A STUDY OF LAPPED SPLICES IN REINFORCED CONCRETE COLUMNS UNDER SEVERE CYCLIC LOADS

by

Kuruvilla Lukose[1]

Peter Gergely[2]

Richard N. White[3]

July 1981 Report 81-11

Progress Report

1. Structural Engineer, Schneider Consulting Engineers, Pittsburgh, PA, (formerly Graduate Research Assistant, Cornell University)

2. Professor, Department of Structural Engineering, Cornell University

3. Professor, Department of Structural Engineering and Director, School of Civil and Environmental Engineering, Cornell University

This report was prepared with the support of NSF Award Nos. PFR78-02399 and CME-8011115. However, any opinions, findings, conclusions, or recommendations expressed herein are those of the authors and do not necessarily reflect the views of the National Science Foundation.

ABSTRACT

Results of the third phase of a continuing investigation of the behavior of lap spliced specimens under high intensity cyclic loading are presented. The purpose of the study was to evaluate the performance of column type lapped splices under reversed cyclic loads and to develop design procedures to ensure adequate seismic loading resistance.

The experimental program consisted of fourteen tests on column specimens with #6 spliced bars at the corners of surrounding #3 stirrups, and subjected to combined bending and shear. The splice length - stirrup spacing relationship was studied in detail. Also investigated were: compression splice behavior, relative orientation of the spliced bars, stiffness deterioration, and bond-shear interaction.

The most significant result is that a reasonable level of ductility in splices under combined bending and shear can be achieved by providing uniformly spaced stirrups along the splice and closely spaced stirrups just outside the high-moment splice end.

The recommended maximum stirrup spacing for splices at least 30 bar diameters long is:

$$s \leq 2.0(A_t L_s/d_b^2) \times 1/(1.25 + 0.2\beta^2 + \beta) ,$$

$$0 \leq \beta \leq 1 \qquad \text{where } \beta = M_\ell/M_y ,$$

for Grade 60 main bars and stirrups, where A_t is the stirrup area crossing the potential splitting crack per splice, L_s is the splice length, d_b is the main bar diameter, M_y is the section yield moment, and M_ℓ is the lower moment at the splice ends. The confinement afforded ensures ductility for limited reversed cycling up to 2.5 times the

yield strain in the splice bars. Changes in stirrup spacing may be required for multiple splice sections, for shears greatly in excess of 120 psi, and for columns under high axial loads. A maximum spacing of the smaller of d/2" and 6" is suggested, where d is the effective depth of the section.

The moment gradient improves splice performance because splice damage primarily occurs only from the high-moment end. Adequate transverse reinforcement is required to resist bond-dowel deterioration near the high-moment end of the splice.

The rate of deterioration of compression splices is reduced because a large fraction of the total force is resisted by direct concrete compression. Bar end bearing resistance becomes effective only after longitudinal cover splitting.

Splices with bars lapped side-by-side and one-above-the-other indicate no significant difference in overall behavior. The performance has yet to be evaluated for large diameter bars and high shear levels.

Reversed cycling above yield results in progressive stiffness reduction, ultimately leading to unstable hysteresis loops with reducing moment resistance.

Bond deterioration arises through longitudinal cover splitting and failure is precipitated by the formation of a cover spalling mechanism. The confinement afforded by cover at incipient failure is negligible.

In horizontally cast specimens the bond resistance of the top splices is less than that of the bottom splices because of the less dense concrete layers at the top.

ACKNOWLEDGMENTS

This work is the outcome of a primarily experimental study conducted at Cornell University on the design of lap splices in reinforced concrete under cyclic loading. The investigation was financially supported through Grant PFR78-02399 provided by the National Science Foundation.

The help of Sam Wheelis, Ernest Pittman, and Jack Powers in the laboratory is gratefully acknowledged. Thanks are due to David Armstrong for typing the manuscript under severe time constraints.

The conclusions and explanations in this report rely heavily on the work of Drs. F. Fagundo and A. Tocci during the first two phases of this project. All beam and column tests from the entire project to date are summarized in Tables 3.1 and 3.2 (pages 47-52). Also, selected conclusions from the first two phases are reproduced in Appendix A.

TABLE OF CONTENTS

LIST OF TABLES

LIST OF FIGURES

NOTATION

A_b, A_s - Area of cross section of spliced bar - in^2

A_t - Area of cross section of stirrup reinforcement - in^2

A_{tr} - Area of transverse reinforcement crossing a potential splitting plane - in^2

b - Width of beam or column - in

C,c - Minimum cover measured to bar surface - in

C_b - Distance between centerline of spliced bar and tension face of beam or column - in

C_c - One half the distance between centerlines of adjacent splices - in

C_s - Distance between centerline of spliced bar and side face of beam or column - in

d - Effective depth of flexural member - in

d_b - Diameter of spliced bar - in

d_s, d_t - Diameter of stirrup bar - in

D_y - Displacement ductility ratio

E_y - Strain ductility ratio

f_b - Average longitudinal bond stress in a spliced bar - psi

f'_c - Concrete compressive strength - psi

f_s - Stress in spliced bar - psi

f_{st} - Stress in stirrup leg - psi

f_{ult} - Ultimate strength of reinforcing bars - psi

f_y - Yield stress of main reinforcing bar - psi

f_{yt} - Yield stress of stirrup reinforcing bar - psi

F_i - Radial bond force resultant per unit length of bar - lb/in

h - Total height of flexural member - in

k - Factor relating maximum stresses in the two spliced bars = $1/(M_y/M_\ell - 0.2)$

K_b - Transverse reinforcing index = $A_{tr}f_{yt}/(Sd_b) \leq 1500$ - psi

K_{tr} - Transverse reinforcing index = $A_{tr}f_{yt}/(600\ Sd_b) \leq 2.5$ - psi

ℓ_s, L_s - Splice length - in

ℓ_d, L_d - Bar development length - in

ℓ_e, L_e - Effective splice length - in

M - Moment at section to which yield penetration occurs - lb/in

M_h - Moment at high moment splice end - lb/in

M_ℓ, M_L - Moment at low moment splice end - lb/in

M_s - Moment at a section of a flexural member - lb/in

M_y - Yield moment of beam or column - lb/in

N - Total number of cycles of reversed loading

N_y - Number of cycles of reversed loading beyond yield

P - Load applied through hydraulic actuator - kip

S,s - Stirrup spacing over splice - in

S_o - Stirrup spacing immediately outside high moment splice end - in

S' - Average spacing between deformation ribs in reinforcing bars - in

T - Tensile force in main reinforcement for splitting failure under combined axial and dowel forces - lb

T_o - Tensile force in main reinforcement for splitting failure without dowel effects - lb

T_{st} - Tensile force in main reinforcement - lb

U - Bond stress - psi

V - Total shear force at a section - lb

V_d - Dowel force in main reinforcement for splitting failure under combined axial and dowel forces - lb

V_{do} - Dowel force in main reinforcement for splitting failure without axial forces - lb

V_{dt} - Dowel force in main reinforcement - lb

α - Inclination of resultant bond force with bar axis

β - Ratio of the lower moment at splice ends and the yield moment = M_ℓ/M_y

Δ - Vertical displacement at the location of the hydraulic actuator - in

Δ_y - Vertical displacement at the hydraulic actuator at first yield of the main bars - in

κ - Factor defined as $2.5/(1.25 + 1/(M_y/M_\ell - 0.2))$

ε - Strain in main reinforcing bars - in/in

ε_{st} - Strain in stirrup legs - in/in

ε_y - Yield strain of reinforcement - in/in

σ_1 - Principal tensile stress in concrete - psi

σ_2 - Principal compressive stress in concrete - psi

σ_{cu}, σ_t - Concrete tensile strength - psi

σ_x - Normal stress in X direction - psi

σ_y - Radial bursting bond stress component - psi

τ - Shear stress - psi

τ_1 - Longitudinal bond stress component - psi

θ - Complement of angle of inclination of bar lug face with bar axis

ρ - Steel ratio = $(\Sigma A_s)/bd$

ϕ - Strength reduction factor

η - Ratio of smaller bar stress to larger bar stress at the two ends of the splice

CHAPTER 1

INTRODUCTION

1.1 The General Problem

Reinforcing bars used in construction are produced in limited lengths due to practical considerations. In normal sized structures, the continuity of reinforcement in beams, columns, and slabs usually results from some form of a connection between any two bars. This is achieved by welding, by using mechanical coupling devices, or by overlapping the two bars over a certain length. Of these, the lap splicing technique turns out to be the most practical and economical choice in most cases. Significant interest therefore attaches to investigating the parameters influencing the behavior of splices under different loading conditions.

The performance of lapped splices under monotonic loads below the yield level is well documented, and present-day design approaches such as the ACI 408 Proposal (1979) or the method suggested by Orangun, Jirsa, and Breen (1975) explicitly include most of the parameters known to affect splice behavior. The situation is quite different for cases involving post-yield cyclic loading, where only a limited understanding has developed to date. Available documentation in this area is mainly behavior-oriented and little was done regarding design methods. Consequently, major seismic codes either do not permit lap splices in regions of inelastic stress reversal or suggest overly conservative designs.

1.2 Objective and Scope

The study presented in the following chapters is a continuation of an investigation into the behavior of lapped splices under inelastic

cyclic loads. In particular, this study investigated tensile and compression lapped column splices under inelastic reversed cyclic loads and attempted to develop design provisions that ensure their adequacy for loads at specified ductility levels.

A total of fifty eight beam-type splice specimens have been tested to date. Nearly all were full scale specimens reinforced with #8 and #10 main bars using #3 or #4 size confining stirrups. Splices were situated in both constant moment and varying moment zones, and subjected to repeated and reversed cyclic loads. The primary variables investigated were loading history and the amount and distribution of confining stirrups. The fourteen column splice specimens were tested primarily to study the behavior of sections spliced at the top as well as the bottom. All splices were subjected to a combination of bending and shear force. The relationship between splice length and the spacing of confining reinforcement was studied in some detail. Also investigated, but in less depth, were concrete cover effects, compression splice behavior, and the effect of the relative orientation of splice bars. The splice design equation developed in Chapter 5 yields results consistent with test observations and explicitly accounts for the moment gradient effect.

1.3 Definitions

The following are the definitions of some of the terms used repetitively in subsequent chapters.

Repeated loading:

A sequence of loads or displacements which vary between zero and a peak in one direction.

Reversed loading:

A sequence of loads or displacements which vary between a peak in one direction and a peak in the reversed direction, thus passing through a neutral point.

Tension stroke:

The portion of a cycle of repeated or reversed loading in which splice bars are in tension.

Compression stroke:

The portion of a cycle of repeated or reversed loading in which splice bars are in compression.

Yield or yield state:

That stage defined by the displacement level at which the splice bars first attain yield stress.

Strain ductility ratio: $\varepsilon/\varepsilon_y$

The ratio of the peak splice bar strain at any displacement level to the yield strain.

Displacement ductility ratio: Δ/Δ_y

The ratio of the vertical displacement at the location of the hydraulic actuator to the displacement at yield.

CHAPTER 2

LITERATURE REVIEW SUMMARY AND GENERAL BOND AND SPLICE BEHAVIOR

2.1 Introduction

This chapter presents a brief summary of the fundamental behavior of deformed reinforcing bars in concrete. Rather than discuss previous investigations chronologically, the approach followed here is to subdivide available information according to the factors known to influence the overall performance of splice and anchored bars in concrete. Behavior under cyclic loading has been a major consideration in this chapter. A more general survey can be obtained from the work of previous researchers in this investigation (Fagundo 1979, Tocci 1981).

2.2 Concrete Strength

Experimental evidence indicates that bond strength increases with an increase in concrete strength. However, the rate of increase of bond strength is less for higher strength concretes. With cover splitting being the primary mode of bond failure, bond strength correlates better with the concrete tensile strength, and attempts have been made to express bond strength in terms of $(f'_c)^n$ with n varying between 0.33 and 0.7 (Zsutty 1977, Lutz 1970, and Chinn 1955).

Tepfers (1973) has shown that there is a limiting, concrete strength (about 9,000 psi) above which splice performance actually worsens. This is a result of the high shrinkage stresses developed by very high strength concretes. These concretes also have the disadvantage of being less ductile and less effective in redistributing stress concentrations (Ferguson 1965). Bond slip curves for high strength concrete specimens show a higher initial slope, a higher ultimate bond stress,

but a smaller total end slip at breakdown (Kemp 1968). Monotonic load tests conducted by Tepfers (1973) showed a direct relation between concrete tensile strength and the maximum steel stress in spliced bars. The overall effect of concrete strength decreases as one gets into longer splice lengths. Cairns and Arthur (1979) state that this is due to the lowering of average bond stresses with larger splice lengths. Bond resistance and concrete compressive strength are also affected by the loading rate. Vos and Reinhardt (1980) and other researchers have shown that higher loading rates result in larger bond and compressive strength.

The correlation of splice behavior with concrete strength is less reliable for repeated and reversed cyclic loading cases. This is because of the extensive concrete cover damage that takes place before splice failure, and also because of the load history dependence of the problem.

2.3 Steel Properties

The use of high strength steel bars in reinforced concrete has resulted in higher levels of bond force. While for monotonic loadings it is enough to study the steel-concrete bond interaction up to the yield level, investigations on inelastic cyclic loadings have necessarily to consider non-linear stress-strain characteristics as well. Elements under seismic influences are likely to be deformed into the post yield stage, and in order to ensure sufficient bar anchorage capacity, a knowledge of the true steel strain hardening properties is required.

In structures subjected to inelastic reversed loadings, the steel behavior is influenced by the Bauschinger effect. This means that if steel is first yielded in one direction, then unloaded, and deformed in the other direction, the yield point in the second direction will be considerably less than that in the first direction. Various stress - strain

relationships are given in Fig. 2.1. The effect of increasing the strain rate is generally to increase the tensile yield point (Fig. 2.2). In some steels, the stress-strain curve may approach that of a perfectly plastic material, and in others, the strain hardening will increase with strain rate.

Hassan (1977) states that after a bar reaches yield, the bond slip behavior depends on the yield plateau length and on the strain hardening modulus. For similar strain hardening moduli, the bond-slip slope decreases with an increase in the length of the yield plateau. For similar yield plateaus, the slope increases with an increase in the strain hardening modulus.

2.4 Bar Size

Several researchers (Mathey and Watstein 1961, Tepfers 1973) have concluded from their experiments that all other variables remaining unchanged, a larger bar diameter results in a lower splice strength. This suggests an inverse relationship between these two variables. Gergely (1969) and Houde (1973) showed that in situations where the confinement provided for an anchored bar is poor, bond splitting indicates little variation with bar size. However, under the confining effect of transverse reinforcement and concrete cover, and the effect of bar end bearing, they found that the extent of bond splitting did show a direct relationship with bar diameter. Morita and Kaku (1973) state that when bars larger than about two inches in diameter are used, it is virtually impossible to attain pullout failures even for considerably large concrete covers. They found that anchorage failures in these situations were brought about by concrete cover splitting.

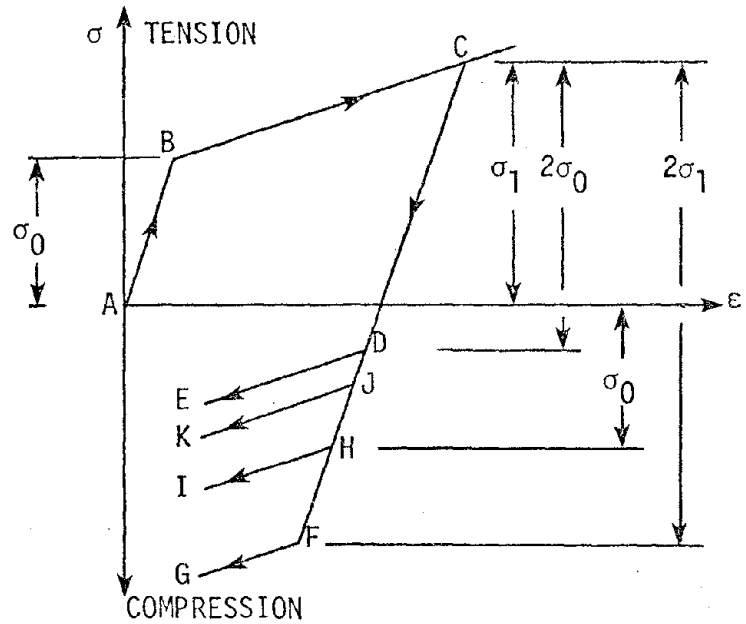

Fig. 2.1. Theories for Bauschinger effect (Mendelson 1968).

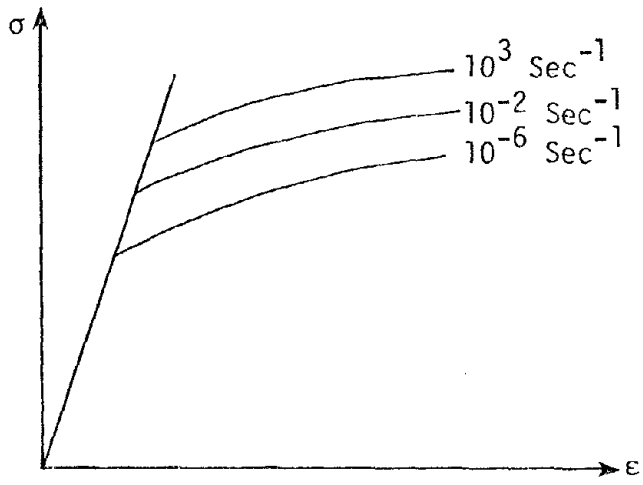

Fig. 2.2. Effect of strain rate. (Mendelson 1968).

The general observations made above also hold for anchored bars subjected to cyclic loading (Jirsa 1971, 1972). Tocci's splice test results (1981) indicate that splices with larger bar diameters sustain fewer reversed cycles above yield. Possible reasons why large diameter bars are more sensitive to load reversals are:

(1) higher stress concentration effects at the bar deformations.

(2) a greater resistance to bending results in large contact zone stresses and possible cover spalling (Fig. 2.3).

(3) for bars in compression, bursting forces due to bar end bearing effects are higher.

An investigation conducted by Tepfers (1973) brings out the influence of splice bar diameter on the effectiveness of concrete strength in splice performance. He states that the reduction in splice strength with increasing bar diameter is more pronounced for high strength concretes (4300 psi) than for concretes with lower strengths (2500 psi). These observations were based on monotonic tests on splices without transverse reinforcement. This behavior is explained by the inability of high strength concretes to redistribute stresses from critical locations to less highly stressed areas. The observed difference is expected to be less in splices where additional confinement is provided by transverse reinforcement.

2.5 Bar Deformations

While the advent of deformed reinforcing bars has resulted in improved bond characteristics, it is important to realize that the force transfer mechanism has undergone a significant change. The now obsolete plain round bars relied on chemical adhesion, friction, and, to some extent, mechanical interlocking with concrete due to the roughness of

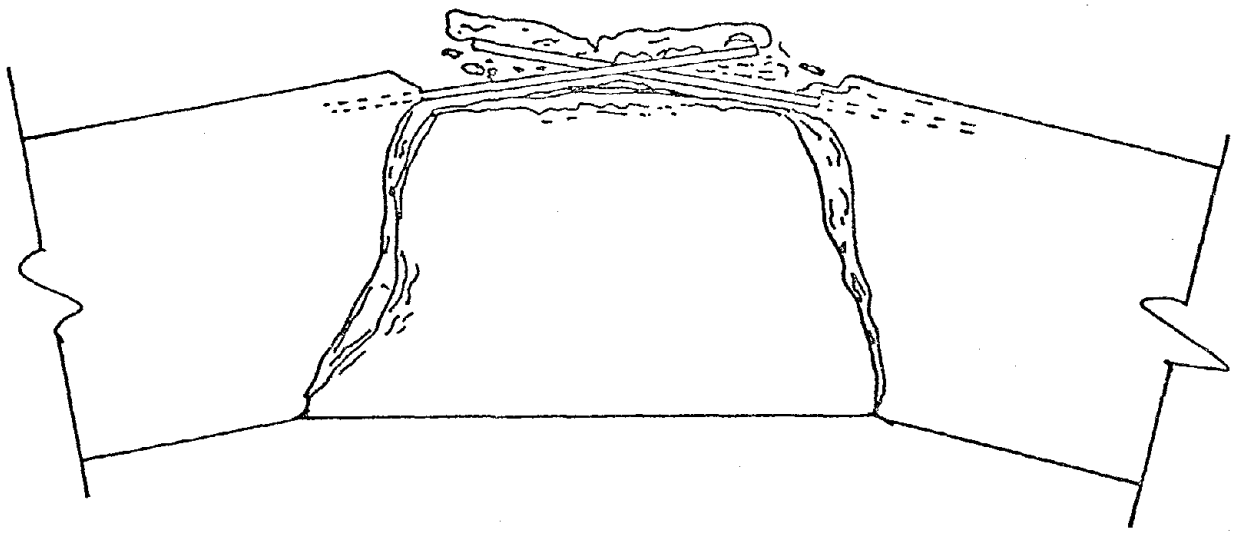

Fig. 2.3. Illustration of the effect of bar stiffness on cover failure. (Fagundo 1979).

the bar surface for force transfer. Pullout type failures were common in these cases. In contrast, present-day deformed bars rely mostly on the mechanical interlocking developed between the lugs and surrounding concrete for force transfer.

The height, spacing, and inclination of bar deformations all influence bond strength. Bars with shallow deformation angles tend to slip along the bar-concrete interface when subjected to axial force. Bars with steeper deformation angles crush the concrete zone directly ahead of each lug. For bars with high closely spaced deformations, a shearing failure of concrete between the lugs is likely to occur. As the deformation spacing is increased, failure shifts to one due to crushing of the concrete zone bearing on the lug face.

Changes in bar surface geometry, within the limits of the ASTM Specifications, have little influence on the behavior of monotonically loaded specimens. In contrast, Hassan and Hawkins (1977) state that bar surface geometry does affect cyclically loaded specimens. They found that bars with deformations inclined to the bar axis were superior to those with deformations perpendicular to the axis.

2.6 Bond Characteristics

It was stated previously that the force transfer mechanism in an anchored bar arises mainly through the interlocking of the bar surface deformations with the surrounding concrete. Contribution to force transfer from chemical adhesion between steel and concrete and friction on the interface layer are small in comparison. The state of forces at the interface of steel and concrete can be described as follows.

When an anchored bar is first loaded, the concrete zone ahead of any lug is subjected to shear stresses and a horizontal direct stress due

to the bearing effect of the lug (Fig. 2.4). The stress states shown in Fig. 2.4 and Fig. 2.5 are equivalent, where θ is equal to the complement of the angle of inclination of the lug face with the bar axis.

σ_1 = principal tensile stress

σ_2 = principal compressive stress

The properties of concrete in tension and compression are expected to be equal at this load level. This state of stress remains unaltered until the tensile stress σ_1 exceeds the concrete tensile strength σ_t. Cracking begins at this stage, and σ_1 is reduced to zero. As a result, a new equilibrium force state develops as shown in Fig. 2.6. It can be seen that

$$\sigma_2 \ell \, \text{Sin}\alpha \times \text{Sin}\alpha = \sigma_y \times \ell \qquad (2.1A)$$

$$\therefore \quad \sigma_2 \, \text{Sin}^2\alpha = \sigma_y \quad \text{and} \quad \sigma_2 \, \text{Sin}\alpha \, \text{Cos}\alpha = \tau_1 \qquad (2.1B)$$

$$\therefore \quad \sigma_y = \tau_1 \tan \alpha \quad \text{or,} \quad \frac{\sigma_y}{\tau_1} = \tan \alpha \; . \qquad (2.2)$$

σ_y can be regarded as a radial pressure inside a thick-walled concrete cylinder, where the internal diameter of the cylinder is equal to the bar diameter, and the cylinder thickness determined by the smallest concrete cover (Tepfers 1973). In current terminology,

σ_y = the radial (bursting) bond component

τ_1 = the longitudinal bond component .

The stresses acting on the concrete interface are shown in Fig. 2.7. Hence, the resultant bond force is inclined at an angle α to the bar axis. The longitudinal component, τ_1 causes changes in the bar force, while the radial component, σ_y creates circumferential tensile stresses in the surrounding concrete. The ratio of these two components is a

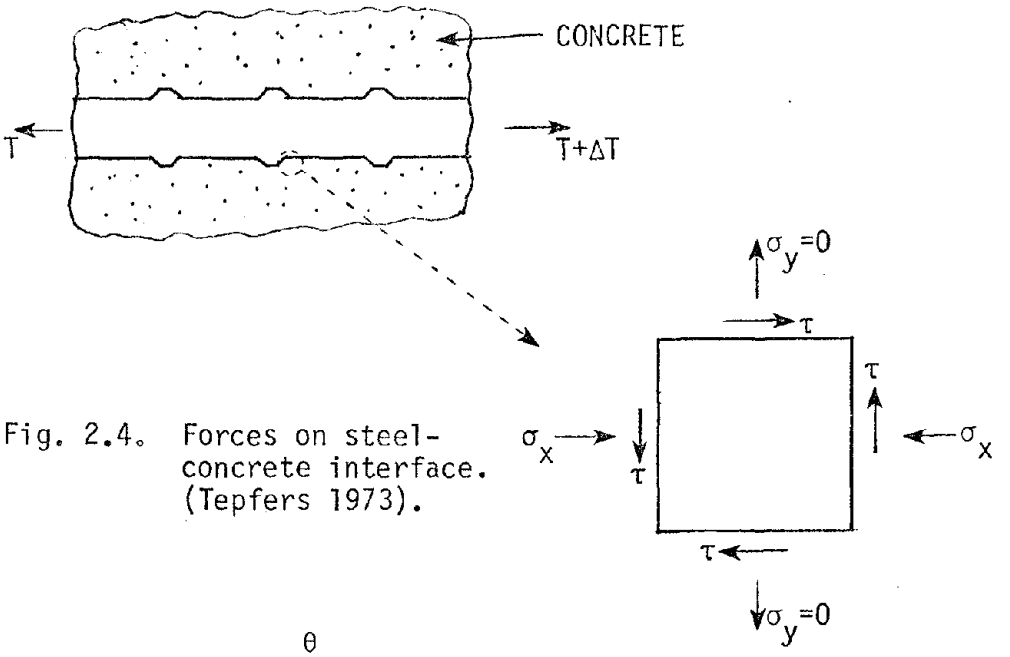

Fig. 2.4. Forces on steel-concrete interface. (Tepfers 1973).

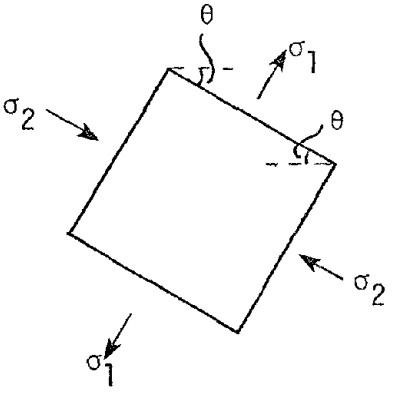

Fig. 2.5. Equivalent state of force.

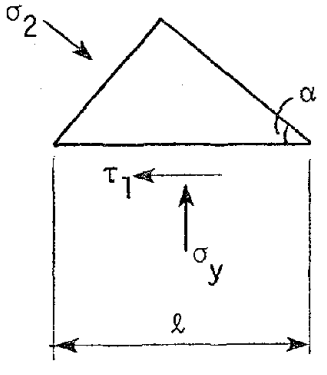

Fig. 2.6. Altered state of force. (Tepfers 1973).

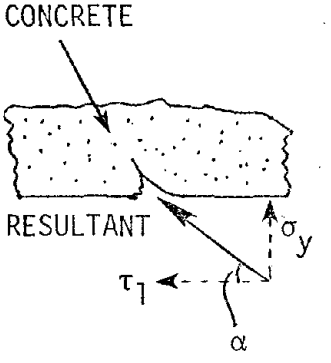

Fig. 2.7. Force on concrete due to bar deformations. (Orangun, Jirsa, Breen 1977).

strong function of the angle α between the resultant and bar axis. Changes in the angle α are seen to occur during the loading process. This is because wedges of crushed and compacted concrete powder which form ahead of the ribs effectively reduce the rib face angle by some unknown angle (Fig. 2.8). Consequently, a change in the relative values of the bond force components also takes place. An anchored bar can fail by:

(1) Shearing of the concrete keys in between the ribs (pullout). This usually occurs in the case of short, well confined anchorage lengths.

(2) Yielding of the bar, as in the case of long anchorage lengths.

(3) Longitudinal cover splitting and a consequent loss of force transfer capacity. This is the failure mode for usual anchorage lengths. Subsequent discussions pertain to this mode.

The resultant bond force in combination with existing concrete stresses produces large diagonal tensile stresses. Internal diagonal cracks develop once the concrete tensile strength is exceeded (Fig. 2.9). The presence of these cracks has been verified analytically (Gergely and Lutz 1967, Hungspreug 1981) and are known to first occur at low bar stress levels. These cracks reduce the stiffness of the surrounding concrete and thereby result in larger deformations due to the same forces. Such a progressive phenomenon results in larger radial and tangential forces and finally brings about longitudinal splitting along the bar axis (Fig. 2.10). Bond stresses can be raised even after splitting due to the loads taken by the concrete cantilevers (Fig. 2.11). However, this will result in higher deformations and slip. For design purposes, Tepfers (1973) states that it is safe to assume that bond resistance attains its peak during longitudinal splitting.

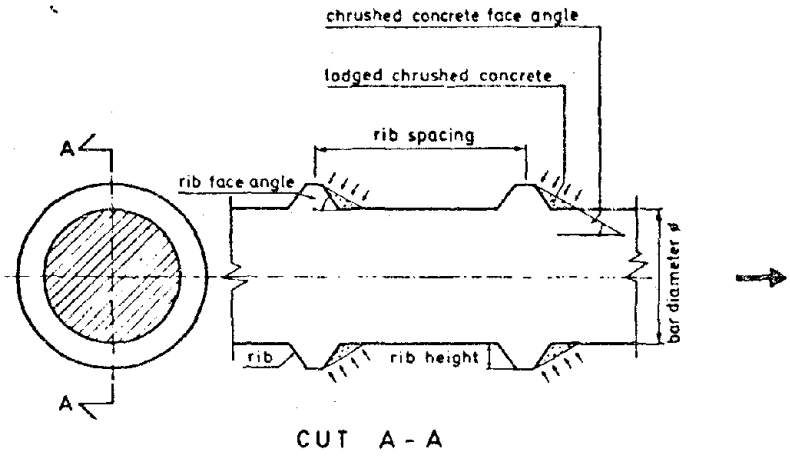

Fig. 2.8. The geometry of a deformed reinforcing bar and the mechanical interaction between the bar and the concrete. (Tepfers 1973).

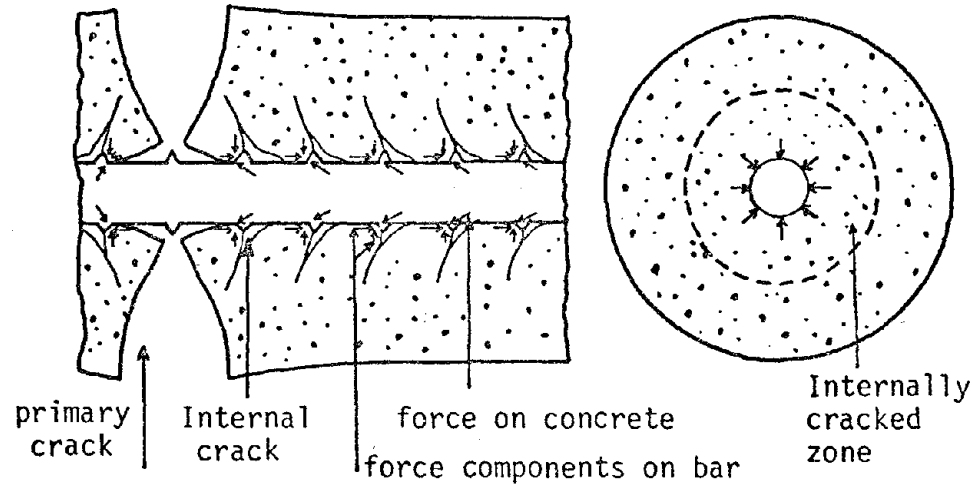

Fig. 2.9. Deformation of concrete around steel reinforcing bar after formation of internal cracks (schematic diagram). (Goto 1971).

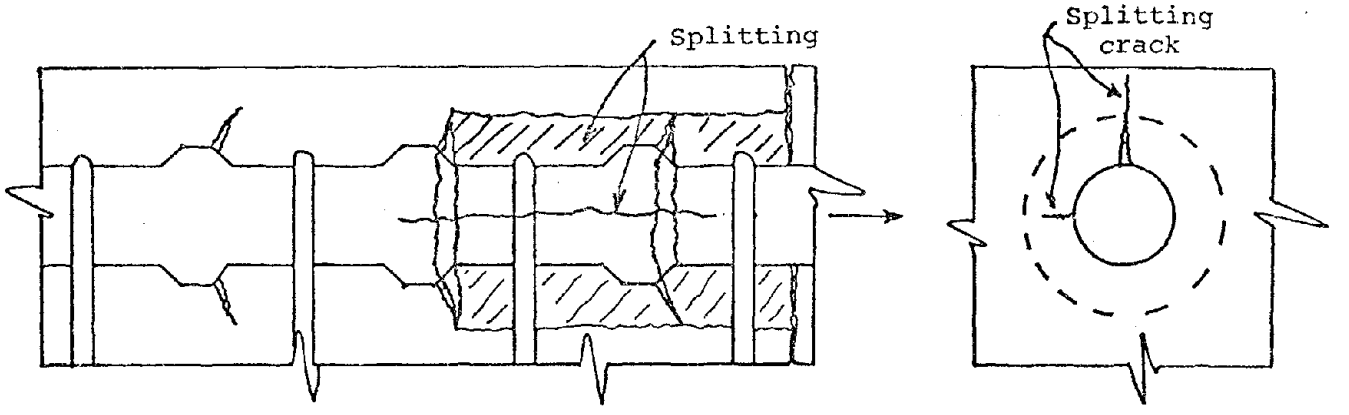

Fig. 2.10. Longitudinal splitting. (Fagundo 1979).

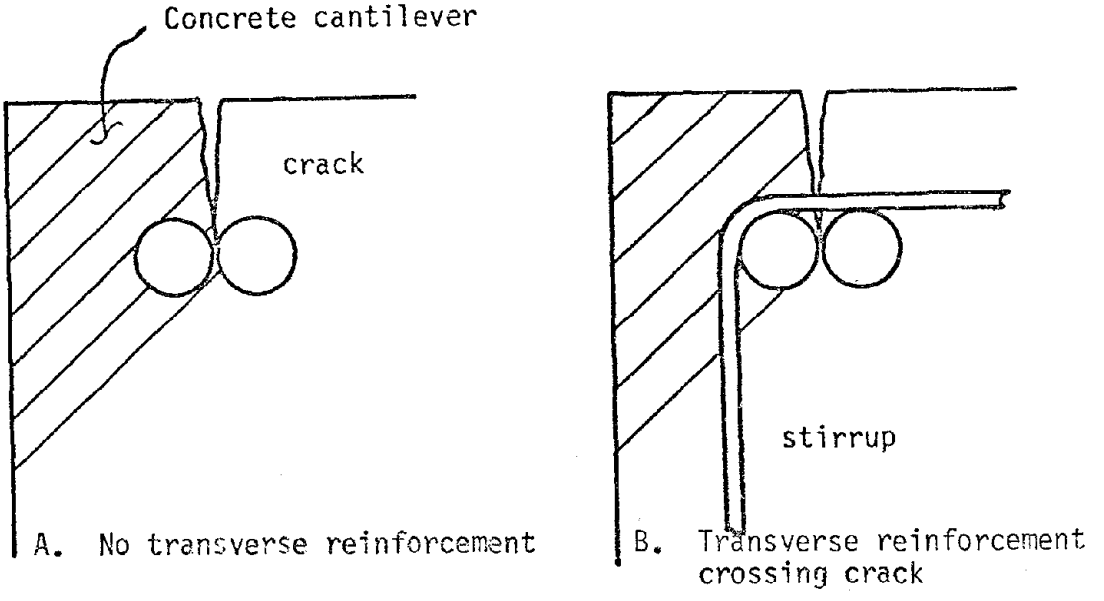

Fig. 2.11. Resistance to radial bond forces after first longitudinal splitting. (Tocci 1981).

With higher bar loads, these splits progress longitudinally and radially and, for splices without transverse reinforcement, failure occurs when the splits reach the surface of the cover and create a cover spalling mechanism.

According to Fagundo (1979), even when splitting is restrained by stirrups, the cover loses its confining capacity when the split reaches the surface. With higher loads, a greater extent of concrete damage becomes due to the crushing of concrete teeth between the lugs (Fig. 2.12). Additional bar slip ensues. The stirrups continue to control the extent of splitting until, at higher levels, failure is brought about by a cover spalling mechanism.

Lapped splices are actually two anchored bars side by side. As the concrete and confining steel have to provide anchorage for both bars, the interaction between bars is important. The bond deterioration process for splices is complicated by the following facts:

(1) Damage propagates from both ends of the splice.

(2) The concrete between bars is subjected to longitudinal bond stresses of opposite sign. This results in stress concentrations at that location.

(3) The bursting effects of the 2 bars are superimposed.

(4) Extensive transverse cracking at high moment locations creates regions of high local bond stress. These are additional locations for the development of splitting.

(5) Bar bending stiffness, although small in comparison to the stiffness of the entire cross-section, can create contact forces at the interface, tending to break through the cover (Fig. 2.3).

Yielding of splice reinforcement is anticipated for splices subjected to severe seismic loading. When this occurs, strains within the

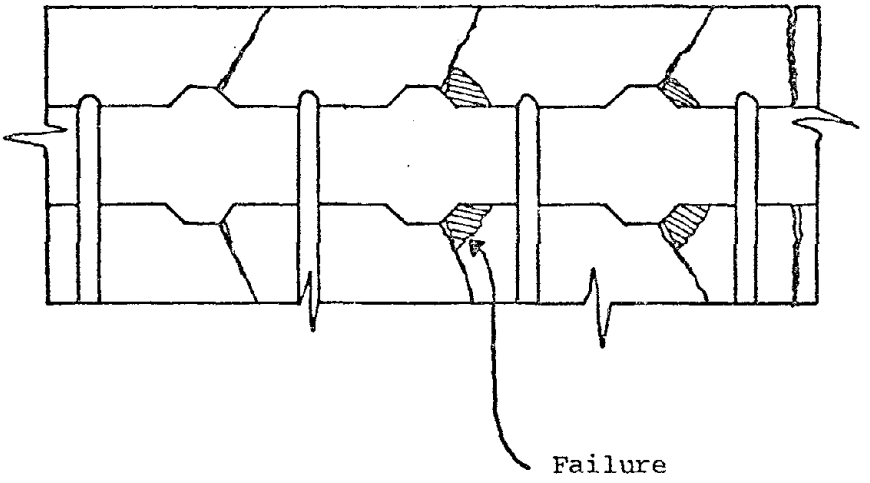

Fig. 2.12. Failure of concrete teeth near bar deformations after extensive longitudinal splitting. (Fagundo 1979).

yielded zone tend to increase at constant loads. The extent of this free elongation is partly restrained by the deformations bearing on the surrounding concrete. Crushing of this concrete zone will permit further elongation. At any rate, the bar force is about constant over the yielded length until strain hardening occurs, and hence, bond forces will not be fully developed over this length. From equilibrium considerations, average bond stresses over the rest of the bar will increase and accelerate the process of bond deterioration. Yielding also results in large structural deformations. Recent investigations suggest that the extent of yield penetration depends on the displacement ductility level, number of post-yield cycles, and on the bar diameter (Gosain and Jirsa 1977, Hassan and Hawkins 1977).

From the above discussion, it is evident that the bond deterioration process can be described only in qualitative terms. This is largely due to a lack of understanding of the interaction of the variables involved such as: concrete strength, transverse reinforcement, bar size, deformation type, and in particular, load history.

2.7 Transverse Reinforcement

Since bond deterioration is brought about largely by radial and circumferential bursting stresses, it follows that overall splice performance can be greatly improved by providing adequate confinement to the concrete at the splice. This confinement comes in the form of lateral reinforcement such as: spirals, closed stirrups, or straight transverse bars. The presence of transverse reinforcement is effective in:

(1) Redistributing stresses after cracking occurs.

(2) Controlling the extent of concrete deterioration.

(3) Imparting ductility to the resisting elements.

While stirrups cannot eliminate splitting in concrete, they effectively restrain the opening of these cracks. They also improve the strength characteristics of the core in resisting the bearing forces of the reinforcement lugs.

The extent of confinement afforded depends on the splitting pattern at failure. Stirrups, to be effective, should cross a potential splitting crack plane. This is particularly important for sections with multiple splices. Tests by Ochoa et. al. (1979) on tension lapped splices under reversed cyclic axial loads indicated that longitudinal splitting and slip were not as well contained for interior bars as for the corner bars. This is attributed to the fact that the corner bars were well confined in two directions by transverse reinforcement, whereas the interior bars had confinement in only one direction. In such cases, additional stirrups binding internal splices should be provided (Fig. 2.13).

The amount and distribution of transverse reinforcement is, perhaps, the most important consideration in designing splices for repeated and reversed cyclic loading into the inelastic stage. Research (Tepfers 1973) suggests that splices should be confined more at their ends, where the forces are high, than at the interior. While valid for monotonic loadings, research at Cornell University (Fagundo 1979, Tocci 1981) shows that under cyclic (repeated and reversed) loadings at and beyond yield, such an arrangement of stirrups is not the best. Due to the progressive nature of cover damage and yield penetration under cyclic loading, once deterioration gets past the splice ends, it will occur over the splice interior at a faster rate due to the poor confinement at those locations. This brings about sudden failures at low ductility levels. With this in mind, a uniform stirrup spacing over the splice is preferable.

Fig. 2.13. Possible stirrup arrangements to improve performance of internal splices. (Fagundo 1979).

The effect of a larger amount of stirrups in controlling the rate of damage penetration into the splice was observed by Fagundo (1979). Fagundo, in testing lapped splices under repeated loading, found that the rate of increase of stirrup strain with bar strain could be greatly reduced by using larger size stirrups (Fig. 2.14). The specimens in which yielding in stirrups was prevented sustained a greater number of cycles above yield than the others. Similar conclusions were stated by Tocci (1981), who performed reversed cyclic loading tests on lapped beam splices. His experiments show that:

(1) The force transfer characteristics of small closely spaced stirrups are better than those of large widely spaced ones.

(2) The zone of influence of a stirrup is small in comparison to stirrup spacing.

Stirrup spacing also has an influence on load-displacement behavior. Both Fagundo (1979) and Jirsa (1971) conclude that to attain a specified deflection, larger loads are required for specimens with closely spaced stirrups, thus indicating improved stiffness characteristics. Morita and Kaku (1973) believe that, for monotonically loaded specimens, there exists an inverse relationship between cover and the effectiveness of an increased number of stirrups. This observation has not been true in the case of cyclically loaded specimens, where the confining effect on concrete cover near failure is negligible.

Many studies, both theoretical and experimental, have been done in an attempt to evaluate the improvement in bond capacity brought about by the provision of transverse reinforcement (Orangun, Jirsa, and Breen 1975, Zsutty 1977, Tepfers 1973). The theoretical investigations make use of equilibrium models, while the experimental studies rely entirely on relationships derived through regression analysis of test data. Kemp

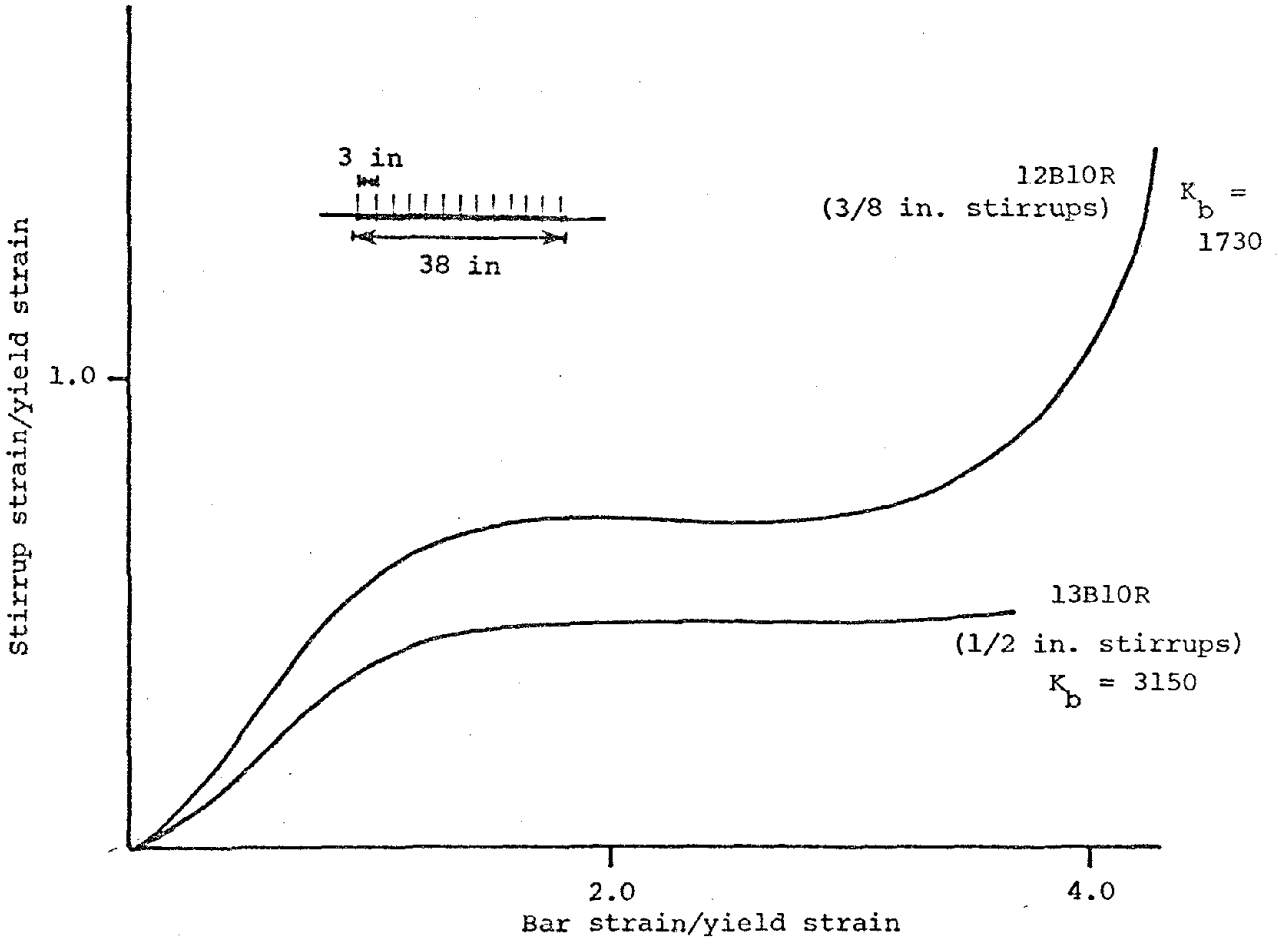

Fig. 2.14. Variation of end stirrups strains with bar strain for beams 12B10R and 13B10R. (Fagundo 1979).

and Wilhelm (1979) point out that since confining stirrups are strained in relation to the crack width, and not directly by applied bond loads, the strain in the stirrups across a bond crack may be nearly constant and relatively insensitive to bond loads. They suggest, therefore, that it might well be a case of strain compatibility rather than equilibrium.

Orangun, Jirsa, and Breen (1975) evaluated the effectiveness of transverse reinforcement over splices in terms of the factor K_b defined as

$$\frac{A_{tr} f_{yt}}{Sd_b} \tag{2.3}$$

where A_{tr} = Area of transverse reinforcement crossing a splitting plane (in^2)
f_{yt} = Yield strength of stirrups (psi)
S = Stirrup spacing (in.)
d_b = Bar dia. (in^2)

and showed, that for monotonic loading, the maximum effective amount of stirrups is attained when K_b has a value of 1500. Fagundo (1979) believes that for splices in a constant moment zone and subjected to repeated cyclic loads, a K_b value higher than 1500 is needed to ensure adequate strength and ductility. In some tests with low K_b values, stirrups went into yield and resulted in sudden failures. He concluded that a K_b value of 3000 is effective and desirable for repeated loading cases.

Stirrups also result in improved bond-slip characteristics, allowing larger bar slips at failure. This is particularly the case for cyclic loading situations, where they are effective in providing confinement at zones of localized damage (Hassan and Hawkins 1977). On the other hand, stirrups act as transverse crack initiators. They are high local stress locations from where splitting cracks usually develop.

2.8 Loading History

There is evidence from a variety of sources that the response of reinforced concrete to repeated and reversed cyclic loads is significantly different from that due to monotonic loads. While the behavior of steel and concrete under cyclic loading is known to a considerable degree, the mechanics of the interaction between these two elements is not well understood.

Stiffness deterioration is, perhaps, the most fundamental manifestation of cyclic loading. This can be due to the progressive cracking of concrete at a damaged location and to the deterioration of the force transfer mechanism between steel and concrete (Bresler and Bertero 1968). Irreversable concrete cracking during the first cycle itself creates stress peaks on the reinforcement at the crack locations which do not return completely to zero upon unloading. The bond deterioration gradually reduces the contribution of concrete towards the overall stiffness and is highly dependent on the type of loading history. Stiffness has a marked influence on the energy dissipation capacity and, as stated by Nielsen (1973), the degradation of stiffness due to bond deterioration results in a loss of energy absorption capacity. In splice elements designed for seismic forces, energy absorption is of prime importance and hence, bond deterioration can result in total failure.

Townsend and Hanson (1977) report that cycles of inelastic loading produce concrete deterioration and modified steel properties, causing changes in the cyclic energy absorption and load displacement curves. Several researchers have observed that when reinforced concrete is loaded beyond the steel yield point, rapid changes occur in the stiffness during the first several inelastic cycles. This concrete deterioration produces unstable load-displacement hysteresis loops which have a decreasing moment

capacity from one cycle to the next, resulting in continually changing structural response characteristics.

Fatigue type tests, where loadings consist of several cycles of low intensity, have been performed by some investigators (Perry and Jundi 1969, Tepfers 1973, Rehm 1976, 1979). The general conclusion is that at low bond stress intensities, specimens can be subjected to several hundred cycles without failure. Failure due to cycling occurs only when the bond intensity is about 70-80% of the ultimate static bond strength. However, these fatigue failure results are of little use in the case of seismic forces. Elements subjected to a small number of high intensity reversed cycles, as in seismic loadings, are not governed by fatigue considerations.

Fagundo's tests (1979) of repeated loading on lapped splices showed that cycling below 80% of the ultimate monotonic bond failure load had only a limited effect on the strength of lapped splices. Although irrecoverable damage due to cracking, splitting, inelasticity, and release of shrinkage stresses prevents the attainment of the initial stage upon unloading, the extent of this permanent damage is low, within the specified loading range. Increasing cyclic loads above 80% of the monotonic capacity results in continuous bond deterioration and larger permanent deformations until loss in anchorage leads to failure. An important conclusion from these tests is that when cyclic loading induces stresses that are below yield, it is the stress level that determines the level of damage. Above yield, the extent of deterioration depends much more on the number of cycles.

In reversed cyclic loading cases, splice damage results from both tensile and compressive bar forces in each cycle. Although tests (Tocci 1981) have shown that bond forces developed in compressive loading

are much less than during tensile loading, it is believed that the end bearing stress of the compression bars leads to significant localized deterioration. Cairns and Arthur (1979) have also recognized this effect in column splice specimens.

According to Goto (1971), cracking patterns are different for monotonic and reversed loading (Fig. 2.15). The solid lines in Fig. 2.15 indicate cracks observed for monotonic loading. The dotted lines represent the cracking pattern anticipated for reversed cyclic loading. If the load level is high enough, the crack systems may join up some distance away from the bar surface. This will result in a zone surrounding the bar within which the concrete can readily pulverise.

Hawkins (1977) states that if displacement ductility ratios in the tensile and compressive half cycles are equal or increase with cycling, the bond deterioration rate is higher than for repeated loads. For low compressive ductilities, the case is similar to repeated loading. Tocci (1981) showed from his splice tests that for similar specimens, reversed loading lead to failures at lower ductility factors than repeated loading. The extent of yield penetration was also less for reversed loading specimens. Tests at the Portland Cement Association conducted by Ochoa et. al. (1979) indicated that the maximum ductility factor for tension lap splices under severe axial load reversals was less than that due to monotonic loads.

2.9 Concrete Cover and its Splitting Patterns

The amount of cover surrounding an anchored bar influences the mode of failure. Orangun, Jirsa and Breen (1975) have shown that the transition between pullout and splitting failures occurs at a C/d_b ratio of about 2.5. In the case of lapped splices, splitting cracks in radial

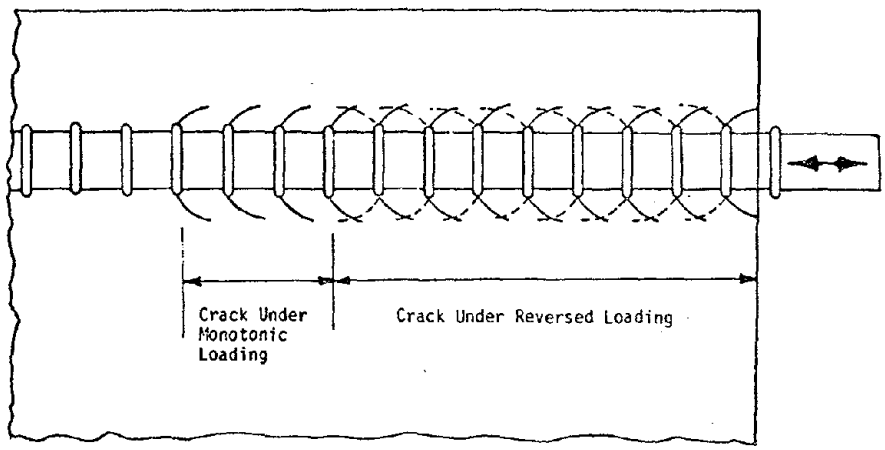

Fig. 2.15. Crack pattern under reversed and monotonic loading. (Goto 1971).

planes are attributed to:

(1) The wedging action of the bar lugs against the adjacent concrete creating circumferential tension and radial compression.

(2) Bending of concrete cover away from the bar due to eccentric longitudinal tensile forces in concrete.

(3) Tension in the cover produced by dowel action of the main bars at transverse cracks where shear exists.

It is important to realize that longitudinal splitting along an anchored bar alters the bond properties in such a way as to produce a uniform distribution of bond stress along the bar length (Tepfers 1973). It also results in improved member ductility and energy absorption.

Depending on the configuration of the spliced bars, the cover ratios, and the cross sectional dimensions, researchers (Ferguson 1969, Tepfers 1973) have identified several possible cover splitting patterns that result in anchorage failure (Fig. 2.16). It is possible, in each of these cases, to derive expressions for ultimate bond strength and required lap length by assuming equilibrium mechanisms between the radial bond forces and the confining force afforded by concrete and transverse steel (Fig. 2.17). The influence of cover in providing confinement is related to the concrete tensile strength, since a splitting failure mode is assumed. The latter property is difficult to evaluate and available data shows wide scatter. Tepfers (1973) reports that the cover splitting pattern at failure is a function of bar size, covers, bar spacing, but largely independent of load history. However, a valid model for a reversed or repeated loading case should account for:

(1) Yielding of main reinforcement (inelasticity).

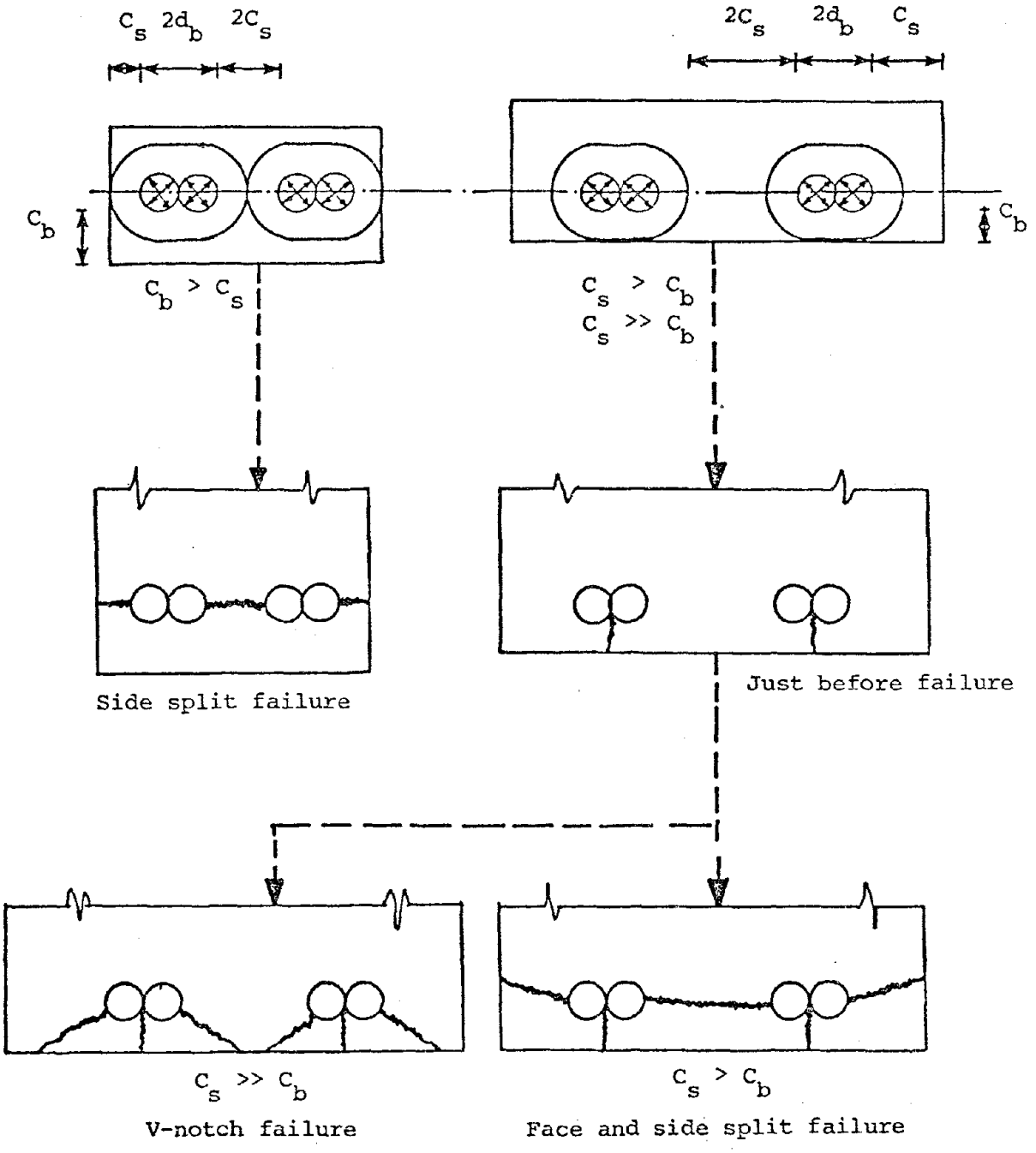

Fig. 2.16a. Basic failure patterns in lapped splices (Orangun, Jirsa, and Breen 1975).

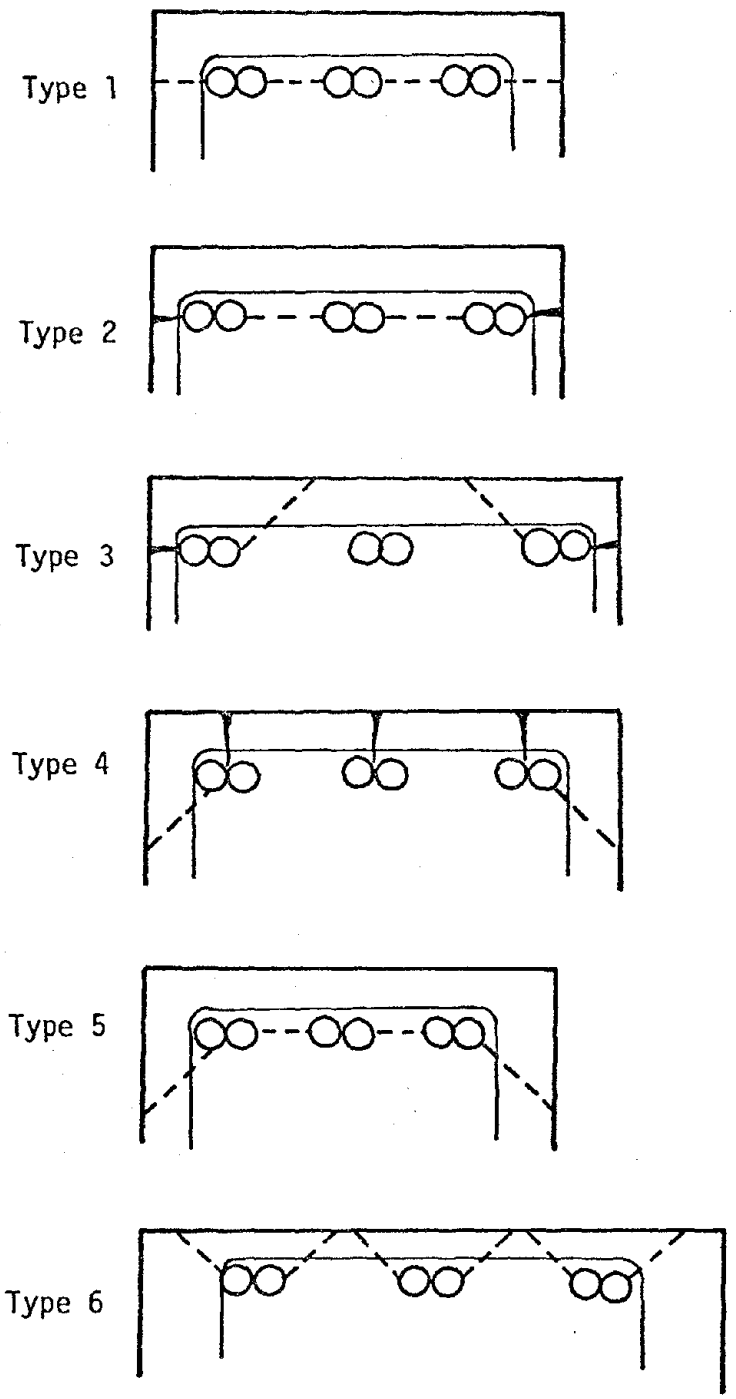

Fig. 2.16b. Ultimate splitting failure patterns with transverse reinforcement. (Tepfers 1973).

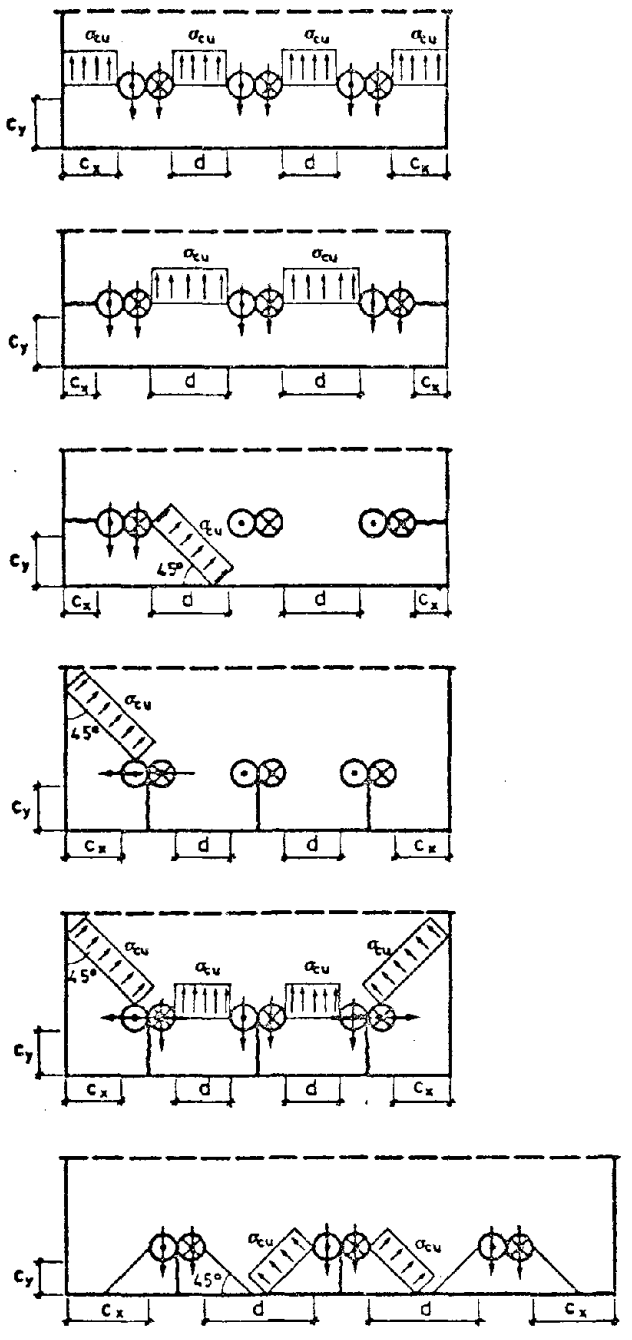

Fig. 2.17a. Splitting failure patterns with stress diagrams. (Tepfers 1973).

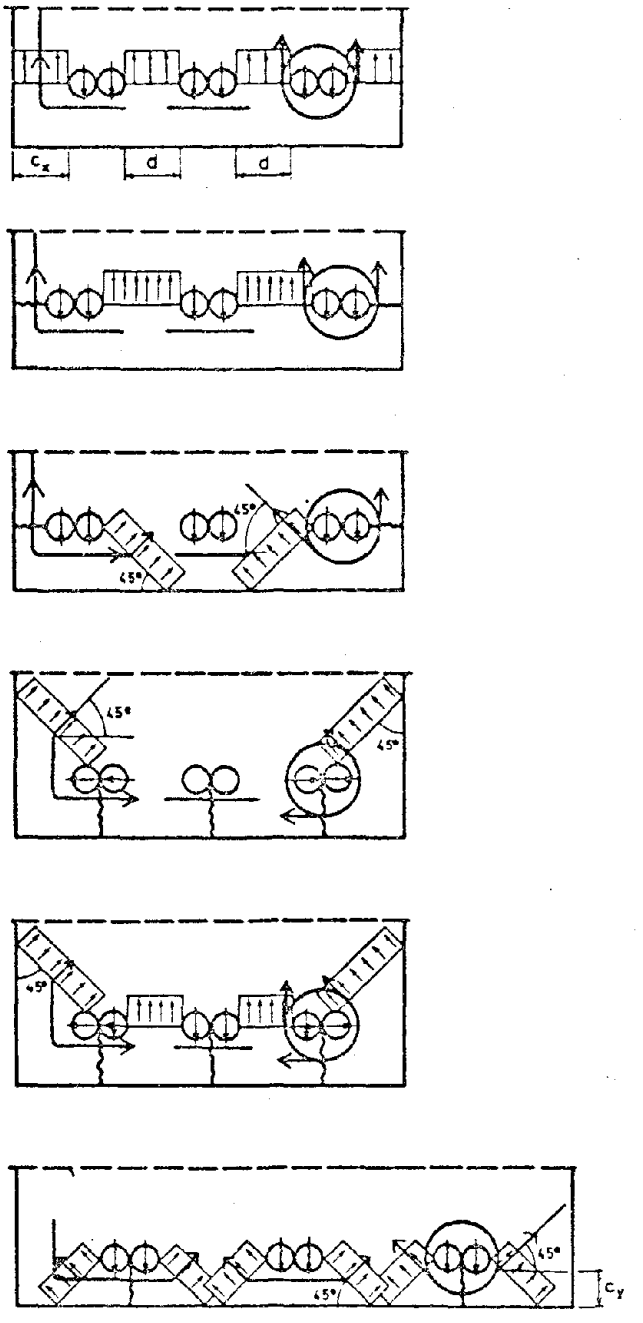

Fig. 2.17b. Ultimate splitting failure patterns with transverse reinforcement and stress diagrams. (Tepfers 1973).

(2) The effect of progressive concrete deterioration on the force transfer characteristics of confining stirrups.

(3) The progressive damage due to dowel action of main reinforcement in shear specimens.

Investigators such as Chinn (1955) and Roberts (1973) have reported an increase in ultimate bond strength with an increase in cover for members under monotonic loads. From the work of Bresler and Bertero (1968), it appears that the influence of cover reduces with cycling and load intensity. Tocci (1981) showed that in the case of lapped splices subjected to inelastic stress reversals, small changes in cover did not result in any appreciable difference in splice strength. This assumes that changes in cover are not so large as to inhibit a splitting failure mode.

2.10 Splice Length

Most researchers agree that the reduction in average bond stress brought about by an increase in splice length improves splice performance. Cyclic loading into the inelastic range brings about the yield penetration effect. The length of a splice bar over which yield penetration occurs develops negligible bond stress. This results in a reduction in anchorage length and a corresponding increase in bond stresses over this length in order to maintain the same load carrying capacity. With this in mind, Fagundo (1979) suggested that splice lengths in these situations be at least $30\,d_b$ long.

Some researchers have indicated that splices can be regarded as anchorage problems, where sufficient development length is provided beyond the region of maximum deterioration. This, however, requires a prior knowledge of the critical section locations which, for seismic

loading situations, may not be easily obtainable. Besides, designs with long splice lengths can lead to overreinforced sections and do not easily attain uniform bond stress distributions.

2.11 Bond Strength Prediction

Attempts at bond strength prediction have been both analytical and experimental. They have been directed towards determining development and splice lengths required to attain the yield strength of deformed reinforcing bars before failure due to bond occurs.

Contributors to the analytical field include Ferguson and Briceno (1969) and Tepfers (1973). In spite of resorting to simplifying assumptions, their work has achieved moderate success when applied to monotonically loaded specimens. The basic procedure involves the selection of a cover splitting pattern depending on observed failure modes (Fig. 2.16). Equilibrium equations are then derived between the resisting and bursting forces, the solutions of which provide an expression for bond capacity. Assumptions made in the assumed distribution of bond forces and in the resisting capacity of cover and transverse steel limit the accuracy of this development. Another limitation is the fact that results are strongly dependent on the value assumed for the angle of inclination α of the resultant bond force.

Statistical formulations rely extensively on collected test data. By the application of regression analysis, the attempt is to relate the geometric and material properties with the bond capacity of the bars in a way that best correlates with data. Considerable work has been done in this area by Orangun, Jirsa and Breen (1975). Their choice of an empirical approach over a theoretical one was mainly because of the difficulty in establishing a value for the inclination α of the bond

force resultant. Using nonlinear regression analysis on several test data, they arrived at expressions for splice and development length, which explicitly account for the bar length, covers, stirrup spacing, bar diameter and concrete strength. Similar expressions have been suggested by Zsutty (1977) and Jimenez (1978). These methods, however, do not directly relate to observed splitting patterns and are of limited use with regard to cyclically loaded specimens.

One instance of this above limitation can be seen from the suggestion (Orangun, Jirsa, and Breen 1975) that splice lengths and development lengths be designed identically. Fagundo (1979) disagrees, and argues that this is valid only for splices with relatively little confinement, where splice failure is precipitated by an anchorage failure of the weaker bar. In contrast, splices with ample confinement, as those designed for cyclic inelastic loads, are characterized by their ability to redistributed forces before failure. In these cases, bond forces on the two splice bars will attain nearly uniform distributions and superimpose, resulting in large radial stress components. Splice lengths under these situations will have to be larger than development lengths.

Hess (1979) used the theory of plasticity in his attempt to solve the problems of anchorage and splicing of reinforcement bars. In this technique, concrete is considered a modified rigid-plastic material, while the reinforcing bars are assumed being rigid-plastic. Then, by equating expressions for internal and external work for a geometrically possible failure mechanism, the load obtained is regarded as being greater than or equal to the true yield load. Internal work expressions are formulated on plain strain assumptions and include contributions from transverse reinforcement. For cases with several failure mechanisms,

a repetitive procedure is required to determine the true upper-bound solution. The author reports some difficulties due to limitations in material modeling and the application of plasticity theory to unreinforced concrete. Tassios (1979) and Takeda and Sozen (1970) attempted predicting bond-slip behavior on the basis of certain sets of rules developed largely by experimental observations. This effort has met with only limited success mainly because of a lack of generality in the results.

Some investigators have analyzed the bond problem through finite element techniques. Tepfers (1973) simplified the anchorage problem to a two-dimensional elastic situation in order to determine the inclination of the bond force resultant. Lutz (1970) used an elastic axisymmetric finite element analysis to model the conditions between two flexural cracks. Similar attempts have been made by Eligehausen (1976) and Bresler and Bertero (1968). However, a realistic model should be three-dimensional, and incorporate inelastic effects, concrete cracking, and separation of the steel-concrete interface. Tocci (1981) analyzed the anchored bar and splice problem using a two-dimensional program incorporating linear elastic fracture mechanics concepts. This is a significant improvement over previous attempts, but is still not a true representation of the problem.

Fagundo (1979) suggested the following design provision for splices subjected to inelastic repeated loads in constant moment zones.

$$S = (A_{tr}\, L_s)/(1.5\, d_b^{\,2}) \qquad (2.4A)$$

$$\text{For } \frac{L_s}{d_b} = 30, \quad S = \frac{20\, A_{tr}}{d_b} \qquad (2.4B)$$

A_{tr} = Area of transverse reinforcement crossing a splitting plane (in^2)

d_b = Spliced bar diameter (in.)

S = Stirrup spacing over splice (in.)

L_s = Splice length (in.)

It should be noted that:

(1) The derivation of Eq. 2.4 is based on equating bursting stresses to confining stresses. However, in view of the large extent of concrete cover damage at imminent failure, the confining influence of concrete is disregarded. The confinement afforded by transverse steel alone is considered.

(2) For splice lengths of at least 30 d_b, splices designed by Eq. 2.4 will withstand about 20-40 cycles of repeated loading up to a displacement ductility of 2 and a strain ductility of about 3.5.

(3) In the development of Eq. 2.4 there exists a direct relationship between stirrup spacing and splice length. Fagundo contends that the larger stirrup spacing brought about by adopting a larger splice length will actually accelerate the bond deterioration process. He concludes, therefore, that a longer splice length is not necessarily a viable option.

(4) For steels with nominal yield strengths of 60 ksi, Eq. 2.4 can be rewritten as

$$\frac{A_{tr} f_{yt}}{S d_b} = 3000 \qquad (2.5)$$

where f_{yt} = yield stress for stirrups (psi).

Recognizing this expression to be equivalent to the definition of the factor K_b, it is concluded that the maximum effective amount of stirrups

in a repeated loading case is double that specified by Orangun, Jirsa and Breen (1975) for monotonically loaded specimens.

Tocci (1981) proposed the following design equation for splices at least 30 d_b in length, and subjected to 15-20 cycles of reversed loading up to a displacement ductility of 2.00 (strain ductility of about 3.5 - 4).

$$S = \alpha \frac{\sqrt{A_t \ \ell_s}}{4 \ A_b} \qquad (2.6A)$$

$$\alpha = \frac{\text{Grade of stirrup steel}}{\text{Grade of spliced bar steel}} \qquad 1 \leq \alpha \leq 1.5$$

A_t = Area of cross section of stirrup bar (in^2)

ℓ_s = Splice length (in)

A_b = Area of cross section of spliced bar. (in^2)

For specimens under combined bending and shear (nominal shear stress $\leq$ 200 psi), the spacing given by Eq. 2.6A can be increased by a factor

$$\sqrt{(2 - M_\ell/M_y} \qquad (2.6B)$$

where

M_y = Moment at high moment end of splice when bar yield occurs.

M_ℓ = Corresponding moment at low moment end of splice.

However, the increased stirrup spacing should not exceed half the spacing required from shear considerations alone.

2.12 Bond-Dowel Interaction

Dowel effects exist only in members subjected to a combination of bending moment and shear, and become apparent only after the formation of flexural shear cracks. At such a stage, shear between sections at a crack is transferred by aggregate interlock, shear forces in the

uncracked portion at the section, forces in transverse reinforcement, and by the dowel action of longitudinal bars. This last effect enhances the extent of local cover splitting (Fig. 2.18) and will thereby affect bond transfer between steel and concrete. Accounting for this dowel effect in the development of a bond theory for lapped splices is hindered by the fact that the extent of total shear transferred by dowel action cannot be estimated accurately enough. Some investigators have suggested that a fair estimate is about 25 percent of total shear. Subsequent tests have, however, indicated that the value is load history dependent.

In an investigation conducted by Jimenez, Gergely and White (1979) it was concluded that:

(1) The dowel capacity for beams is limited to 20-25% of total shear at failure.

(2) Stirrups are beneficial in preventing dowel splitting when placed close to the transverse crack ($\underline{\Omega}$ 1.00")

(3) The dowel capacity is independent of the length of embedment and bar diameter. It increases directly with beam width.

(4) The dowel action over-rides the effect of the wedging action caused by tensile bar forces.

(5) For specimens in which the bars are subjected to combined axial and dowel forces, the dowel capacity of the bar is not influenced by tensile stresses up to 30 ksi. A slight decrease in dowel capacity can be expected when axial stresses are between 40-60 ksi, or when yielding of bars takes place.

Similar investigations were carried out by Krefeld and Thurston (1966). The effect of transverse reinforcement on dowel capacity has been studied to a limited extent by Taylor (1961) and Bauman (1968).

Jimenez, Gergely and White (1979) suggested the following elliptical interaction equation relating the axial and dowel capacities of an anchored bar.

$$(\frac{T}{T_o})^2 + (\frac{V_d}{V_{do}})^2 = 1 \qquad (2.7)$$

T_o = Tensile force in reinforcement required for splitting failure (no dowel effect)

V_{do} = Dowel force in reinforcement required for splitting failure (no axial force effect)

T = Tensile force in reinforcement for splitting failure under combined effects

V_d = Dowel force in reinforcement for splitting failure under combined effects

These components are indicated in Fig. 2.19.

Eq. 2.7 provides a lower bound to experimental data. Tests conducted did not include cases with reversed or repeated cyclic loading. It is likely that the larger bar slips evidenced in inelastic reversed cyclic tests will result in ineffective aggregate interlock and therefore, greater dowel forces (Hawkins and Fourney 1975).

Tests conducted by Kemp and Wilhelm (1979) suggest that there is a weak interaction between bond resistance and dowel force until 80 percent of the dowel capacity is attained. At this point and beyond, bond capacity deteriorates rapidly. A set of interaction curves were developed on this basis (Fig. 2.20). Their tests also showed that the influence of stirrups in resisting dowel forces is greater when large covers are provided. They argue that if stirrups are designed to carry the expected dowel forces, then the ultimate allowable

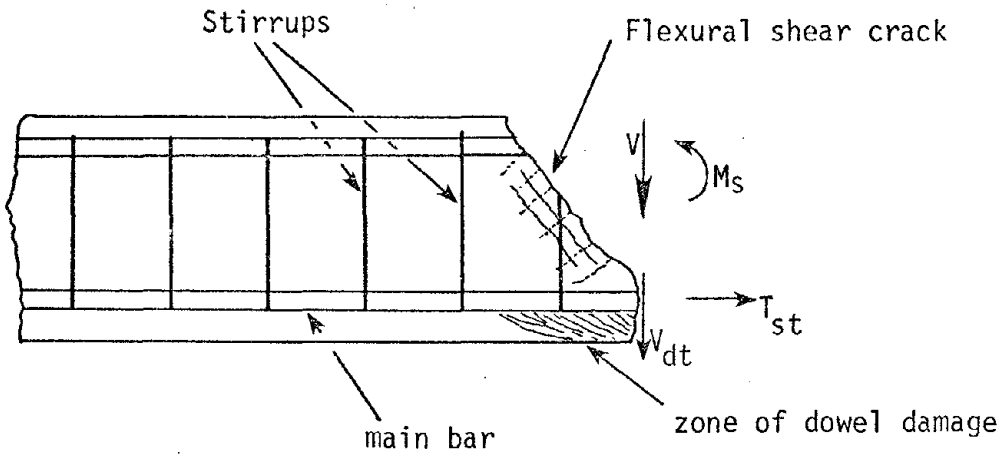

Fig. 2.18. Dowel force damage in flexural specimens. (Tocci 1981).

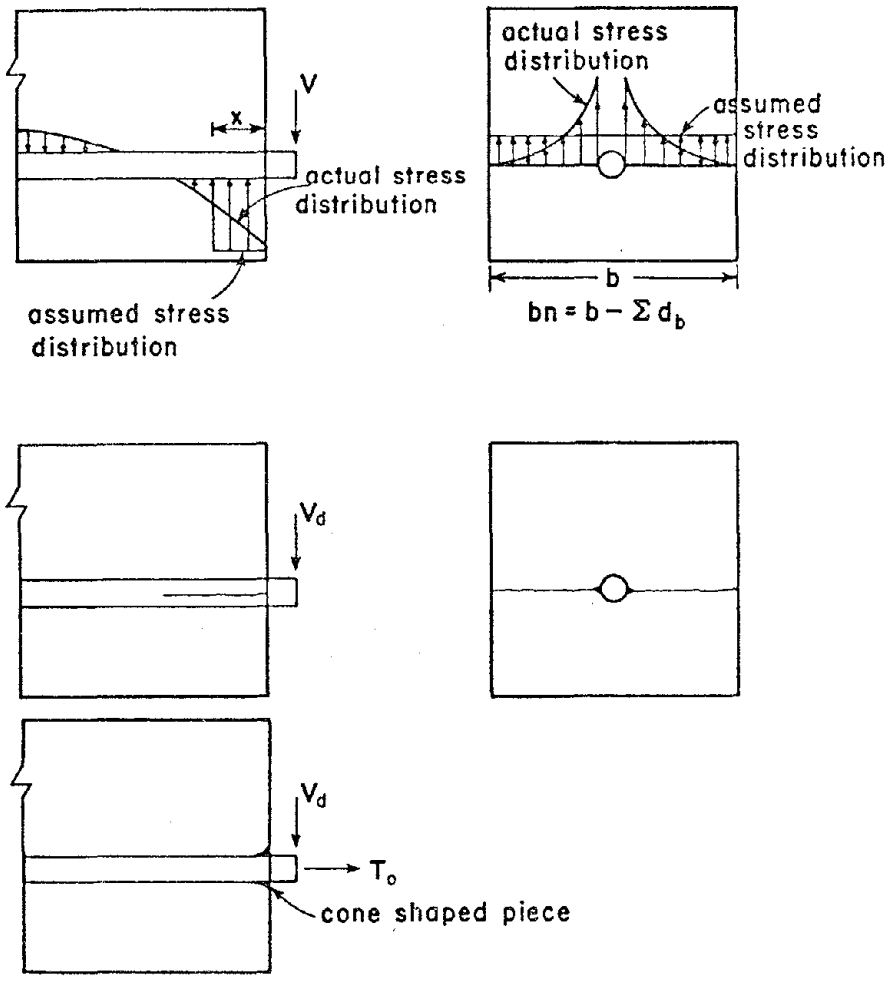

Fig. 2.19. Stress distribution and crack patterns produced by dowel forces. (Jimenez, Gergely, White 1979).

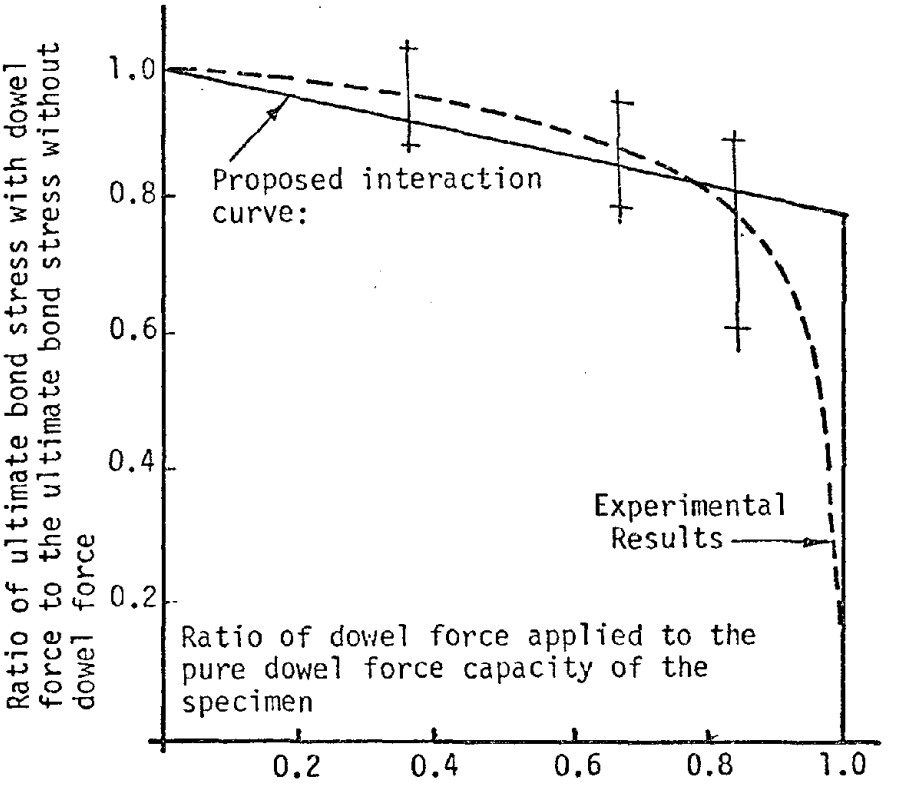

Fig. 2.20. Proposed bond-dowel force interaction curve (Kemp and Wilhelm 1979).

bond stress need not be reduced.

Splice failures from the interaction of bond and dowel forces result when the combined influence of radial bond forces and dowel forces reduce the confinement of the spliced bars to where adequate anchorage ceases to exist. It is pointed out, in this context, that the general agreement that splices subjected to a linearly varying moment undergo less damage than those in a constant moment zone (Ferguson 1970, Tocci 1981) is valid only for moderate shear levels, where the bond-shear interaction is limited. Tests by Tocci (1981) indicate that the critical shear level is at least 180-200 psi for beam splice specimens.

2.13 Compression Splices

Column compression splices, unlike tension splices, cannot be located at low stress locations along the structural element. They have to be designed to develop full strength regardless of location. On the other hand, compression splices do not develop transverse flexural cracks which are locations for splitting crack formation.

Cairns and Arthur (1979) tested lapped splices in reinforced concrete columns under monotonic loads. Their main conclusions were:

(1) In contrast to tensile splices in which complete force transfer occurs within the splice length, compression splice bars are seen to develop bond stresses to a distance of up to 3 d_b outside the splice length.

(2) Large bond stresses are created by end bearing effects at the splice bar ends.

(3) Compression splice strength has two distinct components:

a) a component which provides resistance to counteract the bursting force produced by bond and end bearing.

b) a non bursting component influenced by the concrete compressive strength.

(4) An increase in concrete strength improves splice strength only for short splices.

They reported an improvement in splice performance when ties were provided close to the splice ends. As discussed earlier, the validity of this observation is questionable for specimens under inelastic cyclic loading.

CHAPTER 3

EXPERIMENTAL INVESTIGATION

3.1 Introduction

This chapter describes the experimental procedure followed during the testing of full-scale column splice specimens under inelastic reversed cyclic loads. Tests carried out by Fagundo (1979) and Tocci (1981) during the first two phases of this investigation studied the influence of the amount and distribution of transverse reinforcement on beam type splices subjected to repeated and reversed cyclic load histories. Other parameters such as cover, splice length, bar diameter, and concrete strength were studied to a limited extent. As a result of these tests, it was possible to develop tentative design provisions to ensure splice integrity for a limited extent of inelastic cycling (Section 2.11).

The purpose of this test series was to extend the study to situations in which the top and bottom bars were spliced at the same location (column splices), and to determine whether design provisions could be developed to include these cases as well. Each splice was located at one of the corners of the surrounding tie reinforcement (Fig. 3.1). From the conclusions of the two earlier investigations, it was possible to ascertain the relative importance of the various parameters influencing splice design. Based on this, the column splice tests primarily studied the splice length - stirrup spacing relationship. Other factors such as splice orientation, compression splice behavior, and bond-dowel interaction were also considered. Limitations in the test setup precluded the possibility of investigating direct axial load effects, and hence flexural effects alone were considered.

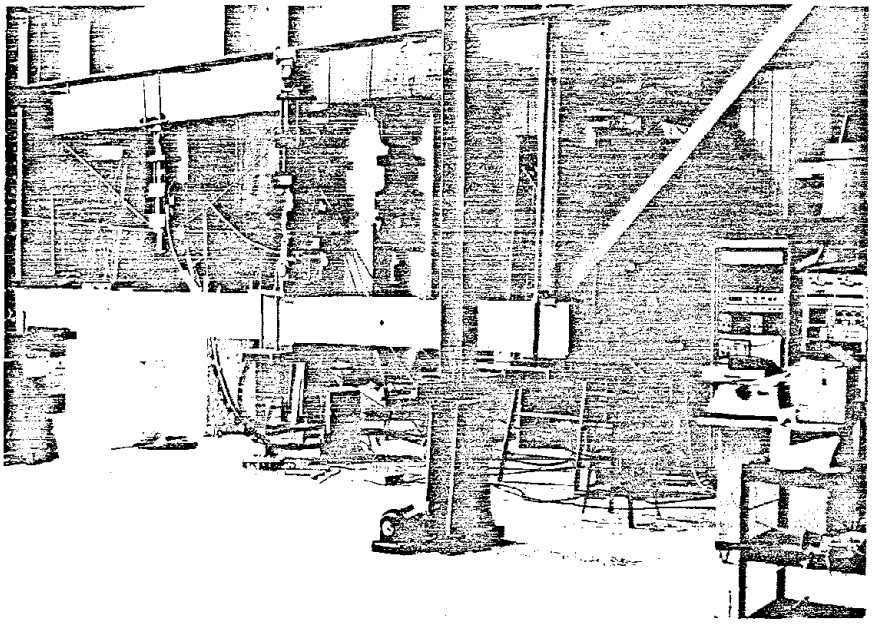

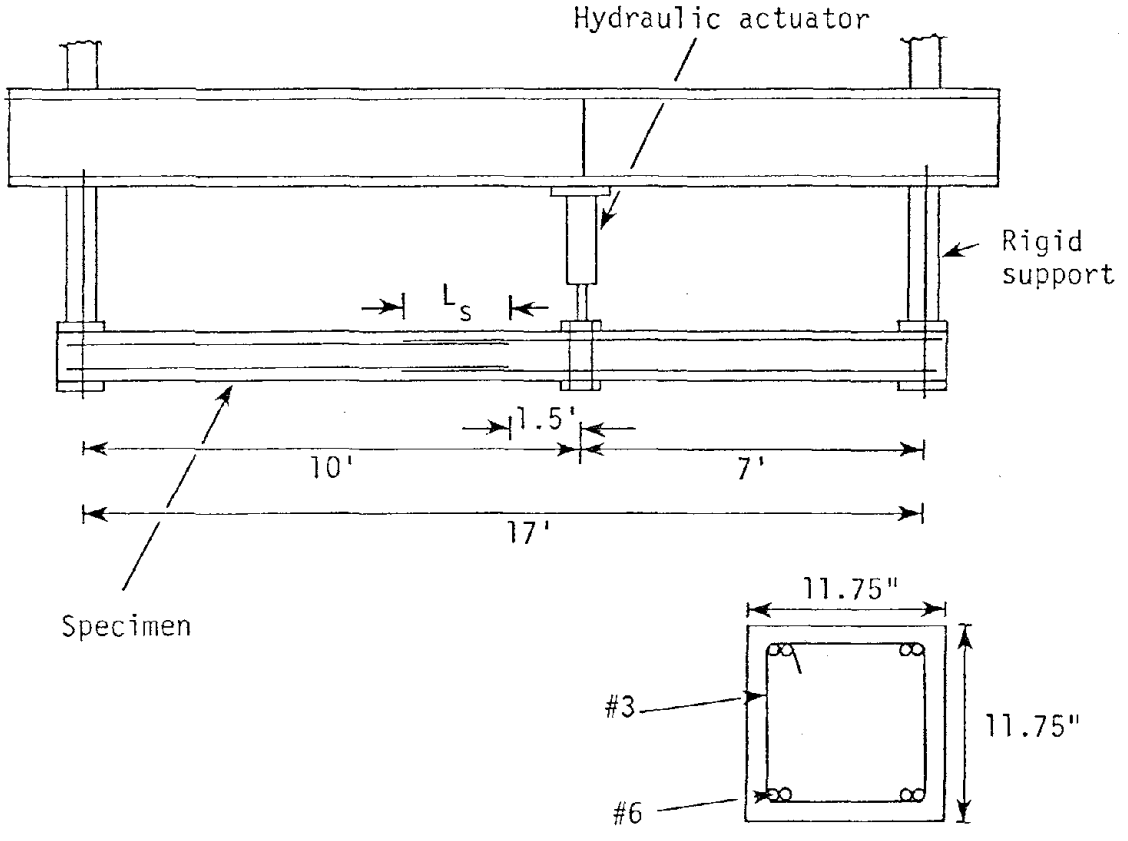

Fig. 3.1. Test setup details.

Table 3.1 summarizes the design details and performance of specimens tested in this and the earlier two studies. A total of 14 column splice specimens were tested, the details of which are in Table 3.2. The first 4 specimens were designed on the basis of Eq. 2.4 (Fagundo 1979) and the remaining 10 followed the design provision given by Eq. 2.6 (Tocci 1981).

Each specimen was loaded as shown in Fig. 3.1. The loading equipment consisted of a single MTS 204.71 hydraulic actuator of 50 kip capacity and a stroke range of ± 3 inches. It produced a linearly decreasing moment over the splice location. This was considered reasonable in view of the fact that columns, typically, are subjected to shear forces and consequently to varying moments. Each specimen was 18 feet long and had a 11.75 inch x 11.75 inch square cross section (Fig. 3.1). It was necessary to locate the splice about 18 inches away from the load in order to prevent the undesirable effect of local compression. Extra longitudinal reinforcement was provided up to the splice so as to ensure that failure would not be controlled by yielding of bars outside the splice.

Test control was achieved by means of a MTS 436 Control Unit, a Hewlett Packard 9825A Calculator-Computer Unit, and a Hewlett Packard 3052A Automatic Data Acquisition System (Fig. 3.2). Fig. 3.3 indicates the flow of command and data during the testing operations. In this particular setup, the HP 9825A Unit was used in controlling the data acquisition system as well as the hydraulic actuator. Hence, test control parameters such as:

1) The number of reversed cycles.

2) The time period per cycle.

Table 3.1 Summary of Splice Test Results

Beam Number	Splice		Transverse Steel		Concrete Cover				Load History	
	d_b	L_s/d_b	$K_b = \frac{A_{tr} f_{yt}}{s d_b}$	(number-size @ spacing)	C_s	C_b	C_c	f'_c (ksi)	Type	# Cycles ($\geq$95% D_y)
1	#10	36	240	3-#3 @ 22"	2-1/2	2-1/4	2-1/2	3.4	monotonic	1(0)
2	#10	36	240	3-#3 @ 22"	2-1/2	2-1/4	2-1/2	3.4	repeated	20(0)
3	#10	36	590	6-#3 @ 9"	2-1/2	2-1/4	2-1/2	3.6	repeated	21(0)
4	#10	36	480	5-#3 @ 22" (not uniform)	2-1/2	2-1/4	2-1/2	3.6	repeated	26(1)
5	#8	36	590	4-#3 @ 11-1/4"	2	1-3/4	2	3.7	monotonic	1(1)
6	#8	36	590	4-#3 @ 11-1/4"	2	1-3/4	2	3.7	repeated	18(2)
7	#8	30	1650	8-#3 @ 4"	2	1-3/4	2	4.4	repeated	27(13)
8	#8	30	1650	8-#3 @ 4" (not uniform)	2	1-3/4	2	4.4	repeated	20(5)
9	#10	30	1760	13-#3 @ 3"	2-1/2	2-1/4	2-1/2	3.9	repeated	26(1)
10	#10	36	1760	16-#3 @ 3"	2-1/2	2-1/4	2-1/2	3.9	repeated	22(7)
11	#8	30	1650	8-#3 @ 4"	2	1-3/4	2	4.2	repeated	16(15)
12	#10	30	1760	13-#3 @ 3"	2-1/2	2-1/4	2-1/2	4.2	repeated	40(38)
13	#10	30	3200	13-#4 @ 3"	2-1/2	2-1/4	2-1/2	4.2	repeated	52(45)
14	#8	30	3000	8-#4 @ 4"	2	1-3/4	2	4.2	repeated	65(55)
15	#8	30	1650	8-#3 @ 4"	2	1-3/4	2	4.2	reversed	45(20)
16	#8	30	1650	8-#3 @ 4"	2	1-3/4	2	4.4	reversed	65(21)

Table 3.1 (continued)

Beam Number	Splice		Transverse Steel		Concrete Cover				Load History	
	d_b	L_s/d_b	$K_b = \frac{A_{tr}f_{yt}}{sd_b}$	(number-size @ spacing)	C_s	C_b	C_c	f'_c (ksi)	Type	# Cycles ($\geq$95% D_y)
17	#8	24	2400	8-#3 @ 2-3/4"	2	1-3/4	2	4.0	repeated	11(0)
18	#8	30	1330	4-#4 @ 9"	2	1-3/4	2	4.0	repeated	21(0)
19	#8	30	1650	8-#3 @ 4"	2	1-3/4	2	3.8	repeated-shear	25(5)
20	#8	30	1650	8-#3 @ 4"	2	1-3/4	2	3.9	repeated-shear	51(10)
21	#10	30	1760	13-#3 @ 3"	2-1/2	2-1/4	2-1/2	3.9	reversed	32(7)
22	#10	30	3200	13-#4 @ 3"	2-1/2	2-1/4	2-1/2	3.9	reversed	58(28)
23	#10	30	1600	7-#4 @ 6"	2-1/2	2-1/4	2-1/2	4.0	repeated	49(10)
24	#10	30	1760	13-#3 @ 3"	2-1/2	2-1/4	2-1/2	4.1	repeated-shear	63(38)
25	#8	30	1650	8-#3 @ 4"	2	1-3/4	2	3.6	reversed-shear	59(24)
26	#10	30	1760	13-#3 @ 3"	2-1/2	2-1/4	2-1/2	3.8	reversed-shear	75(30)
27	#10	36	1760	16-#3 @ 3"	2-1/2	2-1/4	2-1/2	3.6	reversed	53(18)
28	#8	30	1650	8-#3 @ 4"	1-1/2	1-3/4	2	3.9	reversed-shear	62(17)
29	#10	36	1745	9-#4 @ 5-1/2"	2-1/2	2-1/4	2-1/2	3.8	reversed	60(5)
30	#8	36	950	6-#3 @ 7"	2	1-3/4	2	3.5	reversed	48(13)
31	#8	36	950	6-#3 @ 7"	2-1/2	1-3/4	2	4.0	reversed	54(14)

Table 3.1 (continued)

Beam Number	Splice		Transverse Steel		Concrete Cover				Load History	
	d_b	L_s/d_b	$K_b = \frac{A_{tr} f_{yt}}{s d_b}$	(number-size @ spacing)	C_s	C_b	C_c	f'_c (ksi)	Type	# Cycles ($\geq$95% D_y)
32	#10	36	1760	16-#3 @ 3"	2-1/2	2-1/4	3-1/8	4.3	reversed	64(19)
33	#8	30	1650	8-#3 @ 4"	1-1/2	1-3/4	2	3.9	reversed	36(11)
34	#10	45	1070	7-#4 @ 9"	2-1/2	2-1/4	2-1/2	3.9	reversed	56(15)
35	#10	45	1070	7-#4 @ 9"	3-1/8	2-1/4	2-1/2	3.7	reversed	58(23)
36	#8	36	950	6-#3 @ 7"	2	1-3/4	2	3.7	reversed-shear	55(30)

Table 3.1 (continued)

Specimen Number	Desig.	Splice		Transverse Steel		Concrete Cover			Load History	
		Bar Size	ℓ_s/d_b	$K_b = \frac{A_t f_y}{sd_b}$	Number-size @ spacing	C (in.)	C/d_b	f'_c (ksi)	Type	#Cycles ($\geq \Delta_y$)
37	C-1	#6	30	2934	9-#3@3"	2	2.66	3.90	reversed	-
38	C-2	#6	30	2934	9-#3@3"	2	2.66	3.90	reversed	106(42)
39	C-3	#6	40	2200	8-#3@4"	2	2.66	3.40	reversed	114(61)
40	C-4	#6	50	1855	9-#3@4.75"	2	2.66	3.40	reversed	123(50)
41	C-5	#6	30	1760	6-#3@5"	2	2.66	2.91	reversed	79(29)
42	C-6	#6	30	1760	6-#3@5"	2	2.66	2.91	reversed	66(24)
43	C-7	#6	30	1760	6-#3@5"	1.2	1.6	3.47	reversed	78(41)
44	C-8*	#6	30	1760	6-#3@5"	1.2	1.6	3.47	reversed	85(12)
45	C-9	#6	40	1760	7-#3@5"	1.2	1.6	3.80	reversed	82(47)
46	C-10*	#6	40	1760	7-#3@5"	1.2	1.6	3.80	reversed	82(47)
47	C-11	#6	40	1355	6-#3@6.5"	1.2	1.6	3.71	reversed	86(45)
48	C-12*	#6	40	1355	6-#3@6.5"	1.2	1.6	3.71	reversed	82(38)
49	C-13	#6	30	1760	6-#3@5"	1.2	1.6	4.23	reversed	90(50)
50	C-14*	#6	30	1760	6-#3@5"	1.2	1.6	3.52	reversed	78(40)

* - Plane of splice - vertical
C-13, C-14 - Bar end bearing eliminated

Table 3.2. Summary of column splice test results.

Desig.	Purpose	L_s in.	ℓ_s/d_b	S in.	S_o in.	c/d_b	f'_c ksi	Plane of Splice	#Cycles ($\geq \Delta_y$)	Max. Δ/Δ_y	Max. $\varepsilon/\varepsilon_y$	Max. $\varepsilon_{st}/\varepsilon_y$	Type of Failure
C-1	Validity of Eq. 2.4	24	30	3	10	2.6	3.90	Horiz.	-	-	-	-	Accidental overload
C-2	Validity of Eq. 2.4	24	30	3	10	2.6	3.90	Horiz.	106(42)	1.92	2.65	0.66	Bar fracture outside high moment end of splice.
C-3	Validity of Eq. 2.4	30	40	4	10	2.6	3.40	Horiz.	114(61)	2.02	2.81	0.62	Bar fracture outside high moment end of splice.
C-4	Validity of Eq. 2.4	38	50	4.75	10	2.6	3.40	Horiz.	123(50)	2.02	2.50+	0.57	Bar fracture outside high moment end of splice.
C-5	Validity of Eq. 2.6	24	30	5	5	2.6	2.91	Horiz.	79(29)	1.67	2.61+	0.38	Bond-longitudinal cover splitting.
C-6	Validity of Eq. 2.6	24	30	5	5	2.6	2.91	Horiz.	66(24)	1.67	2.52+	0.39	Bond-longitudinal cover splitting.
C-7	Reduced cover	24	30	5	5	1.6	3.47	Horiz.	78(41)	1.84	2.72+	0.46	Bond-longitudinal cover splitting.
C-8	Splice orientation	24	30	5	5	1.6	3.47	Vert.	85(12)	1.00	1.11	0.65	Bond-longitudinal cover splitting.
C-9	Splice length-stirrup spacing relationship	30	40	5°	3.5	1.6	3.80	Horiz.	82(47)	2.08	5.51+	0.21	Localized damage outside high moment end.

+ Failure of strain gage before test termination.
° Spacing governed by d/2 limitation.
Max. ε_{st} on vertical legs for all tests.

Table 3.2. (continued)

Desig.	Purpose	L_s in.	ℓ_s/d_b	S in.	S_o in.	c/d_b	f'_c ksi	Plane of Splice	#Cycles ($\geq \Delta_y$)	Max. Δ/Δ_y	Max. $\varepsilon/\varepsilon_y$	Max. $\varepsilon_{st}/\varepsilon_y$	Type of Failure
C-10	Splice Orientation	30	40	5°	3.5	1.6	3.80	Vert.	82(47)	2.08	4.94+	0.50	Localized damage outside high moment end.
C-11	Splice length-stirrup spacing relationship	30	40	6.5	3.0	1.6	3.71	Horiz.	86(45)	2.06	2.53+	0.21	Bond-longitudinal cover splitting
C-12	Splice orientation	30	40	6.5	3.0	1.6	3.71	Vert.	82(38)	2.06	2.58	0.54	Bond-longitudinal cover splitting
C-13	Compression bar end-bearing	24	30	5	3.0	1.6	4.23	Horiz.	90(50)	2.08	5.02+	0.35	Bond-longitudinal cover splitting
C-14	Compression bar end bearing	24	30	5	3.0	1.6	3.52	Vert.	78(40)	1.87	5.30+	0.48	Bond-longitudinal cover splitting

+ Failure of strain gage before test termination.
∘ Spacing governed by d/2 limitation.
Max. ε_{st} on vertical legs for all tests.

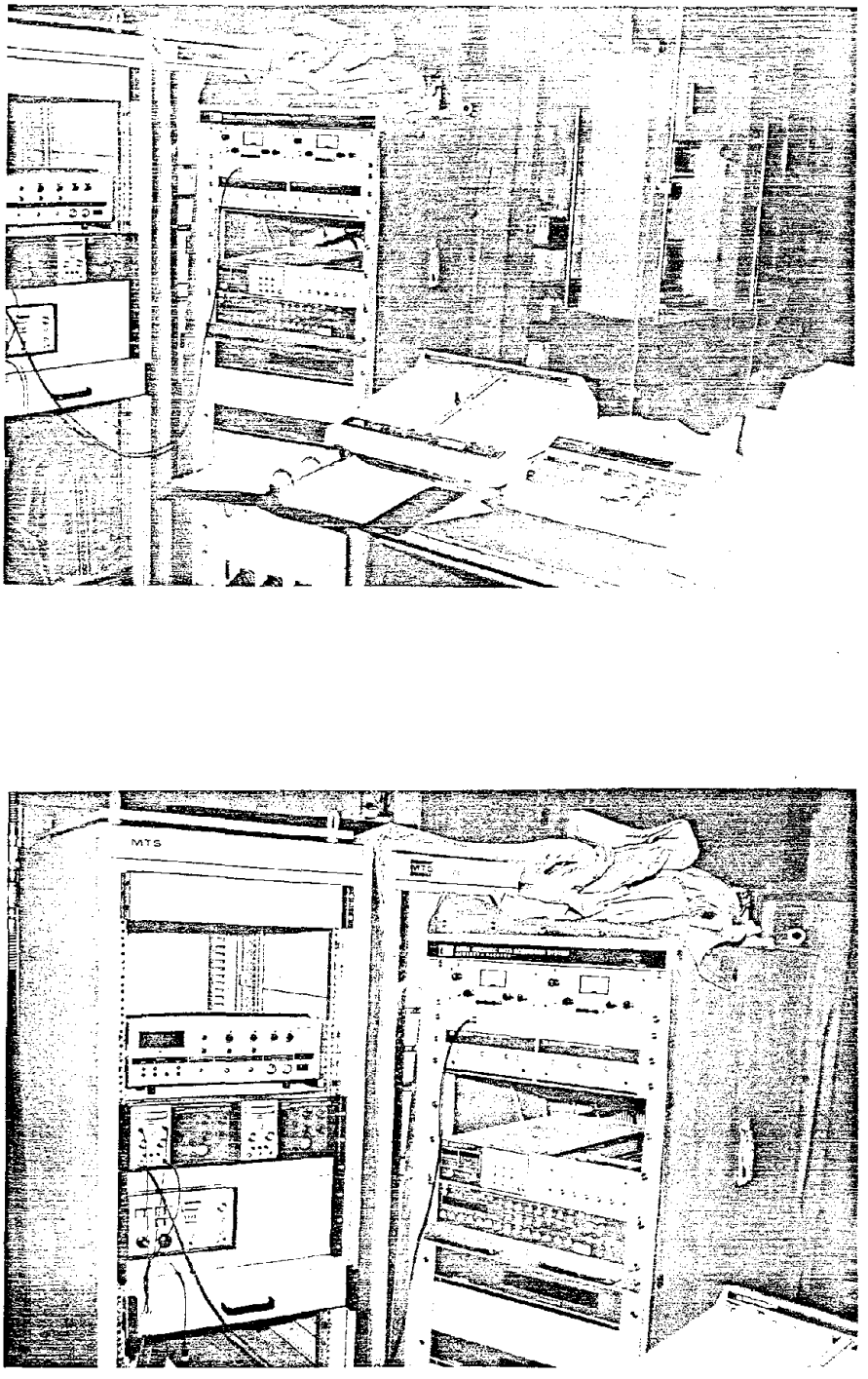

Fig. 3.2. Test control equipment.

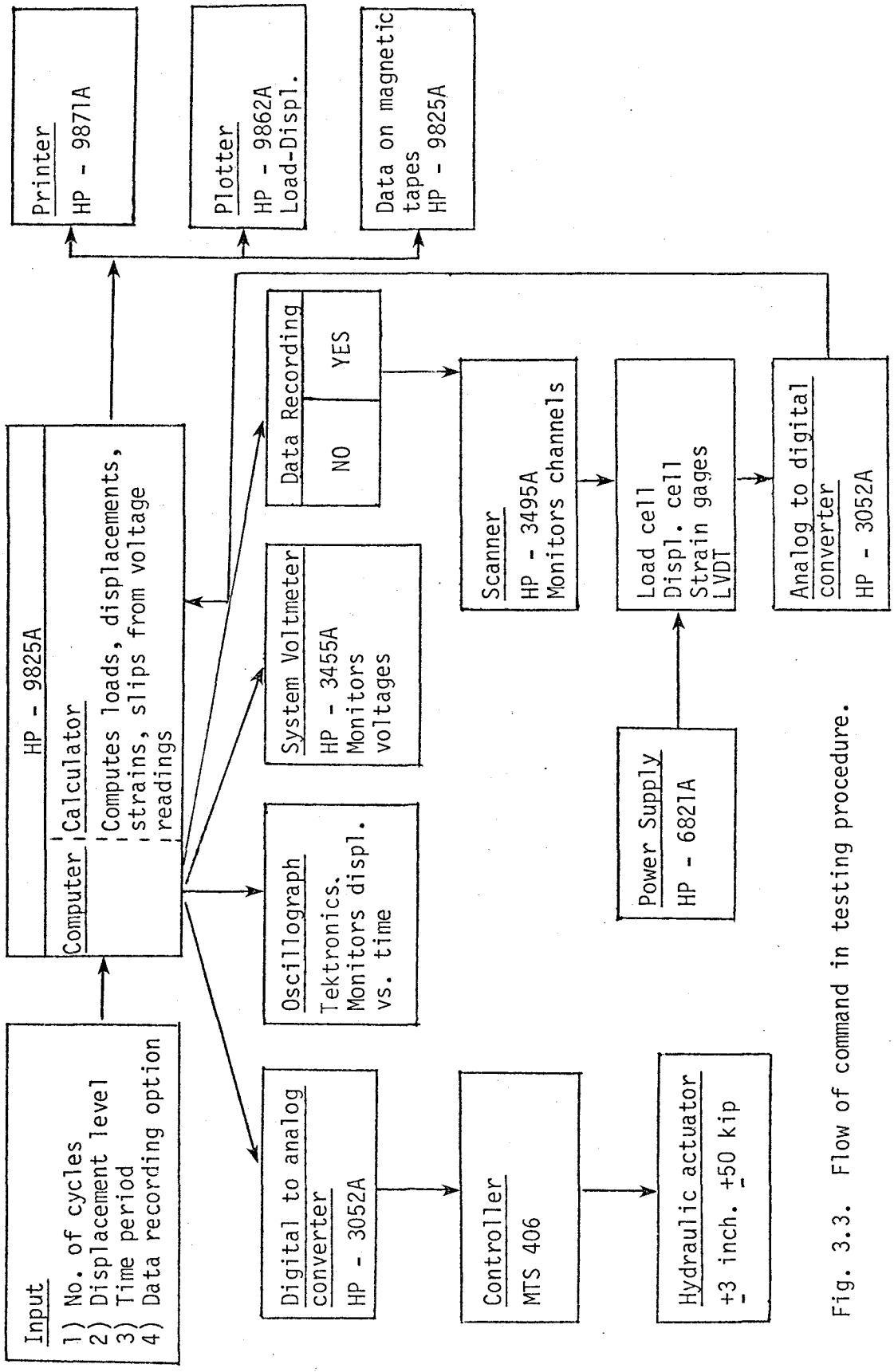

Fig. 3.3. Flow of command in testing procedure.

3) The maximum displacement level.

were input directly through the HP 9825A keyboard. This resulted in excellent coordination between the loading and data acquisition system. All tests were run in a displacement (stroke) controlled mode. With this approach, it was possible to obtain consistent load-deflection relationships even after the main bars had yielded, without the risk of running out of stroke length.

A more detailed diagram of the specimen is shown in Fig. 3.4.

3.2 Instrumentation

Load and displacement at the location of the hydraulic actuator were measured directly through built-in load and displacement cells, respectively. The column specimens were instrumented with electrical resistance strain gages at critical locations on the bars. These were the paper-backed wire type, manufactured by BLH and designated as SR4, A-7. In each specimen, an outer splice bar was gaged at regular intervals at and near the high moment splice end. In addition, the first four stirrups were gaged on the horizontal and vertical legs (Fig. 3.5). Gages were bonded to the bars with Duco cement. Lead wires were soldered on, and the area was moisture proofed either with several layers of hot beeswax or with a special rubberized moisture barrier manufactured by BLH (Fig. 3.6).

In tests C-9 through C-14, splice bar end slips were monitored by means of a displacement transducer. A 0.25" dia. steel rod was cemented in a hole drilled near the end of a splice bar. The lateral movement of this rod, which passed through a 1" dia. hole in the side concrete cover, was monitored by the transducer (Fig. 3.7).

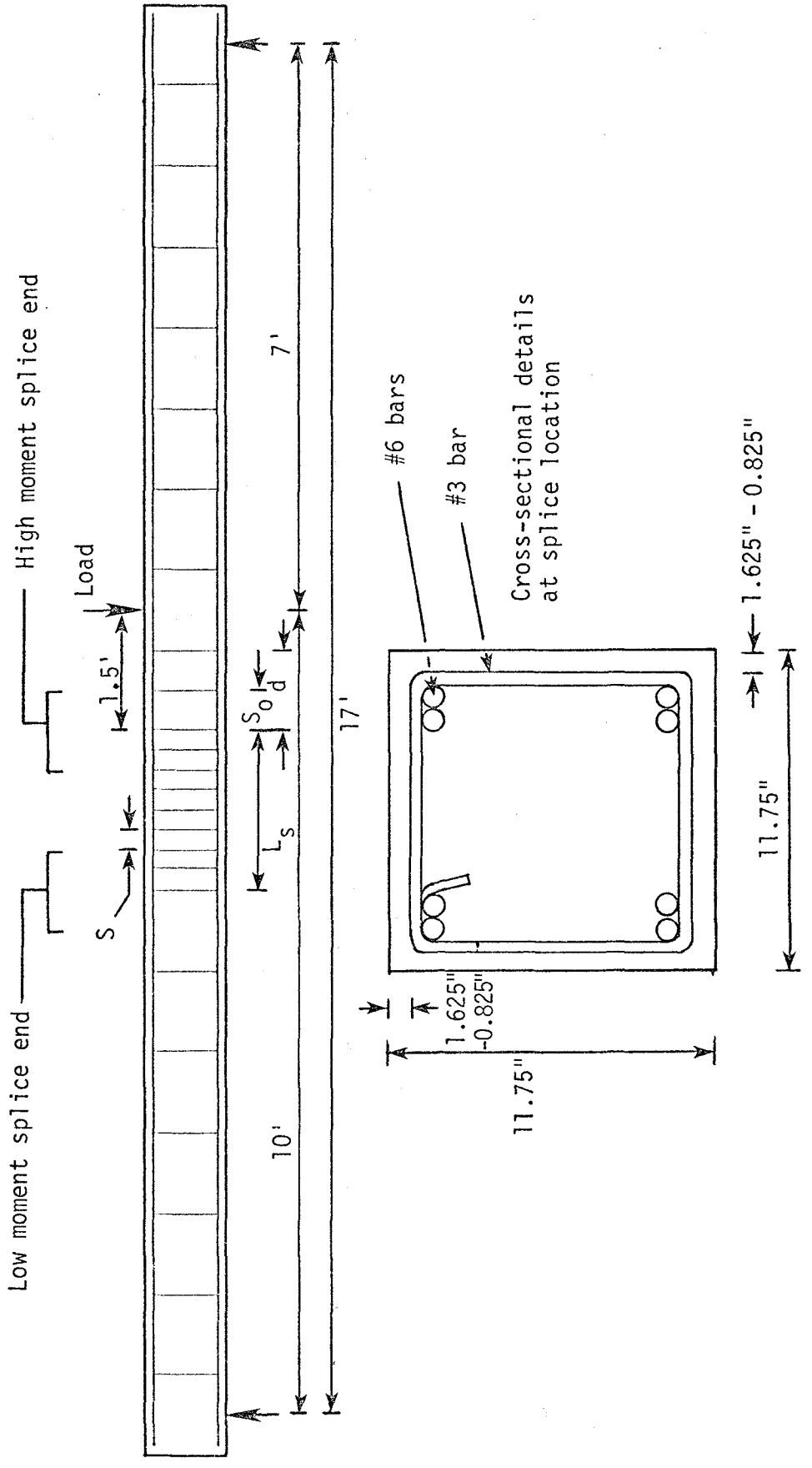

Fig. 3.4. Specimen details.

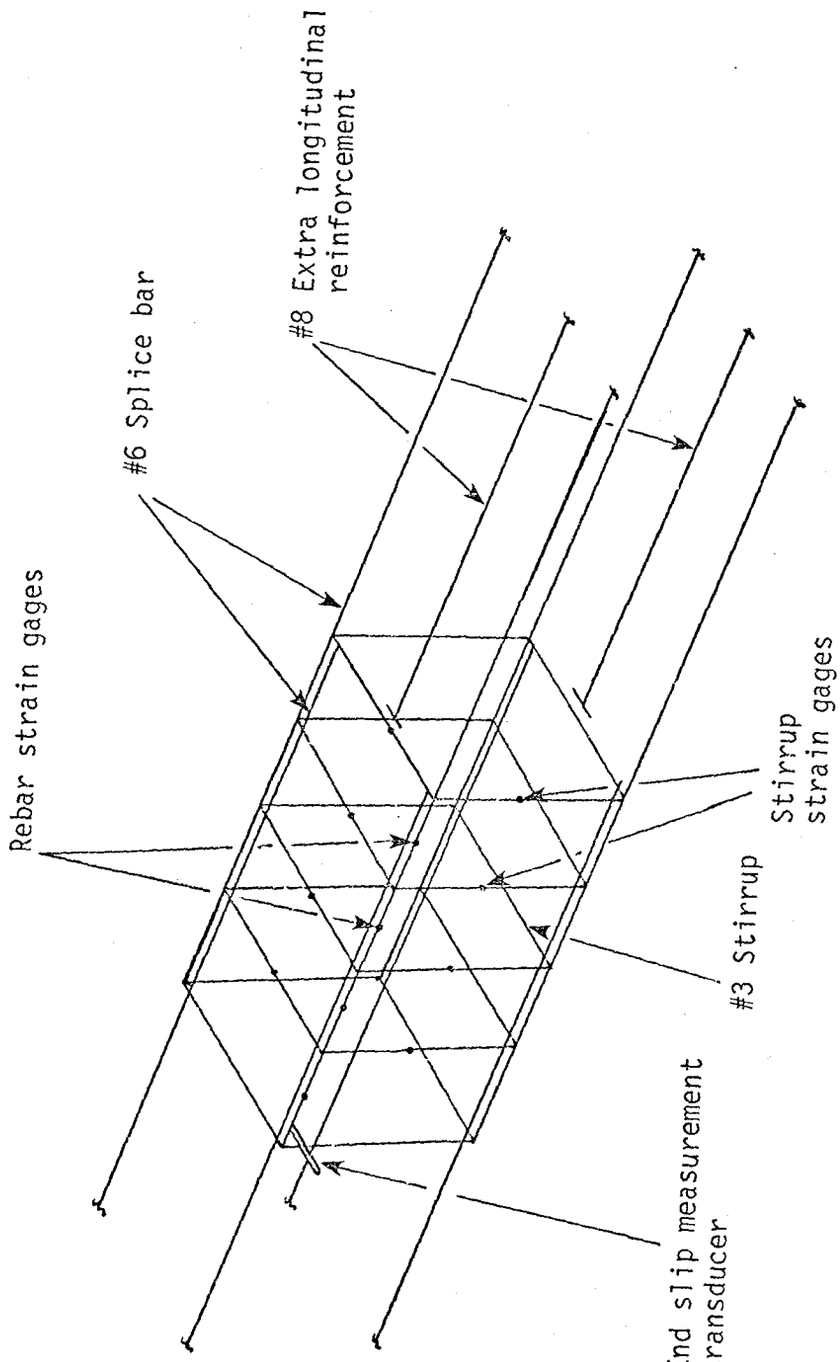

Fig. 3.5. Reinforcement cage layout.

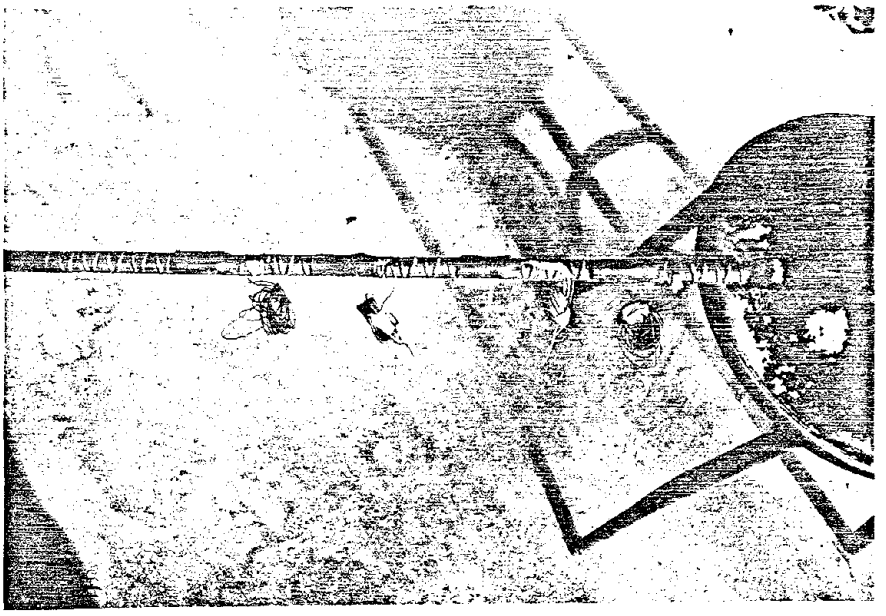

Fig. 3.6a. Strain gage locations on splice bar.

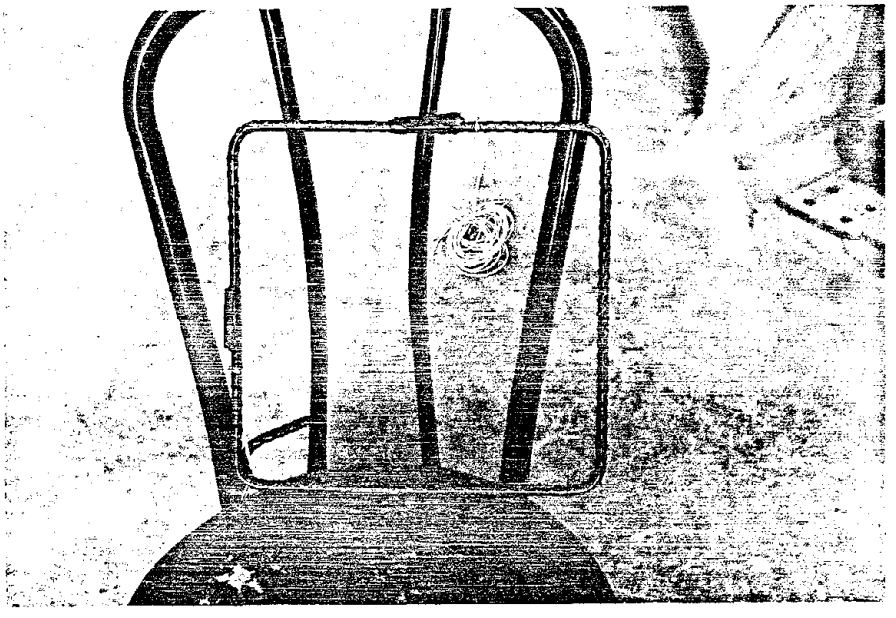

Fig. 3.6b. Strain gage locations on stirrup.

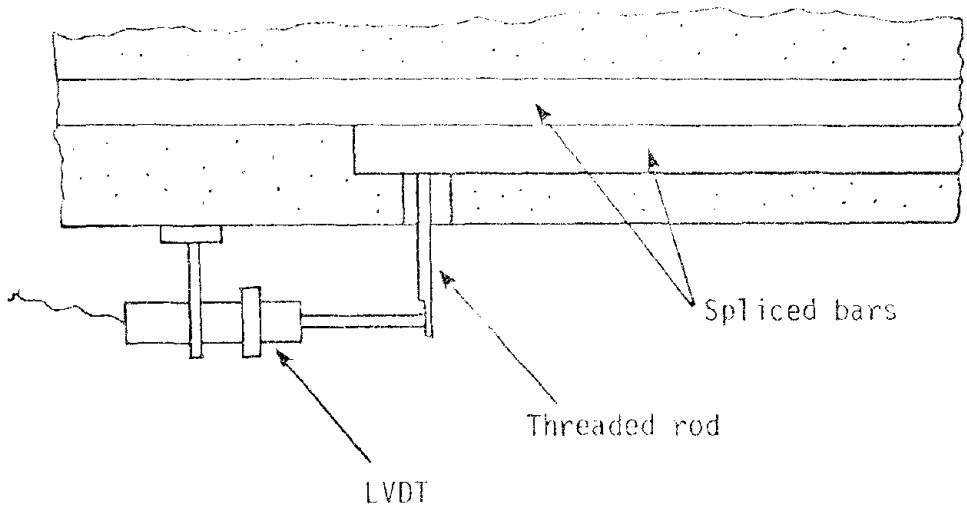

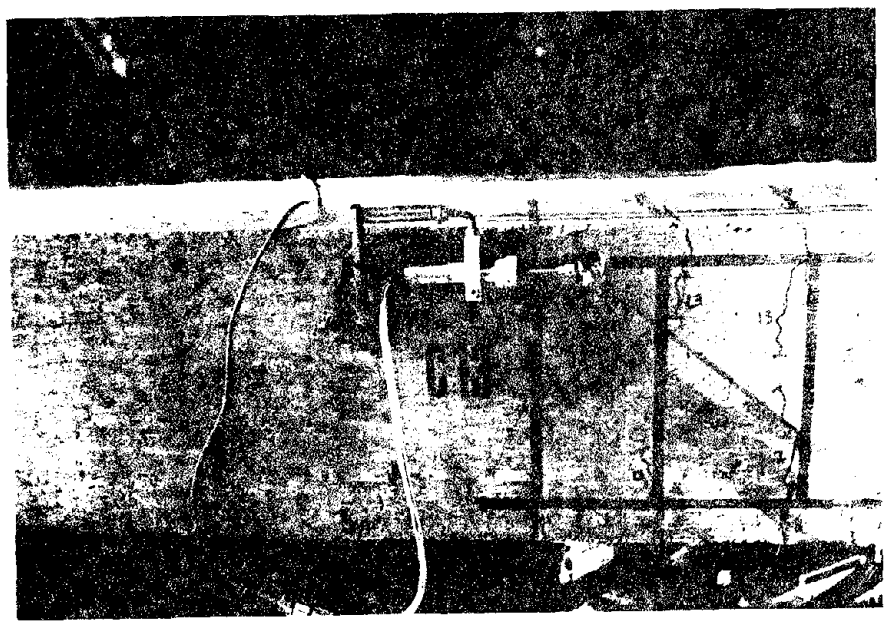

Fig. 3.7. Schematic view and photograph of bar end slip measurement transducer.

3.3 Steel Properties

Main and transverse reinforcement consisted of commercially available deformed bars conforming to ASTM A615. Main bars were of #6 size (0.75" dia.) and the stirrups were #3 (0.375" dia.). Stirrups consisted of closed tie hoops with a 135° cold bend and an extension of 10 bar diameters conforming to ACI 318-77 - Section A-2 (Fig. 3.4). Reinforcing steel properties are given in Table 3.3.

3.4 Concrete Properties

A concrete compressive strength of 3500-4000 psi was attained in most cases. Aggregates were delivered in a mixing truck and consisted of the following grading.

Aggregate	Description	Weight (Lbs/Cubic Yard of Concrete)
NY #1	Crushed Limestone Max. Size 3/4"	300
NY #2	Crushed Limestone Max. Size 1"	1680
Sand		1340

Type III - High Early Strength Portland Cement was used. 7 bags (of 94 lbs each) were needed for each cubic yard of concrete. The concrete was mixed on site prior to casting and a working slump of 3" was usually attained.

3.5 Casting and Curing

The specimens were cast horizontally in reusable 3/4" plywood forms (Fig. 3.8). The mix was placed in 2 or more layers with an overhead bucket and carefully compacted by means of an electric vibrator. Special care was taken while vibrating at the splice region so as not to

Bar Size	Deformation Pattern	Average Rib Spacing S' inch	Tension test results					
			1			2		
			f_y ksi	f_{ult} ksi	% Elong.	f_y ksi	f_{ult} ksi	% Elong.
Main Reinforcement #6	Bamboo Type	0.45	63	104	10.1	65	105	10.5
Transverse Reinforcement #3	V Type	0.20	66	110	11.2	69	108	12.1

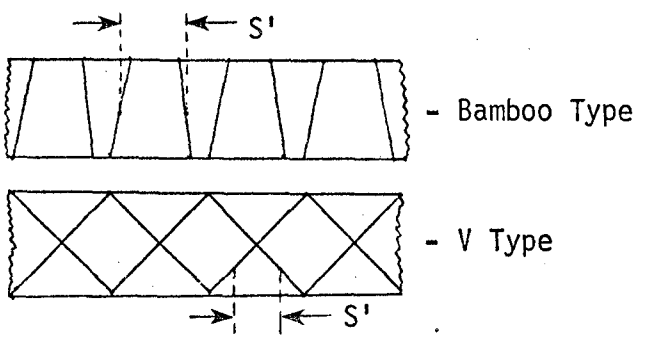

Table 3.3. Reinforcing steel properties.

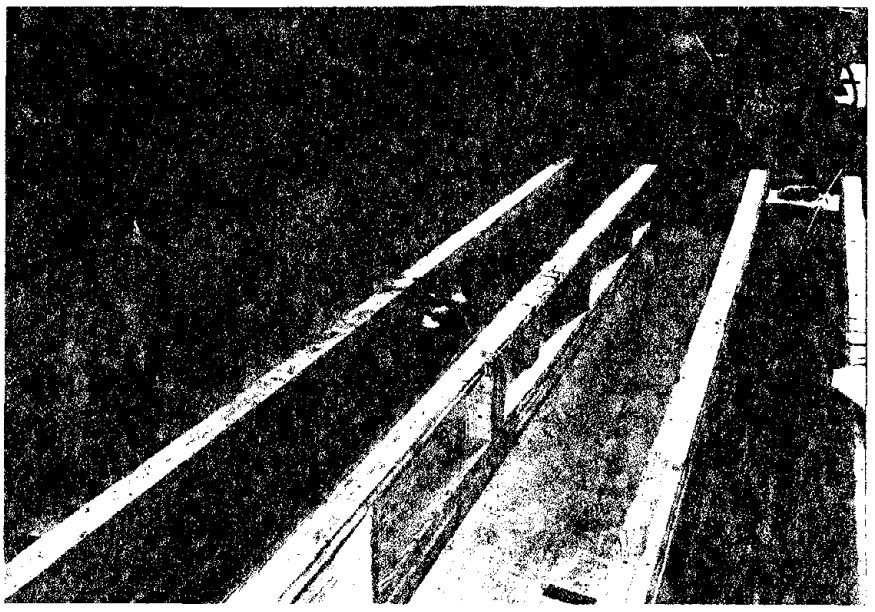

Fig. 3.8. Formwork with specimens prior to casting.

damage the strain gages. Five to six 6"ϕ x 12" concrete cylinders were prepared with each casting operation. The specimens and cylinders were covered with wet burlap and a sheet of plastic a few hours after casting. They were kept moist for approximately 2 weeks. The concrete cylinders were then tested in direct compression to determine their strength.

3.6 Testing Procedure

Displacements were applied in three to four stages up to the point where the spliced bars first attained yield. Each specimen was subjected to an average of twelve reversed cycles at every displacement level. Cracking patterns were observed and marked during the cycling process. Additional cycling was performed at any displacement level if the rate of deterioration was observed to continue during the twelfth cycle. Recordings of load and displacement at the actuator location, bar end slip, and bar strains were made during the first and last cycles of each level. The load-displacement relationship was continuously monitored on the plotting equipment. Displacements were progressively raised above the yield level and the same recording procedure was adopted until the specimen finally failed in some mode. The time period per cycle was always at least 2 minutes, and it was felt that this did not lead to any noticeable dynamic effect.

In order to evaluate the adequacy of the various specimens, an acceptance criteria was developed according to which any specimen was considered satisfactory if it:

1) Sustained 20-40 fully reversed cycles above yield
2) Attained a maximum displacement ductility of at least 1.8
3) Attained a maximum strain ductility of at least 2.5.

3.7 Test Details

3.7.1 Introduction

The following section describes each test in greater detail. The first specimen, C-1 was accidentally overloaded to failure during an early stage of the test and consequently, no useful data could be obtained from it. The test descriptions begin with specimen C-2. Specimens C-2, C-3, and C-4 were designed using Eq. 2.4 proposed by Fagundo (1979), and had progressively larger splice lengths of $30d_b$, $40d_b$, and $50d_b$ respectively. Tests C-5 through C-14 had splice lengths of $30d_b$ and $40d_b$. Stirrup spacings were based on Eq. 2.6 (Tocci - 1981).

Splices lapped in the vertical plane can behave differently from those lapped horizontally for the following reasons.

1) A superposition of large bond forces, shear forces, and splice bar dowel forces can result in high stresses on the vertical legs of the confining ties, possibly resulting in premature failure.
2) The average effective depth 'd' of vertically spliced sections is slightly less than that of corresponding horizontally lapped sections, bringing about bar yield at a lower loads.
3) In splices lapped vertically, the bars in combination have a greater bending resistance than when lapped side by side. This can lead to large contact stresses at the steel-concrete interface and deterioration of concrete cover.

Tests C-8, C-10, C-12, and C-14 were tested with vertically lapped bars to determine the actual influence of the above factors. Their results were compared with control specimens C-7, C-9, C-11, and C-13, respectively.

Test results include plots of load-displacement hysteresis curves, splice bar and stirrup strain variations, bar end slip plots where applicable, and also a brief summary of test observations. For clarity, only selected cycles have been shown in the plots. In all tests, the indicated maximum splice bar strains represent the highest recorded values. In several specimens, inelastic cycling led to strain gage failure before specimen failure. In these cases, true maximum bar strains were actually higher than those shown in the tabulations.

3.7.2 Test C-2

Jack Displacement		No. of Cycles	Cycles Plotted
Inches	Δ/Δ_y		
0.50	0.38	10	-
0.80	0.61	21	first
1.00	0.77	11	first
1.30	1.00	22	-
1.60	1.23	17	first
1.85	1.42	12	first
2.15	1.65	12	-
2.50	1.92	1	first

K_b = 2935
S = 3.0 in. c/c.
S_o = 10.0 in. c/c.
L_s = 24 in. (30 d_b)
C = 2.0 in. (2.66 d_b)
f_y = 60 ksi
f'_c = 3.9 ksi
N = 106
N_y = 42
$(\Delta/\Delta_y)_{max}$ = 1.92
$(\varepsilon/\varepsilon_y)_{max}$ = 2.65
$(\varepsilon_{st}/\varepsilon_y)_{max}$ = 0.66 (Vert. Leg)
Splice Plane: Horizontal

Observations

Specimens C-1 and C-2 were identical and designed based on Eq. 2.4. While testing C-2, flexural cracks appeared at the stirrup locations over the splice during an early part of the test. The growth of these cracks stabilized at a displacement level of 1.00 inch. A transverse flexural crack formed at the high moment splice end and continued cycling led to the progressive widening of this crack. It gradually propagated

towards the concrete core due to the shear force effect. The portion of the splice bars at the high moment end yielded at Δ = 1.3 inch. A flexural crack was observed at the low moment splice end, but did not progressively deteriorate.

The extent of longitudinal splitting of concrete cover over the splice was negligible. Cycling at higher displacement levels led to the spalling of cover at the primary crack located at the high moment end. Much of this localized deterioration was due to the reversing shear stresses and bar dowel forces. Most of the concrete cover at this section was lost subsequently. The spliced bars, having lost practically all confinement at this location, had little resistance to buckling, and consequently experienced large lateral displacements when under compression. This created a high level tension-compression type loading on the bars during the following cycles and finally resulted in failure by bar fracture.

The lack of any significant cover splitting over the splice suggested that C-2 was overconservatively designed.

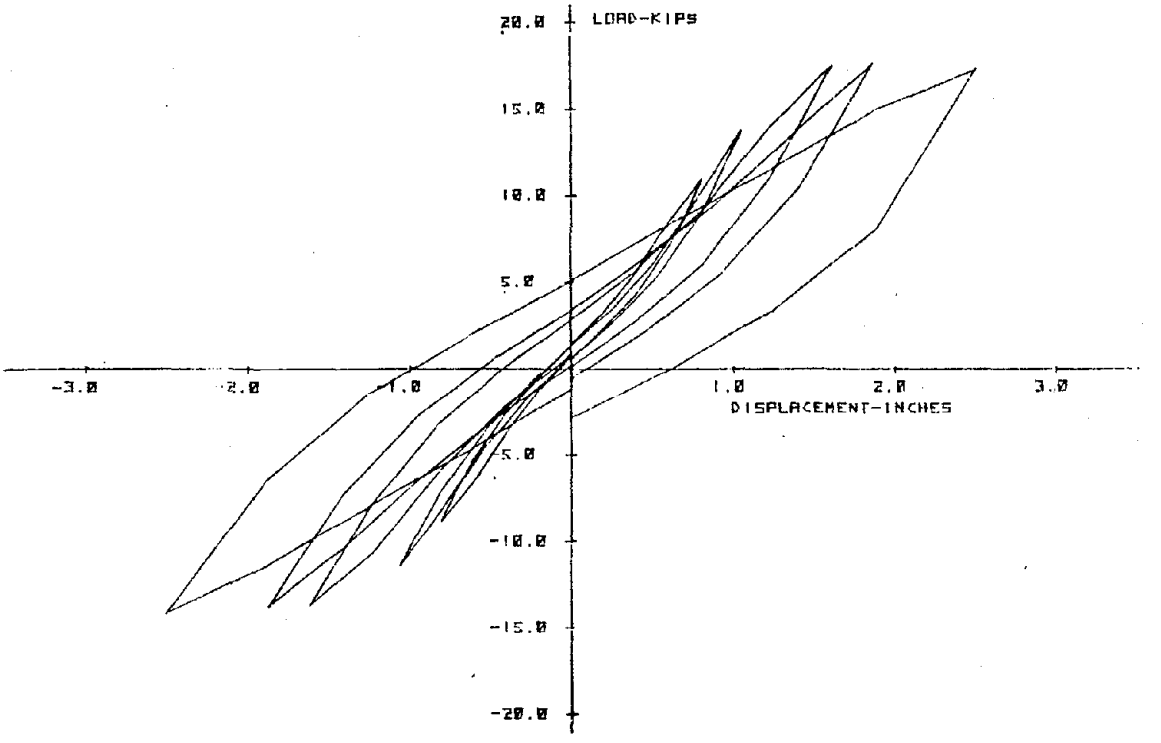

Fig. 3.9a. Load-displacement relationship - Specimen C-2.

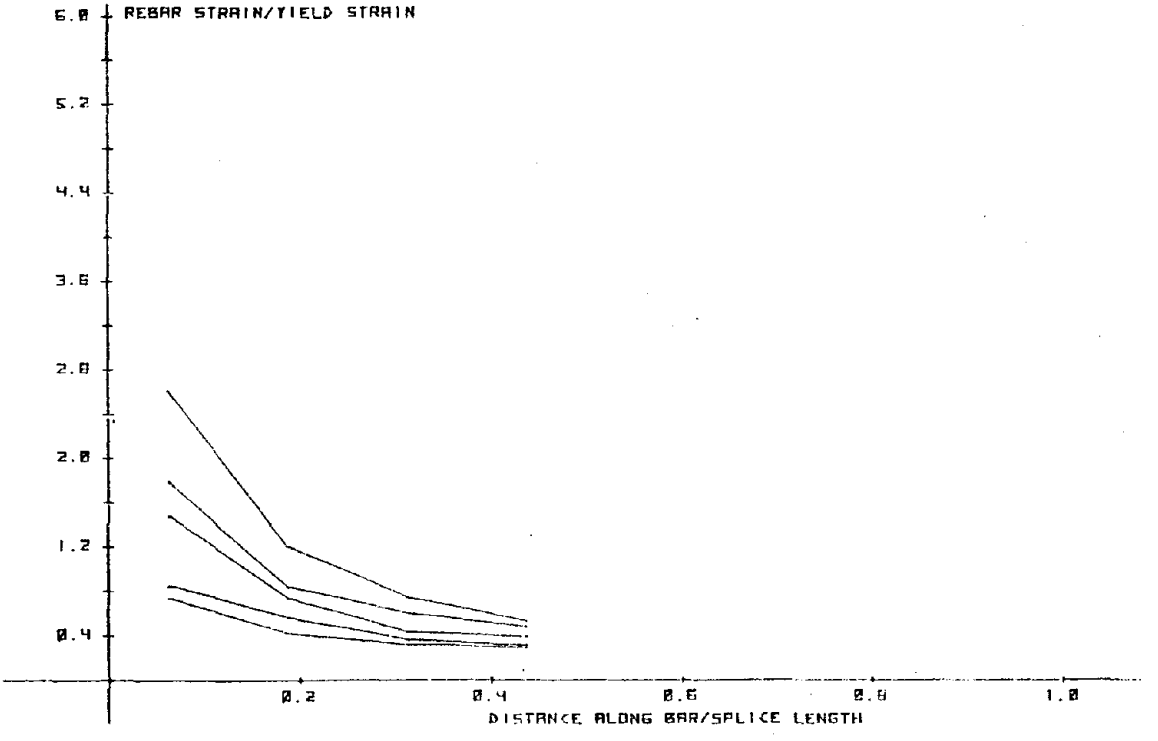

Fig. 3.9b. Main reinforcement strains - Specimen C-2.

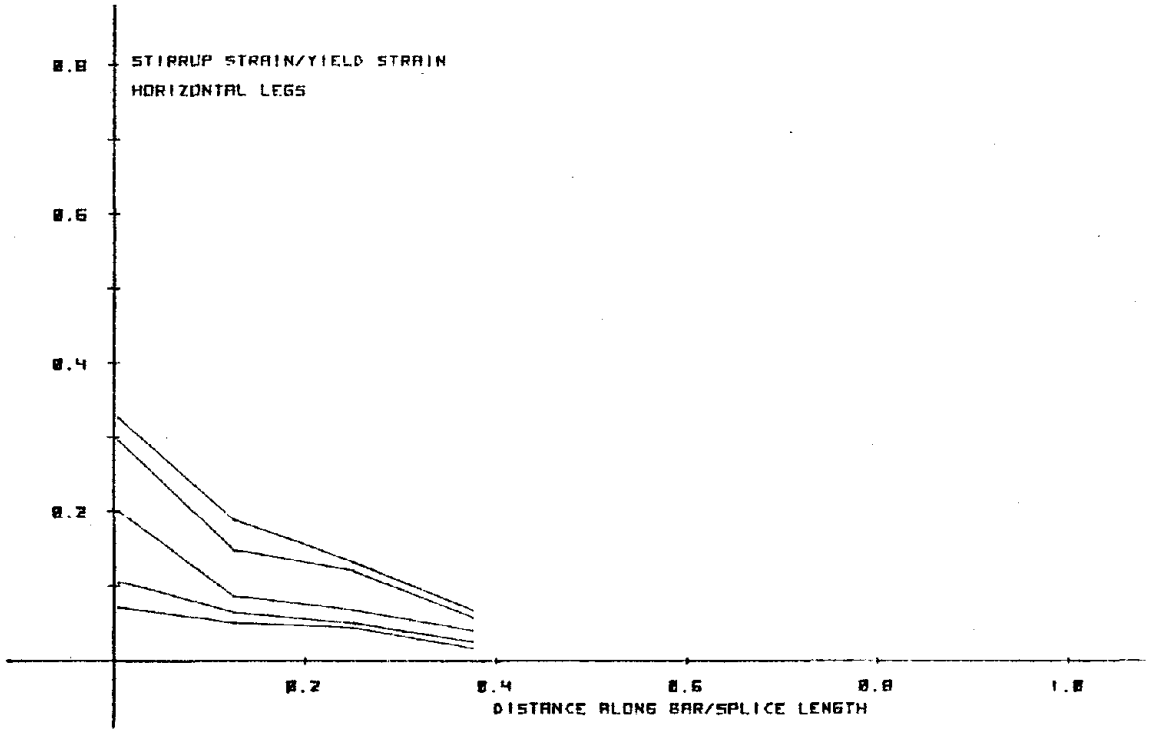

Fig. 3.9c. Stirrup strains - Specimen C-2.

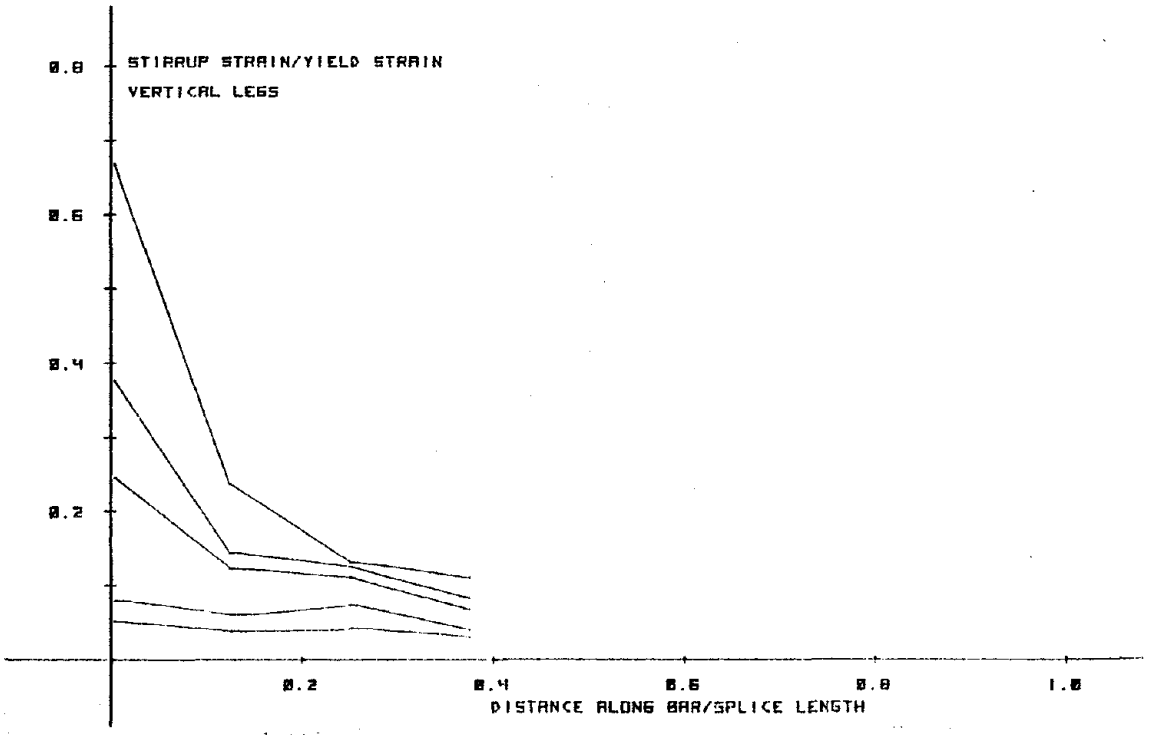

Fig. 3.9d. Stirrup strains - Specimen C-2.

3.7.3 Test C-3

Jack Displacement		No. of Cycles	Cycles Plotted
Inches	Δ/Δ_y		
0.40	0.33	12	last
0.60	0.48	12	-
0.76	0.64	17	first
0.95	0.80	11	-
1.20	1.00	12	first
1.45	1.20	12	first
1.75	1.45	12	-
2.00	1.66	13	first
2.50	2.11	13	first

K_b = 2200
S = 4.00 in. c/c.
S_o = 10.00 in. c/c.
L_s = 30 in. (40 d_b)
C = 2.0 in. (2.66 d_b)
f_y = 60 ksi
f'_c = 3.4 ksi
N = 114
N_y = 61
$(\Delta/\Delta_y)_{max}$ = 2.02
$(\varepsilon/\varepsilon_y)_{max}$ = 2.81
$(\varepsilon_{st}/\varepsilon_y)_{max}$ = 0.62 (Vert. Leg)
Splice Plane: Horizontal

Observations

C-3 was also designed according to Eq. 2.4. It was evident after cycling at the first few displacement levels that most of the damage was again at the transverse crack located just outside the splice high moment end. Flexural cracking developed to a lesser extent over the splice and was usually over the stirrup positions. The splice rebar first yielded at the high moment end at 1.20" displacement. Cycling at higher levels caused further deterioration at the flexural shear crack. A yield penetration of 0.2 ℓ_s into the splice was attained at a displacement level of 2 inches. Stirrups leg strains were all well below the yield value. The highest recorded strain was 0.62 ε_y, on the vertical leg of the first stirrup. Cover splitting to a very limited extent was observed at Δ = 2.00", but did not proceed much beyond the first stirrup position. The splice was practically undamaged beyond this point. The number of load and displacement recordings taken

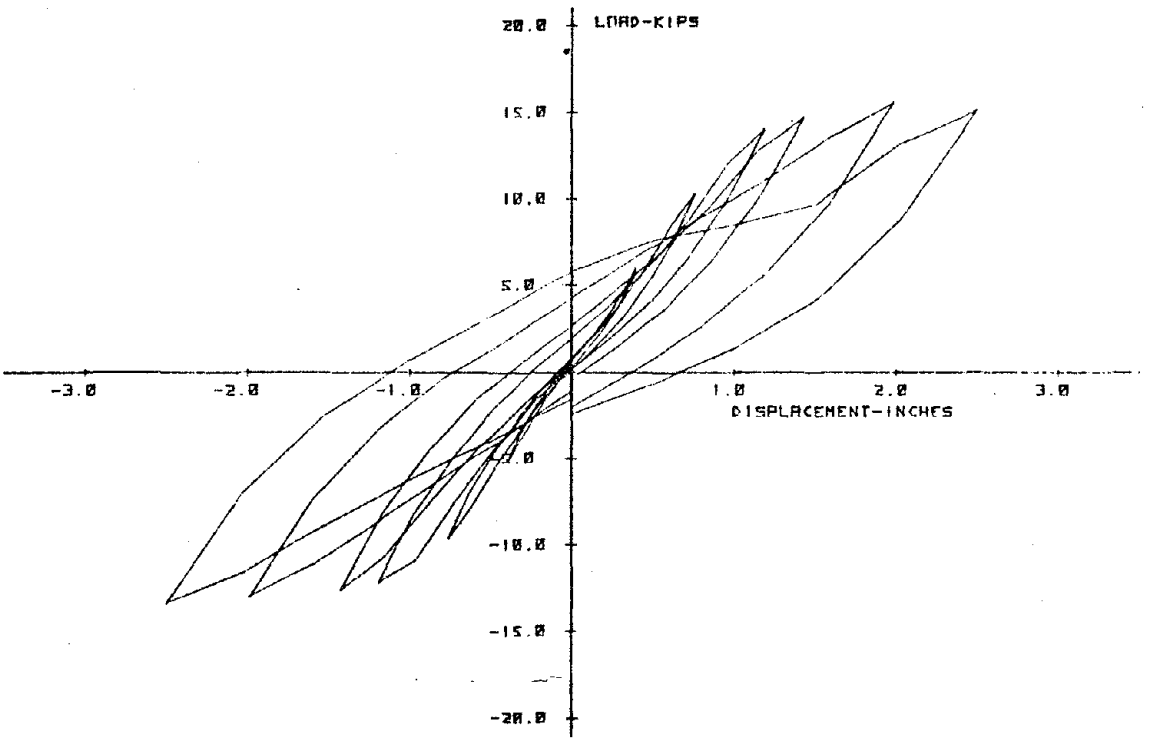

Fig. 3.10a. Load-displacement relationship - Specimen C-3.

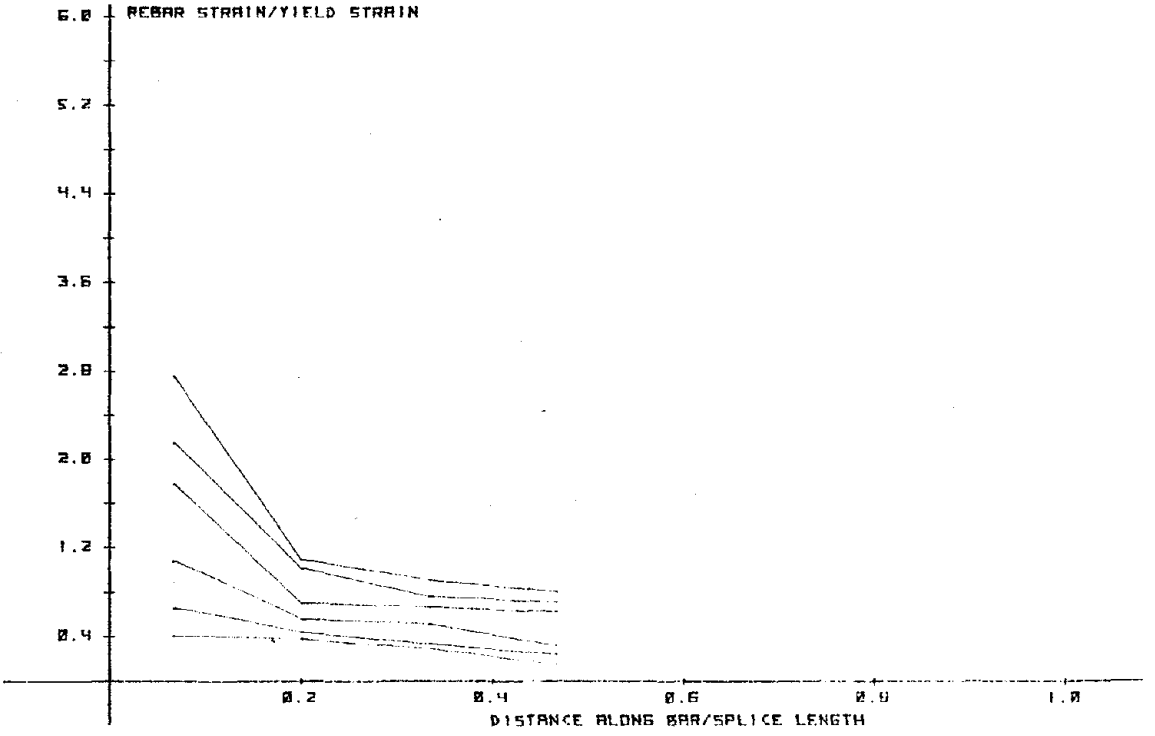

Fig. 3.10b. Main reinforcement strains - Specimen C-3.

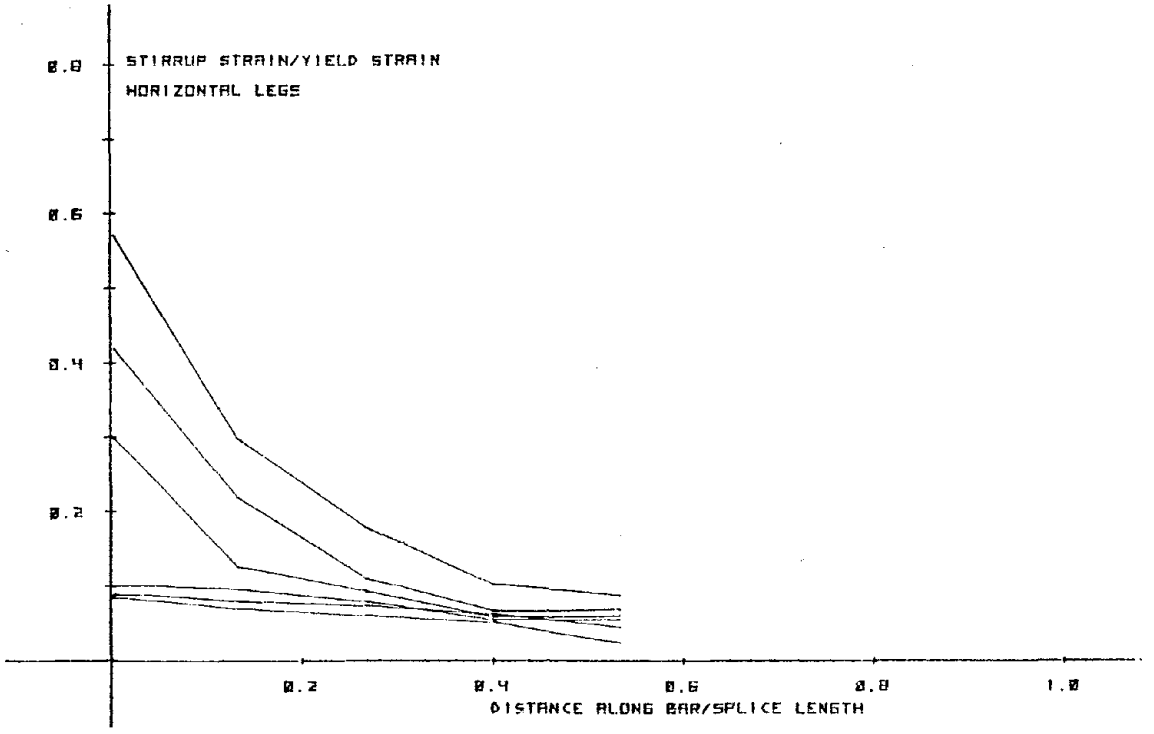

Fig. 3.10c. Stirrup strains - Specimen C-3.

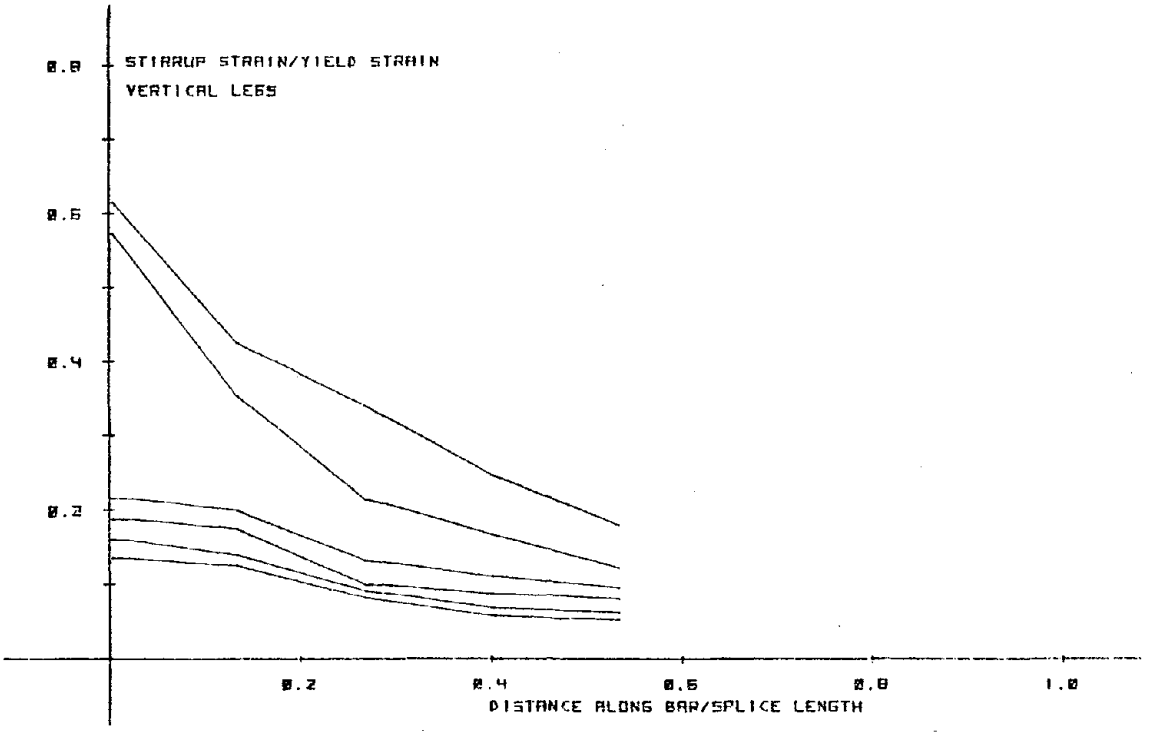

Fig. 3.10d. Stirrup strains - Specimen C-3.

were insufficient to obtain accurate load displacement curves. Failure finally occurred by bar fracture, as in C-2. Specimen C-3 was also regarded as an overconservative splice design.

It is possible that if the damaged portion of the specimen had been better reinforced, a greater extent of splice deterioration would have occurred. However, the possibility of a splice-bond failure was considered very unlikely.

3.7.4 Test C-4

Jack Displacement		No. of Cycles	Cycles Plotted
Inches	$\Delta/\Delta y$		
0.40	0.33	11	-
0.60	0.50	17	first
0.75	0.63	11	-
0.95	0.80	11	-
1.20	1.00	11	first
1.45	1.20	12	first
1.75	1.45	11	first
2.00	1.66	11	-
2.25	1.88	4	-
2.50	2.11	11	first
2.75	2.30	13	first

K_b = 1855
S = 4.75 in. c/c.
S_o = 10.0 in. c/c.
L_s = 38 in. (50 d_b)
C = 2.0 in. (2.66 d_b)
f_y = 60 ksi
f'_c = 3.4 ksi
N = 123
N_y = 50
$(\Delta/\Delta_y)_{max}$ = 2.02
$(\varepsilon/\varepsilon_y)_{max}$ = 2.50*
$(\varepsilon_{st}/\varepsilon_y)_{max}$ = 0.57 (Vert. Leg)
Splice Plane: Horizontal

*Max recorded value, actual value higher.

Observations

The splice design adopted was once again based on Eq. 2.4. Most transverse flexural cracks within the splice occurred during the first 30-40 cycles and were located over stirrup locations, as in Specimens C-1 through C-3. Rebar yield was first observed at the high moment

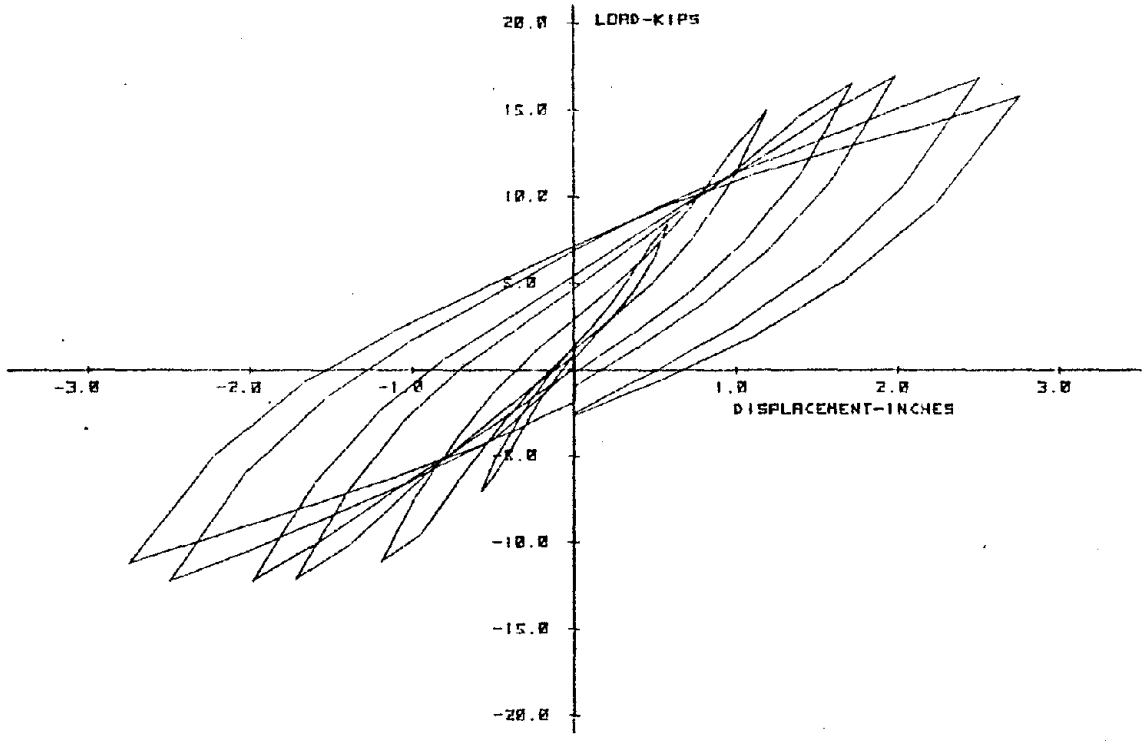

Fig. 3.11a. Load-displacement relationship - Specimen C-4.

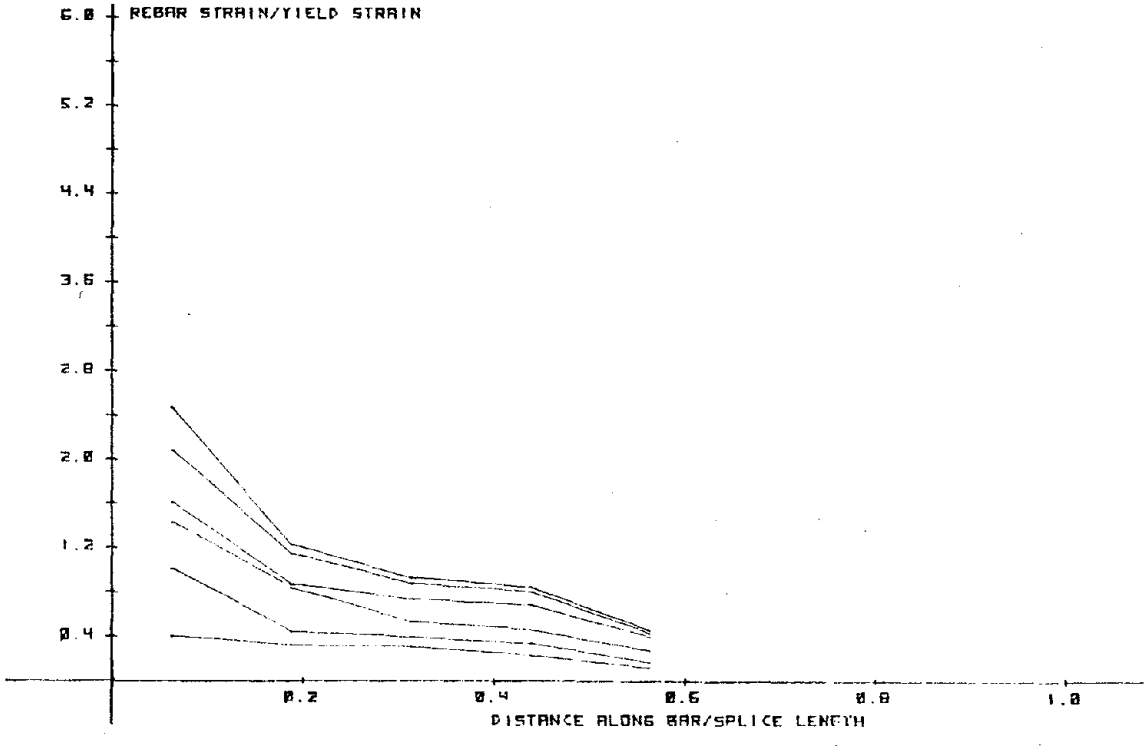

Fig. 3.11b. Main reinforcement strains - Specimen C-4 .

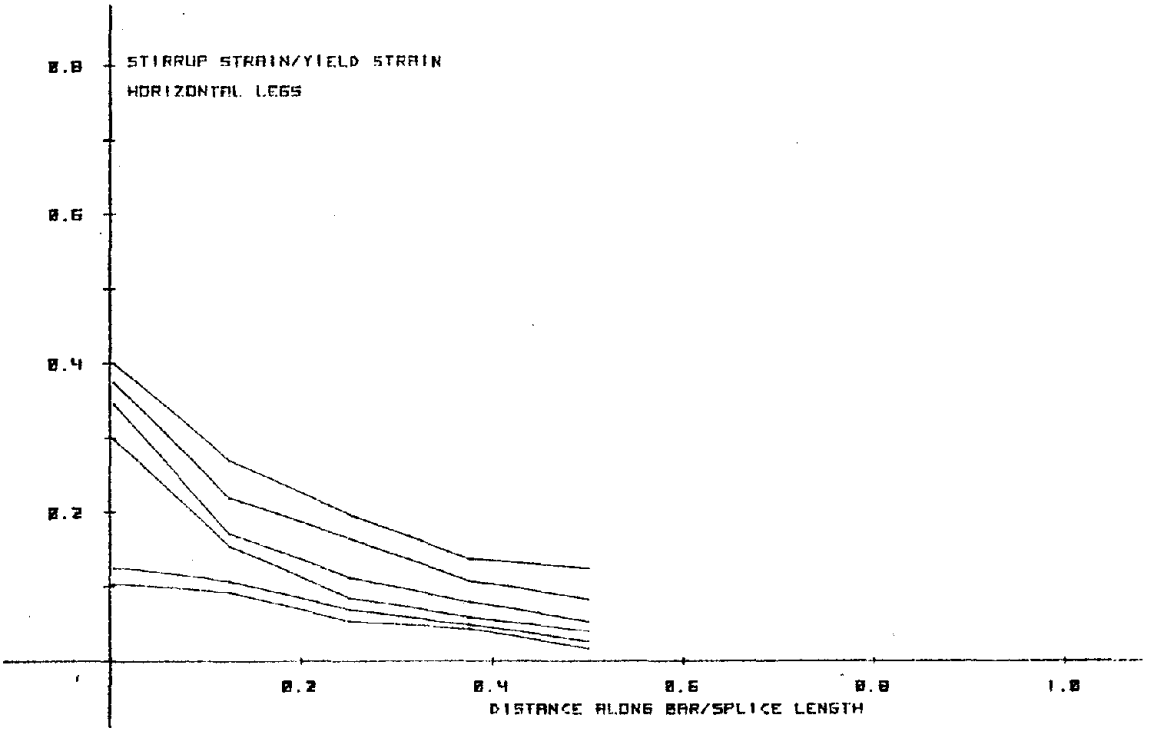

Fig. 3.11c. Stirrup strains - Specimen C-4.

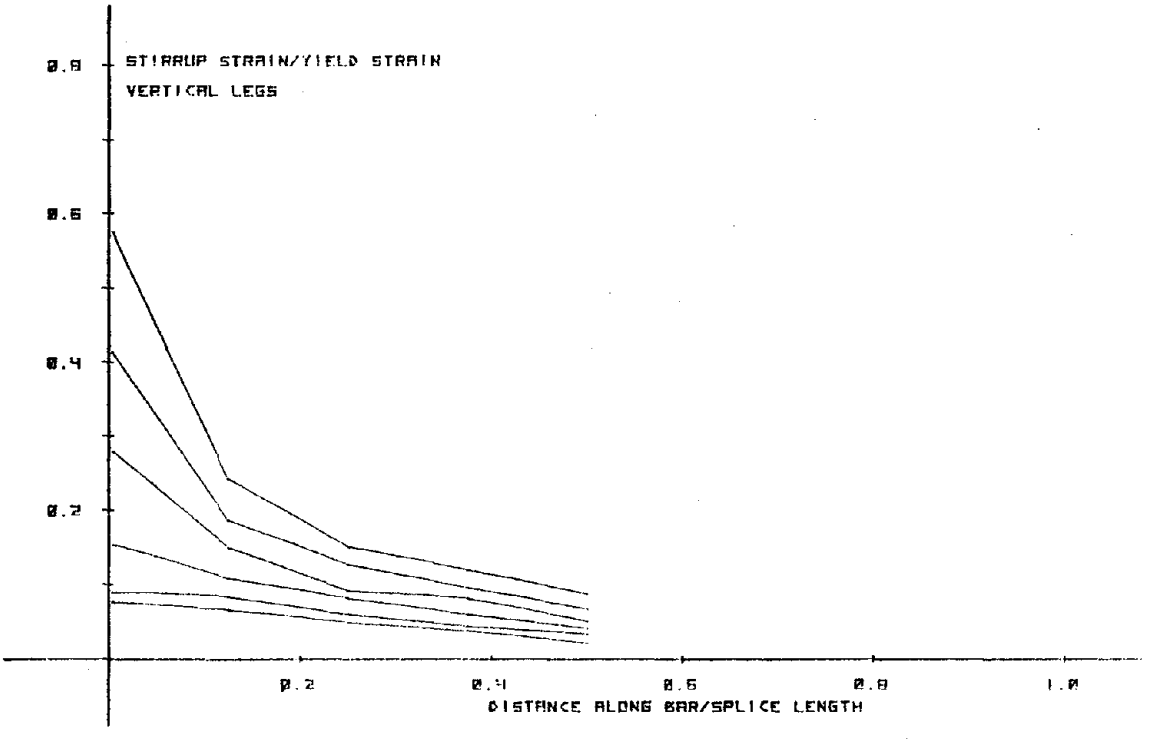

Fig. 3.11d. Stirrup strains - Specimen C-4.

splice end at Δ = 1.2 inches. As in the previous two tests, a flexural crack formed at the high moment end at an early stage and grew wider with subsequent cycling. Concrete cracking propagated towards the core from the top and bottom faces at this section. A localized cover spalling began at Δ = 1.75 in. and, as seen from the P - Δ curves, this was also the stage where load peaks began to level off. Differential movement between the sides of the crack resulted in rebar dowel forces which further damaged cover. An appreciable load shedding tendency was observed at Δ = 2.0 in., the same time as most of the bottom cover at the crack spalled off. With cycling at Δ = 2.5 inches and 2.75 inches, much of the interior core at the cracked section was also destroyed. As in Specimens C-2 and C-3, failure was by bar fracture. The total yield penetration into the splice was 0.19 ℓ_s. The extent of longitudinal cover splitting was insignificant, and as before, it was felt that the splice design was too conservative.

3.7.5 Test C-5

Jack Displacement		No. of Cycles	Cycles Plotted
Inches	$\Delta/\Delta y$		
0.75	0.63	12	first
1.00	0.84	12	-
1.50	1.25	13	first
1.75	1.46	12	last
2.00	1.67	17	last
2.25	1.88	13	first

*Max recorded value, actual value higher.

K_b = 1760
S = 5.0 in. c/c.
S_o = 5.0 in. c/c.
L_s = 24 in. (30 d_b)
C = 2.0 in. (2.66 d_b)
f_y = 60 ksi
f'_c = 2.91 ksi
N = 79
N_y = 29
$(\Delta/\Delta_y)_{max}$ = 1.67
$(\varepsilon/\varepsilon_y)_{max}$ = 2.61*
$(\varepsilon_{st}/\varepsilon_y)_{max}$ = 0.38 (Vert. Leg)
Splice Plane: Horizontal

Observations

Compared to the previous three specimens, C-5 was designed less conservatively using the equation proposed by Tocci (Eq. 2.6). In this specimen, the stirrup spacing, S over the splice was continued up to a distance 'd' outside both ends of the splice. It was observed that this reinforcement was effective in restraining the growth of the end transverse crack. Longitudinal cover splitting was seen on the top and bottom faces at Δ = 1.00". The top splitting did not penetrate along the splice to the same extent as at the bottom. Rebar strains were well into yield at 1.52" displacement. Bottom side splitting occurred at this level. Yield penetration into the splice was about 0.25 ℓ_s at Δ = 1.76". The extent of cover splitting showed an increase at Δ = 2.00". An appreciable load shedding tendency was evident from the load displacement curves, particularly during the downward stroke of each cycle. Further cycling lead to the complete propagation of the bottom face crack, followed by that of the bottom side crack, which resulted in a failure mechanism. Compared to the previous tests, C-5 showed much less damage at the splice high moment end. This test was the first to follow a splice bond failure mode. However, based on the acceptance criteria, it could not be judged as a satisfactory design.

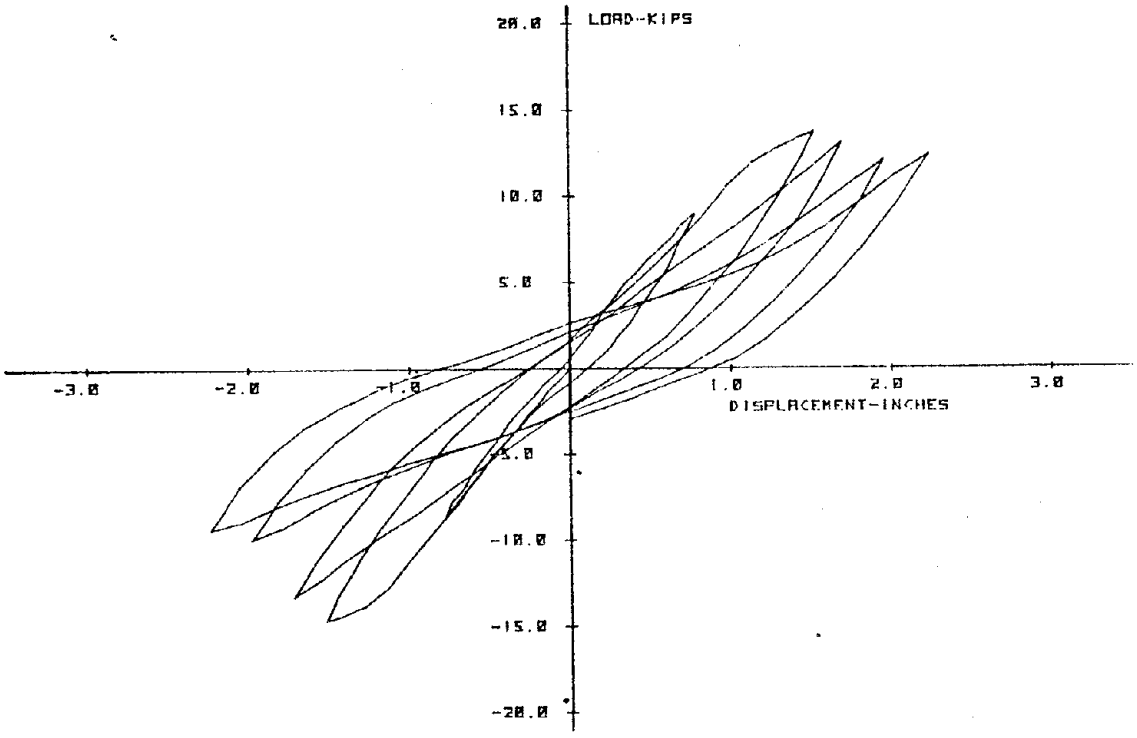

Fig. 3.12a. Load-displacement relationship - Specimen C-5.

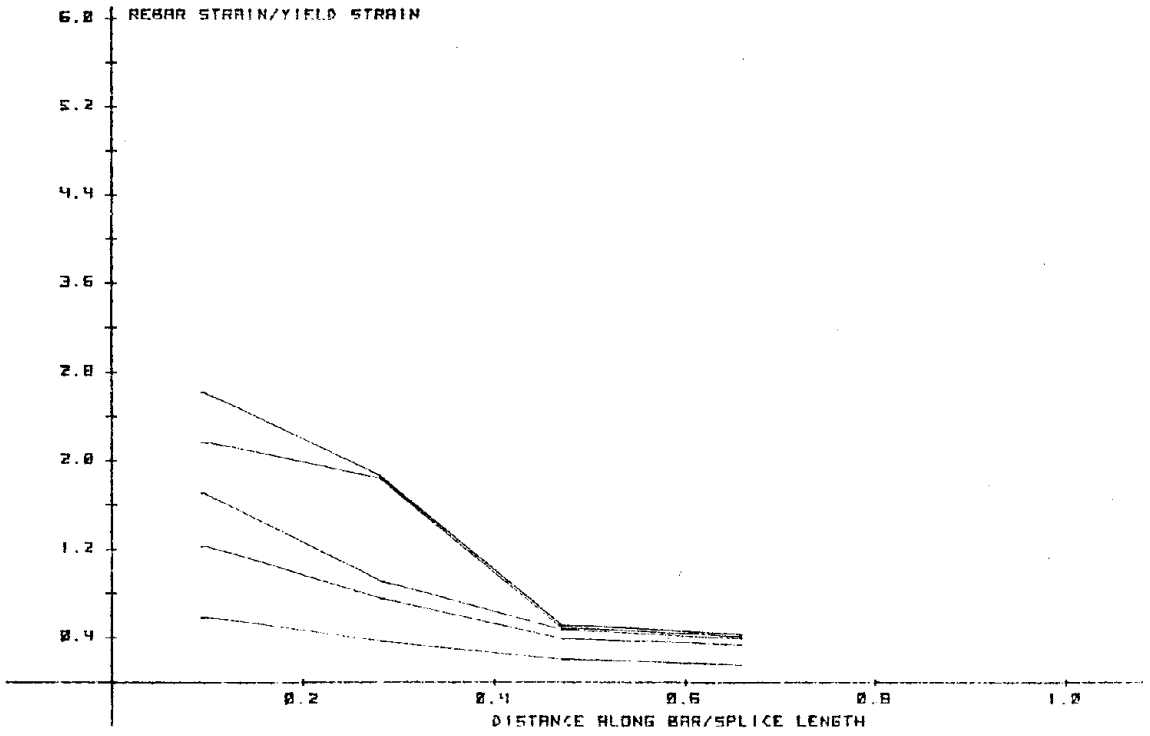

Fig. 3.12b. Main reinforcement strains - Specimen C-5.

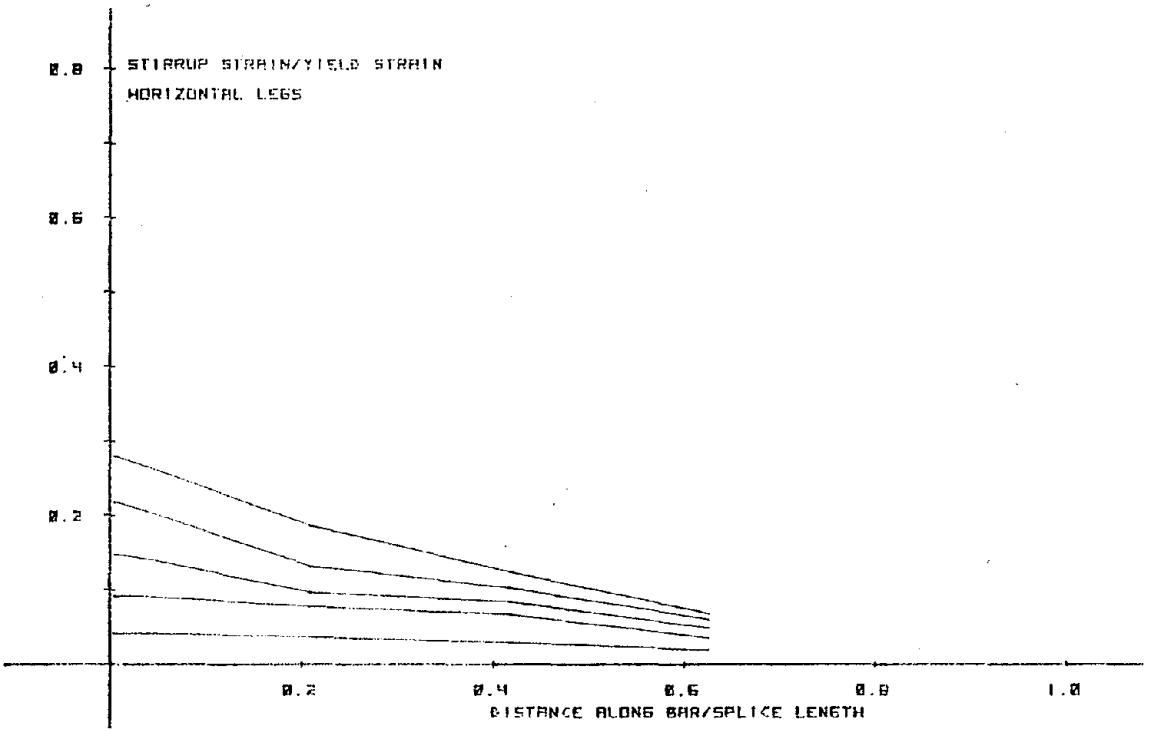

Fig. 3.12c. Stirrup strains - Specimen C-5.

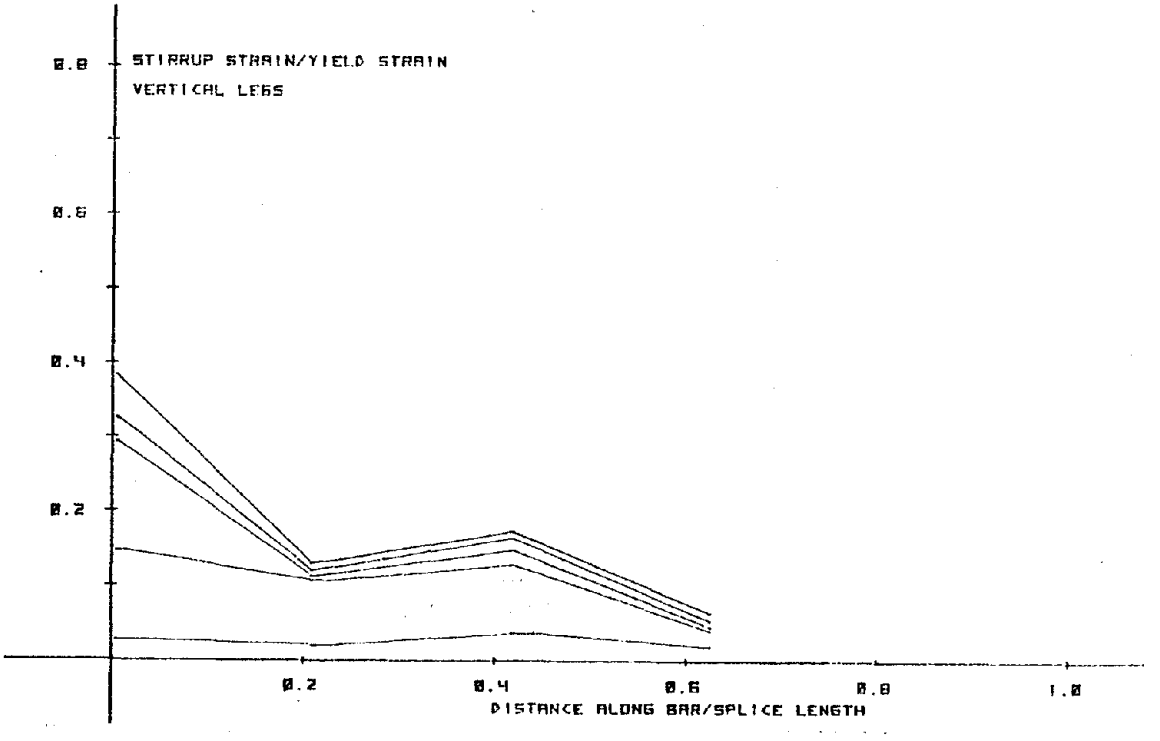

Fig. 3.12d. Stirrup strains - Specimen C-5.

3.7.6 Test C-6

Jack Displacement		No. of Cycles	Cycles Plotted
Inches	Δ/Δ_y		
0.75	0.63	12	first
1.00	0.84	12	-
1.50	1.25	13	first
1.75	1.46	12	last
2.00	1.67	12	last
2.25	1.88	5	first

*Max recorded value, actual value higher.

K_b = 1760
S = 5.0 in. c/c.
S_o = 5.0 in. c/c.
L_s = 24 in. (30 d_b)
C = 2.0 in. (2.66 d_b)
f_y = 60 ksi
f'_c = 2.91 ksi
N = 66
N_y = 24
$(\Delta/\Delta_y)_{max}$ = 1.67
$(\varepsilon/\varepsilon_y)_{max}$ = 2.52*
$(\varepsilon_{st}/\varepsilon_y)_{max}$ = 0.39 (Vert. Leg)
Splice Plane: Horizontal

Observations

C-5 and C-6 were identical specimens. The load history was selected to be the same as in C-5 in an effort to evaluate the repeatability and reliability of the results of C-5. Observations during the test indicated that although a flexural shear crack formed outside the splice high moment end, the extent of damage at that location was controlled by closely spaced stirrups (S_o = 5" c/c). Peak rebar strains were well into yield at Δ = 1.5 inches. As in C-5 the amount of cover splitting at the bottom half was more than that at the top half of the specimen. Load shedding became apparent first at Δ = 1.75 inches and appreciable at Δ = 2.00 inches. Failure in the downward stroke occurred at this displacement level. Although characterized by a splice-bond failure, the maximum ductility factor (Δ/Δ_y) was too low to be acceptable. The vertical leg strains were higher than in C-5. The important point, however, is that both the strain values were well below yield in these

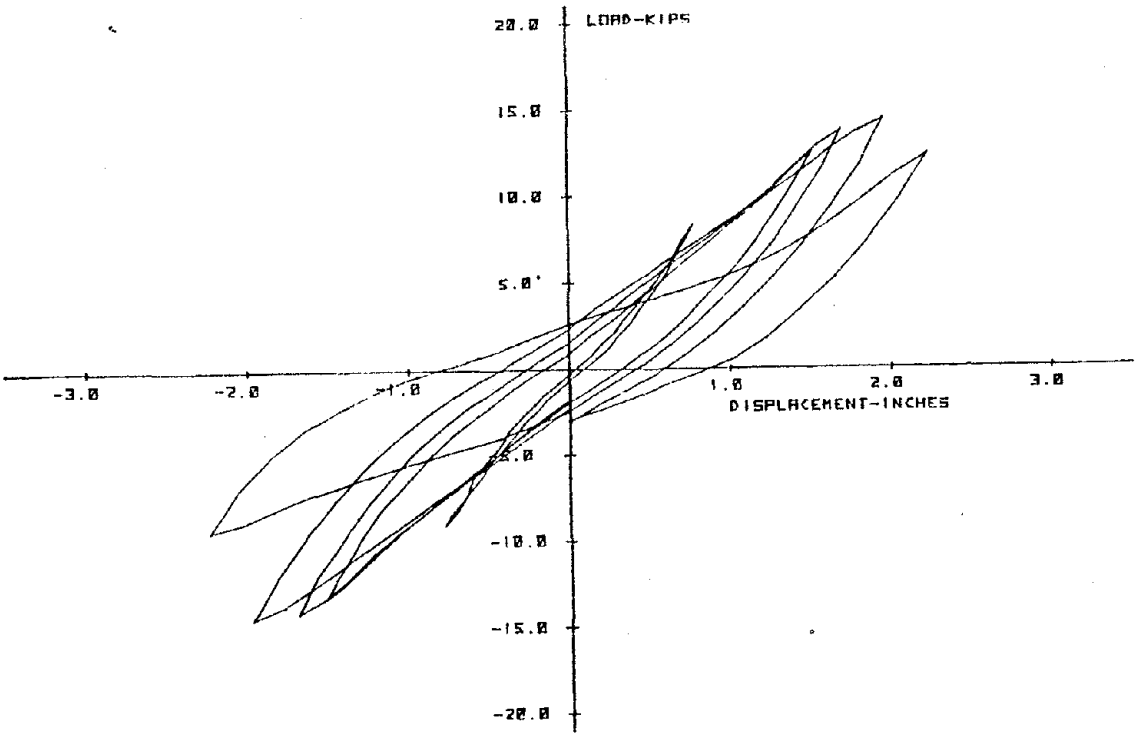

Fig. 3.13a. Load-displacement relationship - Specimen C-6.

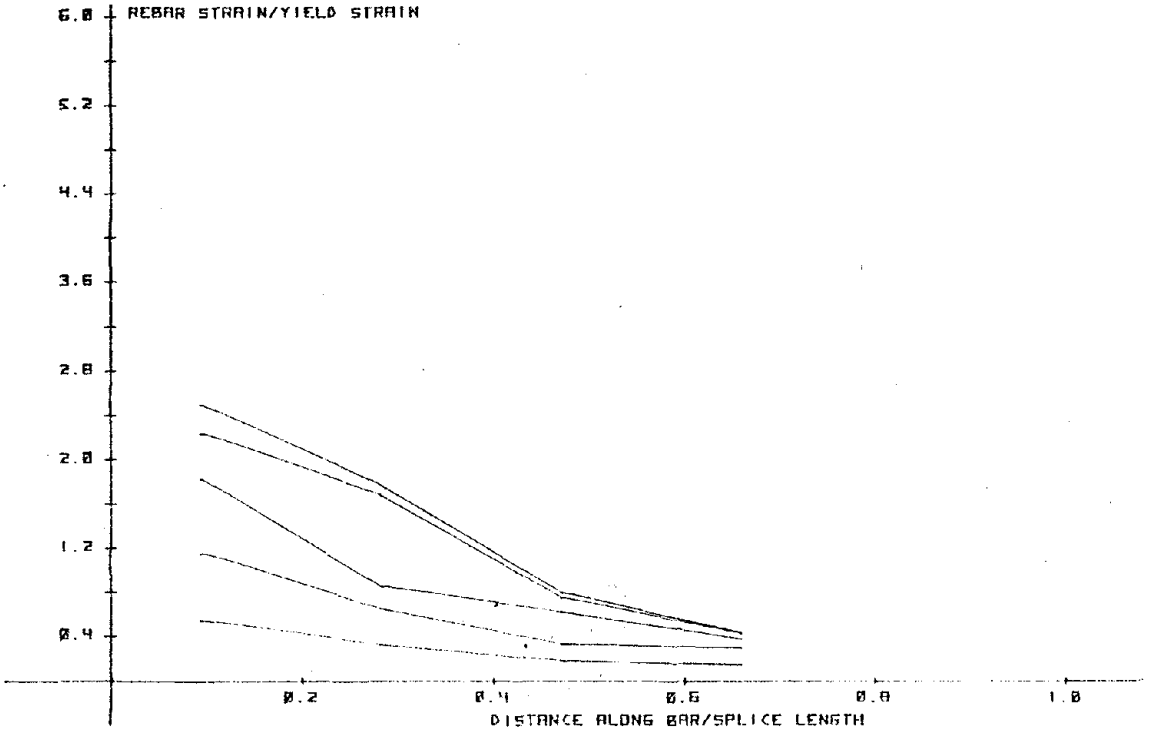

Fig. 3.13b. Main reinforcement strains - Specimen C-6.

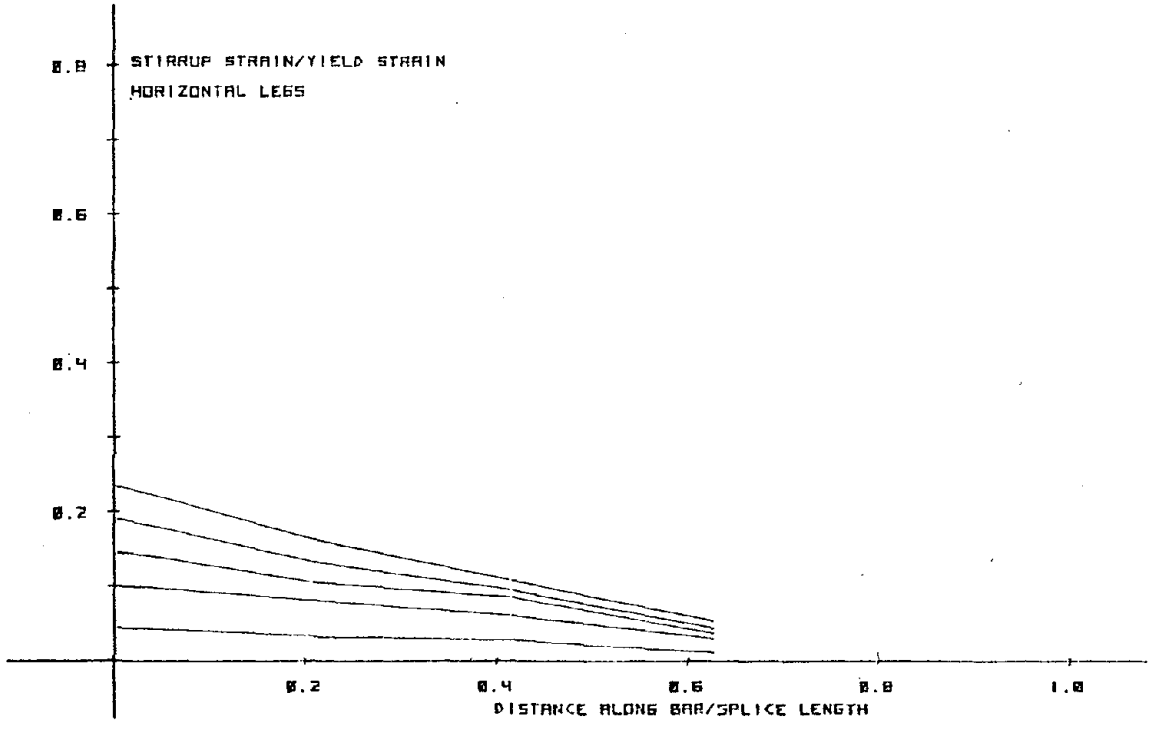

Fig. 3.13c. Stirrup strains - Specimen C-6.

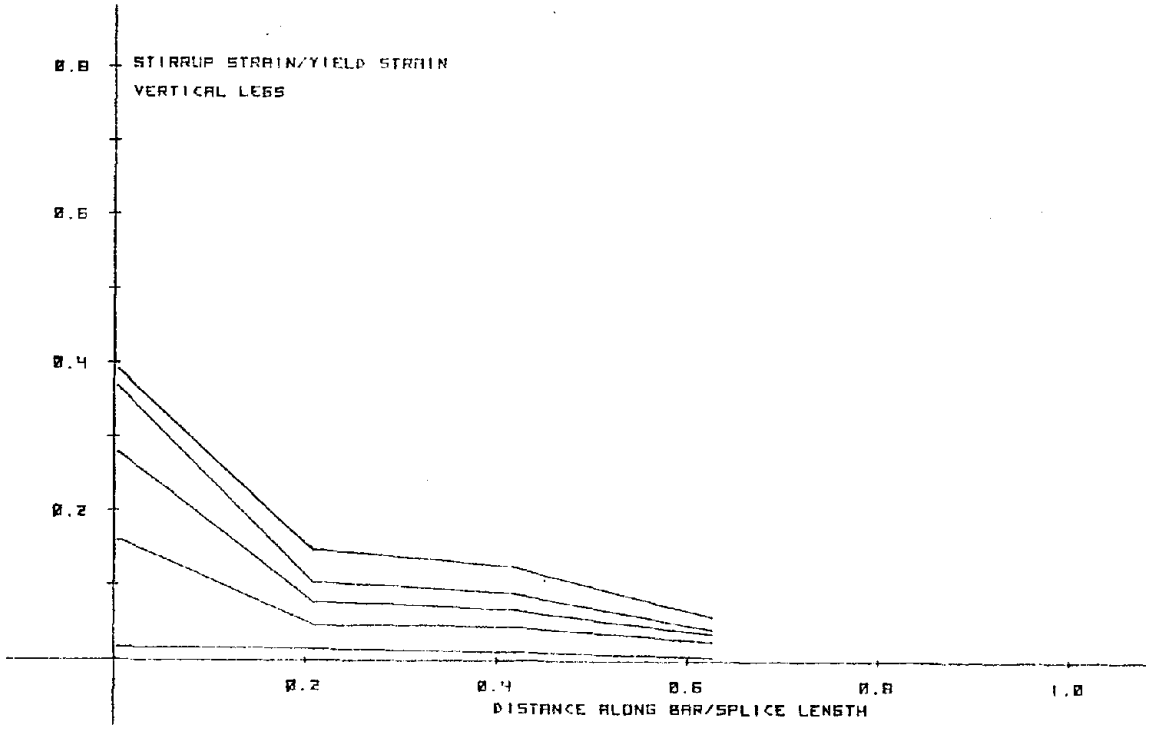

Fig. 3.13d. Stirrup strains - Specimen C-6.

two tests which failed by a cover-splitting mode. The overall performance of this test was similar to that of C-5.

3.7.7 Test C-7

Jack Displacement		No. of Cycles	Cycles Plotted
Inches	Δ/Δ_y		
0.5	0.33	12	last
0.75	0.50	12	-
1.00	0.66	12	-
1.50	1.00	17	first
1.75	1.16	12	first,last
2.00	1.33	12	last
2.50	1.70	5	first
2.75	1.84	1	-

*Max recorded value, actual value higher.

K_b = 1760
S = 5.0 in. c/c.
S_o = 5.0 in. c/c.
L_s = 24 in. (30 d_b)
C = 1.2 in. (1.60 d_b)
f_y = 60 ksi
f'_c = 3.47 ksi
N = 78
N_y = 41
$(\Delta/\Delta_y)_{max}$ = 1.84
$(\varepsilon/\varepsilon_y)_{max}$ = 2.72*
$(\varepsilon_{st}/\varepsilon_y)_{max}$ = 0.46 (Vert. Leg)
Splice Plane: Horizontal

Observations

Specimen C-7 was designed using Eq. 2.6. During the initial stages, the maximum amount of cracking occurred at the high moment end of the splice. The extent of this damage stabilized on further cycling due to the presence of adequate transverse reinforcement in that region. Longitudinal cover splitting was first observed at a 1.00" displacement. The rebar strains were 0.8 ε_y at this level. The splice bars first yielded at Δ = 1.50". The rate of face cover splitting was greater than that at the sides. Bar strains progressively increased with cycling at Δ = 2.00", at the end of which the peak recorded value was 1.86 ε_y. With more cycling, almost complete propagation of the bottom splitting cracks took place. A bar end slip of about 0.1" was

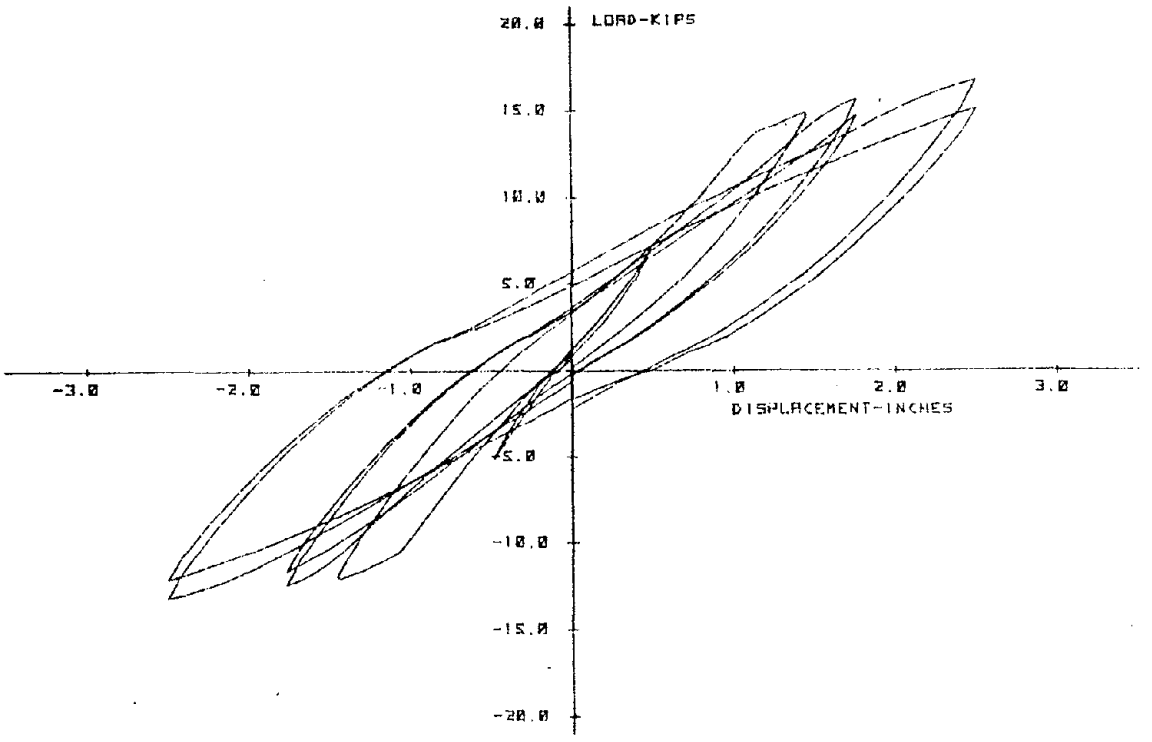

Fig. 3.14a. Load-displacement relationship - Specimen C-7.

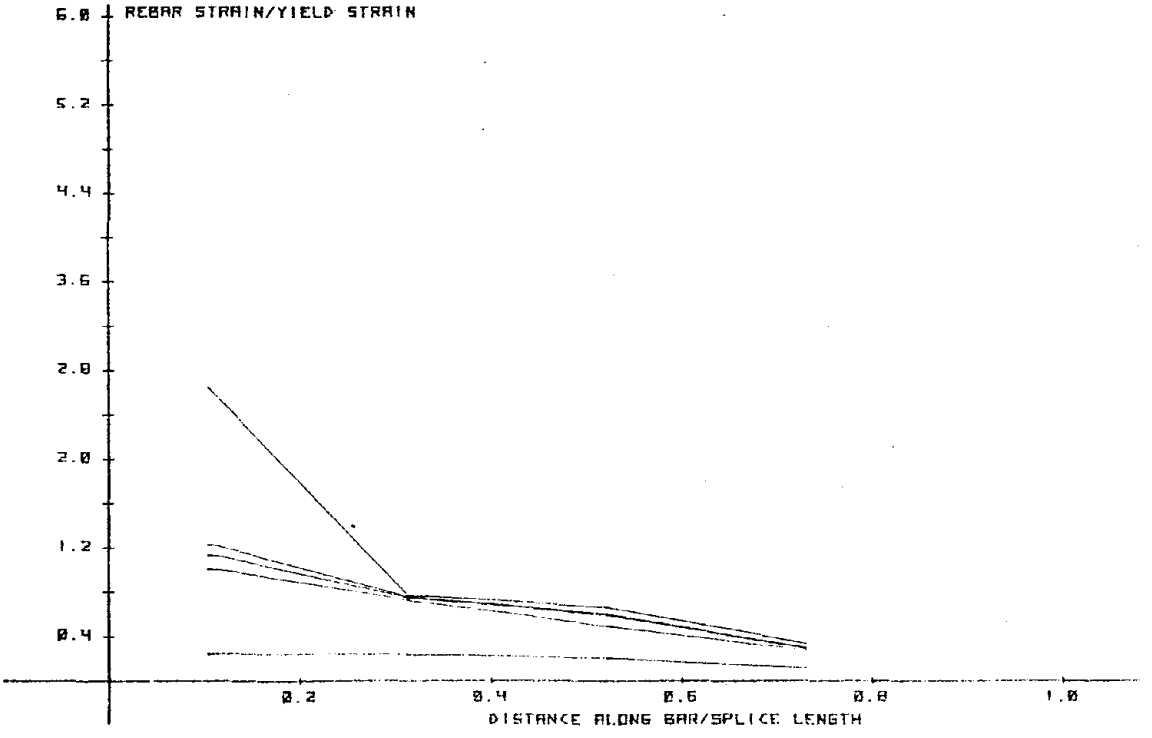

Fig. 3.14b. Main reinforcement strains - Specimen C-7.

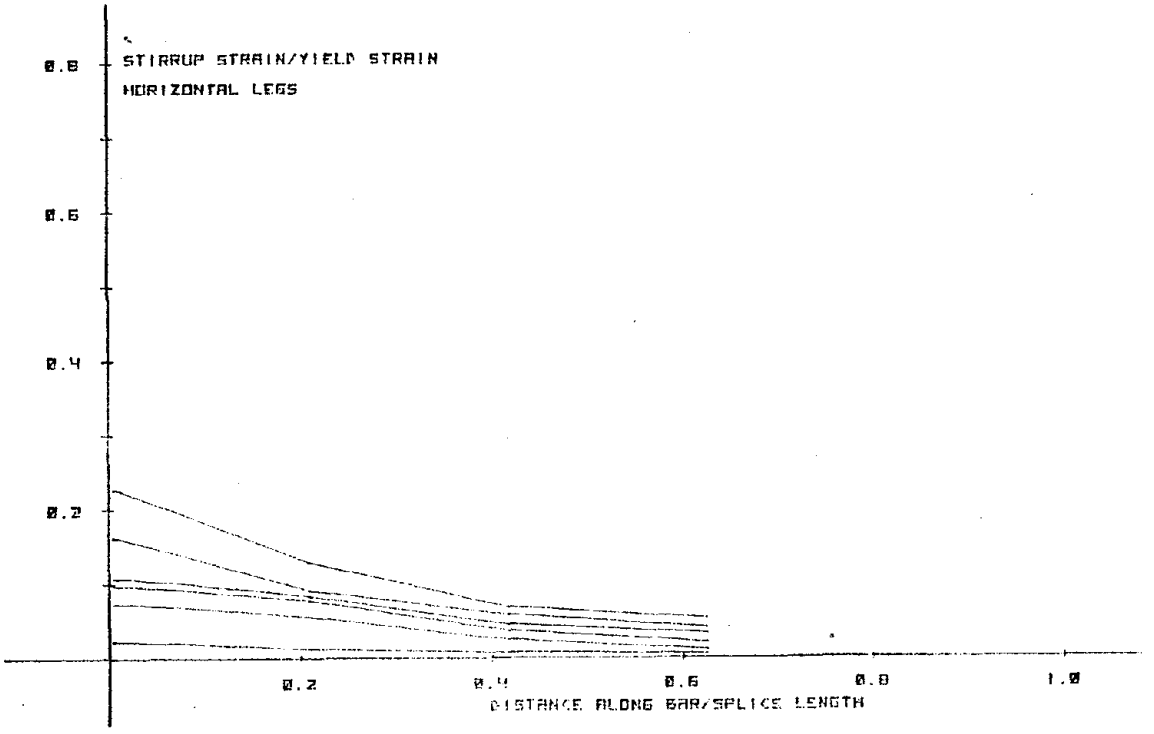

Fig. 3.14c. Stirrup strains - Specimen C-7.

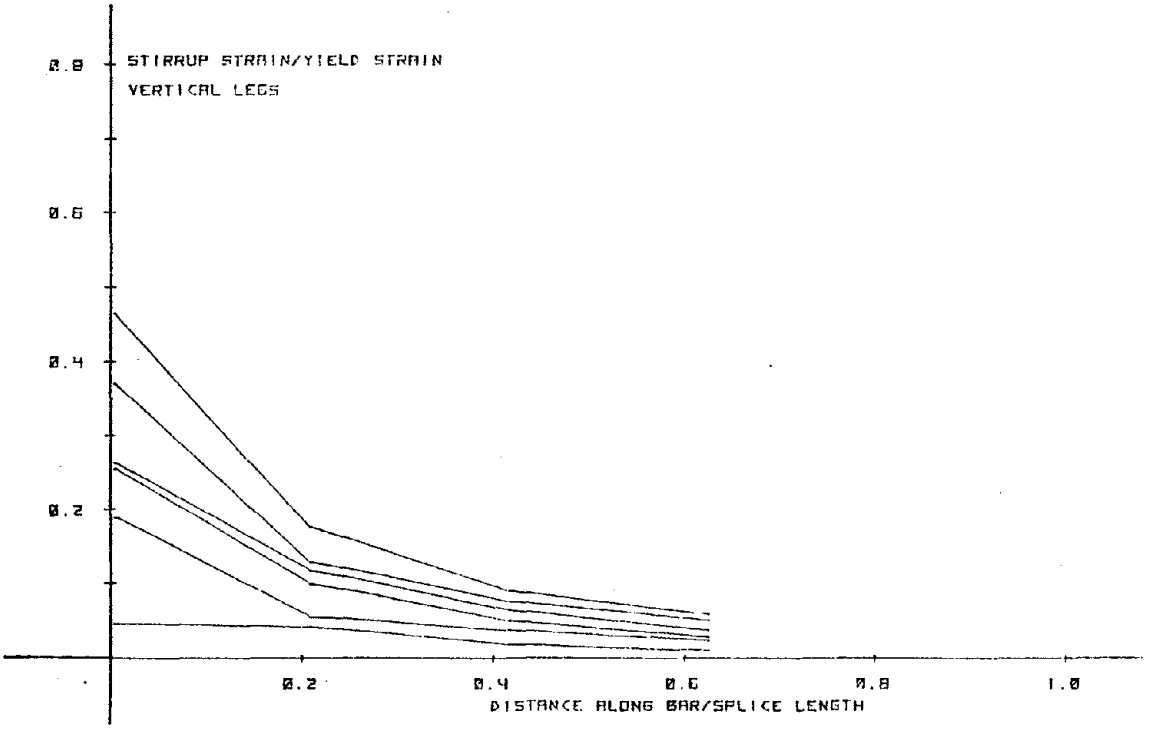

Fig. 3.14d. Stirrup strains - Specimen C-7.

observed visually, but this did not result in a pullout type failure. Testing was terminated before complete destruction. On the basis of the observed displacement and strain ductilities, C-7 was considered to have performed satisfactorily.

3.7.8 Test C-8

Jack Displacement		No. of Cycles	Cycles Plotted
Inches	$\Delta/\Delta y$		
0.50	0.20	12	last
0.75	0.30	12	-
1.00	0.40	12	first
1.50	0.50	12	first
1.75	0.70	12	last
2.00	0.80	12	last
2.50	1.00	12	first, last
2.75	1.10	1	-

K_b = 1760
S = 5.0 in. c/c.
S_o = 5.0 in. c/c.
L_s = 24 in. (30 d_b)
C = 1.2 in. (1.60 d_b)
f_y = 60 ksi
f'_c = 3.47 ksi
N = 85
N_y = 12
$(\Delta/\Delta_y)_{max}$ = 1.00
$(\varepsilon/\varepsilon_y)_{max}$ = 1.1
$(\varepsilon_{st}/\varepsilon_y)_{max}$ = 0.65 (Vert. Leg)
Splice Plane: Vertical

Observations

C-8 was the first test specimen with bars spliced in the vertical plane. In other respects, it was constructed identically to C-7. In comparison to C-7, the splice bar strains increased at a slower rate - being 0.5 ε_y at 1.00" displacement. More cycling produced longitudinal cover splits originating from the sides at the splice high moment end. At 1.75" displacement, longitudinal splits on the top and bottom faces appeared. The peak bar strain, however, was still below the yield value. With cycling at Δ = 2.00", cover splits on the bottom face and sides progressed through the entire length of the splice. The extent of cracking was more on the sides than on the face. Simultaneous face

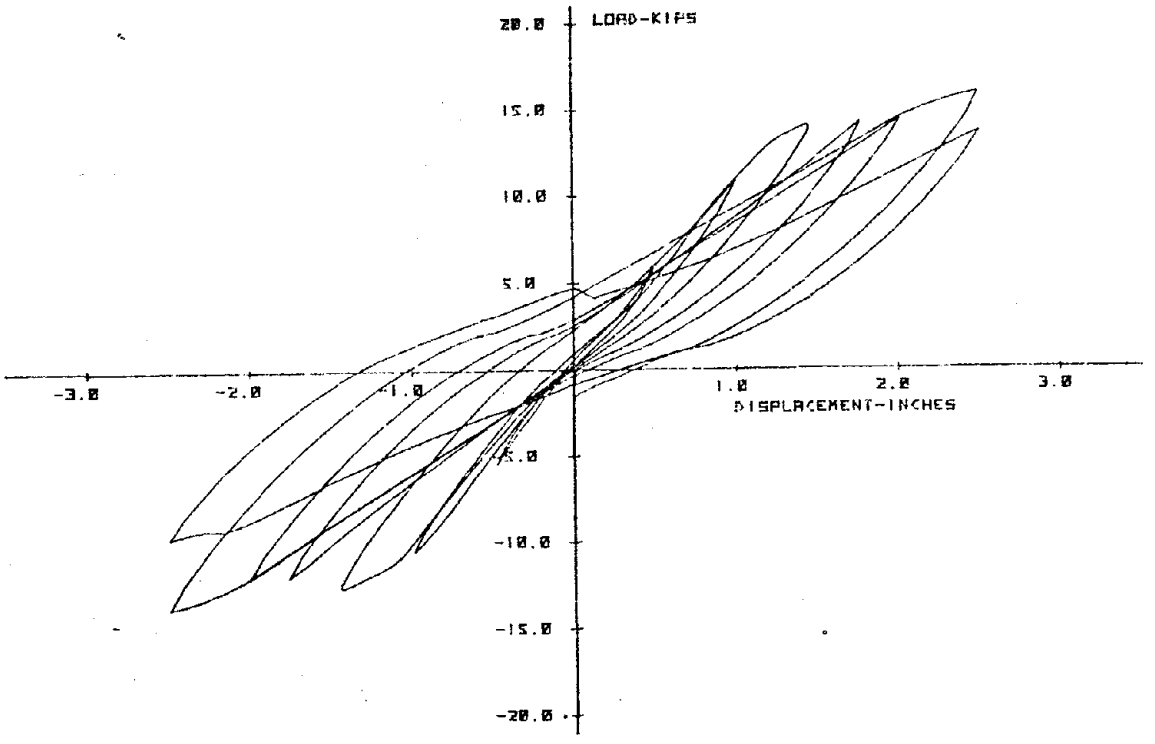

Fig. 3.15a. Load-displacement relationship - Specimen C-8.

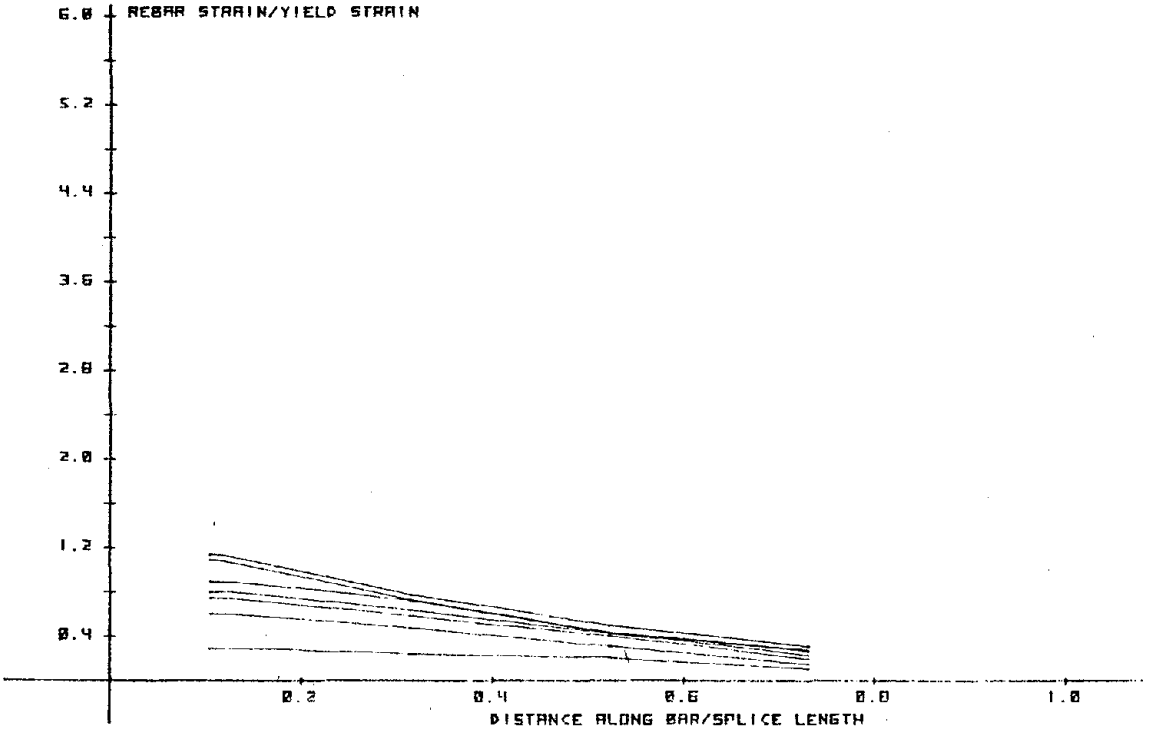

Fig. 3.15b. Main reinforcement strains - Specimen C-8.

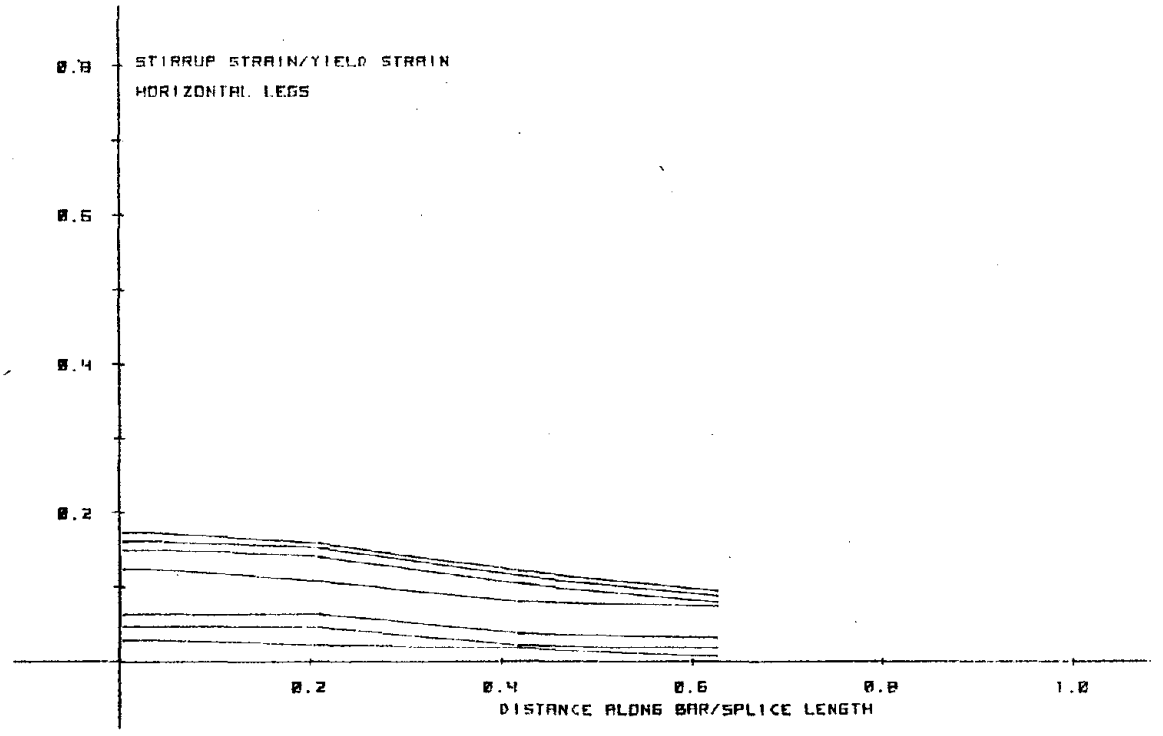

Fig. 3.15c. Stirrup strains - Specimen C-8 .

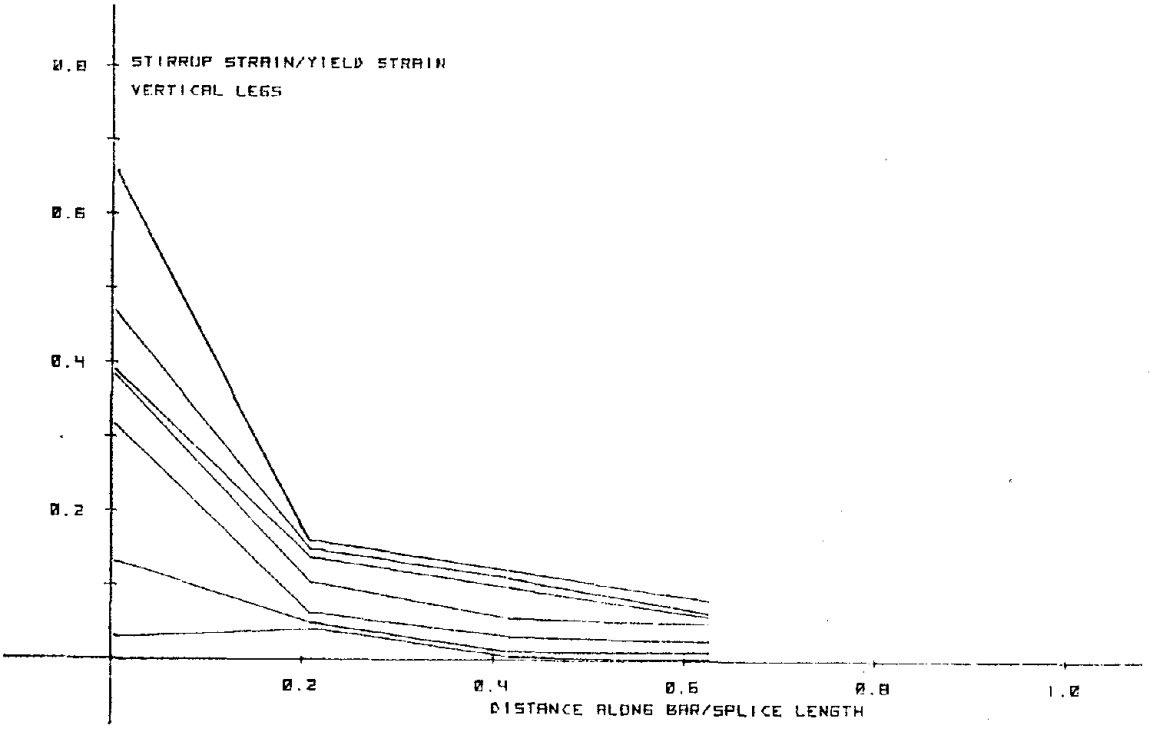

Fig. 3.15d. Stirrup strains - Specimen C-8.

and side cover splitting completed the bond failure mechanism. This resulted in noticeable load shedding during the last cycle at $\Delta = 2.5$". The main bars went into yield only at this level. Bar slips of at least 0.1" were observed visually. From an evaluation of results, it appeared that C-8 performed unsatisfactorily. A comparison with other tests showed this discrepancy to be due to differences in bar instrumentation. This is described in Sections 4.2 and 4.7.

3.7.9 Test C-9

Jack Displacement		No. of Cycles	Cycles Plotted
Inches	Δ/Δ_y		
0.5	0.41	22	first
1.00	0.83	12	first
1.5	1.21	12	first
1.75	1.47	12	first
2.00	1.67	12	first
2.50	2.08	12	first

*Max recorded value, actual value higher.

K_b = 1760
S = 5.0" c/c.
S_o = 3.5" c/c.
L_s = 30 in. (40 d_b)
C = 1.2 in. (1.60 d_b)
f_y = 60 ksi
f'_c = 3.80 ksi
N = 82
N_y = 47
$(\Delta/\Delta_y)_{max}$ = 2.08
$(\varepsilon/\varepsilon_y)_{max}$ = 5.51*
$(\varepsilon_{st}/\varepsilon_y)_{max}$ = 0.21 (Vert. Leg)
Splice Plane: Horizontal

Observations

Splices in Specimen C-9 were lapped in the horizontal plane. The stirrup spacing S was the same as in Specimens C-7 and C-8. This was in order to comply with the ACI-318-77 'd/2' spacing limitation. In an effort to further reduce the damage around the high moment end, stirrups beyond this end section were spaced 3.5 inches c/c. During testing, the splice bars were well into yield at $\Delta = 1.5$", showing strains of 2.6 ε_y. At $\Delta = 1.76$ inches, the yield penetration was 0.17 ℓ_s. Most of

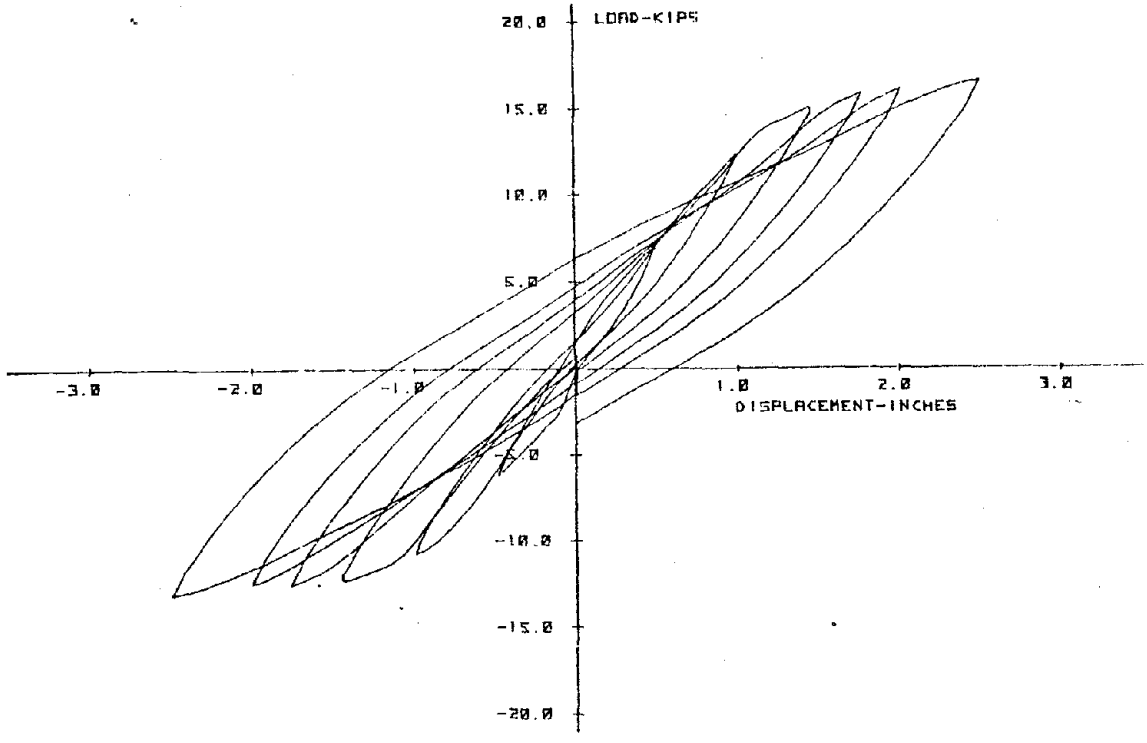

Fig. 3.16a. Load-displacement relationship - Specimen C-9.

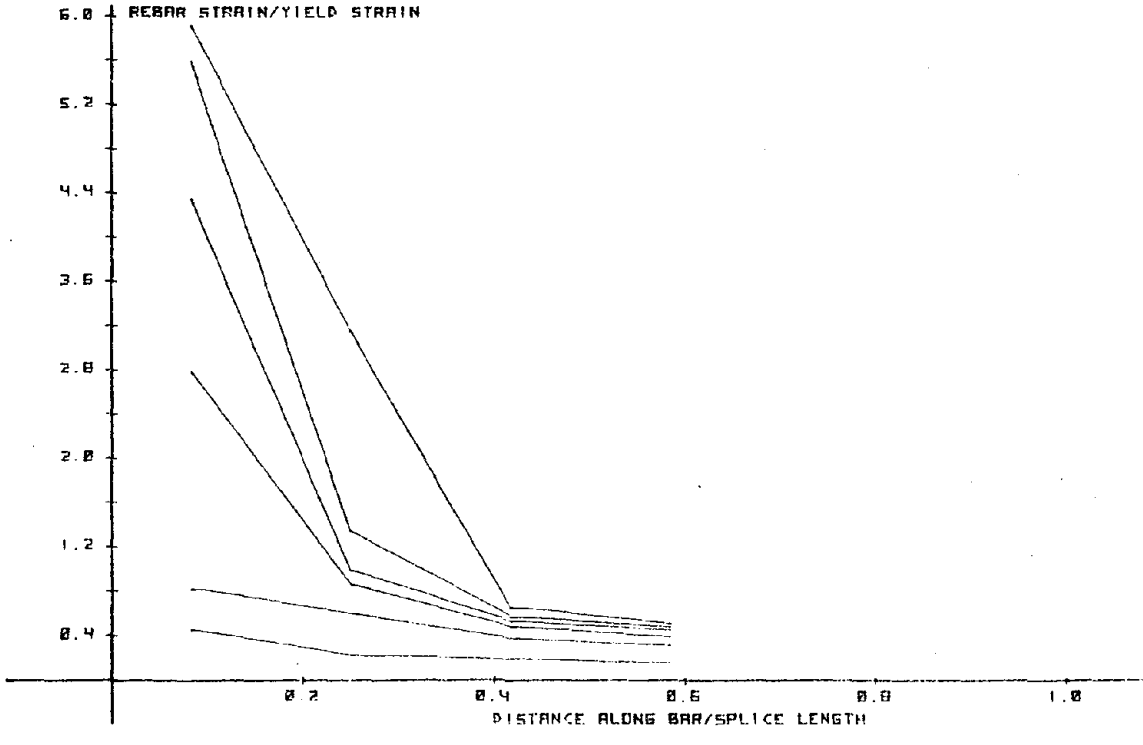

Fig. 3.16b. Main reinforcement strains - Specimen C-9.

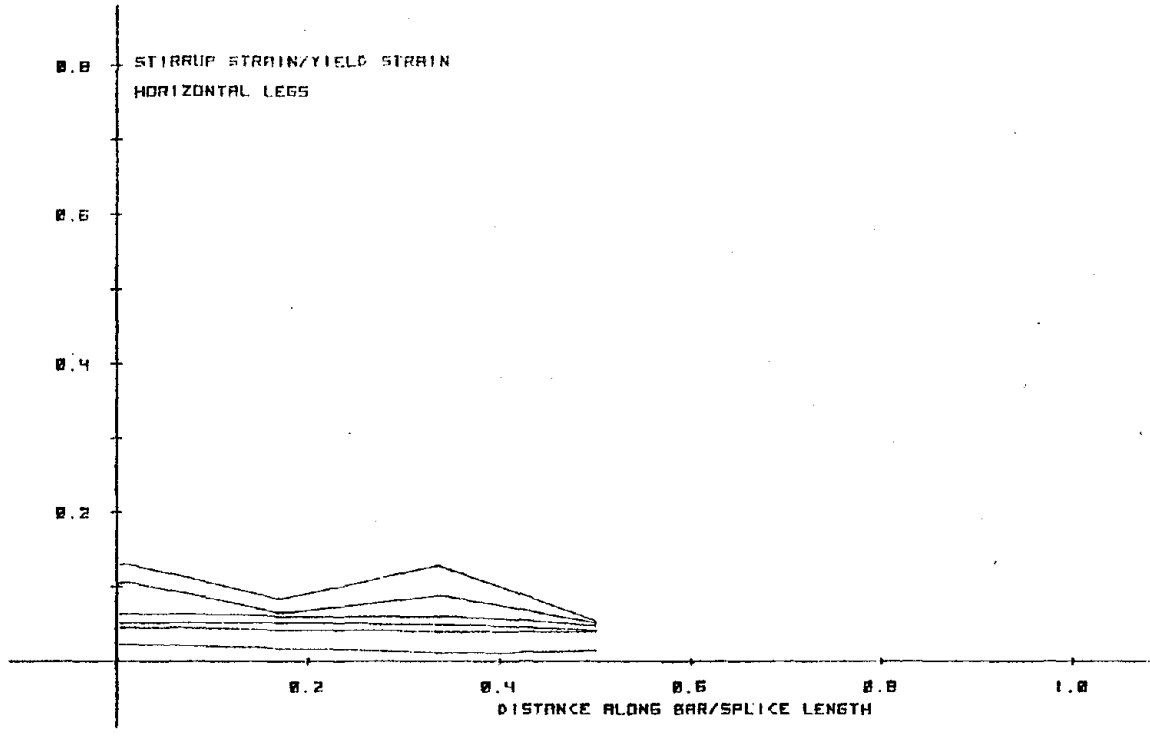

Fig. 3.16c. Stirrup strains - Specimen C-9.

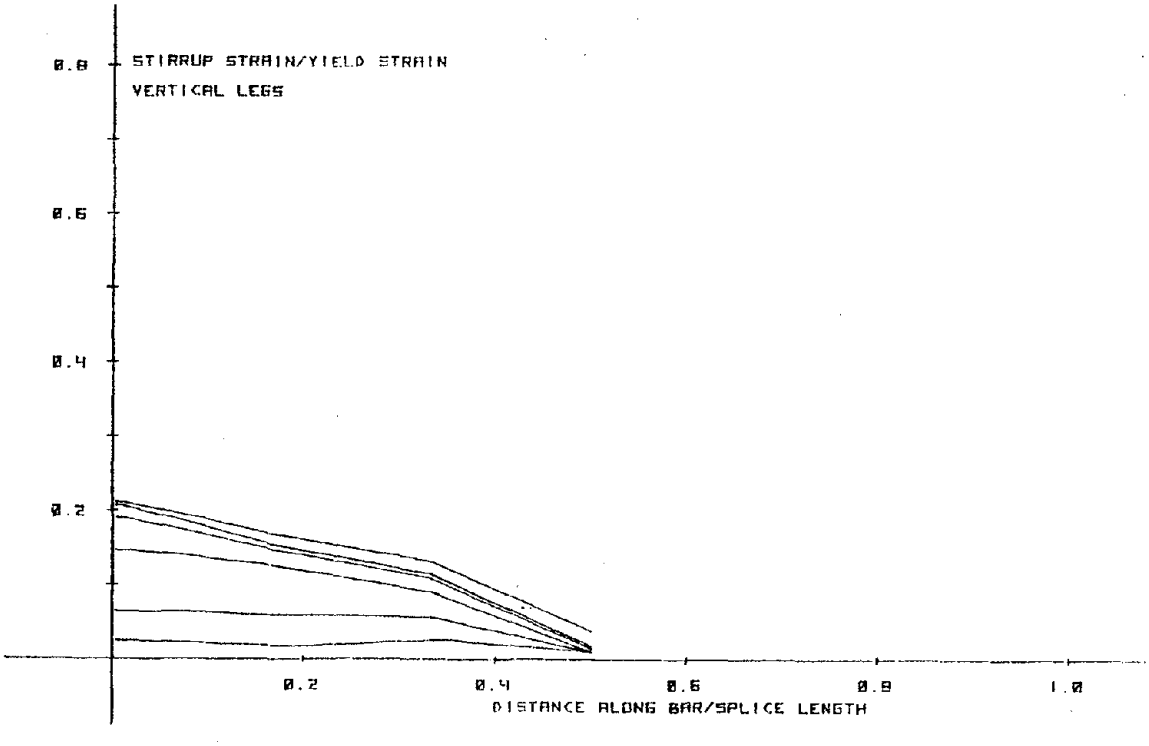

Fig. 3.16d. Stirrup strains - Specimen C-9.

the specimen damage during the rest of the test was at and just outside the high moment end, despite the presence of closely spaced stirrups. The bar end slip measurement transducer recorded values no greater than 0.05". The test was discontinued after cycling at $\Delta = 2.5$", since the splice remained relatively intact thus precluding the possibility of bond failure. Stirrup strains remained relatively low. In spite of high ductility factors, it was difficult to evaluate the results since no significant splice damage occurred.

3.7.10 Test C-10

Jack Displacement		No. of Cycles	Cycles Plotted
Inches	Δ/Δ_y		
0.50	0.41	22	first
1.00	0.83	12	first
1.50	1.21	12	first
1.75	1.47	12	first
2.00	1.67	12	first
2.50	2.08	12	first

*Max recorded value, actual value higher.

K_b = 1760
S = 5.0 in. c/c.
S_o = 3.5 in. c/c.
L_s = 30 in. (40 d_b)
C = 1.2 in. (1.60 d_b)
f_y = 60 ksi
f'_c = 3.80 ksi
N = 82
N_y = 47
$(\Delta/\Delta_y)_{max}$ = 2.08
$(\varepsilon/\varepsilon_y)_{max}$ = 4.94*
$(\varepsilon_{st}/\varepsilon_y)_{max}$ = 0.50 (Vert. Leg)
Splice Plane: Vertical

Observations

C-9 and C-10 were identical except for the orientation of the splice, which was vertical in C-10. While testing, most of the transverse cracking appeared during the first 20 cycles and then stabilized. Face and side splitting appeared first at $\Delta = 1.00$". Maximum rebar strains were beyond yield (1.3 ε_y) at $\Delta = 1.5$" and were assumed to have first exceeded yield at a displacement level of 1.2". With cycling at

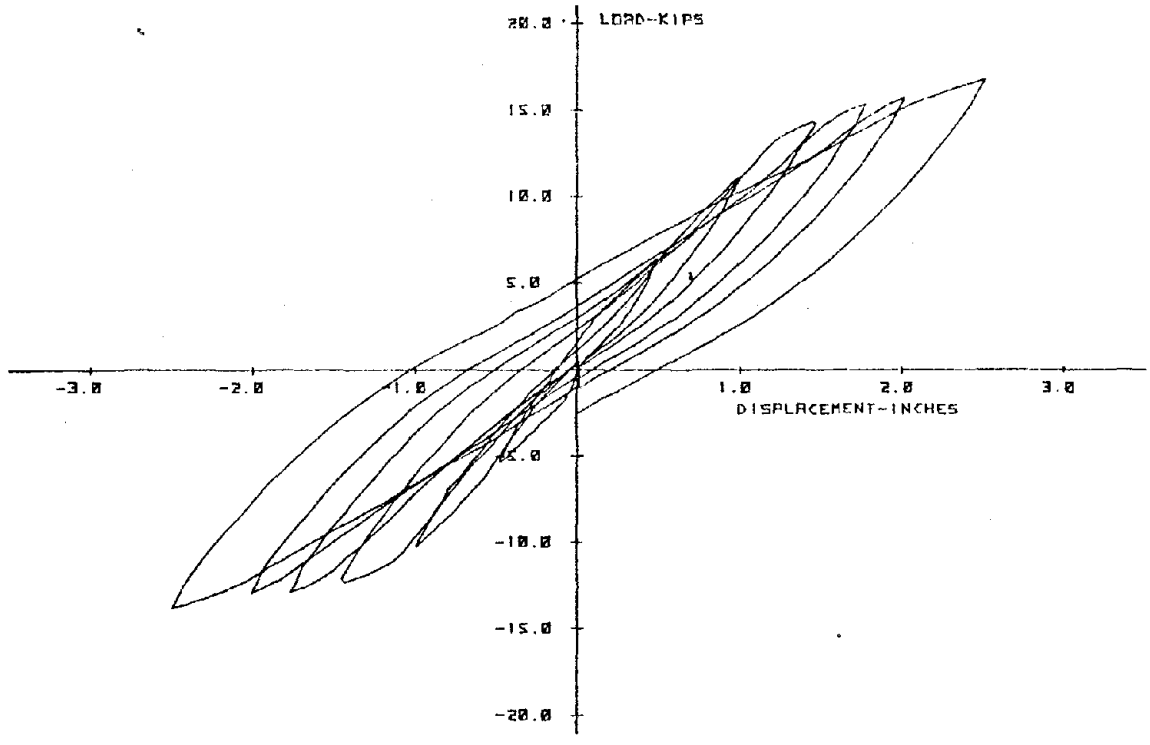

Fig. 3.17a. Load-displacement relationship - Specimen C-10.

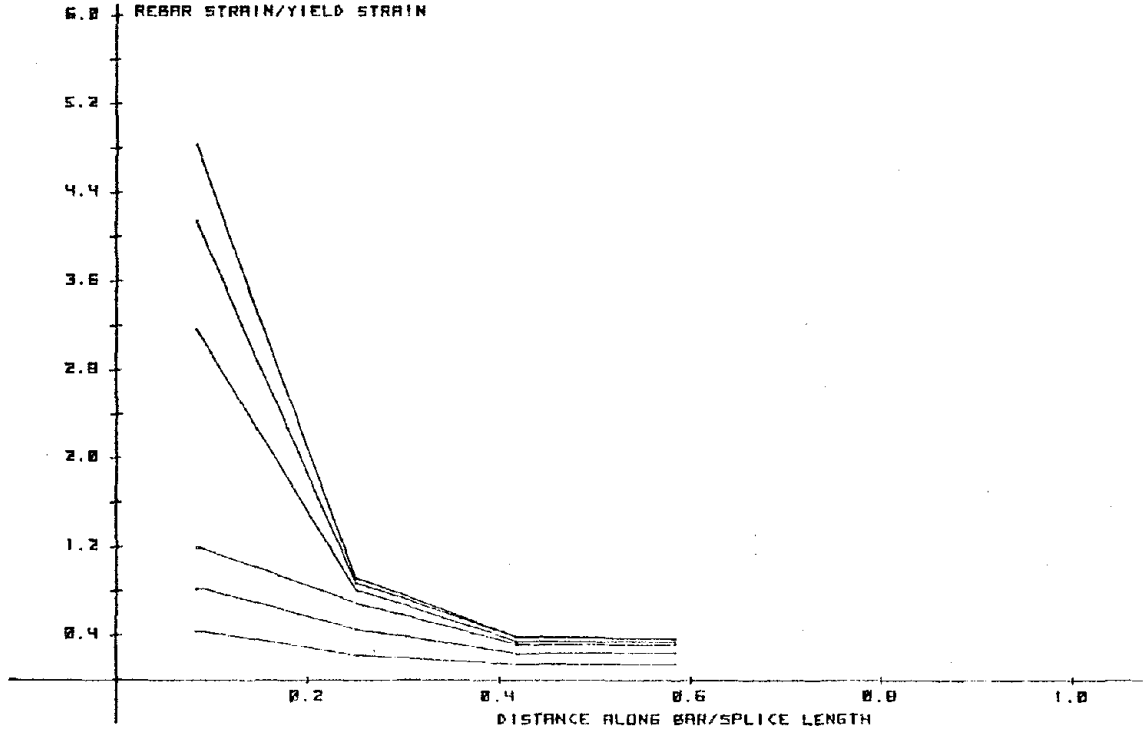

Fig. 3.17b. Main reinforcement strains - Specimen C-10.

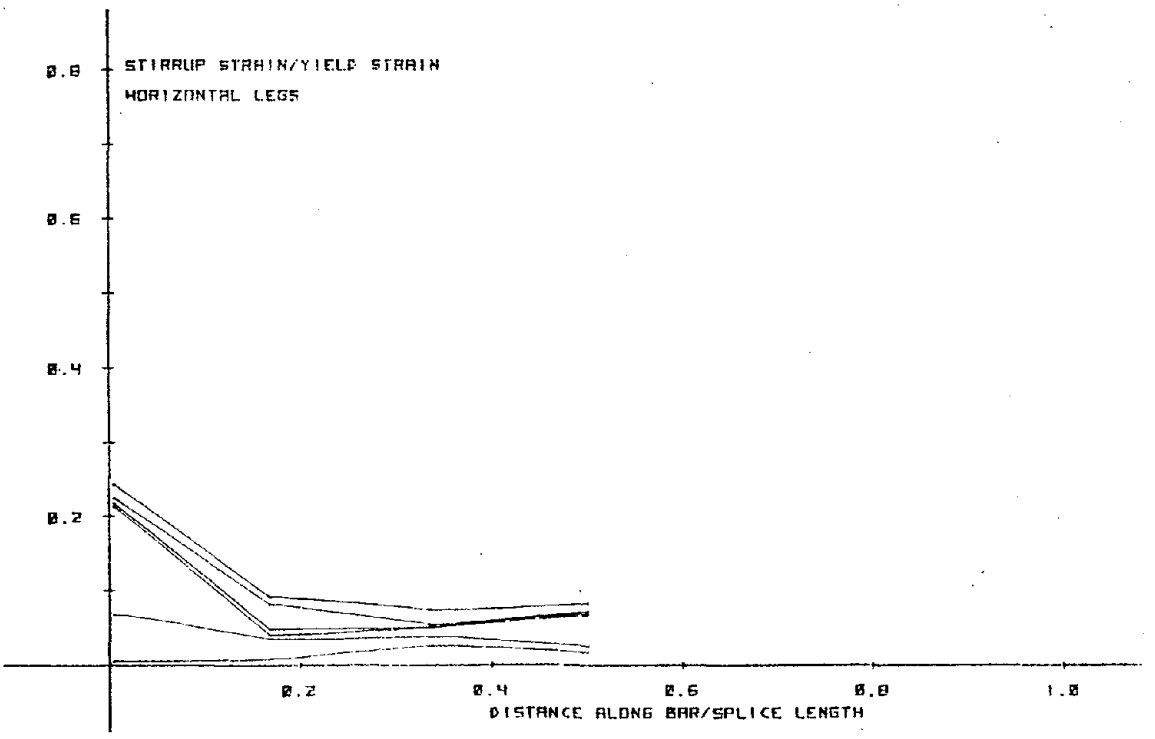

Fig. 3.17c. Stirrup strains - Specimen C-10.

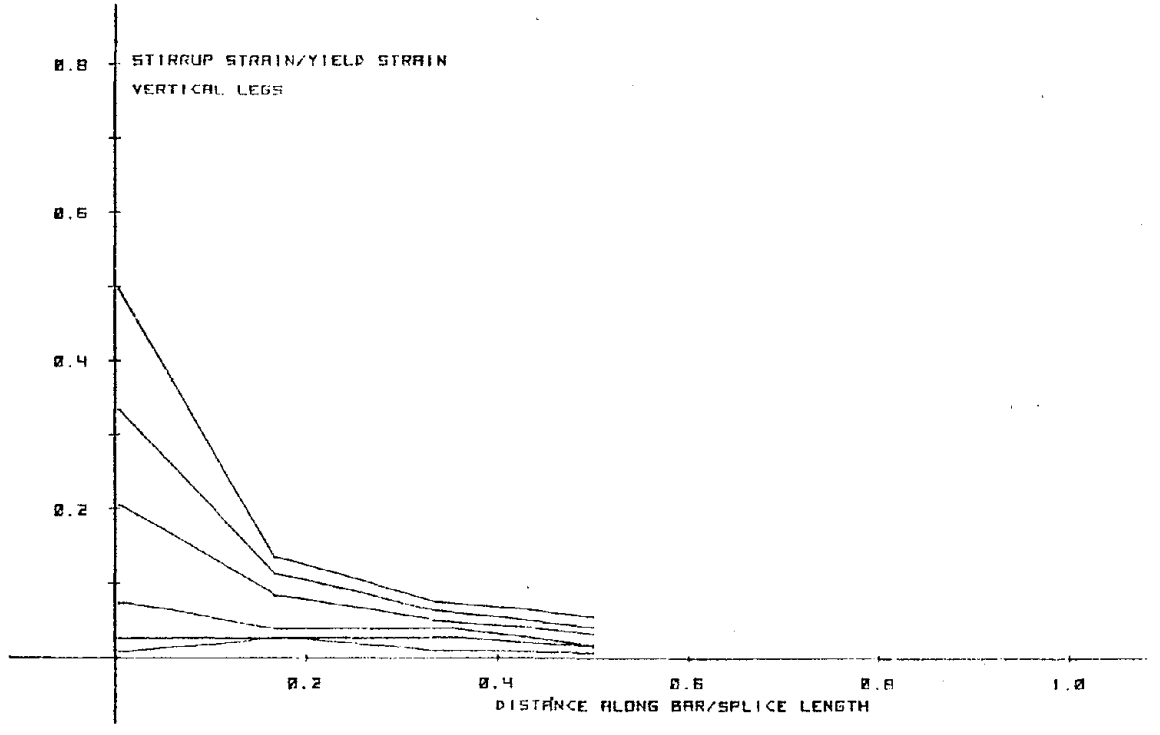

Fig. 3.17d. Stirrup strains - Specimen C-10.

$\Delta = 1.75"$, both face and side cover splitting gradually progressed down the splice length. It stabilized somewhere between the second and third stirrups at $\Delta = 2.00"$. The test was stopped after cycling at $\Delta = 2.50"$ since, as in Specimen C-9, most of the damage was outside the splice. It was clear that additional cycling would not result in a bond failure. Maximum vertical leg stirrup strains were higher than in C-9. As in C-9, the test performance could not easily be evaluated.

3.7.11 Test C-11

Jack Displacement		No. of Cycles	Cycles Plotted
Inches	$\Delta/\Delta y$		
0.5	0.41	22	first
1.0	0.82	17	first
1.5	1.24	12	first
1.75	1.44	12	first
2.0	1.65	12	first
2.5	2.06	11	first

*Max recorded value, actual value higher.

K_b = 1355
S = 6.5 in. c/c.
S_o = 3.0 in. c/c.
L_s = 30 in. (40 d_b)
C = 1.2 in. (1.6 d_b)
f_y = 60 ksi
f'_c = 3.71 ksi
N = 86
N_y = 45
$(\Delta/\Delta_y)_{max}$ = 2.06
$(\varepsilon/\varepsilon_y)_{max}$ = 2.53*
$(\varepsilon_{st}/\varepsilon_y)_{max}$ = 0.21 (Vert. Leg)
Splice Plane: Horizontal

Observations

Test C-11 was a redesigned version of C-9. A stirrup spacing S of 6.5" c/c (obtained from the equation by Tocci) was adopted despite the ACI spacing limitation of d/2" (5") c/c. The cycling levels were the same as in Specimen C-9. Splice bars were well into yield at $\Delta = 1.5"$ and were seen to have just attained yield at $\Delta = 1.1"$. Cover splitting at the faces and sides began at $\Delta = 1.00"$ and steadily penetrated along the splice length at higher cycling levels. Complete face and side splitting occurred at the bottom at the 2.00" displacement level.

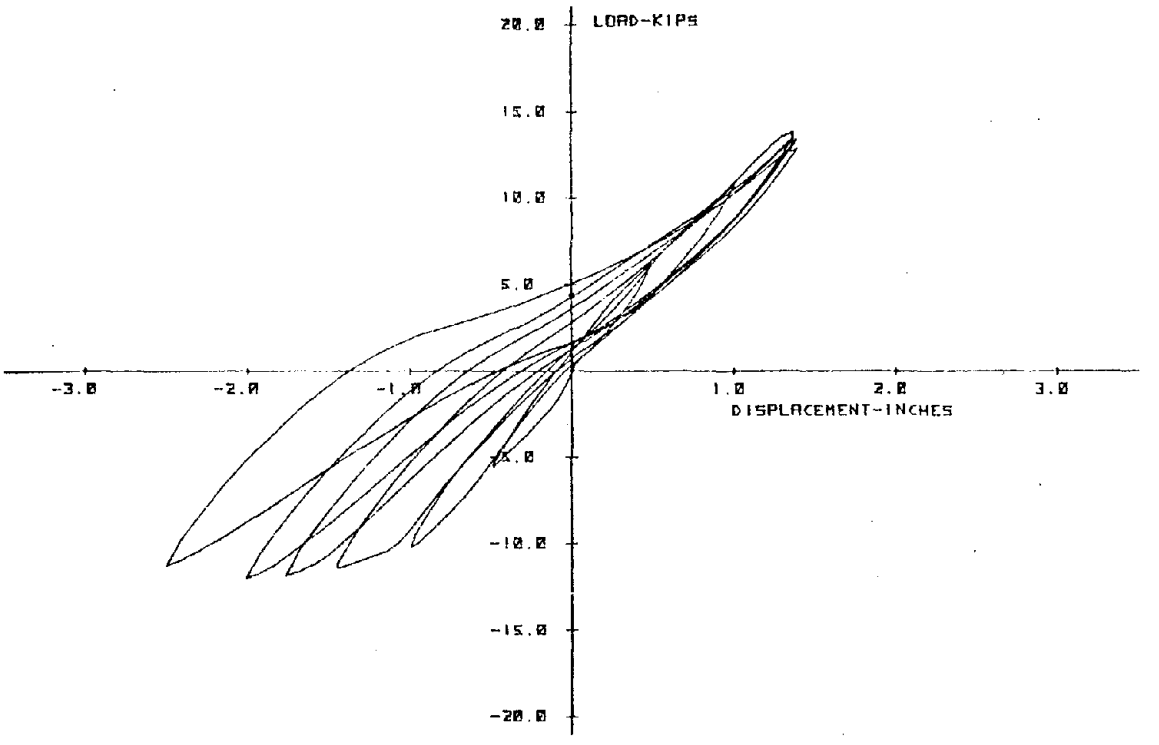

Fig. 3.18a. Load-displacement relationship - Specimen C-11.

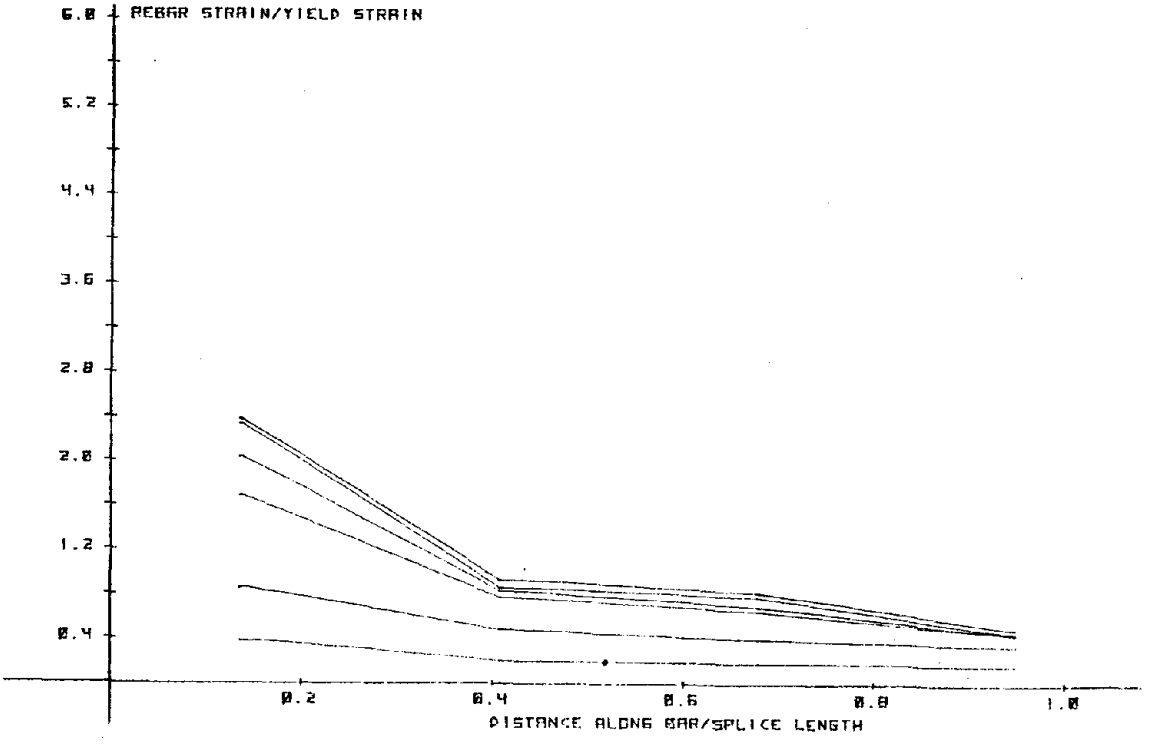

Fig. 3.18b. Main reinforcement strains - Specimen C-11.

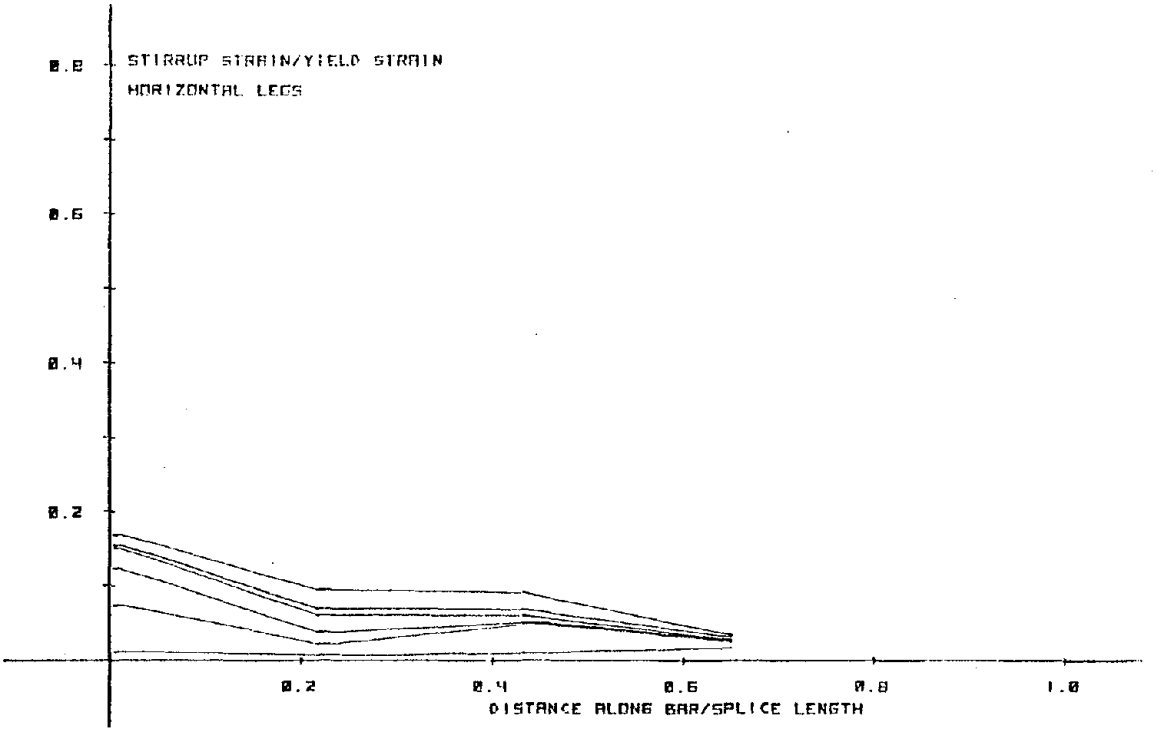

Fig. 3.18c. Stirrup strains - Specimen C-11.

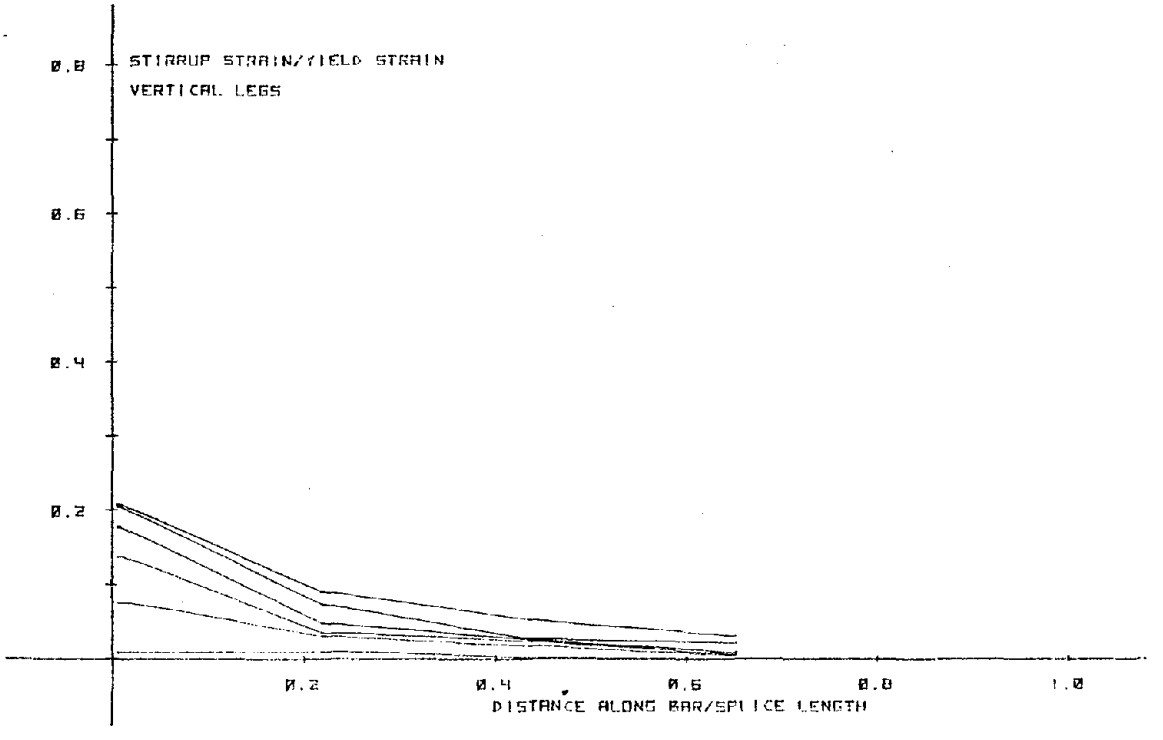

Fig. 3.18d. Stirrup strains - Specimen C-11.

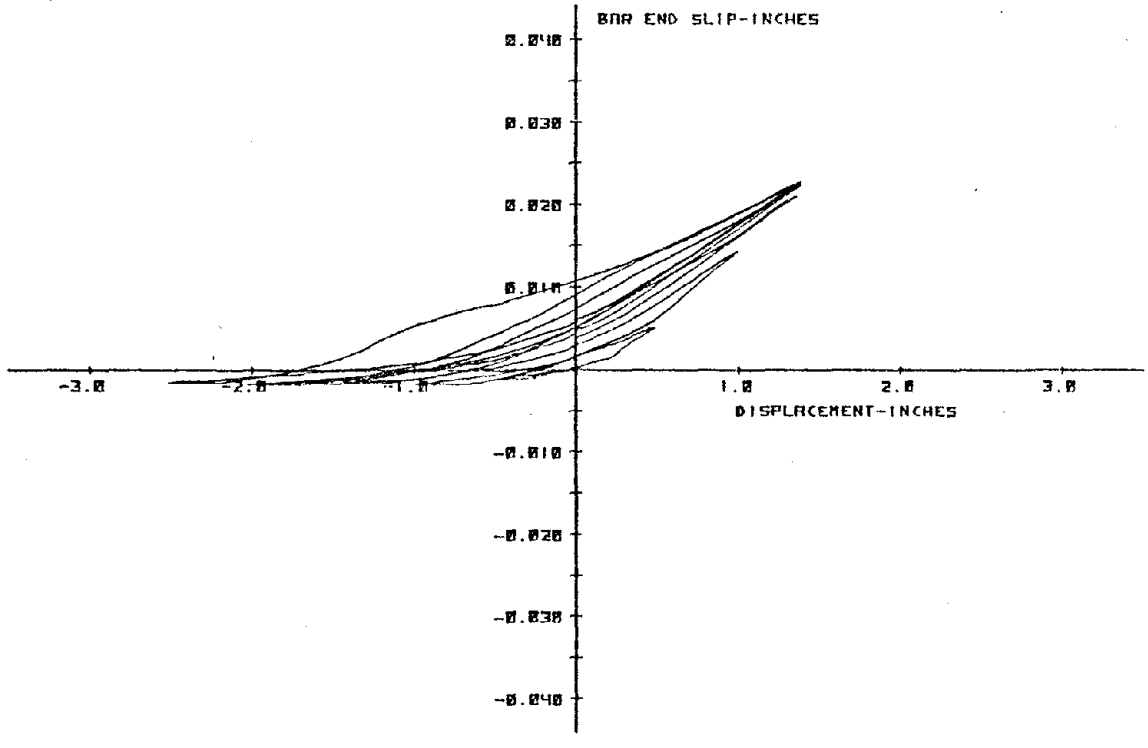

Fig. 3.18e. Bar slip - displacement relationship - Specimen C-11.

This resulted in a bond failure mechanism. Maximum recorded rebar strains were 2.53 ε_y after which the strain gage failed. It is very likely that subsequent strains were even higher. The bottom half of the specimen showed more damage than the top half. The section outside the high moment end was reinforced to about the same extent as in Specimen C-9 but showed much less deterioration compared to Specimen C-9. Due to problems developed in the loading device, the upward stroke was limited to 1.4". Bar and slips measured by the displacement transducer were recorded and plotted at various displacement levels. Based on the acceptance criterion, C-11 performed favorably.

3.7.12 Test C-12

Jack Displacement		No. of Cycles	Cycles Plotted
Inches	Δ/Δ_y		
0.5	0.41	22	first
1.0	0.90	12	first
1.5	1.36	23	first
1.75	1.59	12	first
2.0	1.81	12	first
2.5	2.27	1	first

K_b = 1355
S = 6.5 in. c/c.
S_o = 3.0 in. c/c.
L_s = 30 in. (40 d_b)
C = 1.2 in. (1.6 d_b)
f_y = 60 ksi
f'_c = 3.71 ksi
N = 82
N_y = 38
$(\Delta/\Delta_y)_{max}$ = 2.06
$(\varepsilon/\varepsilon_y)_{max}$ = 2.58
$(\varepsilon_{st}/\varepsilon_y)_{max}$ = 0.54 (Vert. Leg)
Splice Plane: Vertical

Observations

C-12 was a redesigned version of C-10, with splices in the vertical plane. Once again, a stirrup spacing S of 6.5" c/c was adopted. After cycling at the first two displacement levels, considerable face and side splitting was observed at the bottom of the specimen. Several

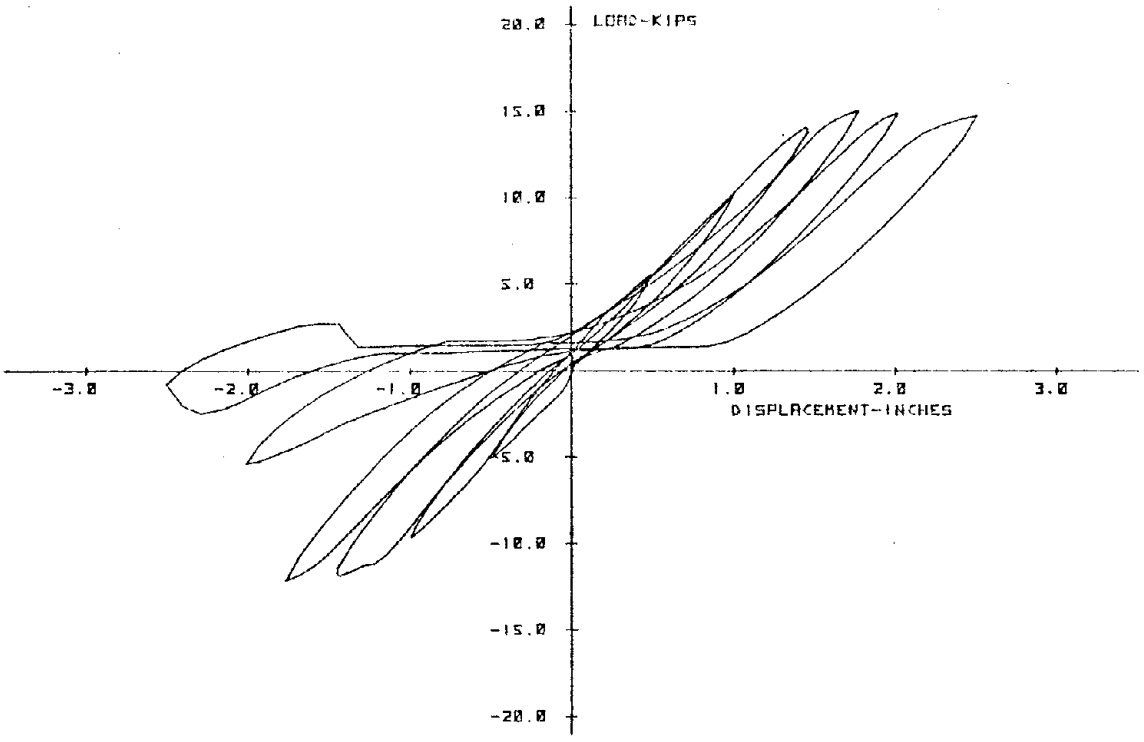

Fig. 3.19a. Load-displacement relationship - Specimen C-12.

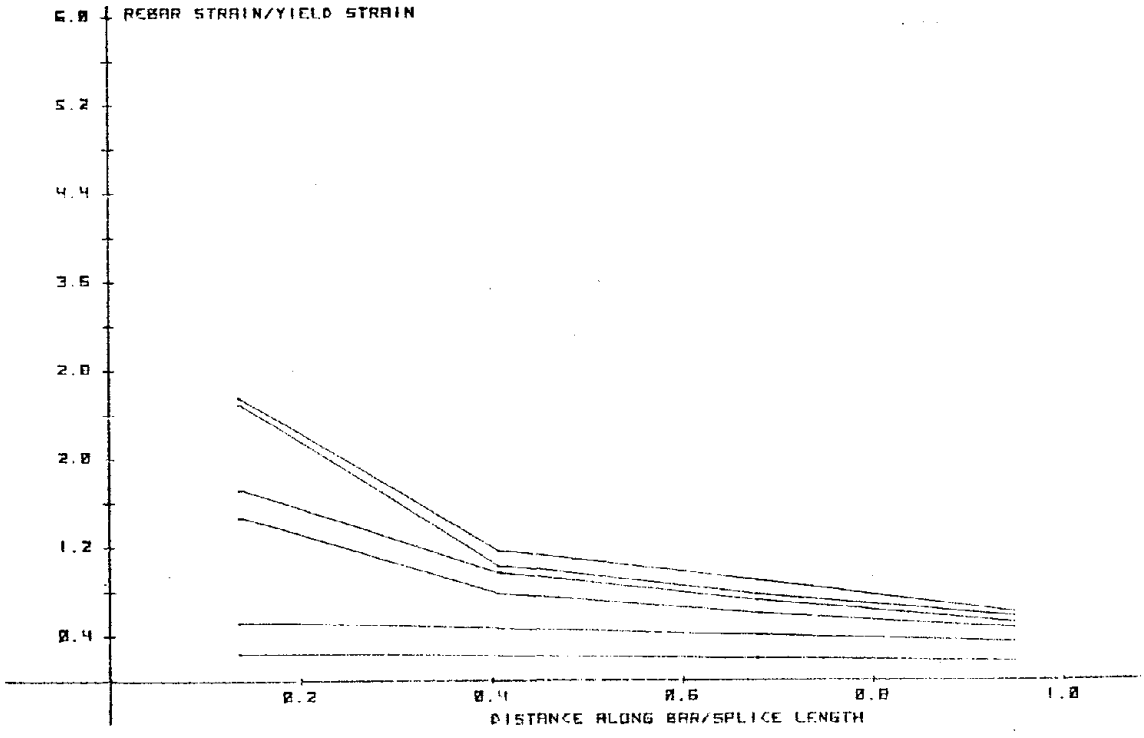

Fig. 3.19b. Main reinforcement strains - Specimen C-12.

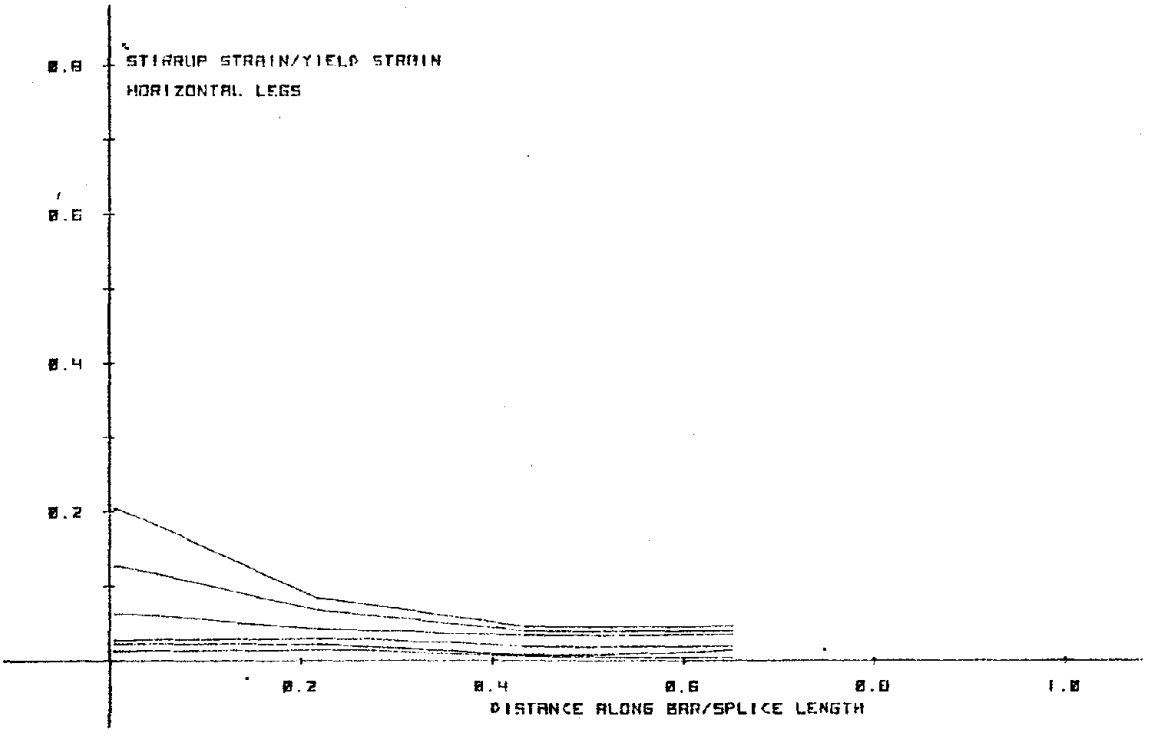

Fig. 3.19c. Stirrup strains - Specimen C-12.

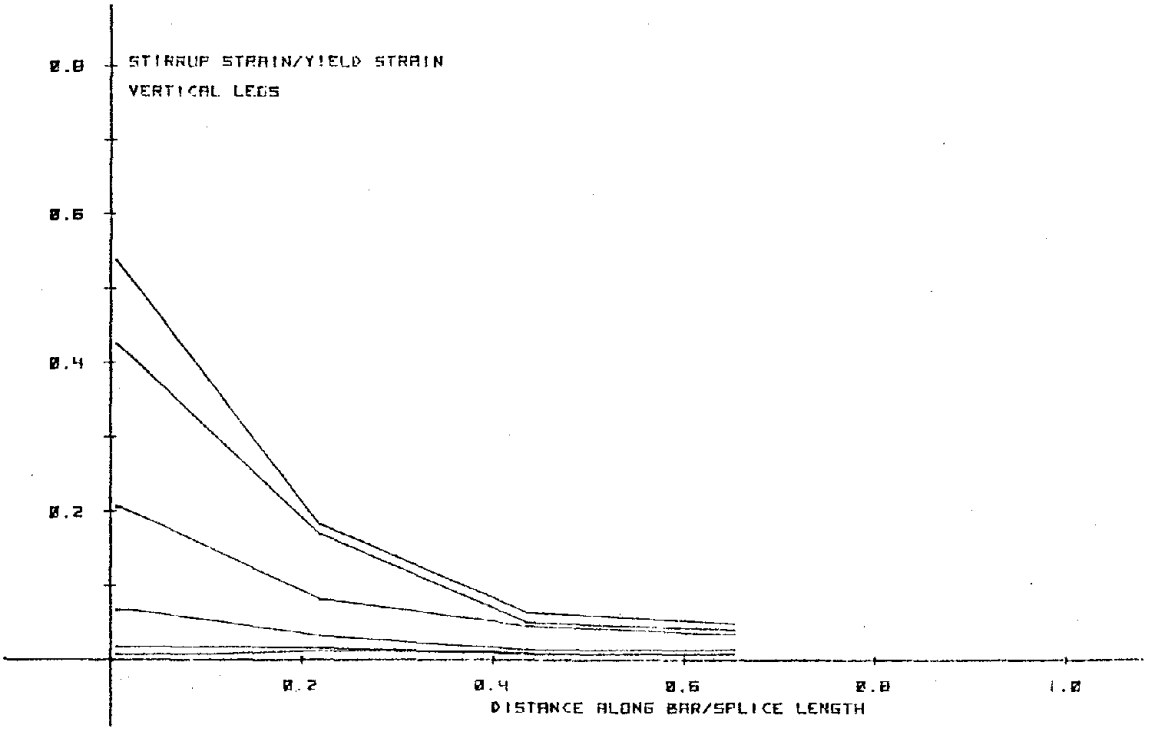

Fig. 3.19d. Stirrup strains - Specimen C-12.

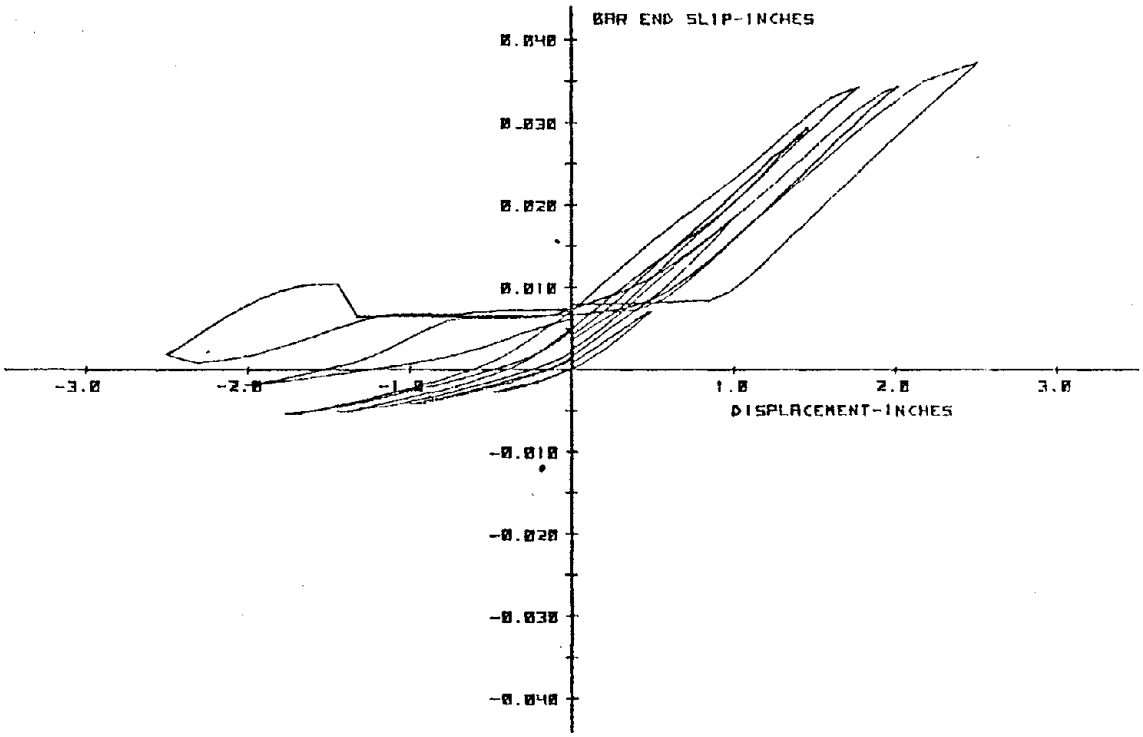

Fig. 3.19e. Bar slip - displacement relationship - Specimen C-12.

cycles were done at $\Delta = 1.5$, as a result of which side cover splitting propagated to 80% of the splice length. Face splitting progressed at a slower rate and became appreciable only at $\Delta = 1.75$". Once again, the lower half of the splice showed more damage than the top. Noticeable load shedding was experienced in the downward direction at $\Delta = 2.00$". The last two load-displacement curves clearly show that failure occurred in the downward direction with virtually no load carrying capacity. At this stage, bottom bar end slips were about 0.25" to 0.50", whereas top bar end slips were recorded as within 0.04". It was concluded from the results that C-12 met the acceptance criteria.

3.7.13 Test C-13

Jack Displacement		No. of Cycles	Cycles Plotted
Inches	$\Delta/\Delta y$		
0.5	0.42	12	first
0.75	0.63	12	first
1.00	0.83	12	first
1.45	1.20	17	first
1.75	1.46	12	first
2.00	1.67	12	first
2.50	2.08	12	first
2.75	2.30	1	first

*Max recorded value, actual value higher.

K_b = 1760
S = 5.00 in. c/c.
S_o = 3.00 in. c/c.
L_s = 24 in. (30 d_b)
C = 1.2 in. (1.6 d_b)
f_y = 60 ksi
f'_c = 4.23 ksi
N = 90
N_y = 50
$(\Delta/\Delta_y)_{max}$ = 2.08
$(\varepsilon/\varepsilon_y)_{max}$ = 5.02*
$(\varepsilon_{st}/\varepsilon_y)_{max}$ = 0.35 (Vert. Leg)
Splice Plane: Horizontal

Observations

This test was carried out to evaluate the influence of the bearing resistance offered by concrete on compression bars. The reinforcement details and load history were the same as in Specimen C-7.

The effect of end bearing was eliminated by attaching styrofoam plugs to the ends of the eight splice bars. Concrete compressive strength was 4.23 ksi, while it was only 3.47 ksi in Specimen C-7.

The first indication of bottom face cover splitting appeared at $\Delta = 0.76$ inches. The main bars went into yield at $\Delta = 1.2$ inches, and the extent of bottom face splitting increased with higher levels of stroke. Some amount of top cover damage was also observed at this stage. However, the side covers were still free of splitting. The second rebar gage yielded at $\Delta = 1.76$", bringing the yield penetration to about 0.35 ℓ_s. Compared to Specimen C-7, the splice maintained better overall integrity, with little evidence of side cover damage even at $\Delta = 2.00$ inches. Cycling at $\Delta = 2.5$ inches and 2.75 inches finally brought about bottom side cover splitting and thereby completed the cover failure mechanism.

This was the first test in which cover splitting occurred all along the top face of the splice as well. A displacement transducer attached to a top splice bar recorded slips at different displacement levels. The slip values for the bar in compression were higher than in C-11 and C-12.

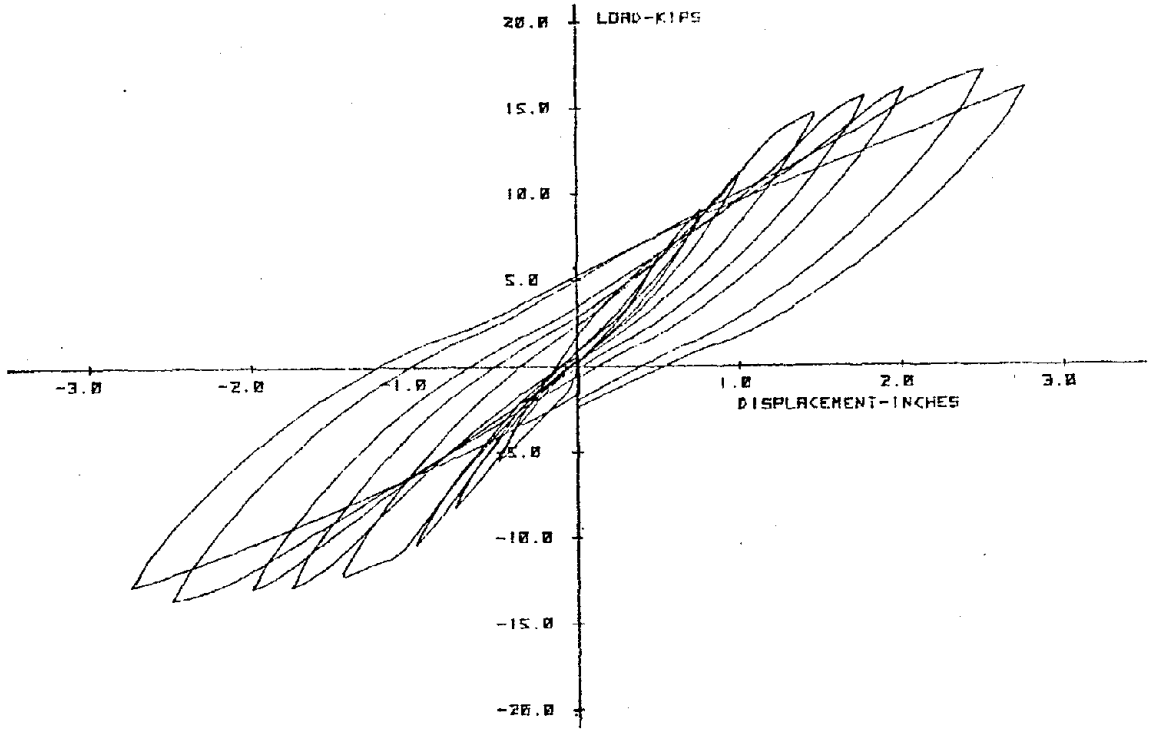

Fig. 3.20a. Load-displacement relationship - Specimen C-13.

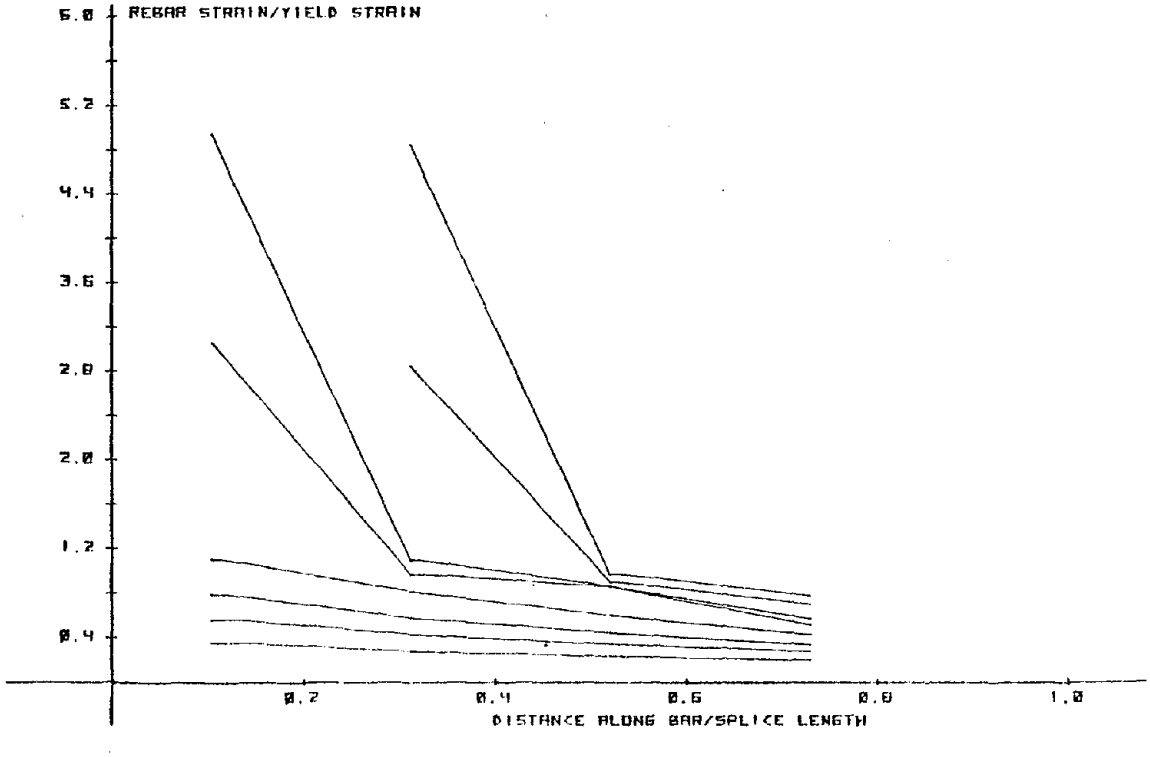

Fig. 3.20b. Main reinforcement strains - Specimen C-13.

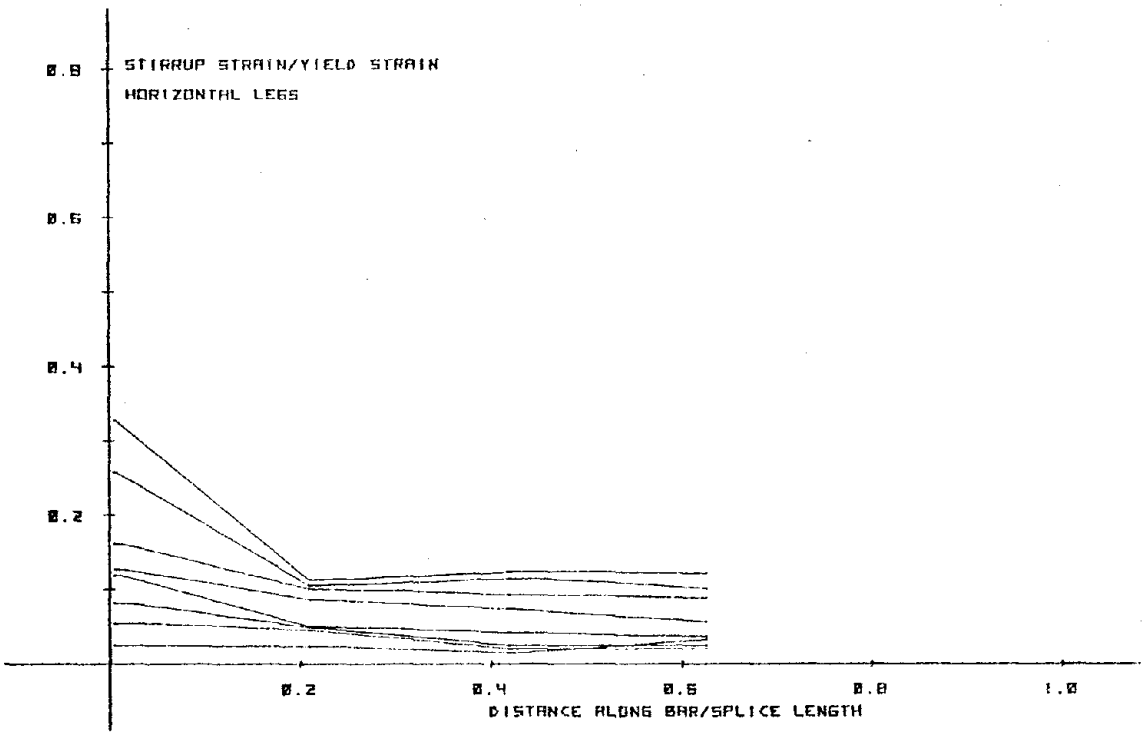

Fig. 3.20c. Stirrup strains - Specimen C-13.

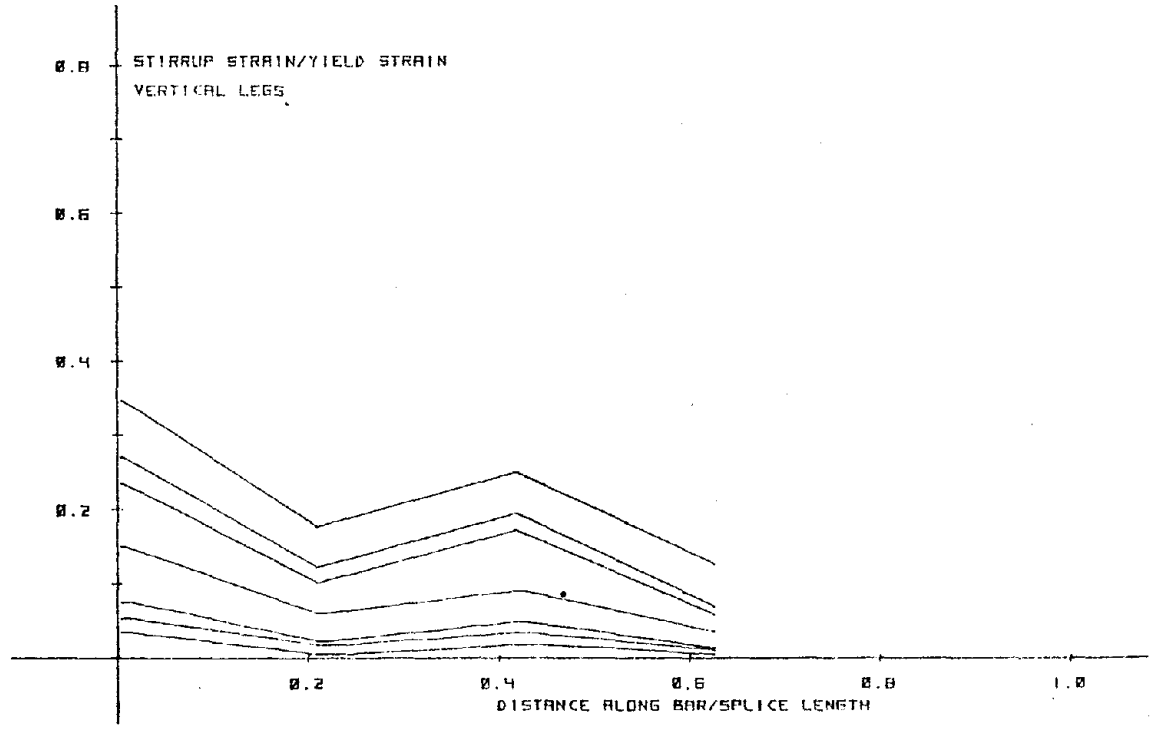

Fig. 3.20d. Stirrup strains - Specimen C-13.

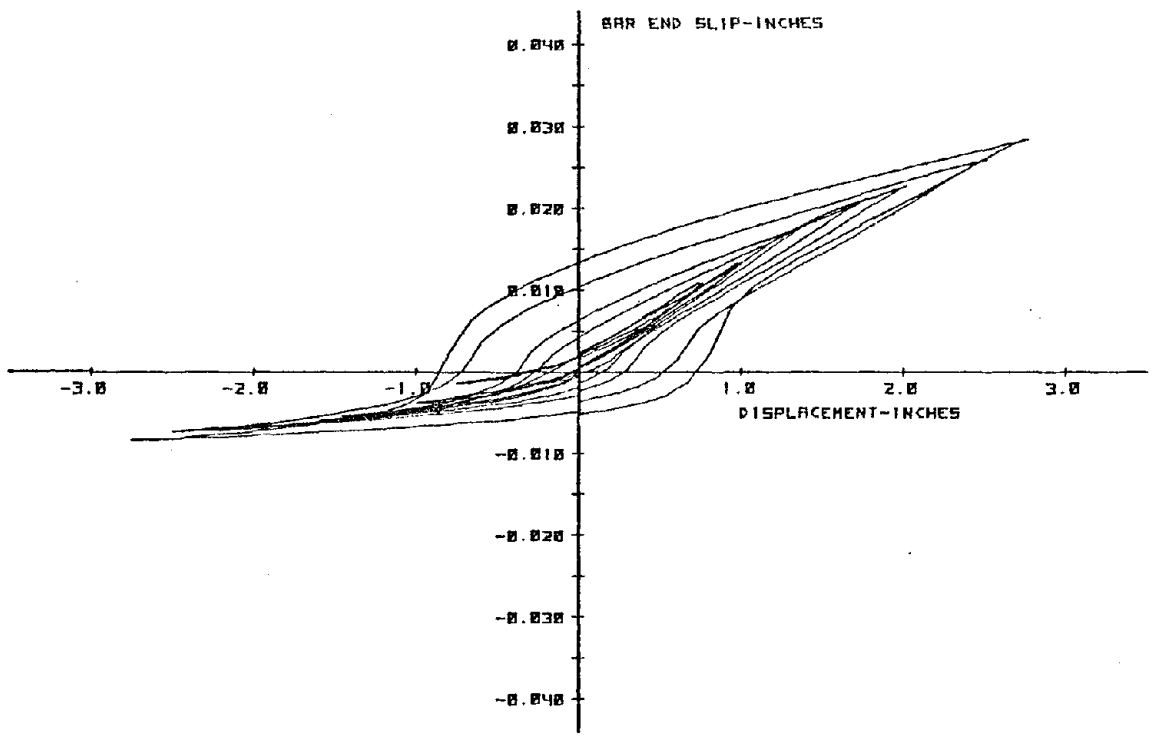

Fig. 3.20e. Bar slip - displacement relationship - Specimen C-13.

3.7.14 Test C-14

Jack Displacement		No. of Cycles	Cycles Plotted
Inches	Δ/Δ_y		
0.5	0.4	12	first
0.75	0.63	12	first
1.00	0.83	12	first
1.45	1.21	12	first
1.75	1.46	12	first
2.00	1.66	12	first
2.50	2.08	6	——

*Max recorded value, actual value higher.

K_b = 1760
S = 5.0 in. c/c.
S_o = 3.0 in. c/c.
L_s = 24 in. (30 d_b)
C = 1.2 in. (1.6 d_b)
f_y = 60 ksi
f'_c = 3.52 ksi
N = 78
N_y = 40
$(\Delta/\Delta_y)_{max}$ = 1.87
$(\varepsilon/\varepsilon_y)_{max}$ = 5.30*
$(\varepsilon_{st}/\varepsilon_y)_{max}$ = 0.48 (Vert. Leg)
Splice Plane: Vertical

Observations

C-14 was conducted in an attempt to investigate the end bearing effect of splices lapped in the vertical plane. Styrofoam plugs were attached to the ends of the spliced bars to eliminate end bearing effects. Splice details and load history were otherwise identical to those of Test C-8. The extent of transverse cracking at low displacement levels was less than in Tests C-11 and C-12. Deterioration at the high moment end was limited. The splice bars first attained yield at $\Delta = 1.2$" displacement. Cycling at $\Delta = 1.45$" lead to the development of side cover splitting at the bottom half of the specimen. At$\Delta = 1.77$", the rate of cover damage at the bottom face and sides increased sharply. Continued cycling lead to the complete propagation of the bottom splitting cracks and the first cycle at $\Delta = 2.00$" indicated failure in the downward direction. The extent of splitting was much less on the top half. A

yield penetration of about 0.25 ℓ_s was attained at failure. Stirrup strains were, in general, low until the failure stage where the first stirrup vertical leg had a strain of 0.48 ε_y.

The bar slip measurement transducer was attached to the end of a top splice bar. It did not record high slips in the compression stroke despite the absence of end bearing. However, splitting along the top face progressed only up to the second stirrup.

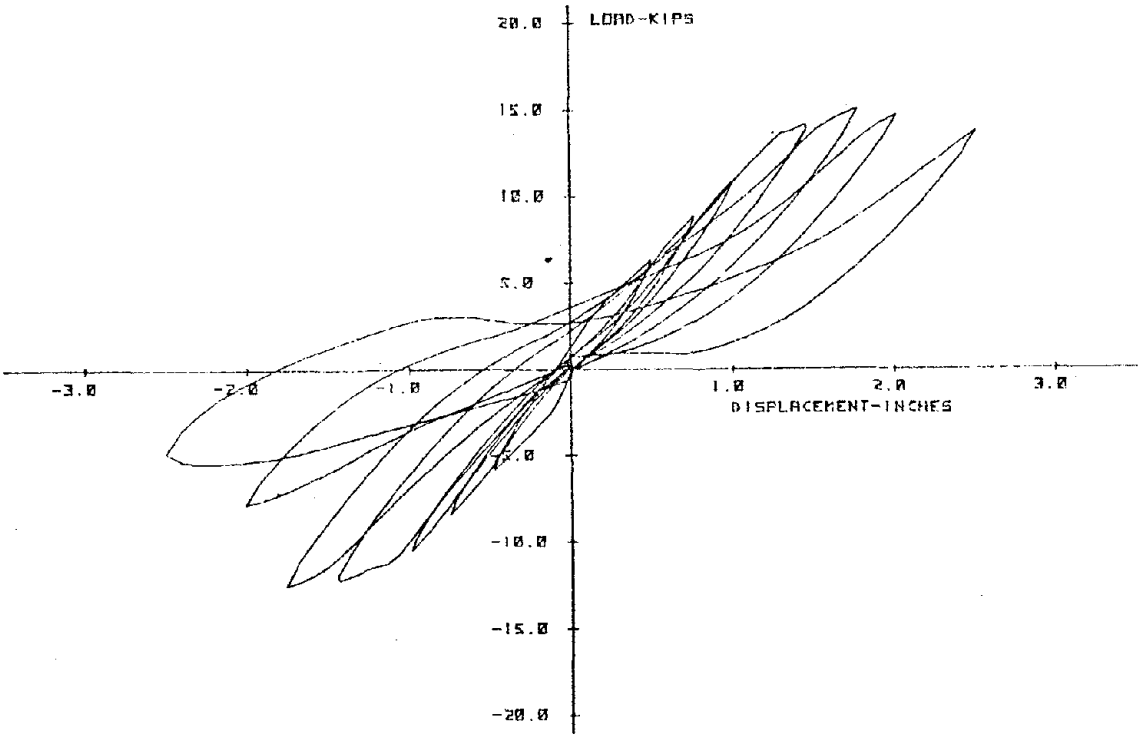

Fig. 3.21a. Load-displacement relationship - Specimen C-14.

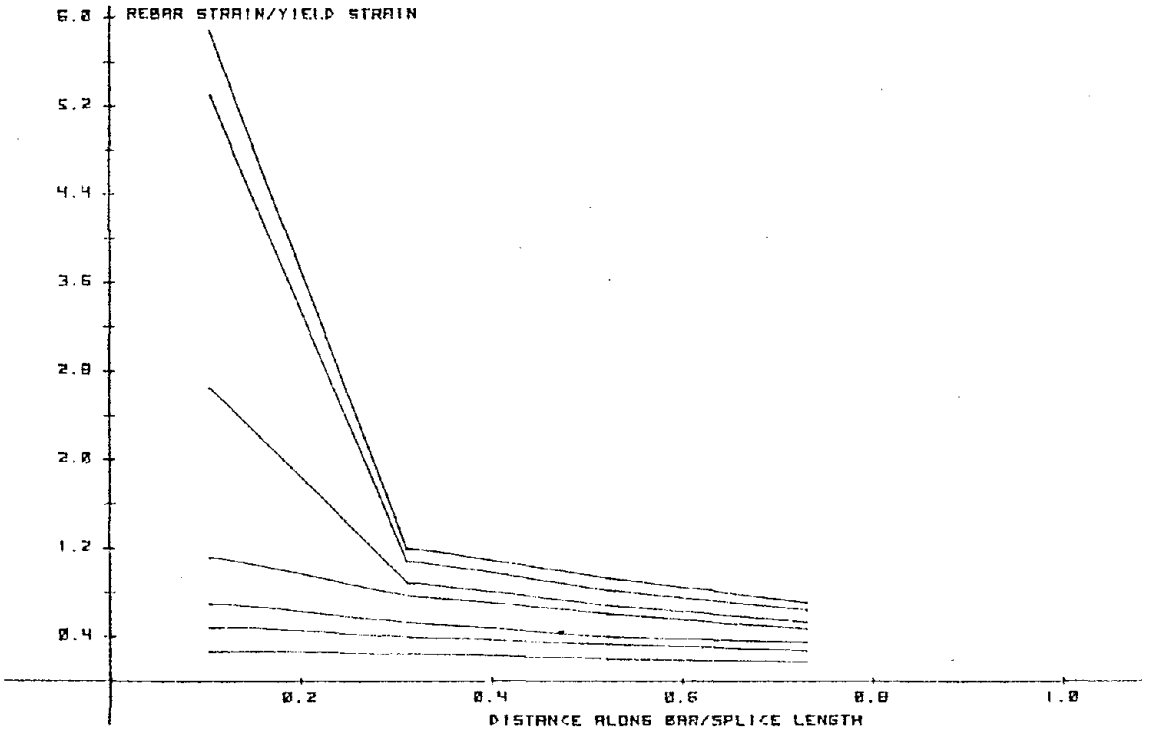

Fig. 3.21b. Main reinforcement strains - Specimen C-14.

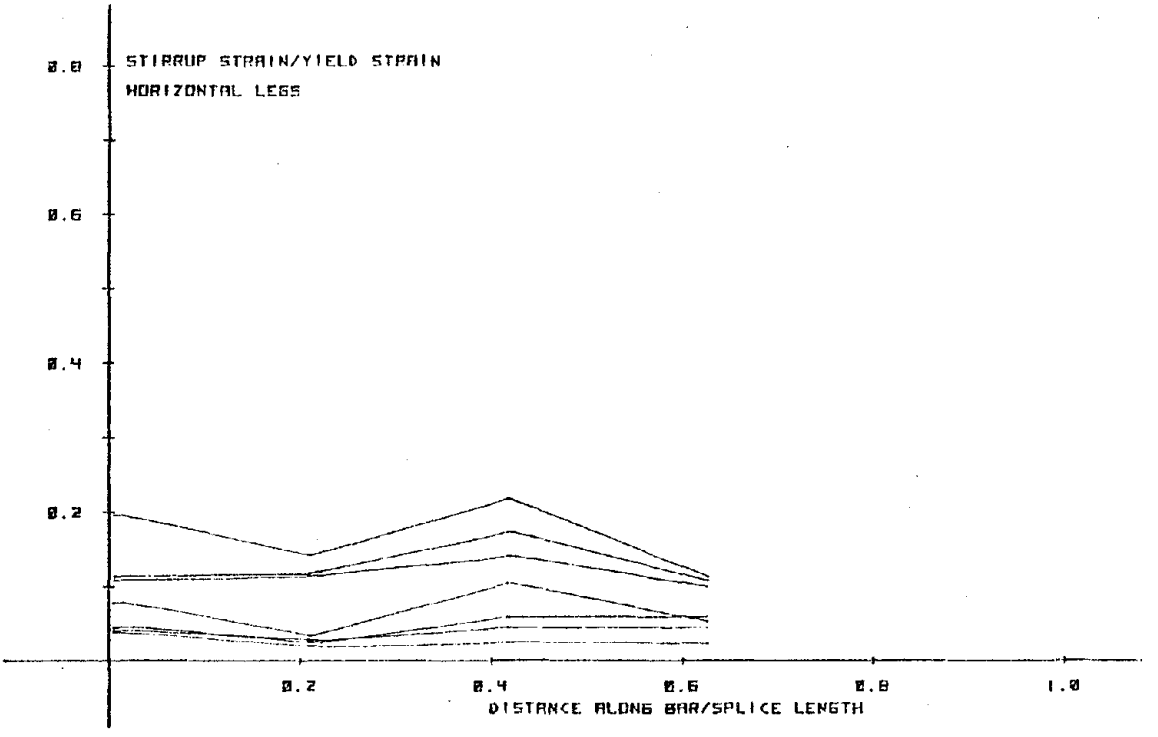

Fig. 3.21c. Stirrup strains - Specimen C-14.

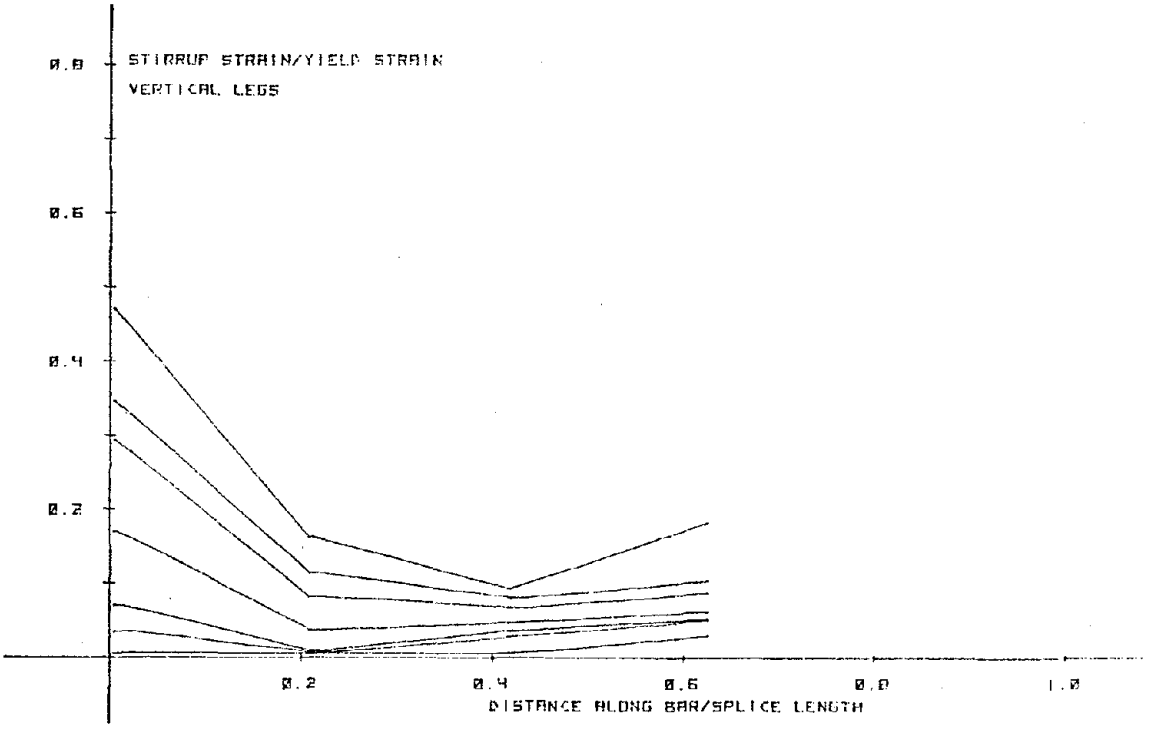

Fig. 3.21d. Stirrup strains - Specimen C-14.

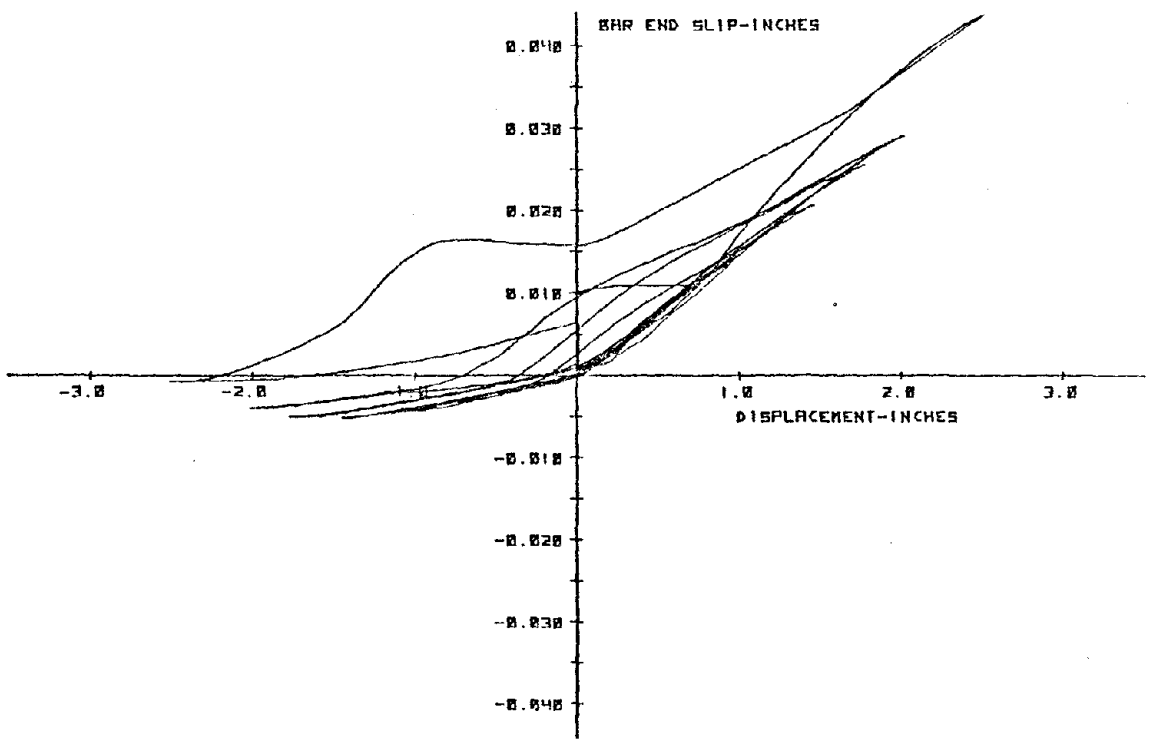

Fig. 3.21e. Bar slip - displacement relationship - Specimen C-14.

CHAPTER 4

DISCUSSION OF EXPERIMENTAL RESULTS

4.1 Introduction

The results of tests on fourteen column splice specimens were presented in Chapter 3. The following discussion of these test results is done in terms of a study of the factors influencing splice behavior under cyclic loads. In each case, relevant tests are discussed and compared with one another in an effort to develop a fundamental understanding of a particular aspect of overall behavior. Comparisons with previous investigations are made where applicable. An explanation of the discrepancies of certain tests is also attempted. Load history, bond-shear interaction, and transverse reinforcement are the main factors influencing splice behavior. Stiffness deterioration, energy absorption, bar strain variation and bar end slip characteristics are discussed as some of the effects of inelastic cyclic loads on spliced members.

4.2 Load-Displacement Relationship

Cyclic loading in reinforced concrete typically results in nonlinear load-displacement characteristics as a consequence of cracking, bar slippage, and bar yield. In this series of tests, plots of the load-displacement relationship at the location of the hydraulic jack were seen to be hysteretic in nature. The area enclosed within these curves is a measure of the energy absorbed by the load resisting system due to the factors mentioned above. In any plot, a comparison of the curves from an early part of the test with those at or near failure shows a gradual increase in the areas enclosed, implying a progressively larger

extent of irrecoverable deterioration. This is accompanied by a loss in stiffness as indicated by the slopes of the curves.

Fig. 4.1 shows the load-displacement relationship at three different stages of reversed cycling at $\Delta = 1.3\Delta_y$ for specimen C-12. It can be seen that specimen deterioration (given by the area enclosed by a curve) produced during the first cycle at this level is greater than that in subsequent cycles. Also, the difference in peak load attained during cycle 1 and cycle 23 is a measure of stiffness reduction. These observations are based on the results of specimen C-12, and although valid in an overall sense for other specimens as well, individual differences can arise on account of differences in the length and orientation of splices, the extent of hoop reinforcement, and concrete strength. These effects are discussed in Section 4.4.

Since all tests were run in a displacement controlled mode, the failure stage was defined as that point during a test when an increase in displacement resulted in a decrease in the corresponding load. This is illustrated in Fig. 4.2 which is a plot of the peak load vs. the peak displacement at different levels of displacement for some typical specimens. In each case the load corresponding to the highest displacement level is seen to be at or beyond the turning point of the curve, indicating the load shedding tendency and hence, failure. The remaining portion of this section aims at rationalizing some of the discrepancies apparent from a comparison of the $P - \Delta$ relationships for all the tests.

Specimens C-5 and C-6 attained a maximum displacement ductility level of about 1.67 and sustained about 28 cycles above yield. However, specimen C-7, which was reinforced identically, sustained 41 cycles beyond yield and reached a maximum displacement ductility of 1.84.

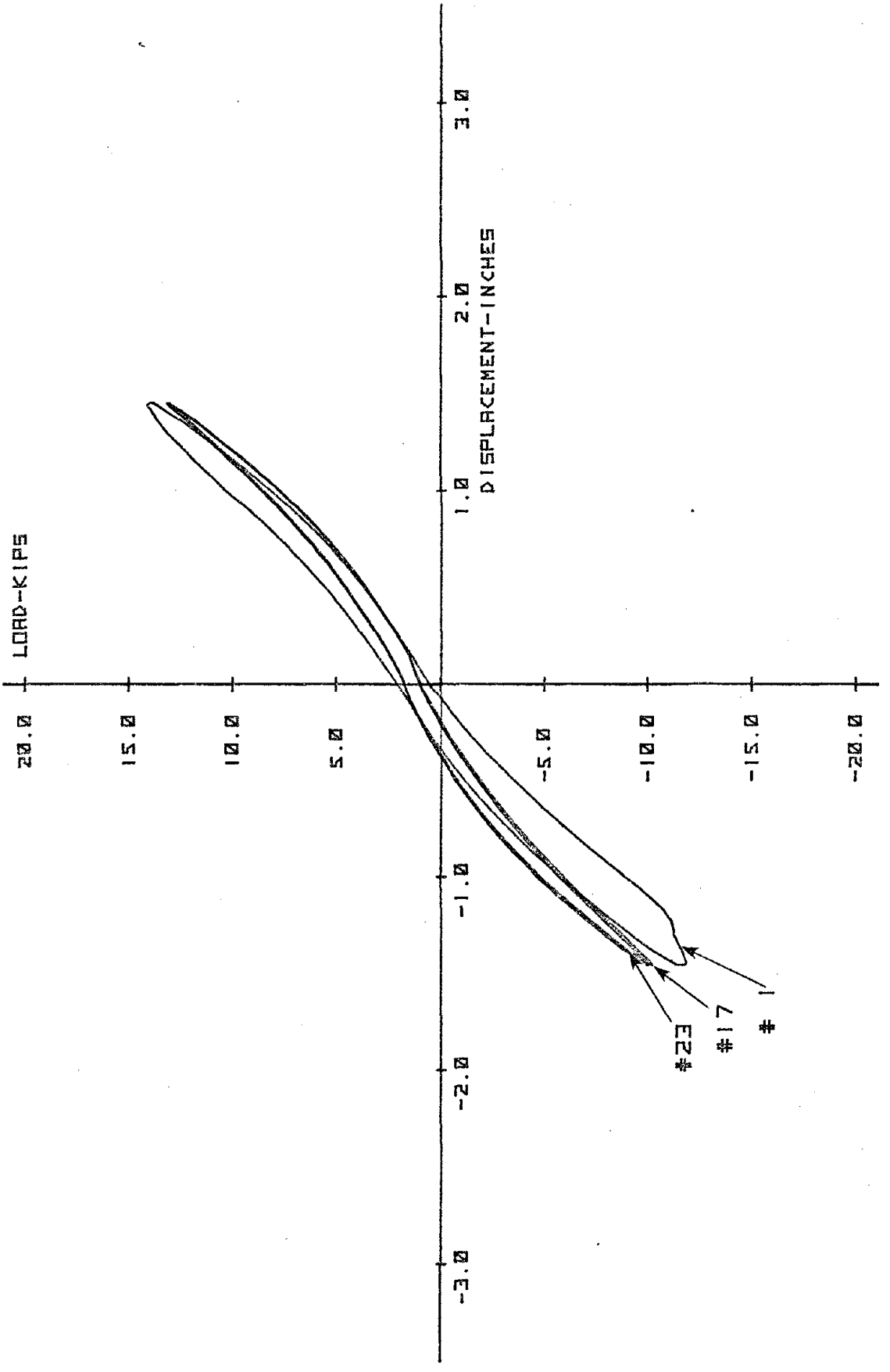

Fig. 4.1. Load-Displacement relationship for C-12 at $1.3\Delta_y$.

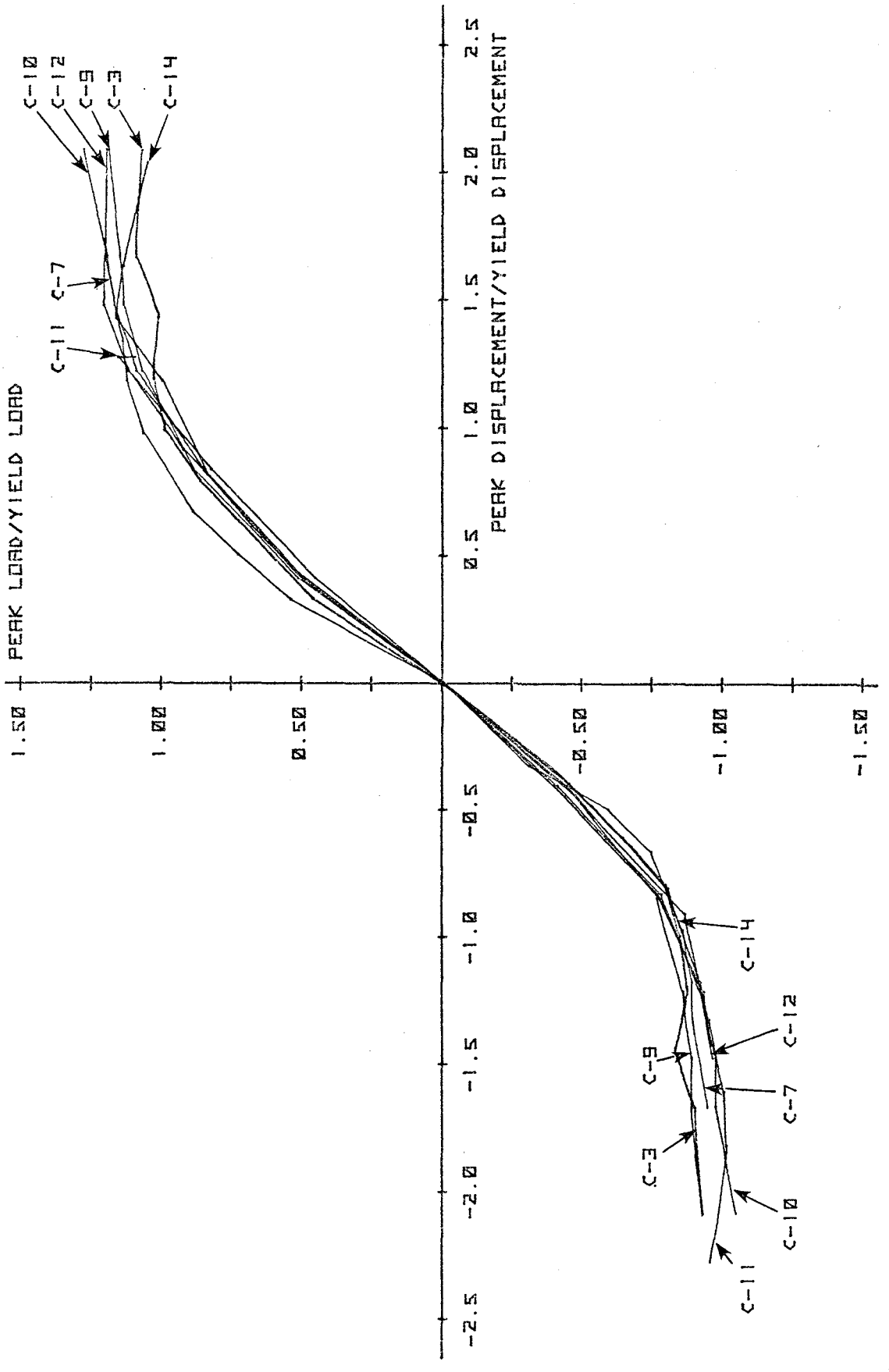

Fig. 4.2. Peak Load - Peak Displacement relationship. Plotted points correspond to first cycle at each level.

This difference in the number of cycles sustained appears to be largely a result of the difference in concrete strength of the two specimens (f'_c = 2.9 ksi for C-5 and C-6, f'_c = 3.47 ksi for C-7). The low concrete resistance in C-5 and C-6 lead to easy concrete cover splitting, particularly at the bottom splices, and resulted in premature failure. It might be argued that a meaningful comparison of tests C-5 or C-6 with C-7 is affected by the fact that their loading histories were different (Section 3.7). However, research (Townsend and Hanson 1977) indicates that cycling at a low displacement level, especially below yield, does not have any significant effect on the load carrying capacity at higher levels. Hence, it is unlikely that differences in load history could have had a major influence on the overall performance of these three tests.

The variables investigated in C-9, C-10, C-11, and C-12 were stirrup spacing and splice orientation. In C-9 and C-11, the bars of each splice were set side by side (horizontally spliced). In C-10 and C-12, they were arranged one above the other, thus forming a vertically lapped splice. Stirrups over the splice were more closely spaced in C-9 and C-10 than in C-11 and C-12. A comparison of C-9 with C-11 and C-10 with C-12 shows large differences in energy absorption capacities and also in ultimate failure modes (Section 3.7). This introduces the question regarding the effect of different failure modes on post-yield splice behavior and is described in Section 4.12.

In examining the behavior of C-11 and C-12, it can be seen that the downstroke displacement ductility of C-12 was considerably less than that of C-11 despite identical concrete strengths. A comparison of C-9 (horizontally spliced bars) with C-10 (vertically spliced bars) shows

no such effect, suggesting that this is not on account of the splice orientation difference. A possible explanation is as follows. Since the upstroke peak in C-11 was limited to 1.4" (due to problems encountered with the MTS hydraulic loading system), the compressive force experienced by the bottom splice bars in any cycle was less than in C-12. This resulted in correspondingly less bottom splice deterioration due to bar end bearing and radial bursting stresses for specimen C-11, and consequently, it exhibited better load carrying characteristics in the downstroke than C-12. It is possible that this disparity is particularly obvious for bottom splice bars due to concrete density variation.

In all the tests, the peak loads in the downward stroke were smaller than those in the upward stroke for any given cycle. The lower stiffness in the downward direction is attributed to the following.

(1) A smaller bottom cover than top cover (due to tolerances in fabrication) resulted in more rapid cover deterioration at the bottom.

(2) Since the specimens were cast horizontally, concrete situated near the bottom was of higher density than at the top. Before testing, each specimen was inverted so that the dense layer became the top surface. The bottom splices, being situated in a weaker concrete matrix, failed before the top splices did. This behavior was observed in all the bond failure tests. In practice, where columns are cast vertically, such a situation is not likely to arise. With this in mind, all displacement ductilities were determined on the basis of the upstroke (+) load shedding characteristics alone.

4.3 Energy Absorption

In seismic resistant design, much effort is directed towards designing elements with large energy absorption capabilities. The fact

that this capacity is closely related to the extent of yield in the main reinforcement is well illustrated in Fig. 4.3, the non-dimensionalized plot of energy absorbed vs. displacement level. The first quantity is defined as the area within the upstroke half cycle of a load-displacement hysteresis loop. This figure compares the relationship for several specimens. An exact numerical comparison of specific cases is difficult to make, since individual variations result on account of differences in the splice design (splice length, amount of transverse reinforcement, concrete strength, etc.). However, a definite increase in the rate of energy absorption at and above the yield displacement level is evident in each of these cases, and the generality of this observation is unaffected by the individual differences listed above.

Fig. 4.1 showed the load-displacement hysteresis curves for Specimen C-12 during the 1st, 17th, and 23rd cycles at a level of $1.3\Delta_y$. The area of the loop at cycle 17 is significantly less than that at cycle 1. However, the areas enclosed by the curves at cycles 17 and 23 are practically the same. This suggests a reduction in the rate of decrease of energy absorption with continued cycling. Ismail (1970) has shown that this behavior is typical of reinforced concrete members cycled at post-yield levels. In other words, unlike low displacement levels where concrete deterioration tends to stabilize after prolonged cycling at a fixed level (indicated by smaller and smaller sized hysteresis loops), cycling at post-yield stages does not lead to a stable condition, and the damage produced is a direct function of the total number of cycles at that level.

Actual behavior is strongly dependent on the type of loading history used. For instance, the load-displacement relationship of a

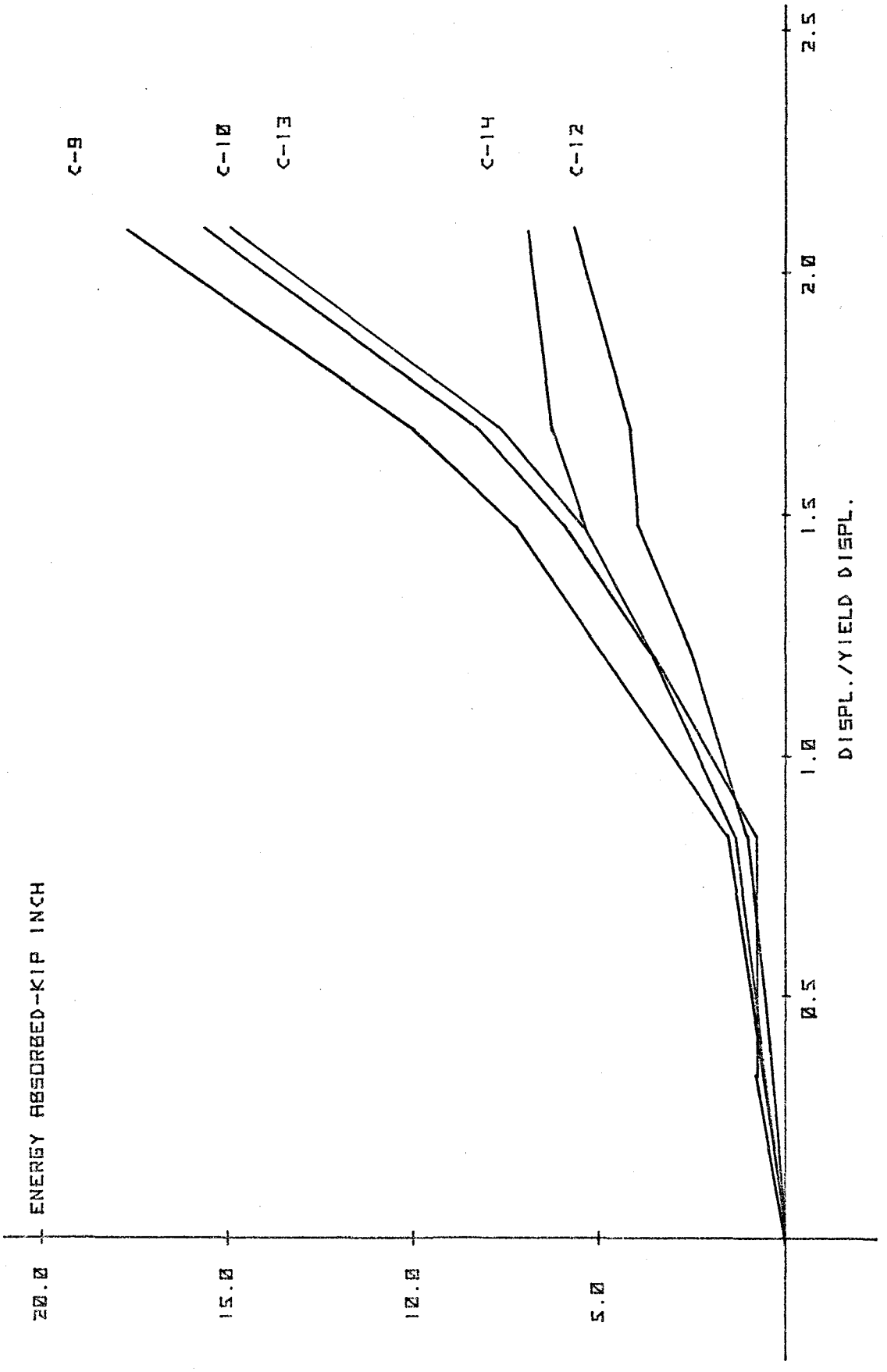

Fig. 4.3. Energy absorbed - Displ. level relationship. Plotted points correspond to first cycle at each level.

specimen subjected to a loading such as in Fig. 4.4a would consist of progressively larger hysteresis curves. The behavior of specimens in this investigation are more typical of the loading shown in Fig. 4.4b.

4.4 Stiffness Reduction

The degradation of the lateral stiffness of a specimen due to reversed cycling at progressively higher displacement levels (as in Fig. 4.4b) is depicted in Fig. 4.5 and Fig. 4.6, where the instantaneous stiffness at the section located under the hydraulic actuator is plotted against applied displacement. These curves are drawn from the data of Tests C-9 and C-12. Each curve represents one complete half cycle from the peak negative displacement (point A in figures) to the peak positive displacement (point B in figures). The following observations are based on these relationships.

The stiffness at zero displacement consistently decreases with reversed cycling. This effect is more pronounced at higher displacement levels. The exact variation is load history dependent and is less for specimens confined by closely spaced stirrups. Nevertheless, reduction in stiffness is probably the most fundamental manifestation of cyclic loading.

The stiffness at any point during the unloading quarter cycle (from A to C) is higher than the corresponding stiffness during the loading quarter cycle (from C to B). This is merely a consequence of the hysteretic nature of the load-displacement curves, whereby the energy provided in attaining a certain load level is greater than that released in returning to the zero load level. As mentioned in Section 4.2, this energy difference represents the amount absorbed by the system. The different paths followed by the load-displacement curve

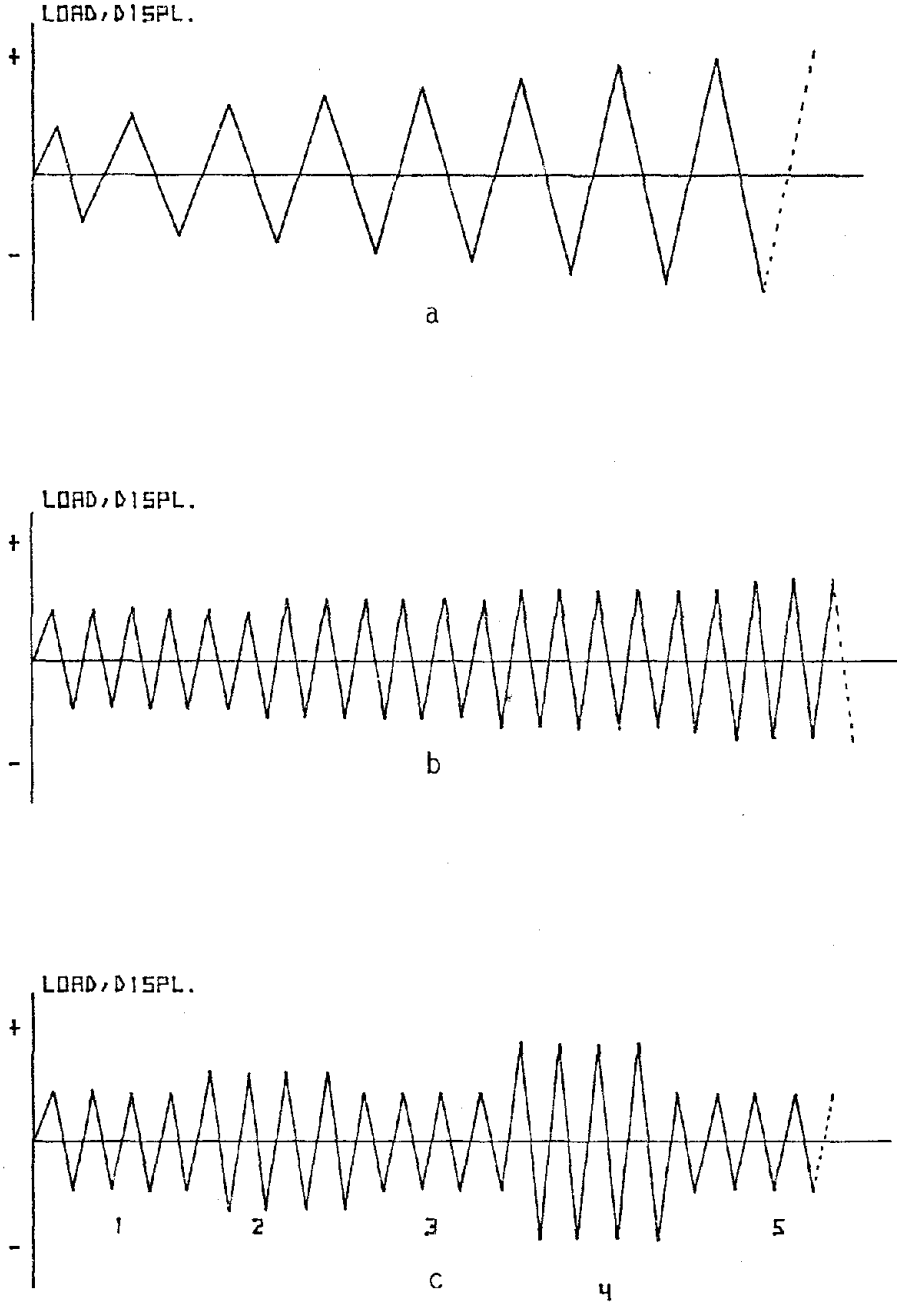

Fig. 4.4. Different loading histories.

during the loading and unloading process results in the unsymmetric nature of the stiffness diagrams.

At a given ductility level (except the very first), a significant drop in stiffness during the loading quarter cycle occurs only when the displacement level exceeds that of the previous cycle. At displacements lower than the peak of the previous cycle, the reinforcement deformations merely bear against concrete wedges crushed and compacted during the preceeding cycle with no additional crushing or cracking taking place. Under these conditions, stiffness increases with displacement. However, beyond the peak of the previous cycle additional concrete and bond deterioration takes place resulting in a sudden reduction in the stiffness contribution due to surrounding concrete. This explains the abrupt stiffness drop evident in Fig. 4.5 and Fig. 4.6. It is interesting to observe that the loading quarter cycle during the very first cycle shows decreasing stiffness right up to the peak displacement at that level in both figures. This is obviously because during this cycle, bond deterioration occurs right from zero displacement up to the peak displacement level. The above observations are consistent with those made by Hassan and Hawkins (1977), that for any particular half cycle, additional bond deterioration takes place if its maximum ductility ratio is greater than or at least equal to that of the preceding cycle.

At low ductility levels (below yield), the stiffness at zero displacement attains a local minimum value. However, after the reinforcing bars yield, the stiffness tends to attain a somewhat constant value during loading from the zero deflection point up to the peak deflection point attained during the preceding cycle. This is probably due to the large inelastic extension of the yielded portion of the spliced

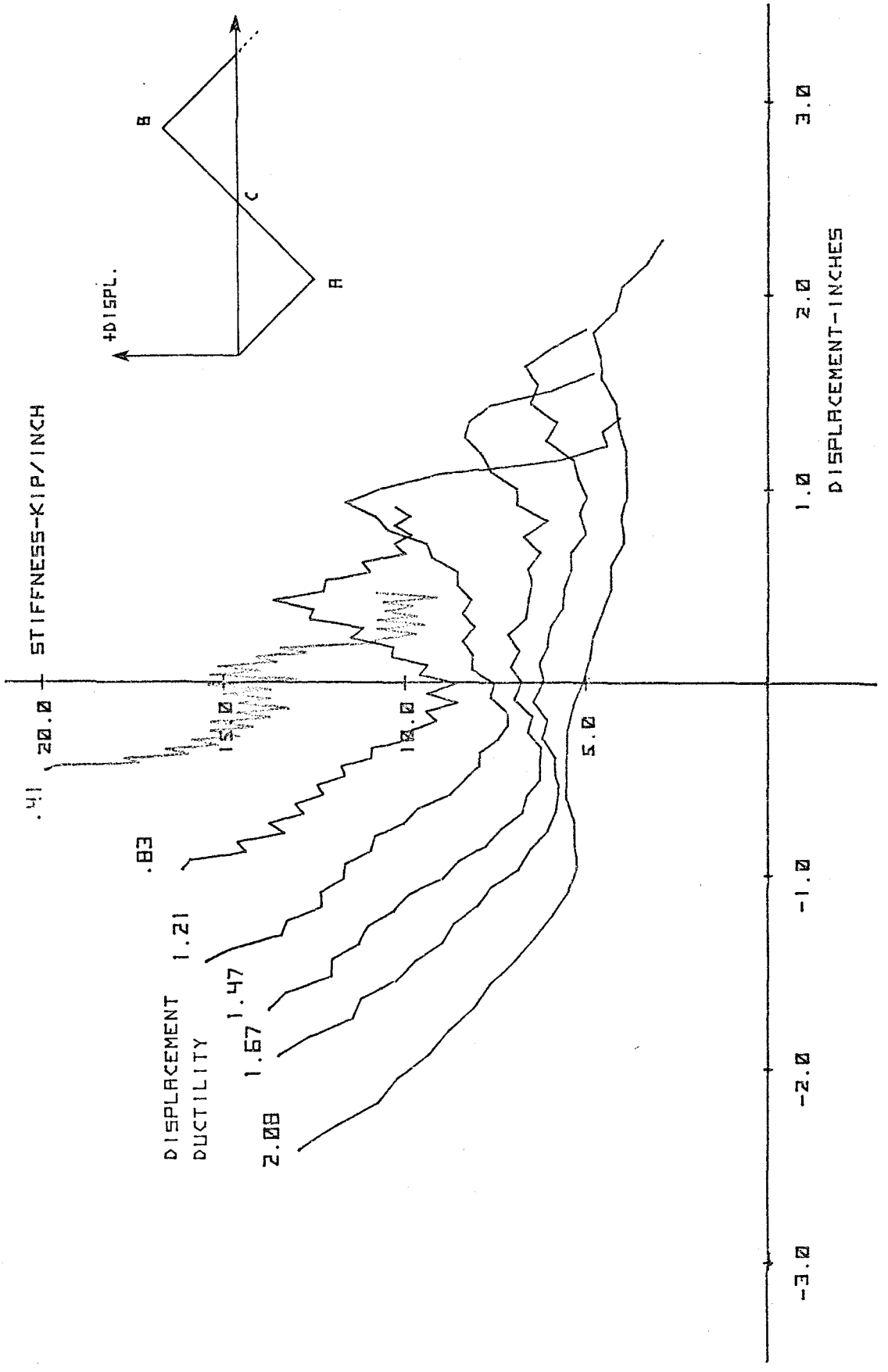

Fig. 4.5. Stiffness - Displacement relationship for Specimen C-9. Plotted curves correspond to the first cycle at each ductility level.

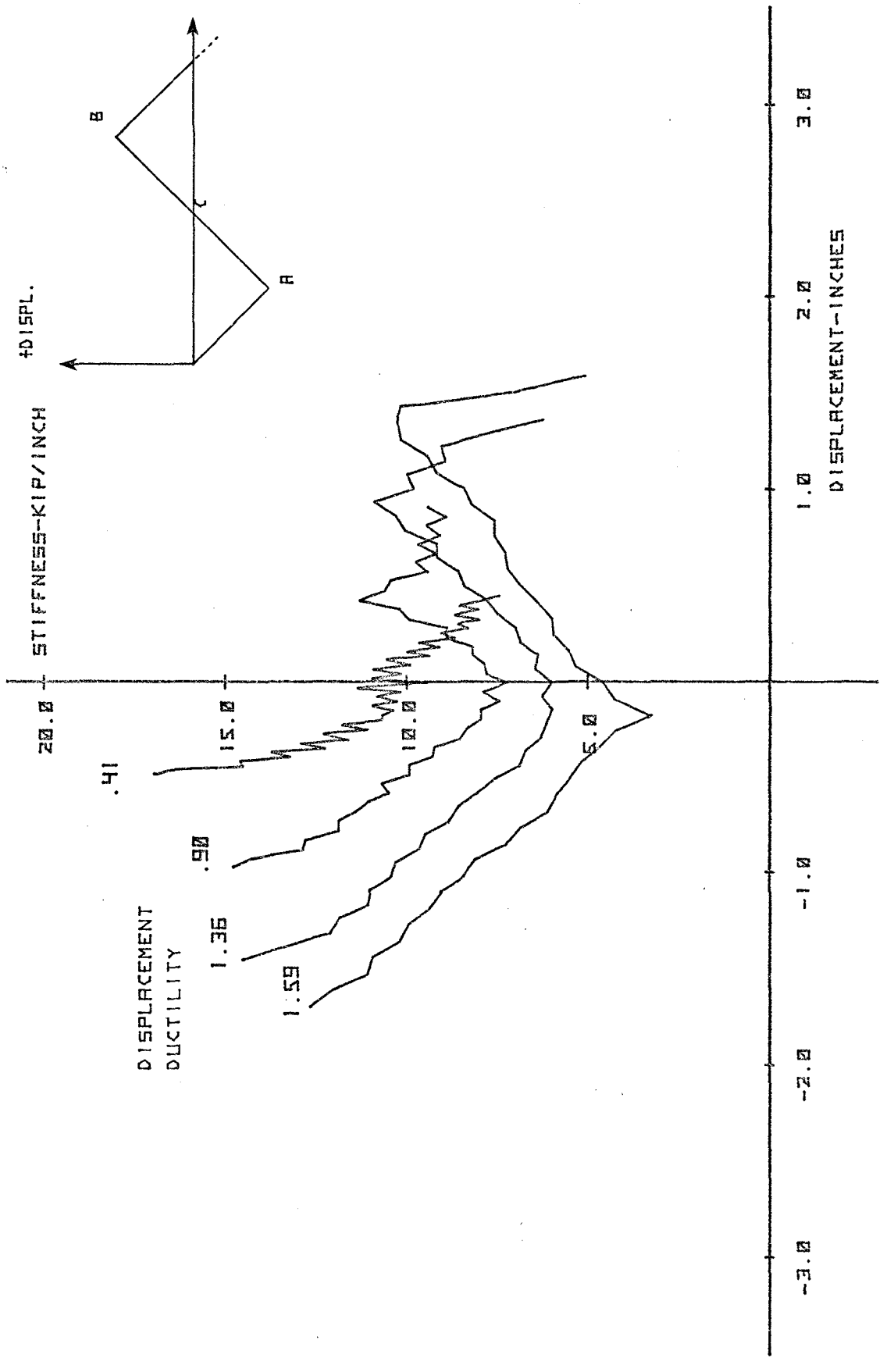

Fig. 4.6. Stiffness - Displacement relationship for Specimen C-12. Plotted points correspond to the first cycle at each ductility level.

bars. The effect is partially restrained by the steel strain hardening effect and by the bearing action of the deformation lugs on surrounding concrete. However, with additional cycling, the surrounding concrete undergoes greater damage and is therefore less efficient in controlling bar elongation. This effect is more obvious in Specimen C-9 (Fig. 4.5) than in Specimen C-12 (Fig. 4.6) because of the higher bar strain levels attained in C-9.

Fig. 4.7 plots the stiffness variation at different cycles during the testing of Specimen C-12. Load-displacement hysteresis curves were plotted for these cycles in Fig. 4.1. Comparing the two figures, it is evident that a loss in energy absorption capacity is accompanied by a degradation in stiffness.

On the practical side, these observations show that it may sometimes be unconservative to design members in seismic regions from initial stiffness considerations alone. In addition to the above, the stiffness characteristics of individual specimens are affected by the following factors.

(1) Splice length: Specimens with long splices have a higher steel ratio (ρ) over a greater portion of their length than those with short splices. Longer splices should therefore result in larger lateral stiffnesses.

(2) Transverse reinforcement: Transverse reinforcement is effective in confining the concrete core particularly at high displacement levels where the extent of concrete cracking is significant. The load carrying capacity of the core improves directly with the amount of confinement provided. Hence, stiffness characteristics can be improved by adopting a small spacing between the stirrups surrounding a splice.

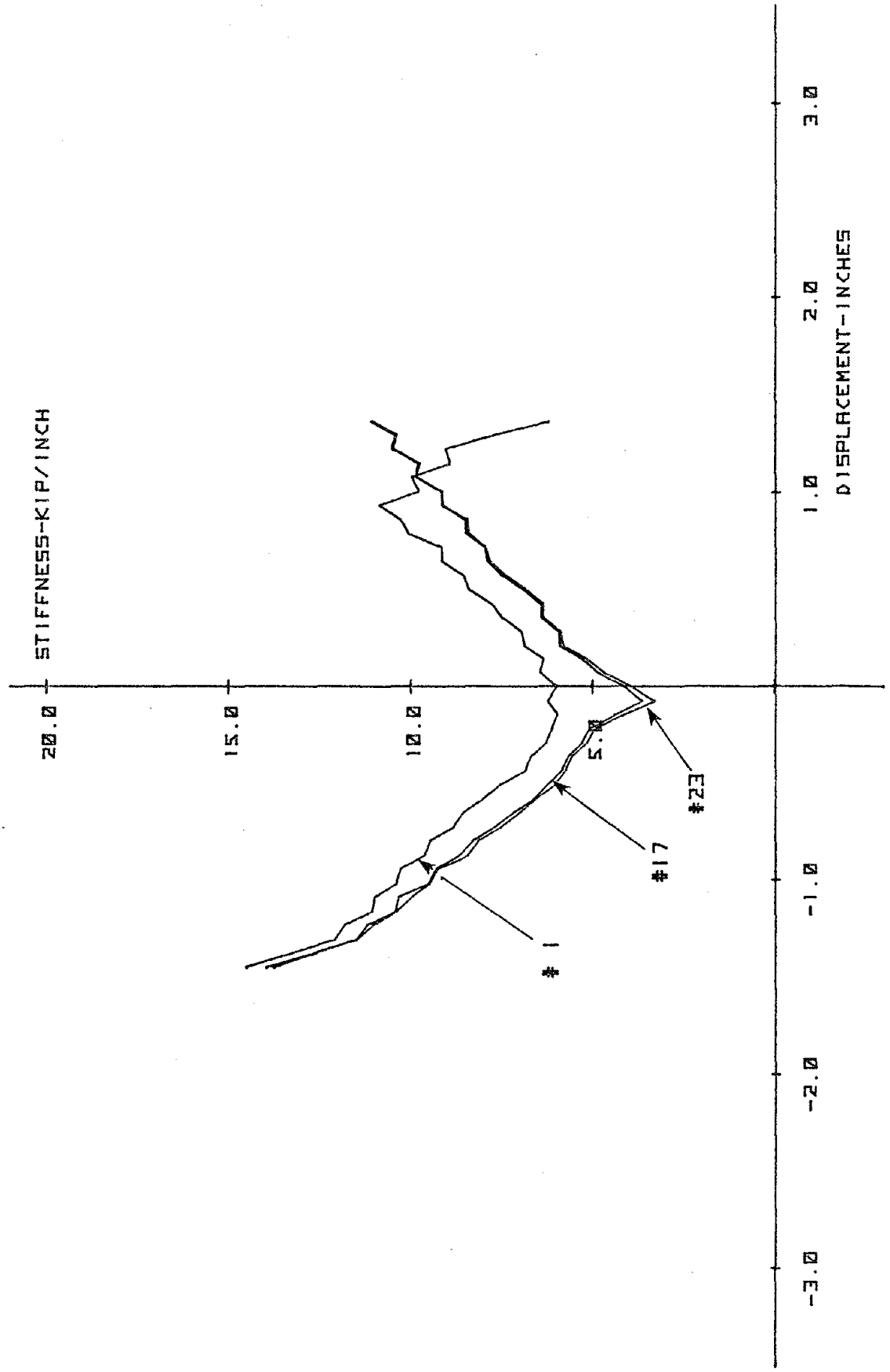

Fig. 4.7. Stiffness-Displacement relationship for specimen C-12 at $1.3\Delta_y$.

(3) Splice orientation: Splices lapped in the vertical plane have a smaller effective depth 'd' than corresponding splices lapped horizontally. For a given moment, this will result in higher average bar stresses in the vertically lapped splice. This is of little consequence at low displacement levels. At higher levels, the bars in the vertical splice will attain yield before those in the horizontal splice, resulting in lower stiffnesses.

(4) Loading history: The exact nature of stiffness degradation is perhaps most dependent on the kind of load or displacement history applied. Fig. 4.7, Fig. 4.5, and Fig. 4.6 are applicable only for a displacement history of the type shown in Fig. 4.4b. Stiffness variations for displacement histories such as in Fig. 4.4a and Fig. 4.4c would be different. For that in Fig. 4.4c, the stiffness at any portion of a cycle would show considerable variation at stages 1, 3, and 5, since research (Townsend and Hanson 1977) shows that cycling at a high displacement level such as stage 4 greatly reduces stiffness at subsequent low levels (such as stage 5) below that at stage 3.

(5) Concrete strength: Higher strength concretes undergo less splice deterioration at any displacement level and thereby attain higher stiffnesses.

4.5 Main Bar Strain Variation

Choosing Specimens C-10 and C-14 as examples, the strain variation along the spliced bars is plotted at various displacement levels in Fig. 4.8. It can be seen that strains at each displacement level are considerably higher in the tensile half cycle than in the compressive half. This is because in the latter case, force transfer occurs by direct concrete compression and by bar end bearing on concrete in addition to

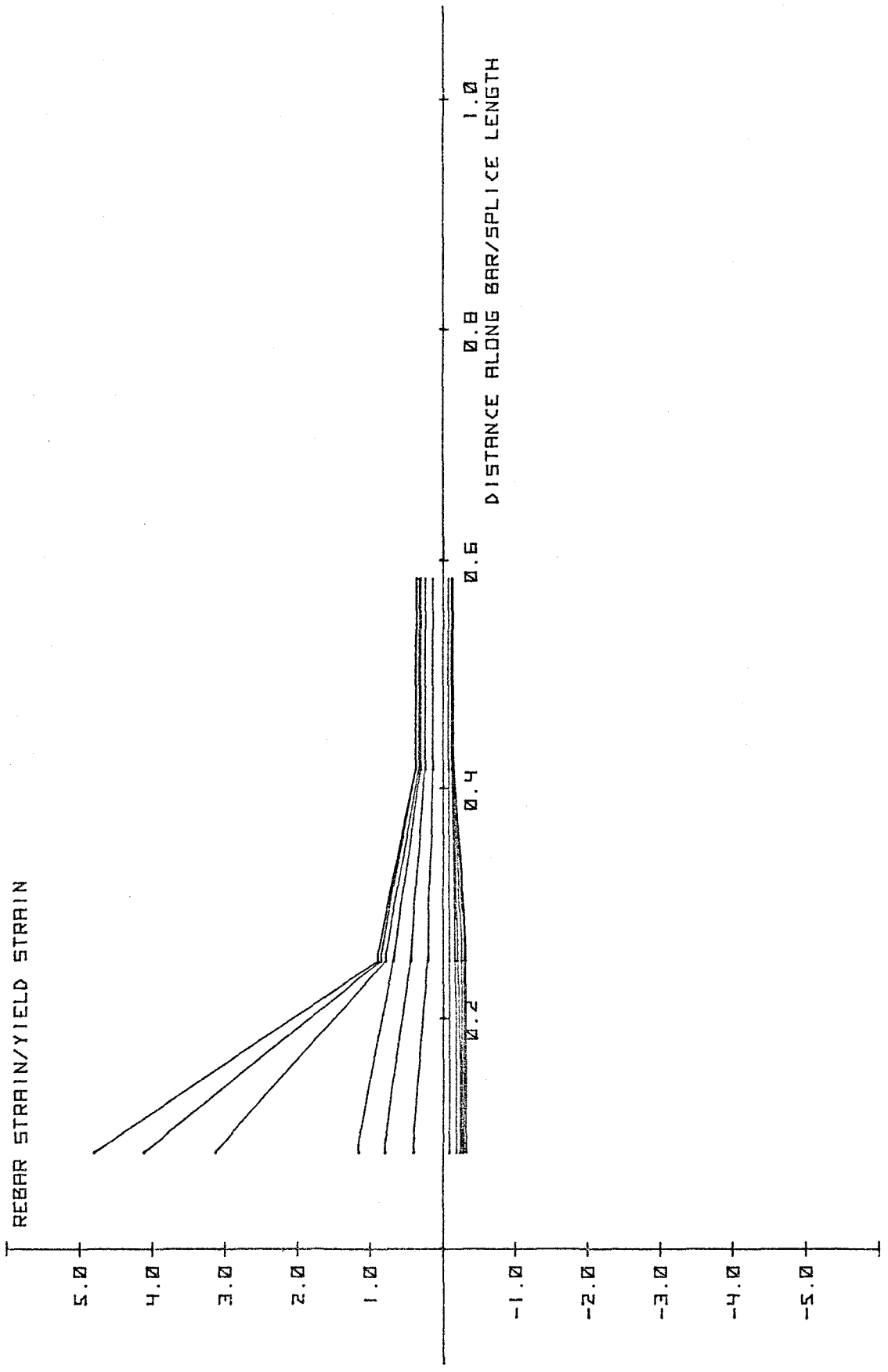

Fig. 4.8a. Tensile and compressive strains along a spliced bar of specimen C-10 at various displacement levels.

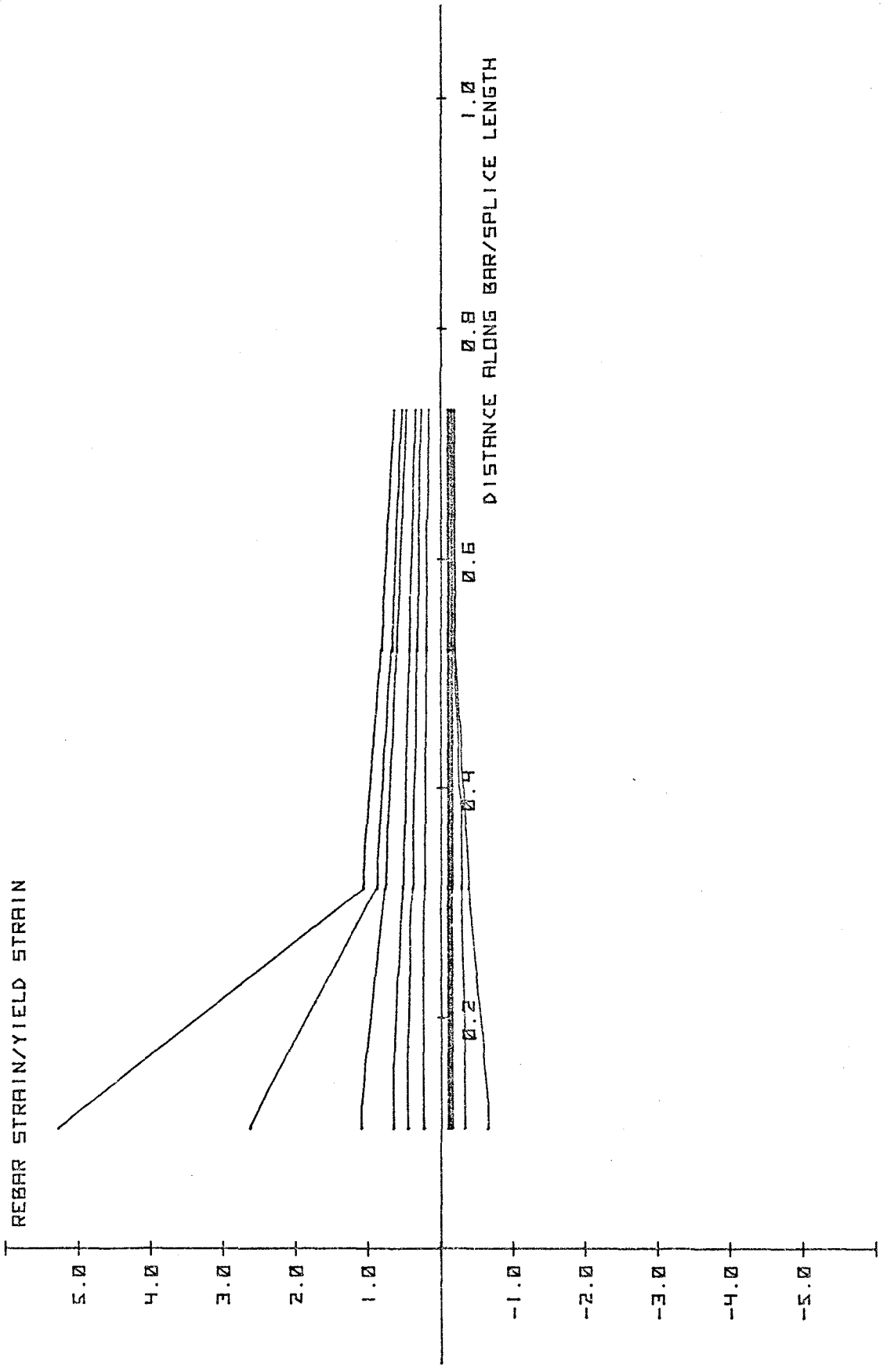

Fig. 4.8b. Tensile and compressive strains along a spliced bar of specimen C-14 at various displacement levels.

bond between the reinforcing bars and surrounding concrete. During the tensile half cycle, all force transfer occurs as a result of bond force, thus resulting in higher bar stresses. Bond stresses, being proportional to the slope of the strain diagram, are also seen to be less in the compressive half cycle. One implication of this is that the mode of failure of a compression splice is different from that of a tension splice (Section 2.13). In this investigation, it is assumed that a well designed tension splice will perform at least as well in compression. However, it should be realized that in real columns, compressive bar strains will tend to be much higher because of creep effects and high direct axial loads. With bending moments, flexural compressive stresses will superimpose on the already existing compression, whereas flexural tension will relieve some of the axial compression. Under these circumstances, the compression splice strength can well become the critical factor. This point is further discussed in Section 4.11.

Certain investigators (Fagundo 1979, Bresler and Bertero 1968) have pointed out that the extent of irrecoverable damage due to cyclic loading increases sharply beyond the stage at which the main reinforcing bars yield. Fig. 4.9 plots the ratio of residual bar strain at zero displacement to the corresponding peak strain at peak displacement at various displacement levels for some typical specimens. The sudden increase in residual strain at and above yield displacement in all these cases is in good agreement with the above observation.

Cairns and Arthur (1979) state that a longer splice length leads to the lowering of average bond stresses. This suggests that if two specimens of different splice lengths are subjected to identical load histories, the longer splices will be less strained than the shorter

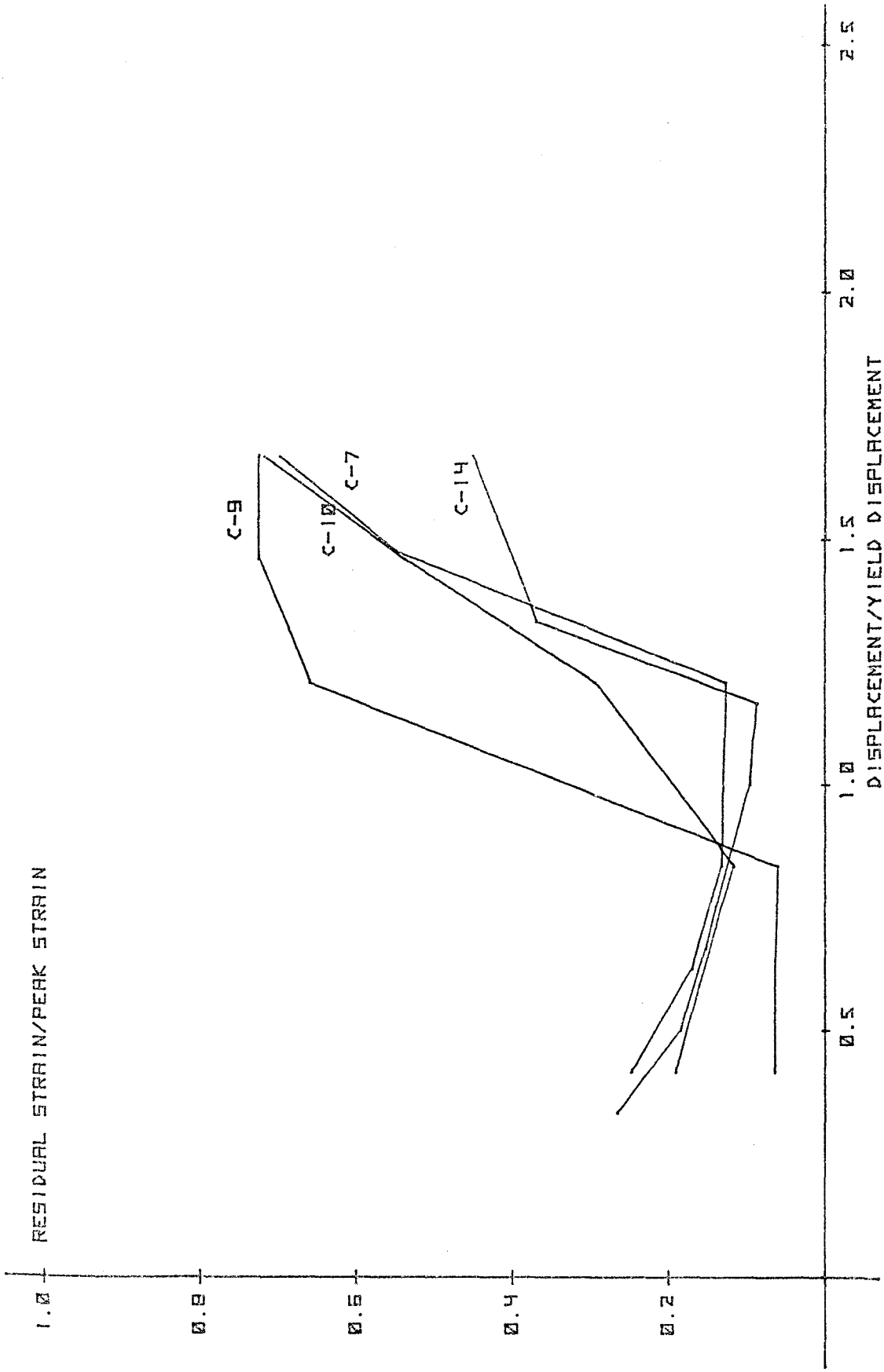

Fig. 4.9. Residual strains at various displacement levels.

ones at any load level.

4.6 Transverse Reinforcement

The amount and distribution of transverse reinforcement is crucial in the design of ductile lapped splices subjected to cycles of inelastic loading. A splice with too little transverse reinforcement could fail due to yield in the transverse steel. A splice having the required amount of steel improperly distributed is characterized by low stirrup strains at failure. The column splice tests utilized closed loop stirrups with the splices situated at the four corners. The advantage of this layout is that potential planes of cover splitting on the face and side are traversed by transverse steel. Design equations developed during the early phase of this investigation (Section 2.11) reflect the fact that splices under reversed cyclic loading require a larger amount of transverse reinforcement than when subjected to monotonic loads. These equations were used in the design of the column splice specimens.

Stirrup strains give an indication of the extent to which the interior core is confined. Radial bursting forces generated by the splice bars are resisted by the stirrup legs and a large strain indicates an effective utilization of transverse steel. In addition, shear and bar dowel forces are also resisted by the vertical legs. Since the column splice test results show that stirrup strains were always well below yield, it is reasonable to infer that for these tests the confining capacity determined by the distribution (rather than total amount) of transverse steel is of importance. This is in agreement with the fact that, within limits, smaller closely spaced stirrups are preferable to larger, widely spaced ones as shown experimentally by Tocci (Section 2.7).

The column splice test results show that the strain in the first stirrup vertical leg was always much higher than in other stirrups. This is a consequence of the force exerted by the dowel action of the splice bars at the location of the main transverse crack. The remaining stirrups were all progressively less strained for two reasons. Firstly, the absence of large flexural shear cracks within the splice resulted in effective shear transfer through aggregate interlock. Secondly, the moment gradient gradually reduced bursting stresses along the splice length.

Maximum stirrup strains recorded for all specimens in this investigation were seen to be well below the yield value. A similar trend was observed in the beam type splice specimens tested under reversed cyclic loading (Tocci 1981). However, stirrup strains were considerably higher in the repeated loading tests conducted by Fagundo (1979). It is possible that the explanation to this lies in the force transfer capacity of the concrete cover surrounding the reinforcement. At very low loads, concrete sections remain virtually uncracked, and consequently, the tensile strain in any stirrup is the same as that of the surrounding concrete. Since a stirrup cross-sectional area is much less than the effective area of the surrounding concrete, a large fraction of the total shear and bursting stress is carried directly by concrete in tension. However, once concrete cracking occurs its tensile resistance is drastically reduced and most of the force has then to be resisted by stirrups. Concrete, although ineffective in carrying direct tensile forces at this stage, is effective in transferring forces from the point of load application to the stirrups. It is unlikely that this force transfer mechanism is affected during early stages of cracking. Hence, stirrup forces,

increase with load as long as the cracking extent is not excessive. It is well established that for cyclic loading tests on splices, the extent of concrete deterioration due to flexural shear cracking and bond effects increases on continued cycling and higher load levels. It is conceivable that after considerable cycling, the amount of concrete damage at the core and particularly at the cover might be severe enough to prevent effective force transfer to the stirrups. Besides, damage to the steel-concrete boundary layer will diminish the wedging forces exerted by the bar ribs, resulting in reduced bursting stresses. This suggests that there are three distinct phases in the stirrup strain variation for splices under cyclic loads. At very low loads, stirrup strains are small due to the force taken through direct concrete tension. With the onset of cracking at higher load levels, concrete is rendered ineffective for primary load resistance and consequently stirrup resist forces at an increasing rate. Beyond this, depending on the level of cycling and load, there exists a third stage where the rate of increase of stirrup force reduces due to ineffective force transfer in concrete.

The above reasoning is presented merely as a possible explanation. Nevertheless, it explains the differences in strain variations among the above mentioned investigations. The repeated loading tests, besides resulting in less bond deterioration per cycle than the reversed cyclic tests, were in most cases subjected to fewer total number of cycles than either the specimens of this investigation or those tested by Tocci. Both these effects resulted in less overall concrete damage near failure and lead to higher stirrup strains through effective force transfer. On the other hand, the total number of cycles for the reversed cyclic tests by Tocci were comparable to those of this investigation. Ultimate

stirrup strain values for these two investigations were therefore similar.

Table 4.1 summarizes the recorded peak strains in the legs of the first stirrup of all specimens. These represent the highest stirrup strains in each test. A comparison of strain values brings out the following observations.

The vertical leg strain levels in C-2, C-3, and C-4 are higher than those of C-5, C-6, and C-7. The main difference in these two sets of specimens lies in the values of S_o. As already mentioned, the high moment end of the splice experienced localized damage. With the formation of reversing flexural shear cracks at that location, much of the additional deterioration was brought about by dowel forces exerted by the reinforcing bars on the concrete cover and on neighboring stirrups. The stirrup spacing immediately outside the splice (S_o) in specimens C-2, C-3 and C-4 was double that in C-5, C-6 and C-7 (10" c/c and 5" c/c respectively). The closer spacing S_o in C-5, C-6, and C-7 resulted in better confinement of the critical section outside the high moment splice end and restricted the growth of flexural shear cracks at that location. Consequently, a significant portion of total shear was resisted by aggregate interlock across these narrow cracks. Also because of the small spacing S_o, some of the adjacent external stirrups traversed the same diagonal tension shear crack as the first splice stirrup, thereby increasing the steel area across the crack. These two effects resulted in relatively low strains on the vertical leg of the first splice stirrup. With larger S_o values, as in C-2, C-3, and C-4, these load sharing mechanisms were far less effective, as evident from the large vertical leg strains on the first stirrup. The extent of flexural shear cracks at all interior sections was far less, and hence the concrete core

SPECIMEN	Splice Plane	L_s/d_b	S inches	S_o inches	Max. horiz. leg εst. x 10^{-6}	Max. vert. leg εst. x 10^{-6}	εst MAX/ε_y^*
C-2	Horiz.	30	3.00	10.00	780	1598	0.66
C-3	Horiz.	40	4.00	10.00	1322	1471	0.62
C-4	Horiz.	50	4.75	10.00	958	1377	0.57
C-5	Horiz.	30	5.0	5.00	668	918	0.38
C-6	Horiz.	30	5.0	5.00	599	931	0.39
C-7	Horiz.	30	5.0	5.00	544	1113	0.46
C-8	Vert.	30	5.0	5.00	414	1563	0.65
C-9	Horiz.	40	5.0	3.50	311	504	0.21
C-10	Vert.	40	5.0	3.50	581	1192	0.50
C-11	Horiz.	40	6.5	3.00	402	506	0.21
C-12	Vert.	40	6.5	3.00	489	1296	0.54
C-13$^+$	Horiz.	30	5.0	3.00	768	836	0.35
C-14$^+$	Vert.	30	5.0	3.00	470	1133	0.48

$^*\varepsilon_y = 2400 \times 10^{-6}$

$^+$ Compression bar end-bearing eliminated.

Table 4.1. Maximum stirrup strains for the column splice tests.

was effective in sharing the total shear force with interior stirrups.

The beneficial effect of adopting an even closer spacing of stirrups (S_o) outside the high moment splice end is evident from comparing vertical leg strains of C-9 and C-11 with those of C-5, C-6 and C-7 in Table 4.1. The strains in the first set of specimens (S_o = 3.5" c/c) is less than in the second set (S_o = 5" c/c). The localized shear damage in test C-6 is shown in Fig. 4.10.

Neither C-9 nor C-10 experienced splice-bond failure. Failure was brought about by a progressive deterioration of concrete at the high moment end, described in Section 3.7. However, some longitudinal cover splitting was observed in both tests, and it was seen that the top face cover split over the first stirrup was more developed in C-10 than in C-9. Due to this, the fraction of bursting stress resisted by tensile forces in the concrete surrounding the horizontal stirrup leg was less in C-10 than in C-9. As a result, the horizontal leg of the first stirrup in C-10 developed a larger force than that in C-9, and this is indicated by their different strain values in Table 4.1.

Tests C-8, C-10, C-12, and C-14 were vertically spliced specimens. High vertical leg strains show the effect of the superposition of bond, shear and dowel forces on the same stirrup leg. This aspect is discussed in Section 4.7.

Stirrup spacing over the splice was 5" c/c for C-9 and 6.5" c/c for C-11. Yet, the stirrup strain diagrams do not indicate any appreciable difference between the two specimens. While this is partly due to the fact that these two tests failed in different modes, it also suggests that there is no significant interaction between the confining capacities of adjacent stirrups. In other words, the zone of influence of

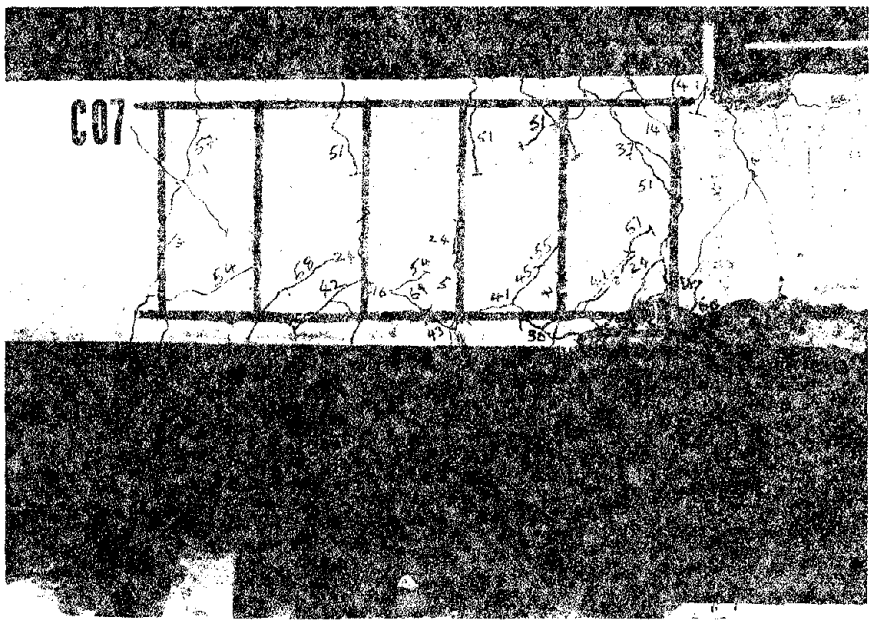

Fig. 4.10. Localized damage due to dowel action in Specimen C-7.

each stirrup is limited.

4.7 Orientation of Plane of Splice

In a lapped splice with equal covers and bars situated at the corners of stirrups with a large spacing between the splices, longitudinal cover splitting first occurs on the face parallel to the splice plane. The layer of concrete between the reinforcing bars is subjected to opposingly directed bond stresses and thus undergoes deterioration at an early stage. Also, Eligenhausen (1976) has shown from finite element analysis models that forces developed between two spliced bars lead to cover splitting on the face parallel to the bars. In a horizontally spliced member, the horizontal legs of the confining transverse reinforcement are stressed more than the vertical ones as a result of this cover damage. The vertical legs provide resistance to shear and bar dowel forces. However, in a vertically spliced member, forces due to all three above effects have to be resisted by the same legs (vertical) of the stirrups.

It is possible that in splices lapped vertically the bars in combination have a greater resistance to bending than when they are lapped side by side. This could result in large contact forces at the steel-concrete interface, particularly for specimens with large diameter bars, and result in a failure of the type depicted in Fig. 2.3. However, due to their large bending resistance, vertically lapped bars are likely to result in less dowel force induced cover damage.

Another effect is that splices lapped in the vertical plane have a smaller effective depth d than corresponding horizontal splices. For a given moment, this will result in higher average bar stresses in the vertically lapped splice, or a somewhat lower stiffness under lateral

loads. Tests C-8, C-10, C-12, and C-14 were conducted and compared with tests C-7, C-9, C-11, and C-13, respectively to determine whether the above effects would result in an adverse condition.

A comparison of stirrup strains (Table 4.1) shows that the vertical leg strain in C-10 is about 2.5 times that in C-9. Similarly, the value in C-12 is 2.6 times that in C-11. The difference is not as pronounced in C-13 and C-14. The relatively high ultimate strains in C-13 in comparison to C-9 and C-11 is probably due to the better force transfer characteristics of the higher strength concrete of C-13. This aspect is further discussed in Section 4.10. The high vertical leg strain in C-7 in comparison to C-9 and C-11 is a consequence of the larger stirrup spacing, S_o of C-7. This effect was explained in Section 4.6. For the same reason the vertical leg strain in C-8 is higher than in C-10, C-12, and C-14. Despite these effects, the absolute strain values are all seen to be well below yield, and a comparison of the maximum ductility factors of the two members in each pair shows no significant difference. The apparently low ductility of C-8 is explained subsequently. In addition, the behavior of the members of each pair was essentially the same despite possible differences in bar bending stiffness and in average effective depth d. Hence, for the #6 main bars and shear stress levels of 120 psi of this investigation, the design provisions of Eq. 2.6 (Tocci 1981) can be considered satisfactory for splices lapped in both orientations.

The apparent discrepancy in the ductility of C-8 when compared to C-10 and C-12 was referred to in Section 3.7 and is explained here. In all tests except C-8, it was the top splice bars which were instrumented. The bottom splice bars were inadvertently instrumented in C-8. As

already explained (Section 4.2), the bottom splices failed before the top ones for all bond failure tests. The poorer force transfer at the bottom splice resulted in the low bar strain values of C-8.

4.8 Bond Splitting

Bonding between concrete and steel enables force transfer in a lapped splice. Splitting of concrete along the splice length occurs mainly as a result of the radial bursting forces. Whether top or side splitting takes place first depends on the relative dimensions of the two covers and on the splice orientation. At any rate, the presence of splitting as such does not imply failure. The specimen will continue to carry loads up to the point where a cover spalling mechanism develops. In all bond failures observed during the column splice testing program, it was seen that considerable longitudinal cover splitting developed prior to failure. Designs that permit substantial cover splitting are preferable for two reasons. Firstly, they result in better ductility and energy absorption characteristics and secondly, they lead to a somewhat uniform bond stress distribution. This justifies the assumption of a uniform bond stress in the development of design provisions. Even in tests where external cover splitting is limited, it is likely that internal cracking and deformation tend to create a uniform bond state.

Several splitting failure mechanisms are possible and have been identified by Tepfers (1973). In this investigation, the face and side split pattern was identified. However, due to the relatively large spacing between splices, the central concrete cover remained intact even at failure (Fig. 4.11). Fig. 4.12 shows the splitting failures in Tests C-5 and C-8.

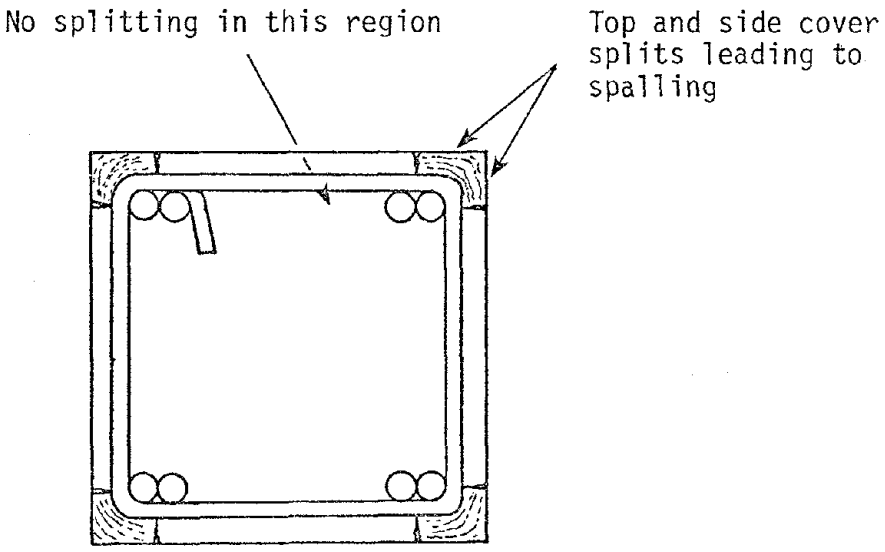

Fig. 4.11. Splitting pattern for specimens in this investigation.

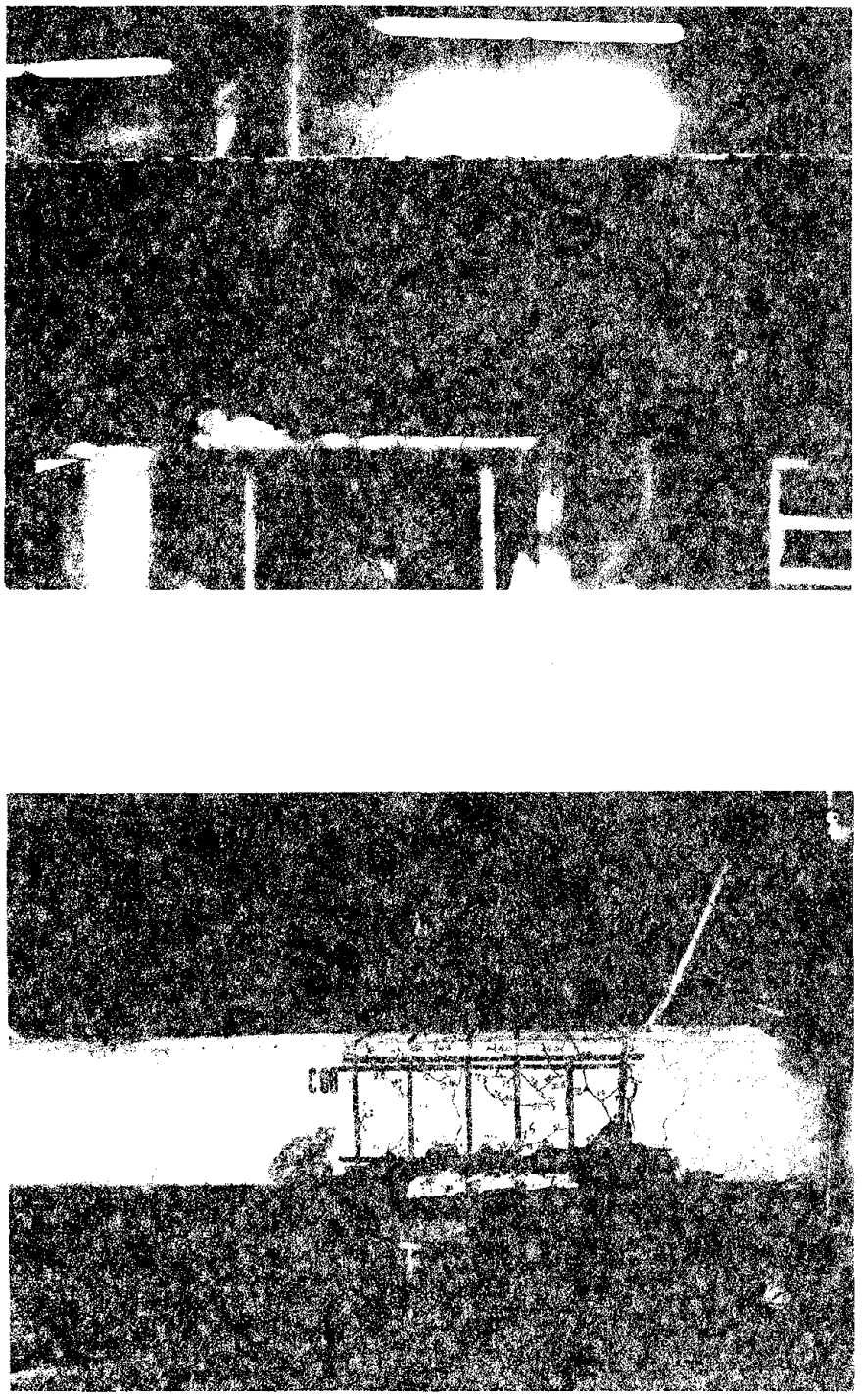

Fig. 4.12. Typical longitudinal splitting splice failures.

4.9 Concrete Cover

Tests C-2, C-3, and C-4 had C/d_b ratios of 2.6. Although this value is not so high as to preclude a bond failure, no significant bond splitting was observed for these tests. This was partly a result of the conservative splice design, but mainly because of inadequate transverse reinforcement at the primary crack location just outside the high moment splice end. As described in Chapter 3, most of the damage was localized at this cracked zone. In tests C-5 and C-6 where this section was transversely reinforced the, extent of longitudinal cover splitting over the splice was appreciable in spite of a C/d_b ratio of 2.6. The remainder of tests had redcued C/d_b ratios (1.6) and were characterized by face and side cover splitting failures (except C-9 and C-10 in which the splice design was over-conservative).

It appears from the above that small changes in cover do not influence splice strength as long as a cover splitting mechanism is attainable. This does not imply that a structure can carry loads even after a loss of cover. Cover, although ineffective as a confinement providing mechanism at and near the failure stage, is an integral part of the mechanism that transfers bond and shear forces from the concrete core to the stirrups. The conclusion made is that as long as the ACI minimum cover specifications are met, and covers are not so large as to prevent a bond splitting failure mode, an explicit consideration of cover is not required in the development of splice design provisions.

4.10 Concrete Strength

Although both C-7 and C-13 were subjected to identical load histories, C-13 (f'_c = 4.2 ksi) maintained better overall splice integrity than C-7 (f'_c = 3.47 ksi). The extent of bottom cover splitting at

various displacement levels was less in C-13 than in C-7. Fig. 4.13 compares the energy absorbed for cycles at different levels of peak displacement. In this, the improved splice integrity of C-13 over C-7 is apparent from its correspondingly lower energy dissipating characteristics.

A comparison of stirrup strains in Table 4.1 shows those of C-13 to be higher than those of C-11 and C-9 even though the S_o values for all three tests were essentially the same (S_o = 3 - 3.5). This is because the higher strength concrete of C-13 experienced less overall deterioration than that in C-11 and C-9 at approximately the same ultimate load level, and was more effective in transferring load to the stirrups. The maximum vertical leg stirrups strain in C-13 is less than in C-7 because of the smaller S_o value, as described in Section 4.6.

No definite conclusions can be formed from a comparison of these two tests since their concrete strengths do not differ by a wide enough margin, and also because of the difference in their fabrication. However, it is felt that the effects mentioned above (higher stirrup strains and lower energy absorption) are likely to be the primary manifestations of high strength concrete. These concretes, being stiffer, are less inclined to permit an even distribution of bond stress and may, consequently, result in splice failures at low average bond stresses due to peak stresses at the end of the splice bars.

4.11 Compression Splice Behavior

As mentioned earlier, this investigation is based on the assumption that an adequately designed tension splice will perform at least as well in compression. For a flexural specimen, transfer of longitudinal tensile forces is entirely contingent on adequate bond between the bar deformations

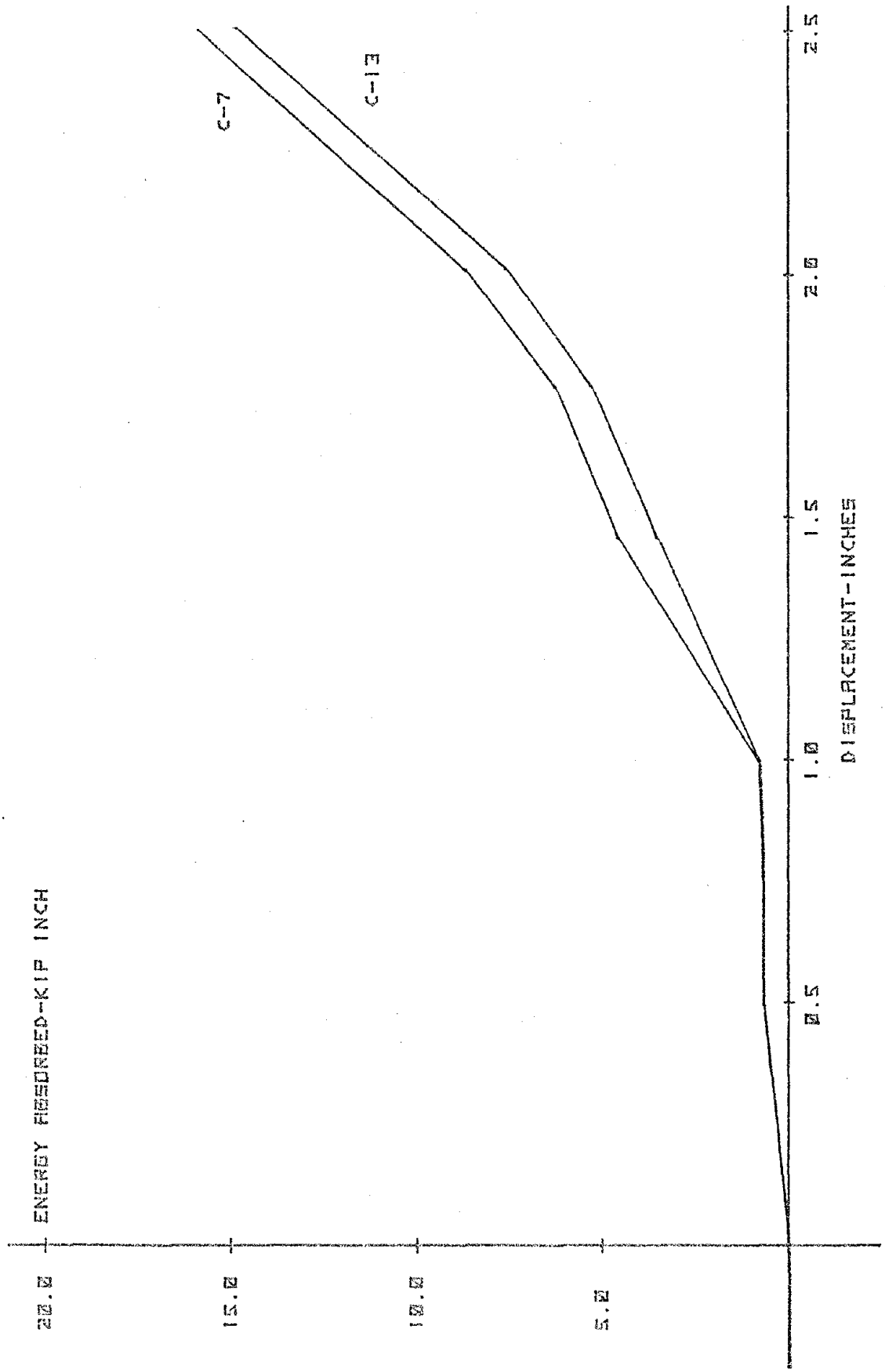

Fig. 4.13. Energy absorption curves for specimens C-7 and C-13.

and concrete. This reduces the problem to one of longitudinal, radial, and circumferential stress resistance and has been discussed in Section 2.6. Compression splices transfer forces by direct concrete compression and bar end bearing in addition to bond. That compression splice bars are stressed to a far less extent than tensile splice bars is evident from Figs. 8a and 8b. Tests C-13 and C-14 were conducted in an attempt to determine the relative contribution of the above effects in a compression splice. These specimens were fabricated with styrofoam plugs at the end of splice bars so as to eliminate end bearing effects. Their reinforcement details were identical to those of C-7 and C-8, respectively.

A comparison can best be made by means of the top bar end slip diagrams. These figures for C-11, C-12 and C-14 (Figs. 4.14, 4.15, 4.17) show a predominance of slip due to bar tension. This is expected in the case of C-11 and C-12 since end bearing on concrete limits slip of a bar under compression. On an average, the peak slip of a bar under compression was one tenth that in tension. During any loading half cycle, deterioration occurs due to inelastic deformation, local crushing, cracking, and bar slip. On unloading, the reverse motion is resisted by friction and the interlocking action at the steel-concrete interface layer. This results in residual slips, residual bar stresses, and incompletely closed cracks. The residual slip effect is evident from the fact that the slip curves are all hysteretic.

Although end bearing effects were eliminated in C-13 and C-14, the curves of C-14 indicate slip resulting mainly from bar tension. For C-13 (Fig. 4.16), a greater poriton of each curve shows slip resulting from bar compression. Recalling that C-13 experienced greater top cover damage than C-14, this shows that bar end bearing resistance becomes

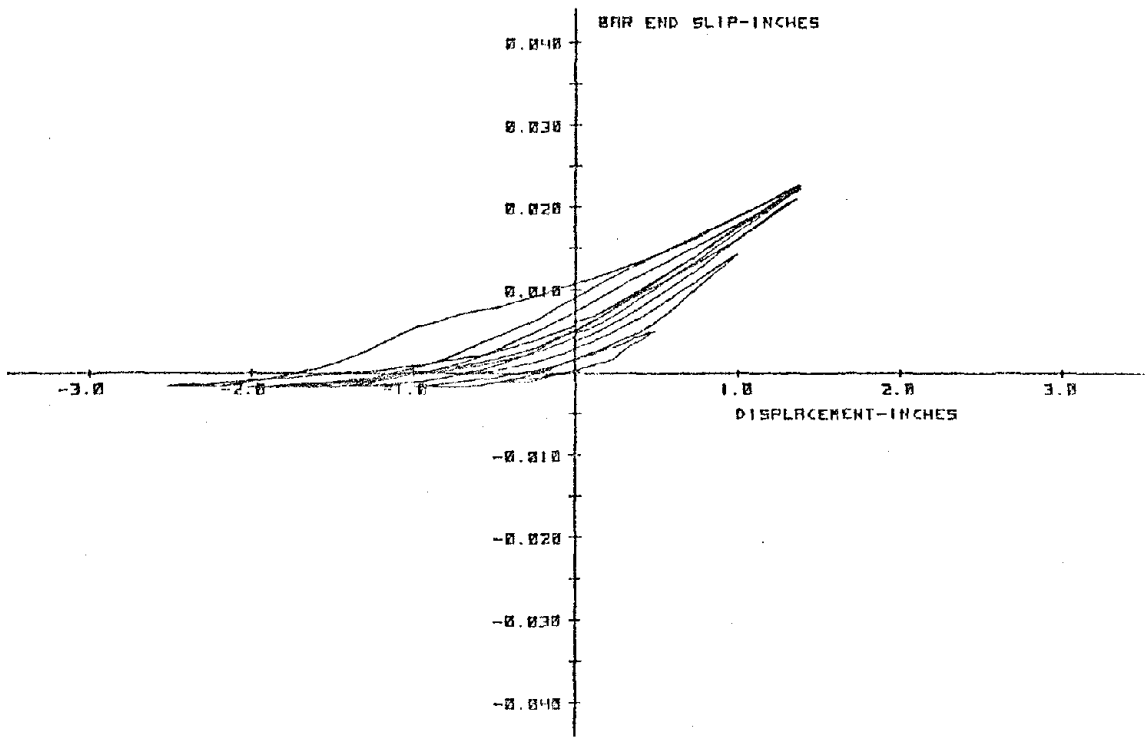

Fig. 4.14. Bar end slip - displacement relationship for specimen C-11.

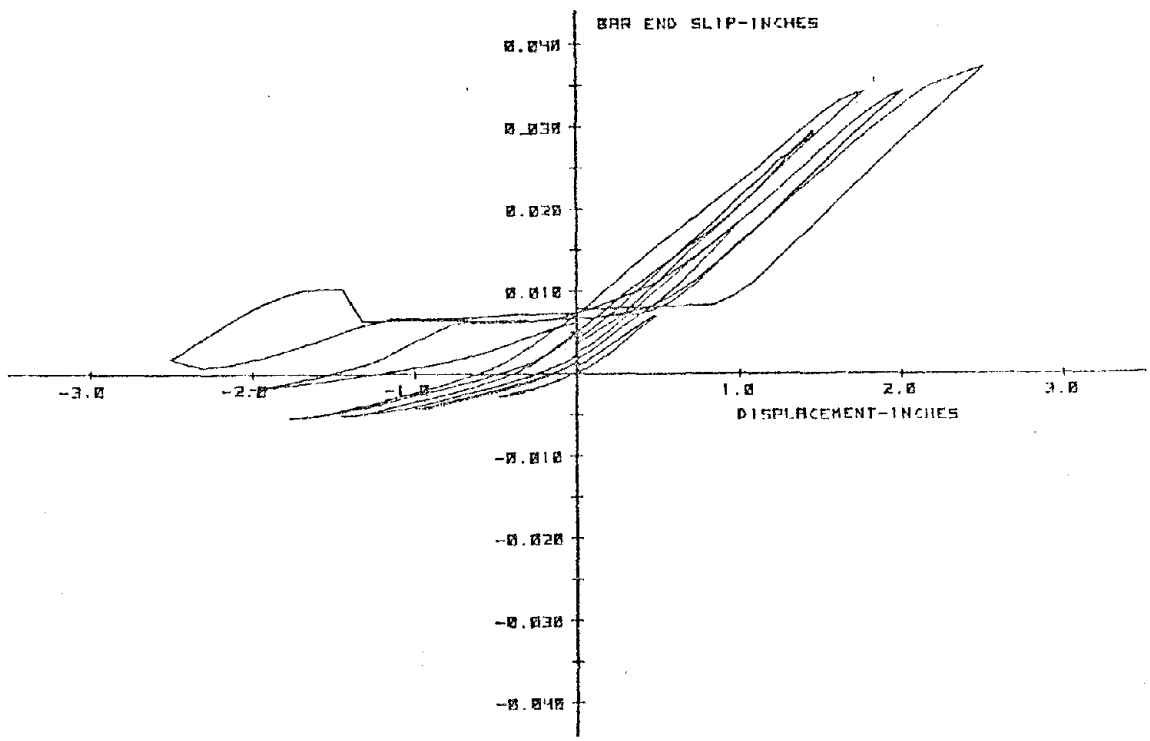

Fig. 4.15. Bar end slip - displacement relationship for specimen C-12.

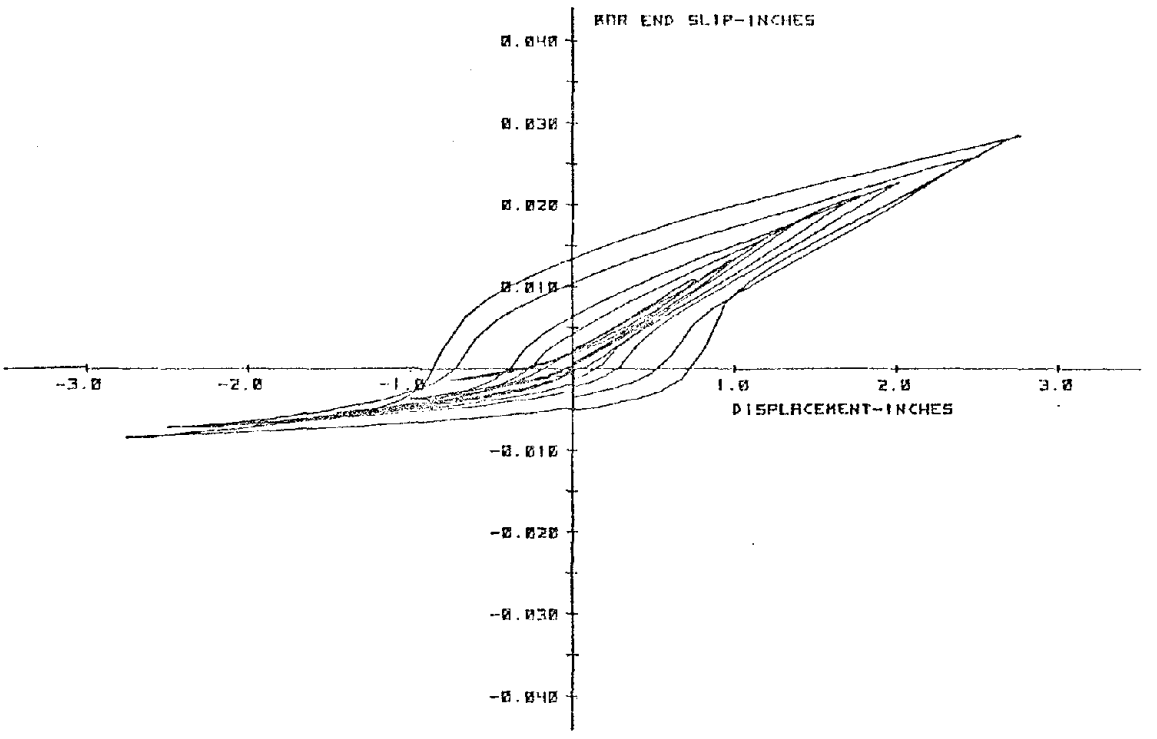

Fig. 4.16. Bar end slip - displacement relationship for specimen C-13.

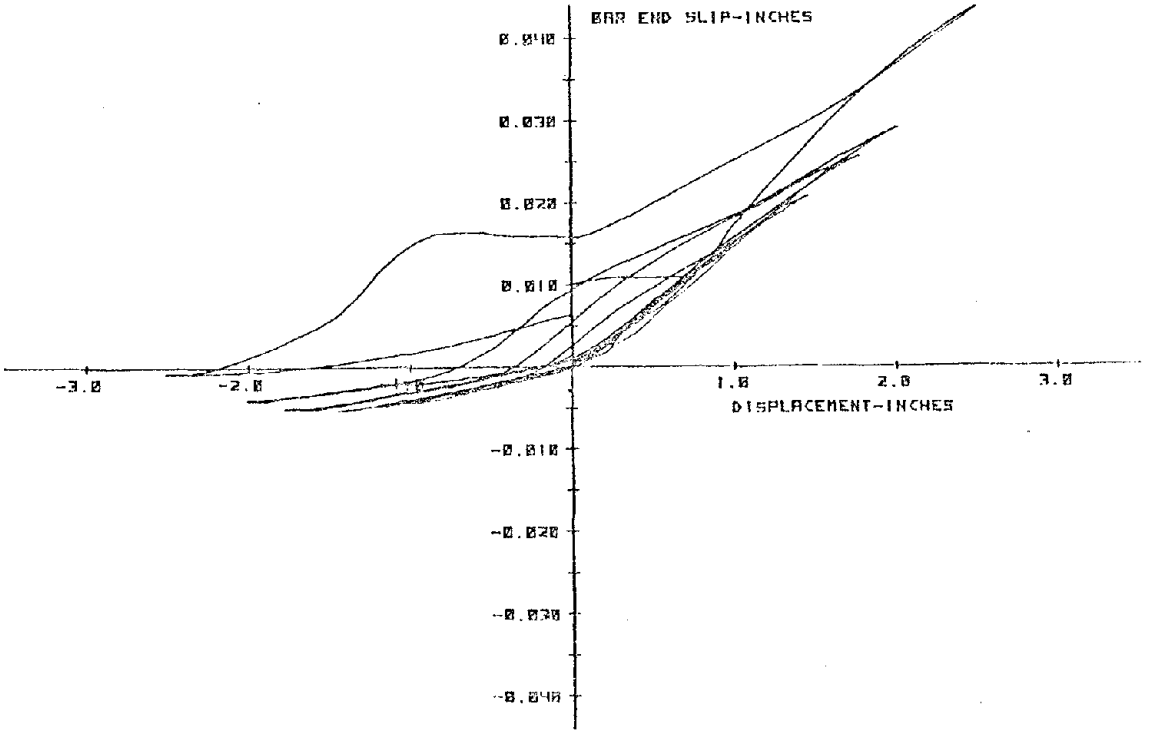

Fig. 4.17. Bar end slip - displacement relationship for specimen C-14.

effective only after cover splitting takes place. Based on the adequate performance of C-13 and C-14, it can be stated that the amount of compression taken by bar end bearing is small in comparison to that resisted by direct concrete compression.

The role of a compression splice is expected to be more critical in the case of real columns subjected to high direct axial loads and bending moment. Depending on the relative magnitudes of axial and flexural stresses, the superposition of these two effects can result in failure due to compression. In these instances, adequate transverse reinforcement should be provided over splices to control localized damage due to bar end bearing, to prevent instability in compression bars, and to resist bond forces.

Tests on compression lapped splices by Cairns and Arthur (1979) show that compression splice strength consists of two distinct components, one relating to the confining forces (transverse reinforcement) that are mobilized to counteract bursting forces produced by bond and bar end bearing, and another related directly to concrete strength. The latter can be interpreted as that portion of the external compressive load resisted by direct concrete compression. From this, it appears that the strength of a spliced compression member can be increased by using higher strength concretes. However, very high strength concretes will have detrimental effects (Section 2.2).

The increase in reinforcement bar stress due to the concrete creep effect is difficult to estimate, as creep depends on the concrete stress level, the concrete strength, and the average ambient humidity besides other factors. All other factors being constant, creep decreases with increasing concrete strength, and this suggests another advantage of

high strength concrete.

In reinforced concrete columns, localized crushing can take place on the compression face at the base due to the superposition of direct axial and flexural compressive stresses at overload. The spread of this damage is typically limited over a length approximated by the effective depth d of the cross section and results in anchorage loss for reinforcement in that zone. Hence, splice lengths at these locations should include an extra length of d to provide adequate anchorage.

4.12 Bond-Shear Interaction

All the column splice specimens were subjected to combined bending and shear. The force to be developed in each anchored splice bar depends on the nature of the moment diagram. Under the moment gradient, the bar located at the high moment end was stressed more than the other. Bond forces were correspondingly higher in this bar. As the second bar was not as highly stressed, average bond forces are less severe for these splices compared to splices situated in a constant moment region. In other words, deterioration of the splice due to cover splitting and yield penetration takes place from both ends for splices situated in a constant moment zone, whereas it occurs from only the high moment end for splices under a moment gradient. However, the interaction of shear forces with bond cannot be neglected and is investigated in this section.

It was observed that in all the tests the region just beyond the high moment end of the splice developed severe flexural shear cracking (Fig. 4.18) due to the following effects:

(1) An abrupt change in stiffness at the section due to different amounts of main reinforcement on either side.

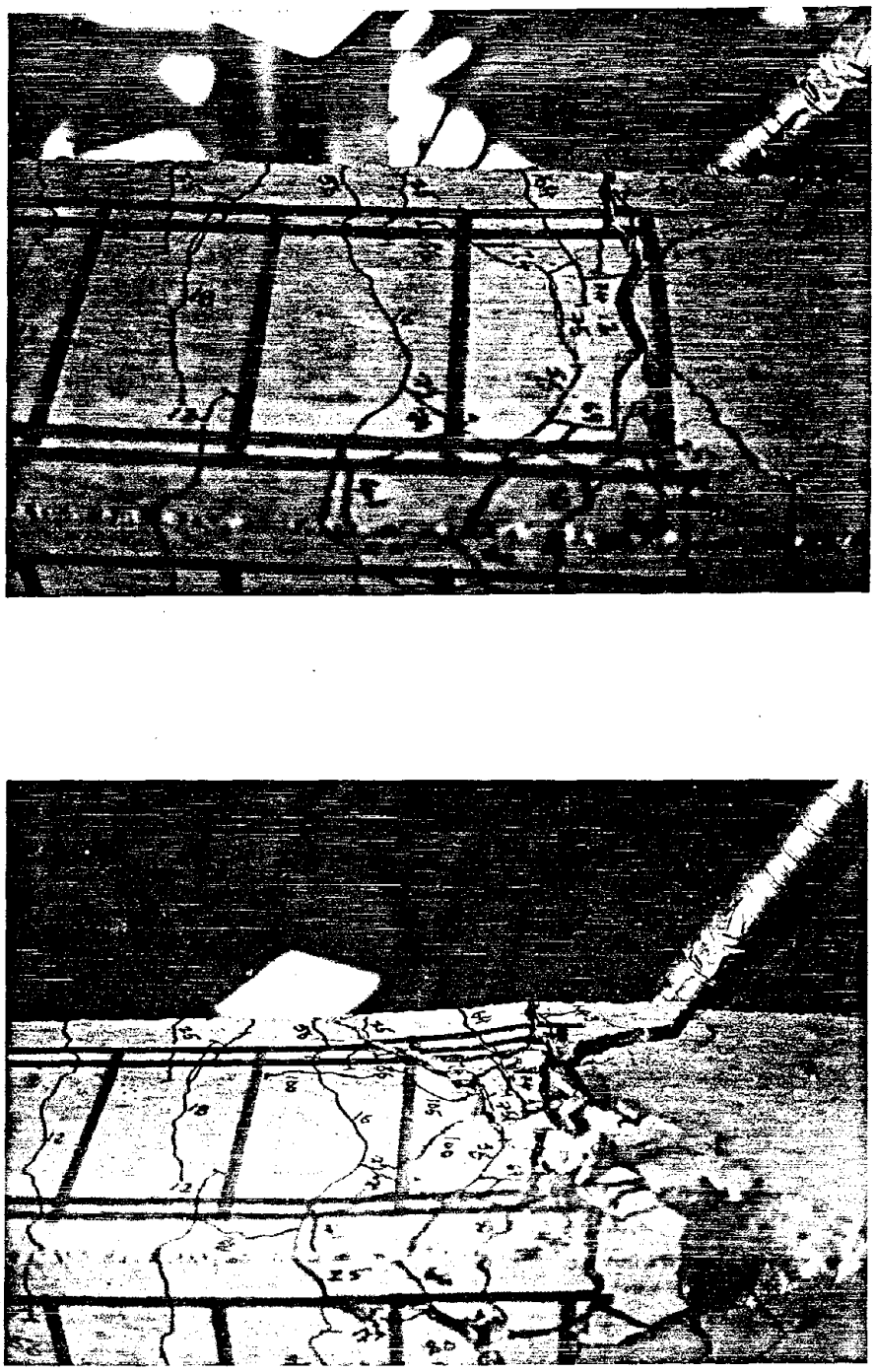

Fig. 4.18. Progressive concrete deterioration at high moment end of splice for specimen C-4.

(2) Stress concentrations at the points where the main bars terminate.

(3) High moments causing transverse flexural cracks which transform into flexural shear cracks. After the formation of this crack, shear resistance at the section is afforded by the uncracked concrete, aggregate interlock, shear reinforcement, and longitudinal bar dowel force. The investigation conducted by Gergely, White, and Jimenez (1979) shows the dowel force effect to be the most significant component in interacting with bond resistance. In particular, the strength of an anchored bar diminishes rapidly as dowel forces approach the bar dowel capacity. Dowel forces develop only at transversely cracked sections and are best resisted by transverse reinforcement. Whether transverse reinforcement can simultaneously resist dowel forces, shear stresses and radial bursting forces is the major point.

Plots of stirrup vertical leg strains show the peak strain to be always on the first splice stirrup (which is also the closest to the primary crack). This behavior was described in Section 4.6. On further cycling, inelasticity, crack width increase, and bar slip reduce the effectiveness of aggregate interlock in transferring shear, thereby increasing the portion transferred by dowel forces and hence producing larger strains on the stirrup leg. This force transfer mechanism is shown in Fig. 2.18. Experiments conducted by Tocci (1981) lead to similar conclusions. Jimenez and others (1979) believe that dowel capacity is related to the net beam width, cover, concrete tensile strength, and transverse reinforcement (Section 2.12). Bar dowel capacity reduces with increasing bar axial tension. Thus, dowel capacity is reduced when the main bars yield.

Damage brought about by dowel action is characterized by localized side cover splitting and spalling. Examination of photographs shows this to be the case in several tests as in Fig. 4.10. Transverse reinforcement close to the crack controls the extent of concrete deterioration due to dowel effects. The effectiveness of this is dependent on the anticipated level of shear and cycling. In this investigation, the shear level was never more than 120 psi. For the extent of cycling done, these tests did not show any premature failures brought on by dowel effects. In other words, transverse reinforcement was effective in resisting dowel, bursting, and shear forces simultaneously. It is possible that higher shear levels and additional cycling can result in greater localized concrete deterioration to the stage where bar anchorage is affected. More research is needed to investigate this possibility.

A possible technique of investigating the influence of dowel forces on bond is by the application of Eq. 2.7 proposed by Jimenez, White, and Gergely (1979). As stated in Section 2.12, the difficulty lies in estimating the fraction of total shear resisted by the dowel mechanism. The problem is more severe for reversed cyclic loading cases, where a gradual reduction in aggregate interlock results in increasing amounts of shear transfer through dowel action. Loading history is thus introduced as an additional variable. Hence, it is clear that an application of Eq. 2.7 is possible only after certain simplifying assumptions are made. This reduces the reliability of results.

The extent of concrete damage at the high moment end of the splice was greatest in Specimens C-2, C-3, and C-4 (Fig. 4.19). They were not reinforced adequately at the critical section. In C-5, C-6, C-7 and C-8, stirrup spacing at the splice was continued through a distance d

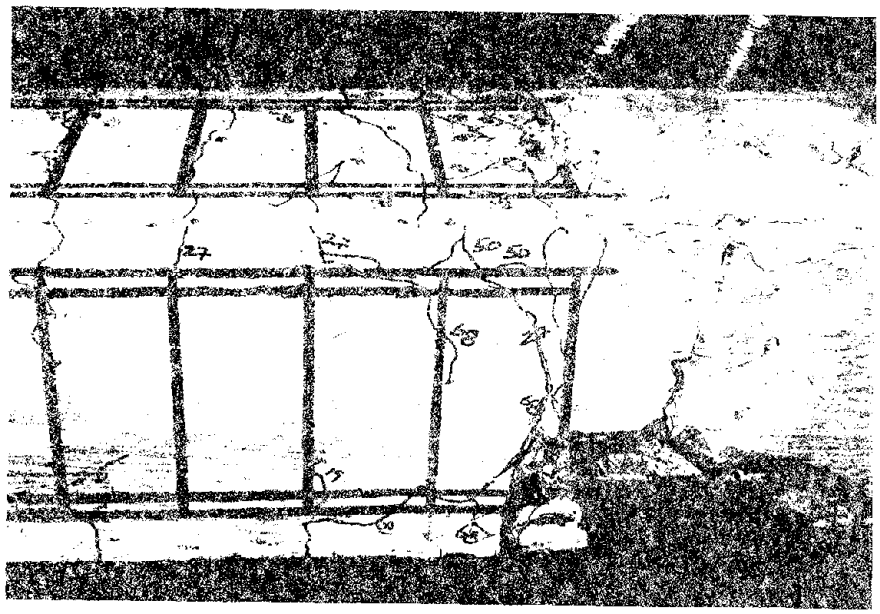

Fig. 4.19. Localized damage outside splice end in specimen C-3 with little deterioration along splice.

(effective depth) beyond the high moment end of the splice. Test observations indicate that concrete deterioration at the critical section was limited in these specimens, resulting in more splice damage than before. When the outer stirrups were spaced at 3 - 3.5" c/c (S_o for C-11, C-12, C-13 and C-14), the integrity of the high moment splice end was even better. Therefore, in specifying S_o, it seems more logical to adopt a fixed value of about 3 - 3.5" c/c rather than S" c/c or $\frac{d}{4}$" c/c to a distance 'd' beyond the high moment splice end. It would be most appropriate to define S_o as an inverse function of the main bar diameter d_b. The exact relationship will have to be determined from experiments.

One important observation is that both C-9 and C-10 experienced considerable concrete damage at the high moment splice end with negligible splice deterioration in spite of an S_o value of 3.5" c/c. This was probably because of the overconservative splice design for these two specimens. This and the above mentioned observations suggest that for lapped splices under combined bending moment and shear force, there always exists the possibility for failure by a localized concrete deterioration at the high moment splice end. It is concluded that:

(1) In cases where excessive concrete covers or closely spaced stirrups over the splice inhibit the extent of longitudinal cover splitting required to cause a splice bond type failure, failure results by a progressive deterioration of concrete at the high moment splice end even for small values of S_o.

(2) The occurrence of a splice-bond type failure is contingent on both a splice design that develops appreciable longitudinal cover splitting and closely spaced transverse reinforcement beyond the high moment end

of the splice.

With the possibility of failure of a reinforced concrete spliced member either by a bond type failure as in C-5, C-6, C-7, C-8, C-11, C-12, C-13, and C-14 or, by a localized concrete deterioration at the high moment end of the splice as in C-2, C-3, C-4, C-9, and C-10, it becomes necessary to compare their performances. In particular, the main question is whether the second set of tests are acceptable from a seismic resistance point of view. In Section 3.6, test acceptance criteria were specified in terms of the total number of post-yield cycles, the maximum displacement ductility, and the maximum strain ductility attained in any test. Test results show that C-9 and C-10 surpass the above criteria. It is also seen that the performance of C-2, C-3 and C-4 was comparable to that of the bond failure tests. Tests C-10 and C-12 were subjected to identical load histories, and yet Fig. 4.3 shows that the energy absorption capacity of C-10 was higher at all displacement levels.

One strong implication of the above observations is that failures characterized by high moment splice end deterioration (as in C-9 and C-10) can be as acceptable as the conventional splice-bond type failures from a seismic resistance viewpoint. The key factor lies in ensuring that the critical section is adequately reinforced (by adopting closely spaced stirrups).

Most seismic codes prescribe stirrup spacings no greater than d/4 at regions where inelasticity is expected. When applied to splices, this could result in stirrup spacings close enough to inhibit the formation of longitudinal cover splitting. The present investigation shows that under these circumstances, lapped splices subjected to combined moment

and shear will undergo concrete damage at the high moment splice end. Thus, for these members, it is important to adequately reinforce the critical sections.

CHAPTER 5

DESIGN RECOMMENDATIONS

5.1 Development of a Splice Design Equation

The following development leads to a design equation for column splices subjected to inelastic reversed cyclic loading under a combination of bending moment and shear force. It is applicable to members with splices at the four corners of closed transverse reinforcement ties as in Fig. 5.1. An equilibrium model approach is followed where it is assumed that at the ultimate stage, failure takes place by bond deterioration.

In a general case, cover splitting patterns depend on relative cover dimensions and on the location of reinforcement. For the tests conducted in this investigation, it was seen that the face and side split mode occurred in all the bond failure specimens. The side split did not extend across the entire width of the cross section because of the relatively large spacing between the two spliced bars at the top and bottom (Fig. 5.1).

The forces at the point of incipient failure are idealized as in Fig. 5.2. As considerable cover damage is expected to occur by this stage, it is reasonable to disregard the small amount of confinement it might afford. With this in mind, the force diagram attributes all confinement to be due to transverse steel. From the equilibrium of these forces

$$A_t f_{st} = (F_1 + F_2)S \qquad (5.1)$$

where F_1 and F_2 are the radial bond force resultants/unit length of each bar of the splice.

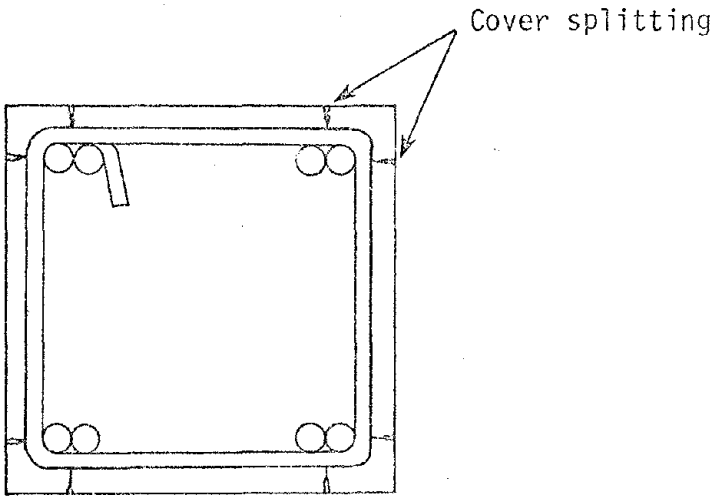

Fig. 5.1. Face and side cover splitting mode.

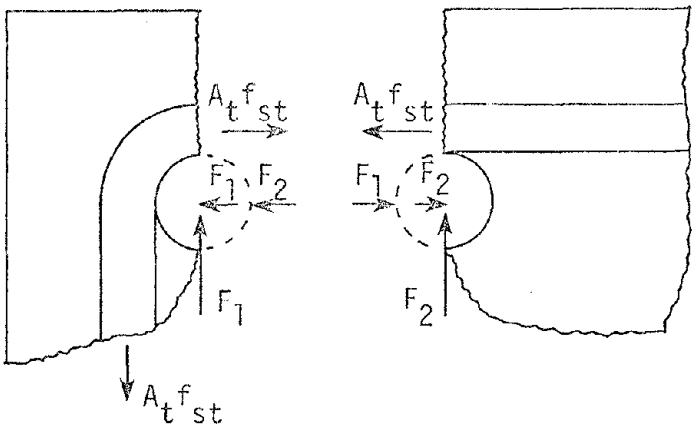

Fig. 5.2. Force diagram.

S = spacing of transverse steel

A_t = area of transverse reinforcement per splice normal to the plane of splitting. For the splitting mode observed in this investigation, A_t = area of 1 stirrup leg.

f_{st} = maximum stress developed in a stirrup leg at incipient failure.

The unit bond force resultants, F_1 and F_2 are proportional to the product of the longitudinal bond stress and the bar diameter. The proportionality constant is the tangent of the angle between the bar axis and the bond force resultant. Several investigators have shown that this angle can vary within a range, depending on the type of loading and the extent of localized damage at the faces of the bar deformation ribs. The typical range lies between 30° and 60°, and it is pointed out that the results are quite sensitive to the value chosen. Assuming a value of 45°, it then follows that the longitudinal bond stress is equal to the radial bond stress at any location along the bar.

Hence, $$F_1 = fb_1 \cdot d_b \qquad (5.2)$$

$$F_2 = fb_2 \cdot d_b \qquad (5.3)$$

where

fb_1 = longitudinal bond stress in one splice bar

fb_2 = longitudinal bond stress in the other splice bar

The longitudinal bond stress at any point along a bar is directly related to the gradient of the bar force diagram at that point. In reality, the force variation in a splice bar is undulating in nature, being higher at the stirrups where the confinement is good and lower at

other locations. However, it has been shown by researchers that cycling at progressively higher levels leads to a nearly linear bar stress variation. Assuming such a force variation, the bond stress on each bar is then uniformly distributed.

Fig. 5.3 shows the stress distribution in the spliced bars at the point of imminent failure. A 20% yield penetration is assumed for bar 1 in the high moment zone. This value is consistent with test observations. Bar 2, being anchored in the low moment zone, is subjected to lower steel stresses. For the extent of yield penetration observed, the stresses in this bar will always be below yield. In other words, yield penetration into the splice takes place only from the high moment end. Referring to Fig. 5.3,

M_ℓ = moment at low moment splice end

M_h = moment at high moment splice end

M = moment at section to which yield penetration occurs.

From statics, it is evident that for a constant shear force along the splice, the moment variation between the splice ends has to be linear. Assuming that the moment at a section is directly related to the sum of the bar stresses at that location, it follows that the total bar stress variation between the splice ends is also linear. Stresses at the yielded portion of Bar 1 can increase above f_y only through strain hardening. In other words, yield penetration occurs under a moment gradient only if strain hardening takes place. In this derivation, contributions to bond force due to strain hardening are disregarded, and it is assumed that all bond development takes place over a length of $0.8\,L_s$ for bar 1. The highest attainable value of M

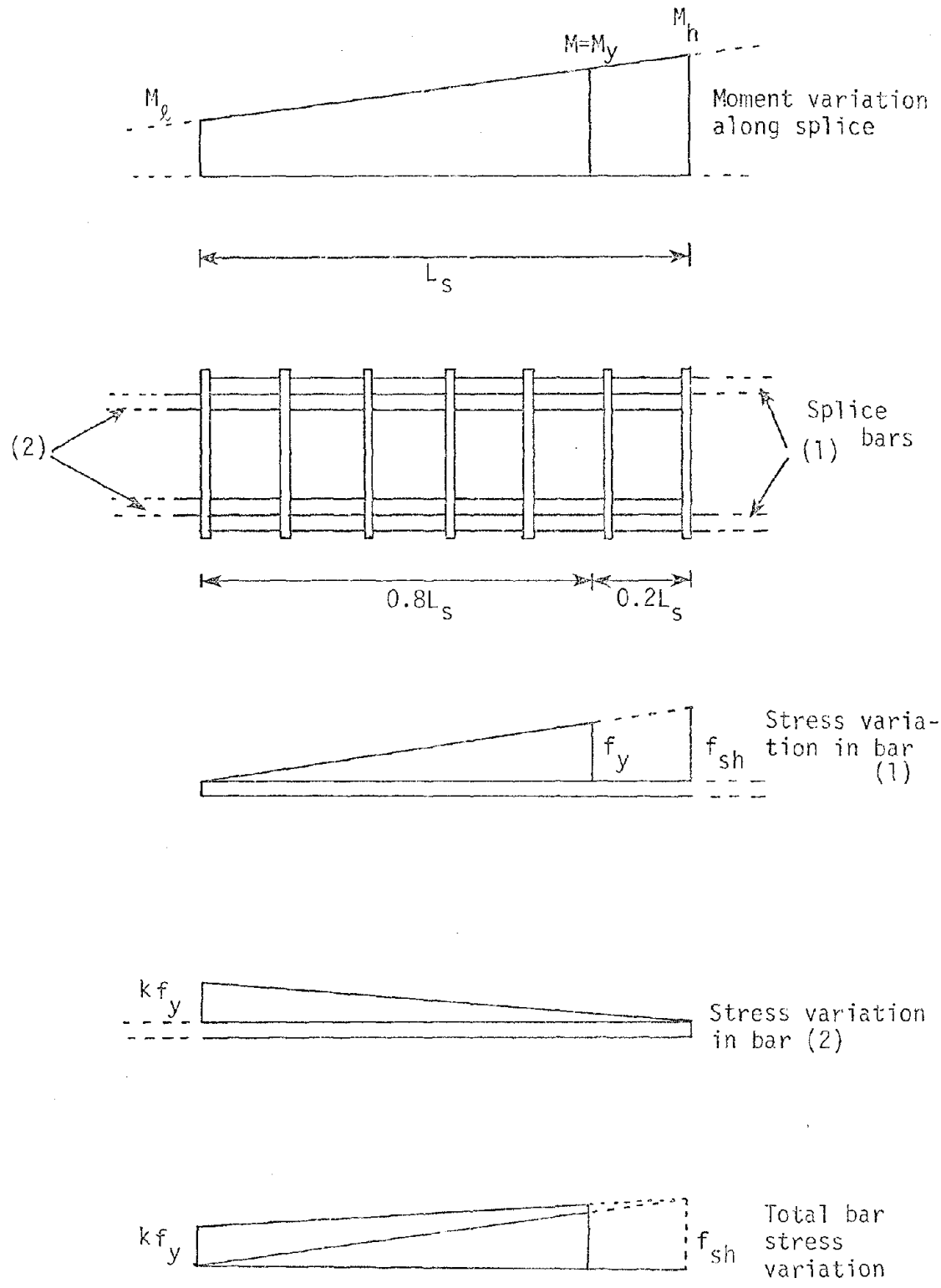

Fig. 5.3. Bar force variation.

is M_y, whereas M_h attains a value in excess of M_y due to strain-hardening, the stresses developed near the free end of bar 2, and possible relocation of the neutral axis.

Recalling that moment and total bar stress are directly related,

$$\frac{M_\ell}{M_y} = (kf_y)/(f_y + \frac{kf_y}{L_s} \times 0.2\, L_s) \tag{5.4}$$

and hence,

$$k = 1/(M_y/M_\ell - 0.2) \tag{5.5}$$

where k is factor relating the maximum stress in bar 2 to the yield stress (Fig. 5.3).

The longitudinal bond stresses are:

$$fb_1 = f_y\, d_b/(0.8\, L_s \times 4) \tag{5.6}$$

and,

$$fb_2 = kf_y\, d_b/4\, L_s \tag{5.7}$$

From Eq. 5.2 and Eqn. 5.3,

$$F_1 = \frac{f_y\, d_b^2}{3.2\, L_s} \tag{5.8}$$

$$F_2 = \frac{kf_y\, d_b^2}{4\, L_s} \tag{5.9}$$

On substitution of these expressions into Eq. 5.1,

$$A_t\, ft_s = (\frac{f_y\, d_b^2}{3.2\, L_s} + \frac{kf_y\, d_b^2}{4\, L_s})\, S \tag{5.10}$$

which can be simplified to:

$$S = \frac{4A_t\, f_{st}\, L_s}{d_b^2\, f_y} \times \left[\frac{1}{1.25 + M_\ell/(M_y - 0.2\, M_\ell)}\right] \qquad (5.11)$$

Eqn. 5.11 determines the stirrup spacing for splices under a moment gradient (moment and shear). For the special case in which the moment is constant ($M_\ell = M_h = M = M_y$), the equation reduces to

$$S = 1.6\, \frac{A_t\, f_{st}\, L_s}{f_y\, d_b^2} \qquad (5.12)$$

which, with suitable substitutions for f_y and f_{st} is identical to Eq. 2.6, proposed by Tocci (1981 - Section 2.11). Before applying Eq. 5.11 to specific cases, a value for f_{st} must be decided upon. Tests in the present investigation indicate a value of 0.55 f_y to be the upperbound. However, this is conservatively taken as 0.5 f_y (half the yield stress).

On substitution, Eq. 5.11 can be rewritten as

$$S = \frac{2.0\, A_t\, L_s}{d_b^2} \times \frac{1}{(1.25 + 1/(M_y/M_\ell - 0.2))}\,, \quad \frac{M_y}{M_\ell} \nleq 1 \qquad (5.13A)$$

A simplified version of the above equation is

$$S = \frac{2.0\, A_t\, L_s}{d_b^2} \times \frac{1}{(1.25 + 0.2\beta^2 + \beta)}\,, \text{ where } \beta = \frac{M_\ell}{M_y} \geq 0 \qquad (5.13B)$$

The error through this simplification is never in excess of 2%. The scope and limitations of the applicability of Eq. 5.13 are listed below.

In view of the uncertainties and approximations involved in any study on reversed cyclic loading and progressive bond deterioration, it seems unreasonable to expect a high level of precision in the development

of design provisions. The above derivation does, admittedly, resort to simplifying assumptions at various stages, however, with regard to the expected level of accuracy, they appear justifiable.

Negative values of (M_ℓ/M_y) lead to an inflection point at some location along the splice. As reversed curvature effects were not considered in this experimental investigation, such cases are conservatively excluded in the above development. Hence, it is necessary to constrain M_ℓ/M_y to be greater than or equal to zero. This can also be satisfied by ensuring that M_y/M_ℓ is not less than unity ($M_y/M_\ell \nless 1$).

In this investigation, any specimen that sustained at least 20 to 40 cycles above yield and attained displacement and strain ductilities of 1.8 and 2.5 respectively were considered satisfactory from a seismic resistance point of view. Data used in the development of Eq. 5.13 was taken only from tests that met or exceeded these requirements.

Specimens in this investigation consisted of #6 bar lapped splices situated at the four corners of #3 closed ties as indicated in Fig. 5.1. The nominal steel yield stress was 60 ksi and concrete compressive strengths ranged from 3.0 ksi to 4.2 ksi. Cover to bar diameter ratios (C/d_b) were limited to 1.6. The nominal shear stresses were always less than 130 psi. Extrapolation of these results for specimens with greatly differing characteristics may not always yield adequate splice designs. For instance, specimens with multiple splices in the same horizontal plane will be characterized by cover splitting patterns as in Fig. 2.16 and Fig. 2.17, which are different from the type assumed in Fig. 5.1 and Fig. 5.2. Similarly, the detrimental effects of high level axial compression causing localized crushing of concrete (Section 4.11) will necessitate splice lengths larger than indicated by Eq. 5.13.

One implication of Eq. 5.13 is that all stirrup legs are stressed to a value of 0.55 f_y. In actual fact, this stress value was attained only on the first stirrup vertical leg. In other words, the assumption is that the limit of structural usefulness is reached as soon as the first stirrup at the high moment splice end attains a stress of 0.55 f_y on its vertical leg. This is normally not the case, since splices continue to carry loads until longitudinal cover splitting progresses over the entire splice length, leading to a cover spalling mechanism. However, errors due to the above assumption are undoubtedly on the conservative side and provide an extra margin of safety against splice failure.

Although concrete confining stresses were excluded from the equilibrium model of Fig. 5.2, higher strength concretes do have an influence on splice behavior as they result in better force transfer capacities and higher overall splice integrity (Section 4.10). Stirrups will, therefore, attain higher stress values f_{st} for higher strength concretes. It is through the increase in f_{st} that Eq. 5.11 reflects the influence of concrete compressive strength, thereby permitting wider stirrup spacings.

Eq. 5.13 assumes that splices fail by a bond mechanism. The region immediately beyond the high moment end of the splice should be adequately reinforced in order to prevent a localized shear-dowel type failure.

5.2 Additional Implications of the Proposed Design Equation

Some of the design implications of Eq. 5.13 are discussed in the following.

1) Fig. 5.4 shows the splice length - stirrup spacing relationship for #6, #8, and #10 main bars and #3 stirrups based on Eq. 5.13. The specimen chosen is shown in the same figure. It represents a realistic situation where column splices are located just above the floor slab or foundation level in storied buildings. The relationship is essentially linear for all three bar sizes and clearly illustrates the option of adopting wider stirrup spacings with longer splices.

2) The change in stirrup spacing due to different moment gradients over the splice can be investigated as follows. Rewriting Eq. 5.13,

$$S = (2.0A_tL_s/d_b^2) \times 1/(1.25 + M_\ell/(M_y - 0.2\ M_\ell))$$

$$= (2.0\ A_t L_s/2.5\ d_b^2) \times 2.5/(1.25 + M_\ell/(M_y - 0.2\ M_\ell))$$

$$= (0.8\ A_t L_s/d_b^2) \times \kappa \qquad (5.14)$$

where

$$\kappa = 2.5/(1.25 + 1/(M_y/M_\ell - 0.2)) \qquad (5.15)$$

A tabulation of κ for different moment gradients over a splice is given in Table 5.1. It is observed that κ varies from 1 for a constant moment zone to 2 for a case where the moment ratio is infinite. Fig. 5.5 shows the stirrup spacing - moment gradient relationship for splices with #6, #8, and #10 bars and of length 30 d_b. Stirrup spacing for other (L_s/d_b) ratios may be obtained by direct proportion. #3 size stirrups are assumed in this relationship.

It should be realized that the effectiveness of transverse reinforcement depends on both, the total amount and the distribution. As mentioned in Section 2.7, the zone of influence of a stirrup is limited, and it is probable that a large spacing obtained from Eq. 5.13

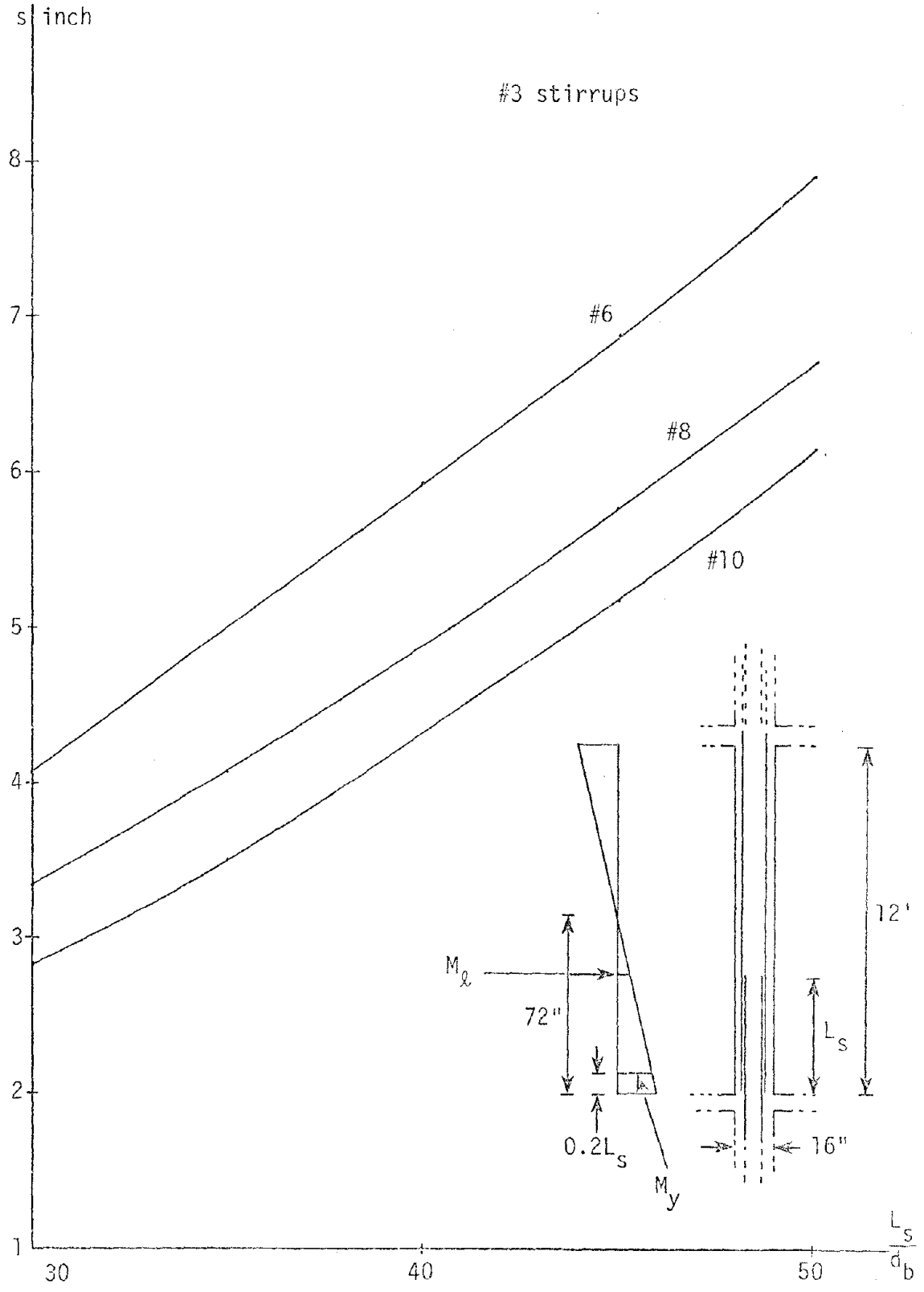

Fig. 5.4. Splice length - stirrup spacing relationship from Eq. 5.13.

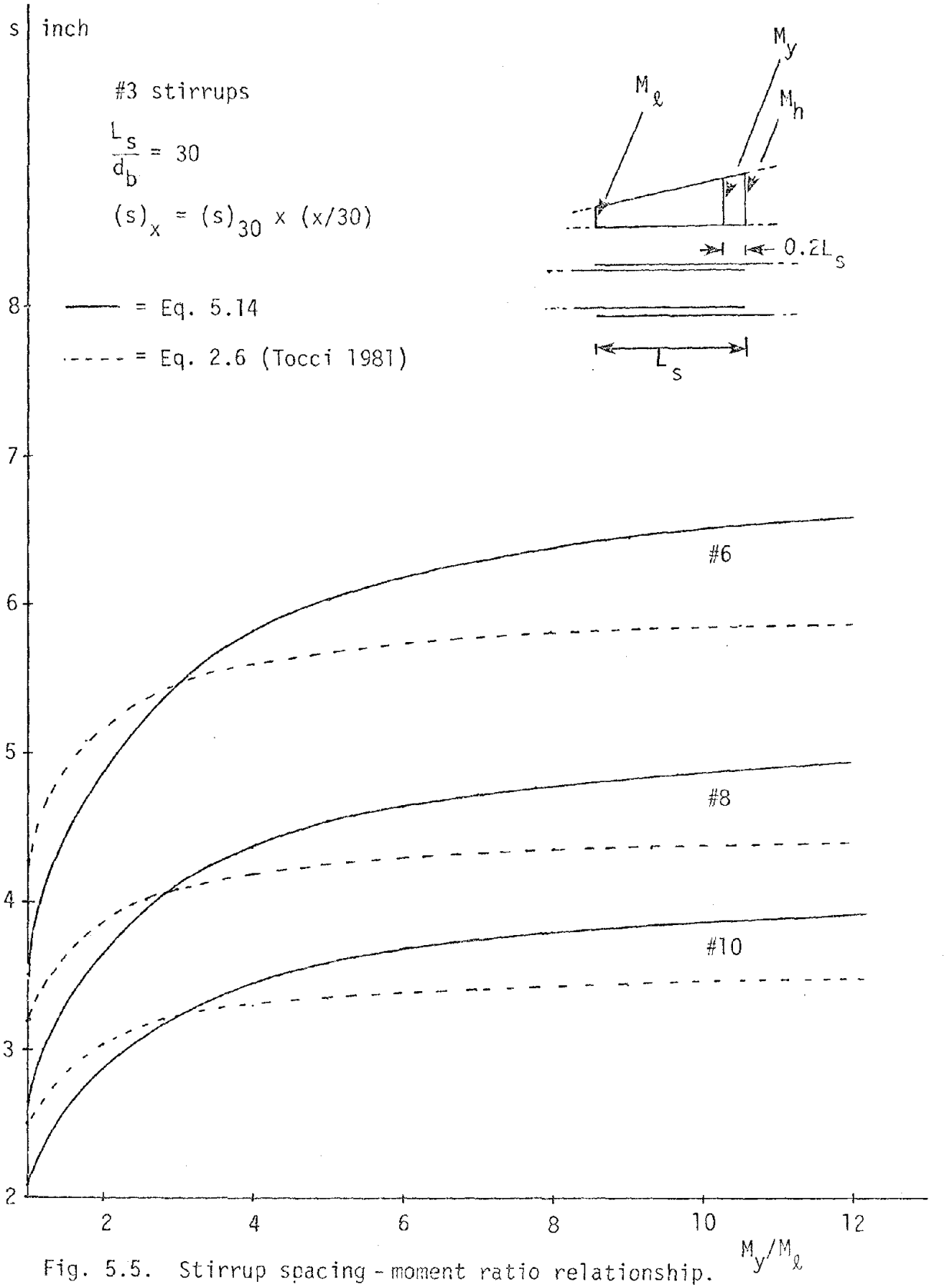

Fig. 5.5. Stirrup spacing - moment ratio relationship.

M_y/M_ℓ	κ
1	1.00
2	1.38
3	1.55
4	1.65
5	1.71
6	1.76
7	1.79
8	1.81
∞	2.00

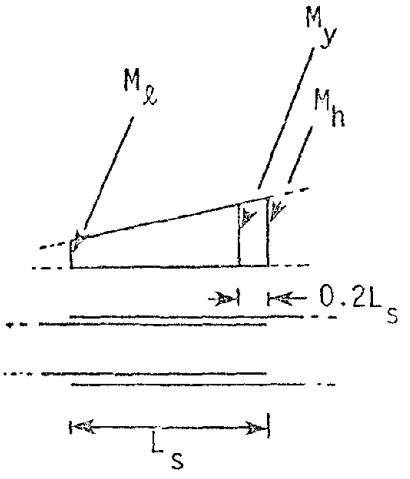

Table 5.1. Relationship between moment ratio and κ factor.

may result in an unfavorable distribution of transverse steel. It is, therefore, appropriate to specify an upper limit to the spacings indicated by Eq. 5.13, and a value of d/2 (d = effective depth) is tentatively selected. This is satisfactory for normal values of d. It is, however, excessive for large d values. In addition, constraints on stirrup spacing and size due to basic code regulations and shear requirements must be satisfied.

Also shown in Fig. 5.5 is a plot of the relationship proposed by Tocci (1981) as given in Eq. 2.6. In comparison to Eq. 5.13 of this investigation, it is conservative for splices located along high moment gradients, but more liberal at constant moment zones.

3) The variation of splice length with moment ratio for a specified stirrup spacing can be determined as follows. Eq. 5.13 is rewritten as

$$L_s/d_b = (S \times d_b)/2A_t \times (1.25 + 1/(M_y/M_\ell - 0.2)) \quad (5.16)$$

Choosing a stirrup spacing S of 4" as an example, Fig. 5.6 shows the relationship between L_s/d_b and M_y/M_ℓ graphically for #6, #8, and #10 bars. #3 stirrups are used in all cases. It is seen that splice length is very sensitive to moment ratio at low values of M_y/M_ℓ. The ratio of splice lengths for moment ratios of 1.00 and ∞ is 2.00. The same factor was seen to be applicable to stirrup spacing (Fig. 5.5).

4) It is instructive to compare the effect of moment gradient suggested in Eq. 5.13 with a relation proposed by Ferguson and Krishaswamy (1971) and Tocci (1981). The change in stirrup spacing prescribed by Eq. 5.13 can be expressed as

$$S_1/S_2 = 2.5/(1.25 + 0.2\beta^2 + \beta) \quad (5.17)$$

$\beta = M_\ell/M_y$

S_1 = Stirrup spacing under a moment gradient

S_2 = Stirrup spacing under a constant moment

The relationship suggested by Ferguson and Krishnaswamy for monotonically loaded specimens at sub-yield levels is

$$\frac{U_1}{U_2} = \frac{2}{1+\eta} \quad (5.18)$$

U_1 = Average bond strength of splice bar under moment gradient

U_2 = Average bond strength of splice bar under constant moment

η = Ratio of smaller bar stress to larger bar stress at the two ends of the splice.

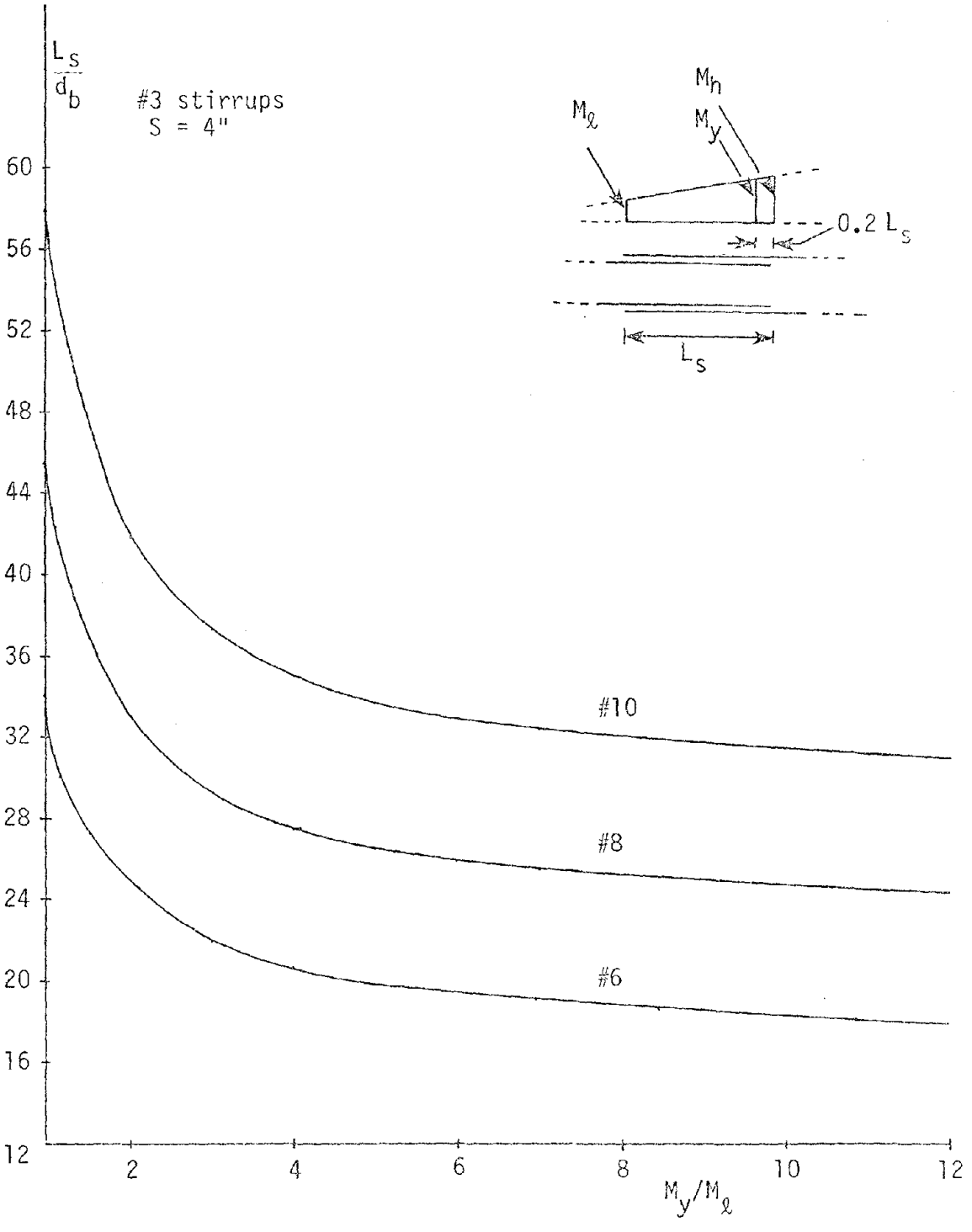

Fig. 5.6. Splice length - moment ratio relationship from Eq. 5.16.

Tocci (1981) stated that stirrup spacings for splices situated at varying moment zones of cyclically loaded beams were related to those at constant moment locations by the factor $\sqrt{2 - M_\ell/M_y}$. Or,

$$\frac{S_1}{S_2} = \sqrt{2 - M_\ell/M_y} \tag{5.19}$$

Assuming that η can be approximated as M_ℓ/M_y and that a larger bond strength U implies a larger stirrup spacing S, Eq. 5.17, Eq. 5.18, and Eq. 5.19 can directly be compared for different values of η as in Fig. 5.7. It is evident that Eq. 5.17 and Eq. 5.18 yield quite similar results, particularly at the two extremes. The relationship suggested by Tocci (Eq. 5.19) is more conservative at high moment gradients than at lower values.

Orangun, Jirsa, and Breen (1975) contend that for cover splitting type failures, a moment gradient has little or no effect on splice length, since an anchored bar is subjected to a maximum stress at the lead end and zero stress at the free end regardless of moment gradient. They showed by a comparison of test and calculated results that there was no tendency for $U_{test}/U_{calc.}$ to become large with smaller η values. This is true in the case of splices subjected to monotonic loads with little or no confinement, and where only sub-yield levels are considered. In these cases, splice strength is determined by the strength of the weaker bar, and the problem reduces to one of ensuring adequate anchorage for each bar. Their tests have shown that splice lengths and bar anchorage lengths are identical. However, well confined splices, such as those designed for cyclic inelastic loads, are characterized by their ability to redistribute forces from highly stressed locations to less critical regions. Bond forces on each bar superimpose, and the

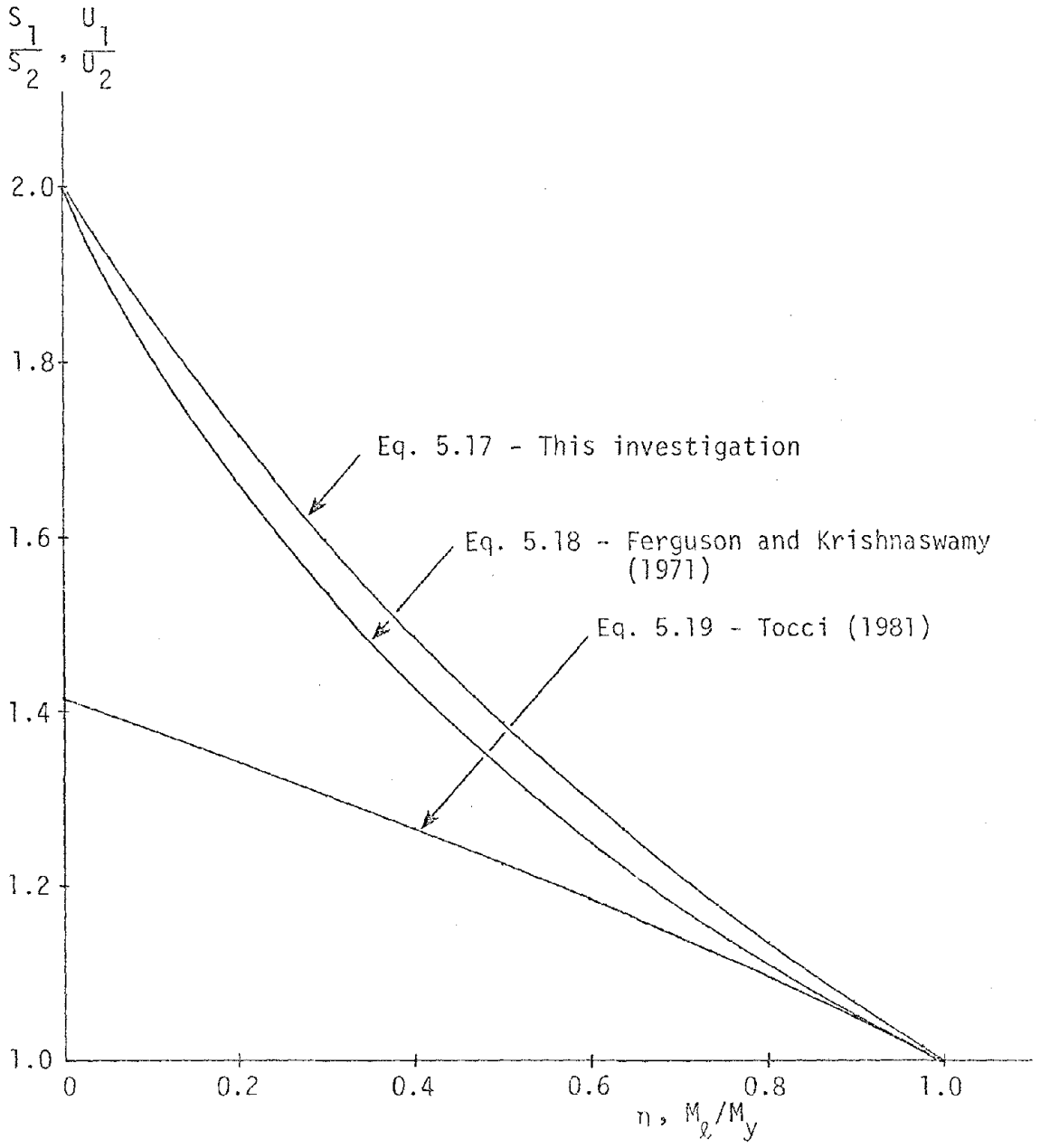

Fig. 5.7. Comparison of Eq. 5.17, Eq. 5.18, and Eq. 5.19.

splice strength is determined by the combined effect of the two bars. Under these effects, moment gradient does have a beneficial effect on splice strength as shown by Fagundo (1979) and Tocci (1981). Eq. 5.18 suggested by Ferguson and Krishnaswamy (1971) is therefore more appropriate in such cases.

5.3 Present Day Design Specifications

All major codes recognize the importance of designing seismic resistant structures with the capacity to deform inelastically. However, since knowledge of structural deterioration under inelastic cyclic loading is limited, codes in this field tend to become excessively conservative.

The ACI 318-1977 Appendix A requires splices to be of the class C type ($L_s = 1.7L_d$), and specifies that stirrup spacing shall be limited by the smallest of $\frac{d}{4}$, $8d_b$, and $24d_s$. Other codes such as SEAOC and the New Zealand Code state that no splice shall be located near a beam column joint where inelasticity is expected. Similar suggestions exist in the German Design Code - DIN 1045. Recent seismic provisions by the Applied Technology Council (ATC) allow splices that are confined by spiral or hoop reinforcement of spacing not exceeding 4" or d/4". It, however, prohibits the use of lapped splices at or near joints and locations where flexural yielding may occur. In practice, such a condition becomes very difficult to satisfy, particularly in the case of columns.

Some of these specifications have inherent inconsistencies. For example, specifying stirrup spacing to be directly related to bar diameter is logical from a bar buckling resistance point of view. For bond resistance purposes, it is in direct contradiction to test observations (Fagundo 1979, Tocci 1981) which indicate an inverse relationship as

appropriate.

Research at Cornell University shows that lapped splices can be designed to withstand inelastic cycling within specified limits of strain and displacement ductility. The following is a comparison of the various splice length - stirrup spacing relationships for a column splice member of the type shown in Fig. 5.8. Tension lap splices alone are considered, and it is assumed that they are situated at a constant moment zone. The assumed cover splitting mode is also shown in Fig. 5.8. The designs studied are:

1) ACI Standard 318-77
2) ACI Standard 318-77 - Appendix A
3) Orangun, Jirsa, and Breen (1975) design approach
4) ACI 408.1R-79 Report design approach
5) Eq. 2.4 (Fagundo 1979)
6) Eq. 2.6 (Tocci 1981)
7) Eq. 5.13 (This investigation)

1) ACI Standard 318-77

It is assumed that the full tensile capacity of the spliced bars have to be developed and that all splicing is done at the same location (no staggering).

Assuming that $\frac{A_s \text{ required}}{A_s \text{ provided}} < 2$,

a Class C type splice is required.

$L_s = 1.7\, L_d$

$L_d = 0.04\, A_b f_y / \sqrt{f'_c} = 31.8"$

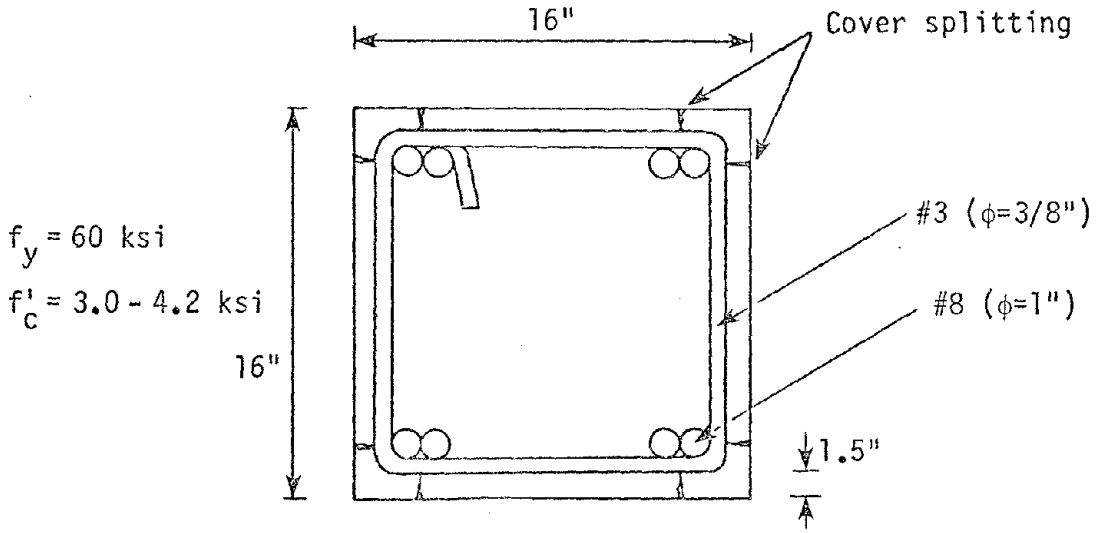

Fig. 5.8. Specimen used for design comparison.

$L_d \nless 0.0004\ d_b f_y = 24"$

$L_s = 1.7 \times 31.8 = 54"$

Compression splice requirements will not govern the design.

Stirrup spacing $S \nless d/2$

$d = 16 - 1.5 - 0.375 - 0.5 = 13.6"$

$S = 6.8"$

2) ACI Standard 318-77 - Appendix A

Lap splice length $L_s \nless 24\ d_b = 24"$

$L_s \nless 12"$

Transverse reinforcement $\nless$ #3

Since inelastic stress reversals are expected, $S \nless d/4$

$\therefore S = \frac{d}{4} = 3.4$

This spacing is required only at those regions of the splice where yielding is expected to occur. Conservatively, it can be used all along the splice length.

$L_s = 54"$, as specified by ACI-318-1977 provision.

3) Orangun, Jirsa, and Breen (1975) design approach

$$L_s = L_d = (10200\ d_b)/\{\sqrt{f'_c}\ (1 + 2.5\ c/d_b + \kappa_{tr})\phi\}$$

c = smaller of clear cover and 1/2 clear spacing of 2 splices.

$\therefore c = 1.5 + 0.375 = 1.875"$

$c/d_b = 1.875 \nless 2.5 \quad \therefore$ O.K.

$K_{tr} = A_{tr} f_{yt}/(600\ S d_b) \leq 2.5$

$A_{tr} = 0.11$ or $0.11 \times 2/2 = 0.11\ in^2$

$\therefore S_{min} = \frac{0.11 \times 60{,}000}{600 \times 1 \times 2.5} = 4.4$ in

$\therefore$ Let S = 4.4" Assume that $\phi = 1$

$L_s = L_d = 10200x1/(\sqrt{3500}\ (1 + 2.5 \times 1.875 + 2.5)) = 21.05$

$= 22"$

$L_s = 22"$

S = 4.4"

4) ACI 408.1R-79 Report design approach

C = cover to bar centre = 2.375"

d = 16 - 2.375 = 13.6"

Clear cover of bar = 1.875" < 2.0"

$\therefore$ Section 1.1.2.1 not applicable

$\therefore L_s = L_d = 5500\ A_b/\phi K\sqrt{f'_c}$

K = smaller of $(K_{tr} + C_s)$ and $(K_{tr} + C_c)$

$K \leq 3d_b = 3$

$C_c = C = 2.375"$

$A_{tr} = 0.11\ in^2$

$K_{tr} = A_{tr}\ f_{yt}/(1500S) \leq 1d_b = 1$

$\therefore S_{min} = 0.11 \times 60000/1500 = 4.4"$

$K_1 = 1 + 2.375 = 3.375 > 3.00$ $\therefore$ Not O.K.

$(K_{tr})_{max} = 3 - 2.375 = 0.625$

$K_1 = 3.0$

$\therefore S_{min} = 7.04"$

$C_s = 2.375$

$A_{tr} = 0.11x2/2 = 0.11$

$\therefore K_2 = 3.0$

Assume $\phi = 1$

$\therefore L_s = L_d = 5500 \times 0.79/(1 \times 3 \times \sqrt{3500}) = 24.48$

$= 25"$

$L_s = 25"$

$S = 7.0"$

5) Eq. 2.4 (Fagundo 1979)

$L_s \nleq 30\ d_b \quad \therefore$ Let $L_s = 30"$

$C/d_b \nleq 1.5$

But $C/d_b = 1.875$. Although the condition is not satisfied, the spacing is calculated for comparison with other designs.

$\frac{A_t f_y}{Sd_b} \geq 3000$ - which is an equivalent form of Eq. 2.4.

$\therefore S \leq \frac{A_t f_y}{3000 x d_b} = \frac{0.11 \times 60,000}{3000 \times 1} = 2.2"$

6) Eq. 2.6 (Tocci 1981)

$L_s \nleq 30\ d_b \quad \therefore$ Let $L_s = 30"$

$S = \frac{\sqrt{(A_t)}\ L_s}{4A_b} = \frac{\sqrt{0.11} \times 30 \times 4}{4 \times 1 \times \pi} = 3.16 \quad \therefore S = 3.2"$

7) Eq. 5.13 (This investigation)

$$L_s \nless 30\ d_b \quad \therefore \text{ Let } L_s = 30"$$

$$s = \frac{2.0\ A_t\ L_s}{db^2} \times \frac{1}{(1.25 + 1/(\frac{M_y}{M_\ell} - 0.2))}$$

Letting $\frac{M_y}{M_\ell} = 1$,

$$S = \frac{2.0 \times 0.11 \times 30}{1} \times \frac{1}{2.5} = 2.6"$$

These results are summarized in Table 5.2. Fig. 5.9 shows the relationship for other values of L_s. The Orangun, Jirsa and Breen (1975) method and the ACI-408-79 method result in rapidly increasing stirrup spacings at low (L_s/d_b) values. Although, in practice, these spacings will be restricted by other requirements (such as shear reinforcement), it is clear that the above two approaches are inapplicable to seismic design situations. This is not surprising, as high level ductility and reversed cyclic loading were never considered in the formulation of these provisions. Eq. 2.4 (Fagundo 1979), Eq. 2.6 (Tocci 1981) and Eq. 5.13 of this investigation all indicate a positive gradient straight line relationship. Eq. 2.4 is on the conservative side. Eq. 5.13 results in lower spacings than Eq. 2.6. However, under a moment gradient influence, Eq. 5.13 is more conservative for low moment gradients, but indicates spacings greater than those of Eq. 2.6 for steep moment gradients (Fig. 5.5).

Desig.	L_s in.	S in.
ACI 318-77	54	6.8
ACI 318-77 - Appendix A	54	3.4
Orangun, Jirsa, and Breen (1975)	22	4.4
ACI 408.1R-79 Report	25	7.0
Eq. 2.4 (Fagundo 1979)	30	2.2
Eq. 2.6 (Tocci 1981)	30	3.2
Eq. 5.13 (This investigation)	30	2.6
Eq. 5.13 (This investigation)	40	3.5

Table 5.2. A comparison of different design approaches for the column section shown in Fig. 5.8.

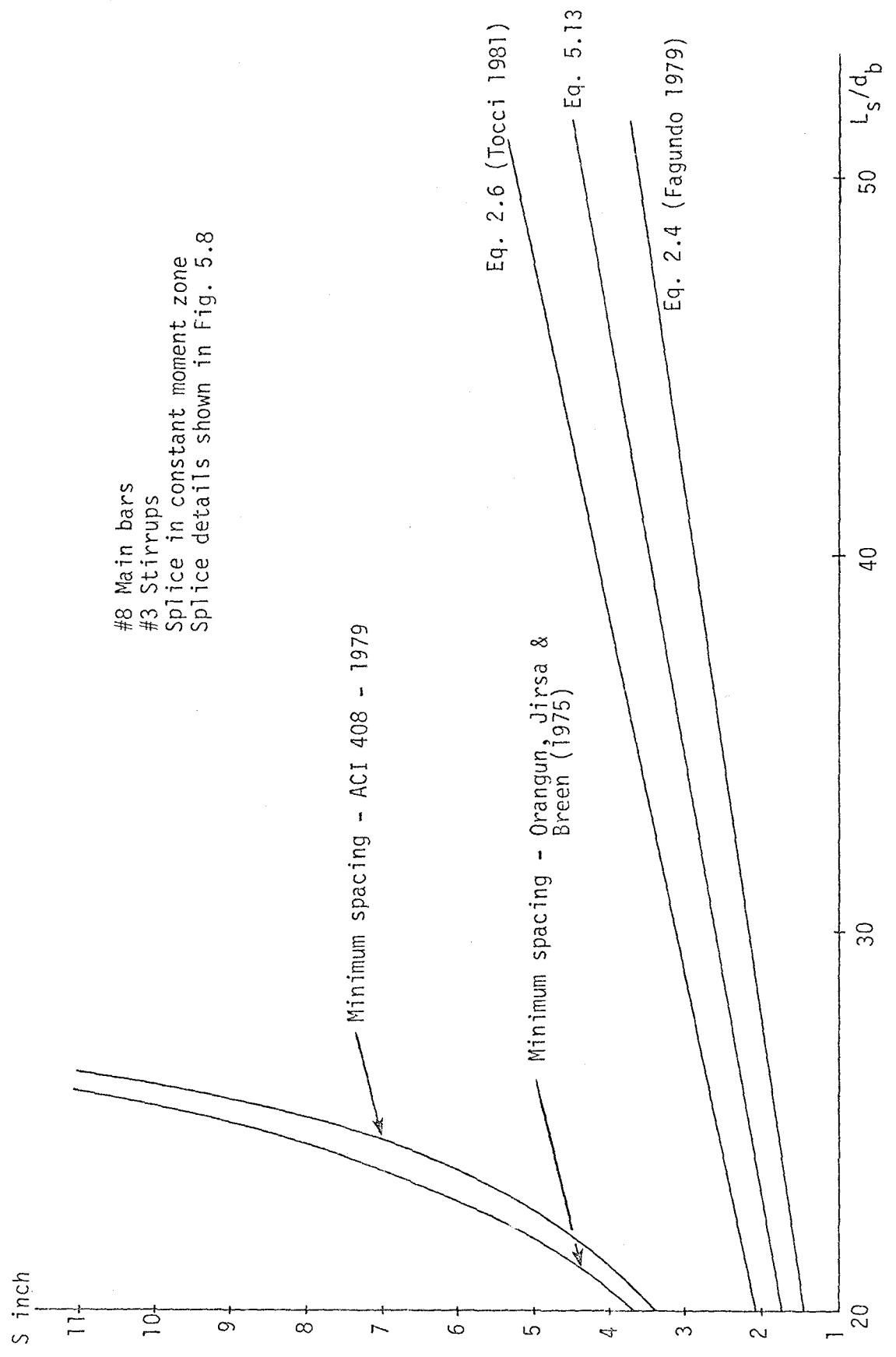

Fig. 5.9. A comparison of different design approaches.

CHAPTER 6

SUMMARY AND CONCLUSIONS

6.1 Summary

This study constitutes the third phase of a continuing investigation into the behavior and design of lapped splices under high level cyclic loads. The first two phases conducted by Fagundo (1979) and Tocci (1981) studied beam type specimens with two longitudinal bars spliced at the same location and subjected to repeated and reversed cyclic loading.

The principal purpose of this research was to study lapped column splices under high level reversed cyclic loading and to re-evaluate the findings of the previous two investigations. The splice length - stirrup spacing interaction was studied in detail. Other factors such as: concrete strength, stiffness reduction, compression splice behavior, and splice orientation were also investigated. Each specimen was eighteen feet long and of square cross-section (11.75" x 11.75"). Four #6 reinforcing bars were lap spliced at the same location and situated at the corners of the surrounding stirrups. Stirrups were #3 size and spaced uniformly along the splice. The reinforcing steel used was of Grade 60 and concrete compressive strengths were between 3.5 ksi and 4.2 ksi. Load was applied through a single hydraulic actuator which produced a linearly varying bending moment and constant shear force over the splice. A total of fourteen tests were conducted, of which Specimens C-1, C-2, C-3, and C-4 were designed using Eq. 2.4, suggested by Fagundo (1979). Specimens C-5 through C-14 were designed by Eq. 2.6, proposed by Tocci (1981). It was necessary to adopt closely spaced stirrups just outside the high

moment splice end in order to prevent a localized shear type failure. Each specimen was subjected to progressively higher levels of cyclic loading until failure. Recordings of load, displacement, and reinforcement bar strains were made at each level using an HP 3052A data acquisition system. Bar end slips were measured in Specimens C-9 through C-14.

Test results are described and an attempt is made to attain a clearer understanding of the behavior of splices under inelastic cyclic loads. This is followed by the development of a splice design equation for specimens of the type tested in this investigation. Relevant comparisons are made with previous studies and with present-day seismic code provisions.

6.2 Conclusions

Several conclusions can be made on the basis of this and the previous two experimental investigations.

(1) Lapped splices for column type specimens can be designed to sustain inelastic reversed cyclic loading within specified limits of ductility. The specimens in this investigation sustained 20-40 cycles of reversed loading at a strain ductility and displacement ductility of at least 2.5 and 1.8 respectively. The amount and distribution of stirrups over the splice and outside the high moment splice end is crucial in ensuring ductility.

(2) The maximum stirrup spacing over tension lap splices at least 30 d_b in length, situated at the corners of stirrups, at shear levels of about 120 psi, and subjected to a limited number of cycles at strain and displacement ductilities of 2.5 and 1.8 respectively is given by:

$$S = (2A_t L_s/d_b^2) \times 1/(1.25 + 1/(\frac{M_y}{M_\ell} - 0.2)) \quad , \frac{M_y}{M_\ell} \leq 1 \tag{6.1}$$

For normal levels of axial load, compression splices will not be stressed as highly as tension splices. The above equation is then conservative for compression splice design. Under high axial loads, adequate compression splice performance may require longer splice lengths and closely spaced stirrups. Eq. 6.1 includes the moment gradient effect by allowing wider stirrup spacings for large values of M_y/M_ℓ (or low values of M_ℓ/M_y).

Eq. 6.1 may be rewritten as:

$$S = (2A_t \ell_s/d_b^2) \times 1/(1.25 + 0.2\beta^2 + \beta) \tag{6.2}$$

where

$$\beta = M_\ell/M_y \tag{6.3}$$

The error in comparison to Eq. 6.1 is never in excess of 2%. Stirrup spacings computed by Eq. 6.1 or Eq. 6.2 should be regarded as maximum allowable values. Actual spacings in individual cases will often be governed by basic code provisions or shear requirements.

(3) Specimens subjected to combined bending moment and shear can fail either by a longitudinal cover splitting mechanism along the splice length, or by a localized shear-dowel type failure at the high moment end. The governing failure mode is determined by the relative amount of transverse reinforcement within the splice and just outside the high moment end. Specimens with closely spaced stirrups beyond the high moment region exhibit significant ductility even for shear-dowel type failures.

(4) Reversed cycling at and above yield results in cumulative concrete deterioration, resulting in continuous changes in the cyclic energy absorption characteristics and in load-displacement relationship. Rapid changes in stiffness occur during the first several inelastic cycles, resulting in unstable load-displacement hysteresis loops which have a decreasing moment capacity from one cycle to the next. Cycling at progressively higher levels of load or displacement finally results in specimen failure.

(5) In any cycle the extent of splice deterioration during the tension stroke far exceeds that during the compression stroke. A significant portion of compressive force is resisted through direct concrete compression. Bar end bearing resistance becomes effective only after the onset of longitudinal cover splitting.

(6) For shear levels of about 120 psi or less, transverse reinforcement over the splice is effective in resisting shear forces in addition to radial bursting stresses. It is also of use in reducing the rate of bar end slip and yield penetration. The moment gradient results in splice damage from only one end and is hence a less severe case than a constant moment zone. Stirrup effectiveness depends on the force transferring capacity of the concrete core and cover at any stage. Small-sized, closely spaced stirrups are preferable to large-sized, widely spaced ones, as the zone of influence of a stirrup is limited. Very closely spaced stirrups inhibit the formation of longitudinal cover splitting and consequently lead to shear-dowel type failures just beyond the high moment splice end. Closely spaced stirrups at this critical location are effective in controlling the extent of localized shear damage. Stirrups over the splice should be uniformly spaced rather than concen-

trated at the two ends.

(7) The onset of splitting does not constitute failure. Loads can be carried beyond the point of initial splitting up to the stage where splitting along two perpendicular faces results in a cover spalling mechanism. The resistance to radial bursting stresses afforded by concrete cover is insignificant at stages near failure. Cover integrity does, however, influence force transfer from interior locations to the stirrups.

(8) Higher strength concrete resists larger compressive forces through direct concrete compression, thereby improving compression splice behavior. These concretes also result in lower energy absorption and better concrete integrity in comparison to lower strength concretes. Very high strength mixes can have detrimental effects due to large shrinkage stresses and cracking.

(9) The influence of the orientation of the two bars of a splice was investigated by comparing the behavior of horizontally spliced specimens (bars side-by-side) with vertically spliced specimens (bars one-above-the-other). It is concluded that the overall performance of specimens of the type used in this research is not significantly affected by the relative positions of the two bars. Further research is necessary to determine the effect of higher shear levels and larger sized splice bars.

(10) The depth of cast concrete has a noticeable effect on bond resistance, particularly for the more workable concrete mixes. The less dense top layers in a horizontally cast beam or column specimen have less resistance to longitudinal cover splitting than the compacted bottom layers. The top concrete layer resistance is further reduced

by shrinkage cracking.

For the sake of completeness, selected conclusions from the results of the first two phases of this investigation have been reproduced in Appendix A.

6.3 Suggestions for Further Research

Concrete cover splitting in this investigation did not extend across the width of the section due to the relatively large distance between the two splices at the top and bottom. Further research is needed to evaluate confinement requirements in sections with multiple splices at a location. Changes in cover splitting patterns will lead to differences in performance and may warrant the use of more than a single confining stirrup at any location in the spliced zone.

The use of offset splice bars has gained popularity because it enables using stirrups of the same size along sections on either side of the splice. However, the cold bending process employed in constructing such a splice results in high stress concentrations at the bend locations. With cyclic loading, this can produce premature failure through bar fatigue . An experimental investigation is needed to decide whether these splices should be used in structures constructed in seismically active areas.

High strength concrete, having a greater splitting resistance, is likely to contribute more to resisting radial bursting stresses than normal strength concrete. Hence, the assumption that the confinement afforded by concrete cover is negligible near failure may not be as valid for these concretes. Also, since concrete ductility reduces with compressive strength, energy absorption capacities will be

lower. Definite conclusions can be arrived at only after actually testing specimens.

While specimens in this investigation showed no significant change in behavior with different splice bar orientations, this effect has yet to be evaluated for large diameter bars and high shear stress levels. The resistance to bending of a combination of two bars arranged one-below-the-other is higher than when laid side-by-side. A high bar bending stiffness can cause cover deterioration due to contact stresses at the steel concrete interface. High shear levels produce bond deterioration through bond-dowel interaction regardless of splice bar orientation.

Limitations in test setup precluded the possibility of applying direct axial loads on the column splice specimens. Although tensile splice behavior is usually more critical than that of compression splices, very high levels of axial load could conceivably produce bar instability, localized end bearing failure, and concrete crushing. Splices might have to be designed more conservatively in these instances. This is yet another possible area for further research.

APPENDIX A

SELECTED CONCLUSIONS FROM THE RESULTS OF THE FIRST TWO PHASES OF THIS INVESTIGATION

A.1 Conclusions from the Investigation Conducted by Fagundo (1979)

1) Lapped splices can be designed to sustain repeated loading to at least twice the yield deflection for the beams tested, which corresponds to over 3 times the yield strain (for f_y = 67 ksi) at the ends of the splice.

2) The splices need to be at least 30 bar diameters in length.

3) Splices must be adequately confined by closely spaced stirrups and the stirrups should be uniformly spaced over the splice length. As the stresses at the ends of the spliced region approach yield, the bursting forces generated by the spliced bars tend to be uniformly distributed along the splice length. As yield penetrates partially along the bars the bursting forces over the middle elastic portion of the spliced region can exceed those at first yield.

4) Stirrup spacing for splices of at least 30 bar diameters in length subjected to a limited number of cycles up to $2D_y$ (or 3 times the yield strain at the ends of the splice) should be:

$$s \leq 20 \frac{A_{tr}}{d_b} \qquad (A.1)$$

for Grade 60 reinforcement (main bars and stirrups).

This limit was arrived at three independent ways: (a) using a simplified equilibrium analysis of the bursting forces and confining forces for uniform stirrup strains equal to less than 0.15%, (b) assuming

that the elongations of stirrups is proportional to the elongation of the main bars at the ends of the splice, and (c) assuming twice the maximum effective amount of stirrups specified for monotonic loads. All three derivations were based on the test results.

5) The ACI 408 proposal is adequate for monotonic loads up to yield and for repeated loads below 80% of the monotonic failure load. Unless at least the maximum amount of stirrups specified by ACI 408 is used, spliced regions will probably fail during the first hundred cycles at or above 80% of the monotonic bond failure load.

6) For equal side and bottom cover, bottom splitting occurred first. Bottom splitting creates vertical cantilevers between the splitting cracks and the sides of the beam, and these cantilevers bend outward due to the bursting effect leading to sudden side splitting.

A.2 Conclusions from the Investigation Conducted by Tocci (1981)

1) Seismic codes are unnecessarily restrictive concerning the use of lap splices. Most codes for the seismic resistant design of reinforced concrete structures prohibit the use of lap splices in regions where flexural yielding is anticipated. This suggests that lap splices are not reliable under conditions of cyclic, inelastic straining. The current study indicates that splices may be designed where yielding is anticipated under certain conditions.

2) Reversed cyclic loads are more detrimental to splice performance than repeated loads, particularly for large diameter bars. Reversed bending of the bars, end bearing during compression loading of the splice and large curvature that alternates in sign contribute to increased cover damage when loads are reversed.

3) Cyclic, post-yield loading induces progressive deterioration of the force transfer mechanism, yield penetration along the splice length and, for members with typical amounts of confinement, progressive longitudinal splitting. As yield penetrates along the bars, bond and therefore bursting forces over the central, elastic portion of the splice can exceed those at first yield.

4) Principal circumferential stresses generated by bond cause longitudinal splitting along the bond length. In flexural members with typical amounts of confinement, bond failure results when longitudinal splitting produces a mechanism for cover spalling. When confinement is large, the mode of failure changes from bond splitting to pullout. Stirrups uniformly spaced along the splice length are effective in increasing confinement and are essential to member ductility when bond splitting is the anticipated mode of failure.

5) Although yielding of one or more stirrups in a splice region is often sufficient to induce a bond splitting failure, it is not a necessary condition. Cumulative damage to the concrete cover can result in loss of reinforcement anchorage before stirrup strains reach yield, particularly when #4 stirrups or larger are used.

6) The closer the spacing of stirrups along the splice length, the less important is the cover as a factor influencing splice strength. With closely spaced stirrups the effectiveness of the cover is reduced since transverse cracks, which typically form at stirrup locations, are points of weakness from where longitudinal splitting originates.

7) The monotonic design provisions proposed by ACI Committee 408 indicate that the contribution of concrete is added to the contribution of transverse steel to obtain total splice confinement. However,

accumulative cover damage makes its contribution at ultimate unreliable in the case of cyclic, post-yield loading. Therefore, cover has been neglected in formulating the design provisions given here.

8) The key to understanding the interaction of shear and bond is the dowel forces which result after the development of transverse shear cracking. The large flexural-shear crack that develops at the high-moment end of the splice can induce substantial dowel action. Dowel action is a significant factor influencing splice strength because it is known that dowel forces approaching the dowel capacity of a section rapidly reduces the anchorage capacity of reinforcement. The failure of two splices under the combined action of moment and shear was explained in terms of an index of bond-dowel interaction.

9) Finite element fracture analyses were used to assess the effectiveness of confinement for splicing and the developing of straight reinforcement. Results indicated that spliced bars required greater confinement for equivalent bond lengths or inversely, that splice lengths need be longer than corresponding development lengths for equal amounts of confinement. The principal merit of analysis based on fracture mechanics is that parameter studies can be conducted to evaluate the relative influence of cover, transverse steel, splice spacing, etc. without the time and expense required for extensive experimental programs. Undoubtedly, experimentation is required for verification purposes and to study parameters not readily modeled, such as load history.

10) The stirrup spacing for splices at least 30 bar diameters in length subjected to a limited number of cycles up to 2Dy (3-5 times the yield strain at the splice ends) should be:

$$s \leq \alpha \frac{\sqrt{A_t \ell_s}}{4 A_b} \leq 6" \qquad (A.2)$$

where: $\alpha = \frac{\text{grade of stirrup steel}}{\text{grade of spliced bar}}$

If more than two bars are spliced at a section, equation A.2 can be used without modification when the clear distance between the splice is greater than $4d_b$ or additional transverse steel is used as indicated in Section 2.7 and Figure 2.13. When shear stresses are below 250 psi the stirrup spacing may be taken as the product of the spacing calculated by equation A.2 and the following factor:

$$\sqrt{2 - \frac{M_\ell}{M_y}} \qquad (A.3)$$

However, when a splice is subjected to combined moment and shear, stirrup spacing should be the smaller of the spacing required for bond or half the spacing required for shear. In addition, the spacing of stirrups calculated in this way should be continued for a distance d from the high moment splice end.

REFERENCES

ACI Committee 215, "Considerations for Design of Concrete Structures Subjected to Fatigue Loading," ACI Journal, Vol. 71, No. 3, March 1974, pp. 97-121.

ACI Committee 318, "Building Code Requirements for Reinforced Concrete (ACI 318-77)," ACI, Detroit, 1977.

ACI Committee 408, "Bond Stress - the State of the Art," ACI Journal, Vol. 63, No. 11, Nov. 1966, pp. 161-1190.

ACI Committee 408, "Opportunities in Bond Research," ACI Journal, Vol. 67, No. 11, Nov. 1970, pp. 857-867.

ACI Committee 408, "Suggested Development, Splice, and Standard Hook Provisions for Deformed Bars in Tension," ACI Journal, Vol. 1, No. 7, July 1979, pp. 44-46.

Applied Technology Council - in Association with the Structural Engineering Association of California (ATC-SEAOC), "Tentative Provisions for the Development of Seismic Regulations for Buildings," ATC Pub. ATC 3-06, 1978.

Aristizobal-Ochoa, S.D., Fiorato, A.E., Russell, H.G., and Corley, W.G., "Earthquake Resistant Walls - Tests of Lap Splices," Progress Report to NSF Submitted by PCA, Research and Development Construction Technology Laboratories, Nov. 1977.

Aristizobal-Ochoa, S.D., Fiorato, A.E., "Tension Lap Splices Under Severe Load Reversals," Portland Cement Association, Research and Development Series, Summary Report No. 1639, 1979.

Arthur, P.D., and Cairns, J.W., "Compression Laps of Reinforcement in Concrete Columns," The Structural Engineer, Vol. 56B, No. 1, March 1978.

Baumann, T., "Versuche zum Studium der Verdubelungswirkung der Biegezugbewehrung eines Stahlbetonbalken," Material Prüfungsamt Für Das Bauwesen Der Technischen Hochschule, München, Bericht No. 77, 1968.

Blume, J.A., Newmark, N.M., and Corning, L.H., "Design of Multistory Reinforced Concrete Buildings for Earthquake Motions," Portland Cement Association, Skokie, Illinois, 1961.

Bresler, B., and Bertero, V., "Behavior of Reinforced Concrete Under Repeated Load," Proceedings ASCE, Vol. 94, ST6, June 1968, pp. 1567-1590.

Bertero, V., and Vallenas, J., "Confined Concrete: Research and Development Needs," Proceedings of a Workshop on Earthquake-Resistant Reinforced Concrete Building Construction, University of California, Berkeley, July 1977.

Bresler, B., and Bertero, V., "Behavior of Reinforced Concrete Under Repeated Load," Proceedings ASCE, Vol. 94, ST6, June 1968, pp. 1567-1590.

Broms, B.G., "Technique for Investigation of Internal Cracks in Reinforced Concrete Members," ACI Journal, Vol. 62, No. 1, Jan. 1965, pp. 35-44.

Cairns, J., and Arthur, P.D., "Strength of Lapped Splices in Reinforced Concrete Columns," ACI Journal, Vol. 76, No. 2, Feb. 1979, pp. 277-296.

Chinn, J., Ferguson, P.M., and Thompson, J.M., "Lapped Splices in Reinforced Concrete Beams," ACI Journal, Vol. 52, Oct. 1955.

Code of Practice for the Design of Concrete Structures DZ 3101: Part 1, Draft New Zealand Standard, Standards Association of New Zealand, Oct. 1978.

Eligehausen, R. and Rehm, G., "Lapped Splices of Deformed Bars Under Repeated Loading," Beton-U. Stahlbetonbau, Heft 7, 1976, pp. 170-174 (in German).

Eligehausen, R., "Übergreifungsstö Be Zugbeansprunchter Rippenstäbe mit Geraden Stabenden," Universität Stuttgart, Berlin, 1979.

Fagundo, F., "The Behavior of Lapped Splices in Reinforced Concrete Beams Subjected to Repeated Loads," Ph.D. Thesis presented to Cornell University, Ithaca, NY, January 1979.

Ferguson, P.M., and Breen, J.E., "Lapped Splices for High Strength Reinforcing Bars," ACI Journal, Vol. 62, No. 9, Sept. 1965, pp. 1063-1078.

Ferguson, P.M., and Briceno, A., "Tensile Lap Splices, Part 1: Retaining Wall Type, Varying Moment Zone," Research Report No. 113-2, Center for Highway Research, The University of Texas at Austin, July 1969.

Ferguson, P.M., and Krishnaswamy, C.N., "Tensile Lap Splices, Part 2: Design Recommendations for Retaining Wall Splices and Large Bar Splices," Research Report No. 113-3, Center for Highway Research, The University of Texas, Austin, April 1971.

Ferguson, P.M., and Thompson, J.N., "Development Length of High Strength Reinforcing Bars," ACI Journal, Vol. 59, No. 7, July 1962.

Ferguson, P.M., and Thompson, J.N., "Development Length of Large High Strength Reinforcing Bars," ACI Journal, Vol. 62, No. 1, Jan. 1965, pp. 71-94.

Ferguson, P.M., and Breen, J.E., "Lapped Splices for High Strength Reinforcing Bars," ACI Journal, Vol. 62, No. 2, 1965, pp. 1063-1078.

Gergely, P., "Experimental and Analytical Investigations of Reinforced Concrete Frames Subjected to Earthquake Loading," Workshop on Earthquake Resistant Reinforced Concrete Building Construction, University of California, Berkeley, July 11-15, 1977.

Gergely, P., "Splitting Cracks Along the Main Reinforcement in Concrete Members," Department of Structural Engineering, Cornell University, 1969 Report to Bureau of Public Roads, U.S. Department of Transportation, pp. 90.

Gergely, P., White, R.N., and Fagundo, F., "Bond and Splices in Reinforced Concrete for Seismic Loading," AICAP-CEB Symposium, Vol. 2, Rome, May 1979.

Gergely, P., and White, R.N., "Seismic Design of Lapped Splices in Reinforced Concrete," Proc. Seventh World Conference on Earthquake Engineering, September, 1980, Vol. 4, pp. 281-288.

German Standard DIN 1045, Concrete and Reinforced Concrete Structures: Design and Construction, (English Translation) London. British Standards Institution, 1972.

Gosain, N.K., and Jirsa, J.O., "Bond Deterioration in R.C. Members under Cyclic Loads," Proc. 6th World Conference on Earthquake Engineering, New Delhi, 1977.

Goto, Y., "Cracks Formed in Concrete Around Deformed Tension Bars," ACI Journal, Vol. 68, No. 4, April 1971, pp. 244-251.

Hassan, F.M., and Hawkins, N.M., "Anchorage of Reinforcing Bars for Seismic Forces," Reinforced Concrete in Seismic Zones, ACI SP53-15, 1977.

Hassan, F.M., and Hawkins, N.M., "Prediction of the Seismic Loading Anchorage Characteristics of Reinforced Bars," Reinforced Concrete in Seismic Zones, ACI SP53-16, 1977.

Hassan, F.M., and Hawkins, N.M., "Effect of Post-Yield Loading Reversals on Bond Between Reinforcing Bars and Concrete," Report SM73-2, Department of Civil Engineering, University of Washington, Seattle, Washington, March 1973.

Hawkins, N.M., "Development Length Requirements for Reinforcing Bars Under Seismic Conditions," Workshop on Earthquake Resistant Reinforced Concrete Building Construction, University of California, Berkeley, July 11-15, 1977.

Hawkins, N.M., Kabayashi, A.S., and Fourney, M.E., "Reversed Cyclic Loading Bond Deterioration Tests," SM-75, Department of Civil Engineering, University of Washington, Seattle, November 1975.

Hawkins, N.M., "Fatigue Characteristics in Bond and Shear of Reinforced Concrete Beams," Fatigue and Concrete SP-41, ACI, 1974, pp. 203-236.

Hess, U., "The Anchorage Strength of Reinforcement Bars at Supports," Final Report, Plasticity in Reinforced Concrete, Volume - Band 29, IABSE Colloquium, Copenhagen, Denmark, 1979.

Hungspreug, S., Gergely, P., Ingraffea, A.R., and White, R.N., "Local Bond Between a Reinforcing Bar and Concrete Under High Intensity Cyclic Load," Report 81-6, Department of Structural Engineering, Cornell University, January 1981.

Houde, J., "Study of Force-Displacement Relationships for the Finite Element Analysis of Reinforced Concrete," Structural Concrete Series No. 73-2, McGill University, Montreal, Dec. 1973.

Ismail, M.A.F., "Bond Deterioration in Reinforced Concrete Under Cyclic Loading," Ph.D. Thesis, Civil Engineering Department, Rice University, Feb. 1970.

Ismail, M.A.F., and Jirsa, J.D., "Behavior of Anchored Bars Under Low Cycle Overloads Producing Inelastic Strains," ACI Journal, Vol. 69, No. 7, July 1972, pp. 433-438.

Ismail, M.A.F., and Jirsa, J.D., "Bond Deterioration in Reinforced Concrete Subjected to Low Cycle Loads," ACI Journal, Vol. 69, No. 6, June 1972, pp. 334-343.

Jimenez, R., White, R.N., and Gergely, P., "Bond and Dowel Capacities of Reinforced Concrete," ACI Journal, Vol. 76, No. 1, Jan. 1979, pp. 73-92.

Jimenez, R., Gergely, P., and White, R.N., "Shear Transfer Across Cracks in Reinforced Concrete," Report 78-4, Department of Structural Engineering, Cornell University, Ithaca, N.Y., Aug. 1978.

Jirsa, J.O., and Brown, R.H., "Reinforced Concrete Beams Under Load Reversals," ACI Journal, Proceedings V. 68, No. 5, May 1971, pp. 380-390.

Jirsa, J.O., and Ismail, M.A.F., "Bond Determination in Reinforced Concrete Subjected to Low Cycle Loads," ACI Journal, Proceedings V. 69, No. 6, June 1972, pp. 334-343.

Jirsa, J.O., Lutz, L.A., and Gergely, P., "Rationale for Suggested Development, Splice, and Standard Hook Provisions for Deformed Bars in Tension," ACI Journal, Vol. 1, No. 7, July 1979, pp. 47-61.

Kemp, E.L., Brezny, F.S., and Unterspan, J.A., "Effect of Rust and Scale on the Bond Characteristics of Deformed Reinforcing Bars," ACI Journal, Vol. 65, No. 9, Sept. 1968, pp. 743-756.

Kemp, E.L., and Wilhelm, W.J., "Investigation of the Parameters Influencing Bond Cracking," ACI Journal, Vol. 76, No. 1, Jan. 1979, pp. 47-71.

Krefeld, W.J., and Thurston, C.W., "Contribution of Longitudinal Steel to Shear Resistance of Reinforced Concrete Beams," Journal of the American Concrete Institute, Vol. 63, No. 3, March 1966, pp. 325-344.

Lin, I.J., "Anchorage Characteristics for Reinforcing Bars Subjected to Reversed Cyclic Loading," Masters Thesis Presented to the University of Washington, Jan. 1978.

Lutz, L.A., "Information on the Bond of Deformed Bars from Special Pull-Out Tests," ACI Journal, Vol. 68, No. 11, Nov. 1970, pp. 885-887.

Lutz, L.A., "Analysis of Stresses in Concrete Near a Reinforcing Bar Due to Bond and Transverse Cracking," ACI Journal, Proceedings V. 67, No. 10, October 1970, pp. 778-787.

Lutz, L.A., and Gergely, P., "Mechanics of Bond and Slip of Deformed Bars in Concrete," ACI Journal, Vol. 64, No. 11, Nov. 1967, pp. 711-721.

Lutz, L.A., Gergely, P., and Winter, G., "The Mechanics of Bond and Slip of Deformed Bars in Concrete," Report No. 324, Department of Structural Engineering, Cornell University, Aug. 1966.

Mathey, R.G., and Watstein, D., "Investigation of Bond in Beam and Pull-Out Specimens with High-Yield Strength Deformed Bars," ACI Journal, Vol. 57, No. 9, March 1961, pp. 1071-1090.

Mendelson, A., "Plasticity; Theory and Application," Macmillian, New York, 1968.

Morita, S. and Kaku, T., "Local Bond Stress-Slip Relationship under Repeated Loading," Proceedings of Seminar on Earthquake Engineering with Emphasis on the Safety of Reinforced Concrete Structures, University of California, Berkeley, Sept., 1973.

Morita, S., and Kaku, T., "Splitting Bond Failures of Large Deformed Reinforcing Bars," ACI Journal, Vol. 76, No. 1, Jan. 1979, pp. 93-110.

Nielsen, N.N., Takeda, T., Sozen, M.A., "Reinforced Concrete Response to Simulated Earthquakes," Journal of the Structural Division, ASCE, Vol. 96, No. ST12, Dec. 1970, pp. 2557-2574.

Nilson, A.H., "Bond Stress - Slip Relations in Reinforced Concrete," Report 345, Dept. of Structural Engineering, Cornell University, Ithaca, N.Y., Dec. 1971.

Ochoa-Aristizobal, S.D., Fiorato, A.E., "Tension Lap Splices Under Severe Load Reversals," Portland Cement Association, Research and Development Series, Summary Report No. 1639, 1979.

Orangun, C.O., Jirsa, J.O., and Breen, J.E., "A Reevaluation of Test Data on Development Length and Splices," ACI Journal, Vol. 74, No. 3, March 1977, pp. 114-122.

Orangun, C.O., Jirsa, J.O., and Breen, J.E., "The Strength of Anchored Bars: A Reevaluation of Test Data on Development Length and Splices," Research Report 154-3F, Center of Highway Research, The University of Texas at Austin, Jan. 1975.

Perry, E.S., and Jundi, N., "Pullout Bond Stress Distribution Under Static and Dynamic Repeated Loadings," ACI Journal, Vol. 66, No. 5, May 1969, pp. 377-380.

Rehm, G., "The Fundamental Law of Bond," Proceedings, Symposium on Bond and Crack Formation in Reinforced Concrete, Stockholm, 1957 (translated RILEM, Paris, 1958).

Rehm, S., and Eligehausen, R., "Bond of Ribbed Bars Under Repeated Loads," ACI Journal, Vol. 76, No. 2, Feb. 1979, pp. 297-309.

Rehm, G., and Eligehausen, R., "Lapped Splices of Deformed Bars Under Repeated Loading," Beton-U. Stahlbetonbau, Heft 7, 1976 pp. 170-174 (in German).

Roberts, N.P., and Chung-Tai Ho, R., "Behavior and Design of Tensile Lapped Joints in Reinforced Concrete Beams," Civil Engineering Public Work Review, Vol. 68, No. 798, Jan. 1973, pp. 35-45.

Roy, H.E.H., and Sozen, M.A., "Ductility of Concrete," Proc. of the International Symposium on Flexural Mechanics of Reinforced Concrete, Miami, 1964.

Structural Engineers Association of California (SEAOC), Seismology Committee, "Recommended Lateral Force Requirements and Commentary," San Francisco, California, 1974.

Takeda, T., Sozen, M.A., and Nielsen, N.N., "Reinforced Concrete Response to Simulated Earthquakes," Journal of the Structural Division, ASCE, Vol. 96, No. ST12, Dec. 1970, pp. 2557-2574.

Taylor, H.P.J., "Investigation of the Dowel Shear Forces Carried by the Tensile Steel in Reinforced Concrete Beams," Cement and Concrete Association Report No. TRA 431, Nov. 1961.

Tassios, T.P., "Properties of Bond Between Concrete and Steel Under Load Cycles Idealizing Seismic Actions," Symposium on Structural Concrete Under Seismic Actions, CEB, Rome, 1979.

Tepfers, R., "A Theory of Bond Applied to Overlapped Tensile Reinforcement Splices for Deformed Bars," Publication 73:2, Division of Concrete Structures, Chalmers Teknisica Hogskola (Chalmers University of Technology), Goteborg, Sweden, 1973.

Tepfers, R., "An Investigation of the Fatigue Strength of Concrete," Statens Råd för Byggnadsforskning, Report 86, Stockholm, 1978.

Tocci, A.D., "The Behavior and Strength of Lapped Splices in Reinforced Concrete Beams Subjected to Cyclic Loading," Ph.D. Thesis, Department of Structural Engineering, Cornell University, May 1981.

Townsend, W.H., Hanson, R.D., "Reinforced Concrete Connection Hysteresis Loops," Reinforced Concrete in Seismic Zones, ACI SP53-13, 1977.

Viwathanatepa, S., Popov, E.P., and Bertero, V.V., "Deterioration of Reinforced Concrete Bond Under Generalized Loading," ACI 1977 Annual Convention, San Diego, California, March 1977.

Vos, I.E., and Reinhardt, H.W., "Bond Resistance of Deformed Bars, Plain Bars and Strands Under Impact Loading," Report 5-80-6, Dept. of Civil Engineering, Delft University of Technology, September 1980.

Watstein, D., and Mathey, R.G., "Strains in Beams Having Diagonal Cracks," ACI Journal, Proc. V. 55, No. 4, December 1958.

Winter G., and Nilson, A.H., "Design of Concrete Structures," 8th ed., McGraw-Hill, New York, N.Y., 1978.

Zsutty, T., "An Empirical Study of the Behavior of Bond Test Data," Presented at the 1977 Annual Convention, American Concrete Institute, San Diego, March 1977.